APRIL 1986

ENVIRONMENTAL SCIENCE & TECHNOLOGY

ES&T

SCF processing
Page 319

It's only right for them to know

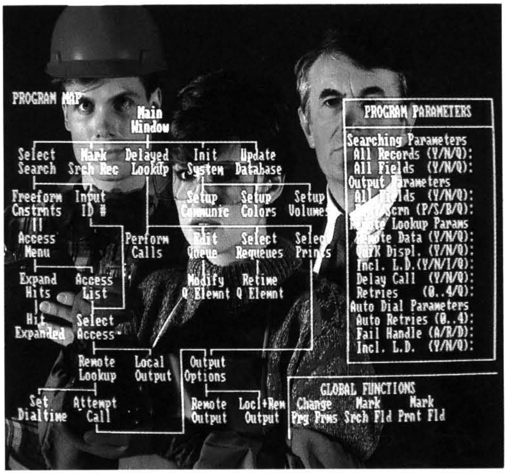

CHEMPRO™ HAZARDOUS CHEMICAL DATABASE

Federal right-to-know laws require that complete safety data on all chemicals used in the workplace be kept **accessible, on site, at all times.** To help keep your employees safe and to help you comply with these laws, we've developed ChemPro, a microprocessor database that gives you **fast** access to accurate, reliable information on over 4100 potentially hazardous chemicals.

Emergency information in seconds. Hit emergency key for FIRE, SPILL, or POISON, and enter chemical name. In seconds, a concise emergency screen displays fire fighting, decontamination or first aid procedures.

Safety information on over 4100 hazardous chemicals. ChemPro contains a carefully selected subset of data on each of the chemical entries stored in the National Library of Medicine's (NLM) vast Hazardous Substance Data Bank (HSDB). Each ChemPro entry contains concise technical and safety information culled from HSDB records, including: biodegradability, biological warning signs, chemical/physical properties, environmental impact, flammability, hazardous reactions, manufacturing/use information, storage/handling instructions, substance identification, and toxicity.

Direct access to the Hazardous Substance Data Bank. For even more extensive technical information on each of its chemical entries, ChemPro features a built-in communications package allowing registered NLM users to interface directly with the larger HSDB. Just open an account with the NLM and you have direct access to **twice** as much information on every chemical in your ChemPro database.

Plus planned nonobsolescence. When you subscribe to our quarterly update service, we'll upgrade your database with new entries to keep your records nearly as up-to-date as the NLM itself.

Search and print data from thousands of entries. Runs on the IBM Personal Computer AT® for massive storage capability and fast searches. A chemical name, synonym, Chemical Abstract Service (CAS) or HSDB number takes you directly to an entry. If you don't know the name, you can search for an entry using a keyword, molecular formula — even a fragment of the name from a torn label. Help windows appear at a keystroke to guide even a novice through the program.

Tailor the program to your individual usage habits, and cut search time drastically. Merely preset program parameters to skip prompts you don't want, and to query you only on the options you want it to.

For more information on ChemPro, call your Fisher Rep today. Or call 412-562-8383 about a low-cost demo disk.

Fisher Scientific

Environmental Science & Technology

For officers and advertisers, see page 334.

Please send *research* manuscripts to Manuscript Reviewing, *feature* manuscripts to Managing Editor. For editorial policy and author's guide, see the January 1986 issue, page 30, or write Janice L. Fleming, Manuscript Reviewing Office, *ES&T.* A sample copyright transfer form, which may be copied, appears on the inside back cover of the February 1986 issue.

Environmental Science & Technology, ES&T (ISSN 0013-936X), is published monthly by the American Chemical Society at 1155 16th Street, N.W., Washington, D.C. 20036. Second-class postage paid at Washington, D.C., and at additional mailing offices. POSTMASTER: Send address changes to *Environmental Science & Technology,* Membership & Subscription Services, P.O. Box 3337, Columbus, Ohio 43210.

SUBSCRIPTION PRICES 1986: Members, $28 per year; nonmembers (for personal use), $42 per year; institutions, $164 per year. Foreign postage, $8 additional for Canada and Mexico, $16 additional for Europe including air service, and $23 additional for all other countries including air service. Single issues, $15 for current year; $17 for prior years. Back volumes, $198 each. For foreign rates add $2 for single issues and $8 for back volumes. Rates above do not apply to nonmember subscribers in Japan, who must enter subscription orders with Maruzen Company Ltd., 3-10 Nihon bashi 2 chome, Chuo-ku, Tokyo 103, Japan. Tel: (03) 272-7211.

SUBSCRIPTION SERVICE: Orders for new subscriptions, single issues, back volumes, and microfiche and microform editions should be sent with payment to Office of the Treasurer, Financial Operations, ACS, 1155 16th St., N.W., Washington, D.C. 20036. Phone orders may be placed, using Visa, Master Card, or American Express, by calling toll free (800) 424-6747 from anywhere in the continental U.S. Changes of address, subscription renewals, claims for missing issues, and inquiries concerning records and accounts should be directed to Manager, Membership and Subscription Services, ACS, P.O. Box 3337, Columbus, Ohio 43210. Changes of address should allow six weeks and be accompanied by old and new addresses and a recent mailing label. Claims for missing issues will not be allowed if loss was due to insufficient notice of change of address, if claim is dated more than 90 days after the issue date for North American subscribers or more than one year for foreign subscribers, or if the reason given is "missing from files."

ES&T

CONTENTS

Volume 20, Number 4, April 1986

FEATURES

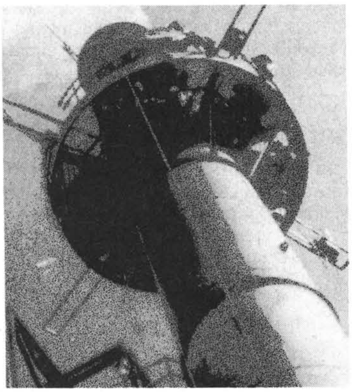

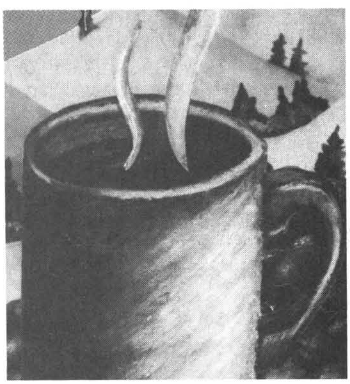

REGULATORY FOCUS

VIEWS

DEPARTMENTS

UPCOMING

Victim compensation
Environmental engineering education

ESTHAG 20(4) 305–416 (1986)
ISSN 0013 936X

Credit: p. 330, Robert Suddarth Photographers

Cover: Donna K. Cantor; at Bourbon Street Restaurant, Holiday Inn, Bethesda, Md.

RESEARCH

NOTES

CORRECTION

* To whom correspondence should be addressed.

■ This article contains supplementary material in microform. See ordering instructions at end of paper.

ES&T

GUEST EDITORIAL

Writing wrongs

Perhaps I am becoming cantankerous, or simply hypersensitive, but it seems to me that every scientific, technical, and nontechnical magazine I read contains at least one article sprinkled with mathematical-grammatical errors right out of the fifth grade. These errors are distracting and, rightly or wrongly, can undermine the reader's confidence in the accuracy of the data and in the technical competence of authors, reviewers, and editors.

The most common is the times-greater/times-as-great error. For example, 50 ppm is not five times (500%) greater than 10 ppm; it is four times (400%) greater. The error in using five times greater is 25%. Of course, 50 ppm is five times as great as 10 ppm. In the same family of errors are times-higher/times-as-high, times-larger/times-as-large, times-faster/times-as-fast, and so on.

Times excess also occurs. I find that usage of times greater, higher, larger, and faster is almost always incorrect, when data are available to verify the correctness; I am forced to assume that similar but uncheckable statements must be wrong just as frequently. Attempts to make calculations from these statements can be fraught with error. If we are not careful, we may lose the specific meaning of these phrases, just as we have of others such as "biweekly," which, at least in the United States, now means every two weeks *and* twice a week.

Almost as common are the times-less, times-smaller, times-lower errors. Times colder and orders of magnitude less can be included here. All are mathematically and grammatically impossible. For instance, 10 ppm is neither five times (500%?) less nor even four times (400%?) less than 50 ppm. It is 80% less. Alternatively, 10 ppm is one-fifth of 50 ppm. The limit is 100% less.

Naked decimal points are becoming embarrassingly frequent, streaking across computer printouts and through the literature, spawned by the software writers. We learn, in about the fifth grade, that 0.63 is correct, .63 is wrong, and −.63 is unforgivable. There is, of course, a practical reason for this. However, sportswriters regularly compound the error when reporting a batter hitting .250 *percent.* One hit in 400?

I am no expert in the field of grammar, so when even I observe these particular errors my faith in the rest of the article is shaken. It is difficult sometimes to get the fact accepted that there is an error or, if there is acceptance, to have steps taken to prevent a recurrence.

Education is the answer, of course—not just through high school and college, but by way of the journalists' bible, the stylebook. A stylebook in some form is the ultimate authority for virtually all writers. Stylebooks vary and may disagree, but every organization uses one, whether it has been written in house or by others. It is disappointing to find that some stylebooks contradict the fundamentals taught in our schools. The stylebook of one of the nation's largest weekly news magazines contradicts itself by defining watt, w, as a traditional unit and, on the opposite page, stating that watt, W, is metric.

I believe it is important to keep a sense of proportion when leveling criticism, but we must not let these errors breed and get out of hand. I am not proposing anything as grandiose as calling on the English-speaking world to rise up and slay these semantic dragons, but I hope that writers, reviewers, and editors and the editors of individual stylebooks will take note and update accordingly. Then, for all of us, it may be the end of writing wrongs.

Kenneth A. Hooton

Kenneth A. Hooton is the senior chemical consultant for the Salt River Project in Phoenix, Ariz. He has degrees from London and Arizona State universities and, over the past 40 years, has practiced chemistry and semantics in Africa, Europe, and the United States. To his friends, he is the consummate which doctor.

0013-936X/86/0920-0307$01.50/0

ES&T CURRENTS

INTERNATIONAL

The United Kingdom will abandon its program of research into ocean wave power, but it will support research on solar-heated homes, energy from waste, and windmills. About £14 million will be allocated for work on the latter three forms of renewable energy, but the British government will lose the benefits of the £17 million dedicated to ocean wave energy research. Energy Minister David Hunt says that British government policy will "support the winners in nonconventional energy options. We are concentrating our resources on the most promising options." The British government will, however, continue to follow other countries' wave energy research, especially that of Norway.

FEDERAL

EPA's proposed operating budget for fiscal year 1987 is $1.376 billion, a 7.6% decrease from the fiscal year 1986 level appropriated by Congress. The 1987 figure includes a 4% decrease from EPA's 1986 budget *after* the Gramm–Rudman–Hollings deficit reduction law has cut the 1986 budget by 3.6%. About $295 million has been proposed for research, which is a $17.3-million decrease from estimated 1986 funding. The drinking-water program will likely suffer a $7-million cut to $84 million, and the air program may be cut by almost $21 million to $239.3 million. The hazardous waste program, however, is expected to receive an increase of $7 million over the fiscal 1986 appropriated level to $256 million. Reagan administration officials proposed these figures Feb. 5.

The Office of Management and Budget (OMB) has no authority to cause EPA to miss a statutory deadline, according to a decision handed down Jan. 28 by Judge Thomas Flannery of the U.S. District Court for the District of Columbia. The Environmental Defense Fund sued EPA last May, on the grounds that an OMB review of proposed underground tank rules made the agency miss a 1985 mandatory deadline for final issuance of these rules. Government attorneys had argued that President Reagan's Executive Order 12291 of Feb. 17, 1981, allows OMB to review proposed regulations to ensure that they meet Reagan administration policies. Judge Flannery rejected the government's argument, noting that the missed deadline was mandated by Congress in the 1984 amendments to the Resource Conservation and Recovery Act.

Thomas: Superfund may be shut down

All cleanups required by Superfund will cease by July if Superfund has not been reauthorized or if Congress has not provided short-term funding by April 1, according to EPA Administrator Lee M. Thomas. Superfund and its taxing authority expired Sept. 30, 1985. Since then, the House and Senate have been unable to agree on the size of a new fund or on how to raise the money. EPA issued a Superfund shutdown schedule Jan. 29 that would require the agency to inform contractors of contract terminations and employees of furloughs. As things stand now, by April 1, EPA will allocate $1 million each month for emergency cleanups through July 1—about 20% of the funds available in January. Had Superfund been reauthorized, the new law would have provided funding for five years. Thomas proposed legislation in February to furnish $861 million to Superfund to keep the program alive for a year.

The U.S. Fish and Wildlife Service reports that 10 national wildlife refuges are contaminated by toxic chemicals and another 74 may be in danger of contamination. In February, William Horn, the Department of the Interior's assistant secretary for fish, wildlife, and parks said that the service has begun to clean up four contaminated refuges and plans to start work on another five. EPA is cleaning another refuge. Contaminants include selenium (Kesterson Refuge, Calif.), asbestos fiber (Great Swamp National Wildlife Refuge, N.J.), DDT (Wheeler Refuge, Alaska), PCBs (Crab Orchard, Ill.), and mustard gas and plutonium (Johnston Island in the central Pacific Ocean).

EPA recently proposed limits on NO_x emissions from new industrial boilers. To help boiler operators comply with the regulations, EPA has developed a method, called reburning, that destroys NO_x formed during combustion. This technique calls for the expansion of the combustion zone within the boiler. A mixture of natural gas and ambient air is diverted to a secondary zone above the primary combustion zone. Hydrocarbon radicals created in the secondary zone are estimated to reduce NO_x emissions by 50% or more if the reburning technique is coupled with other emission control systems.

STATES

Pennsylvania is delaying a $3-million, low-interest loan program for homeowners to radon-proof their homes. Last October, Gov. Richard Thornburgh announced that 2–9% loans would be made by the Pennsylvania Housing Finance Agency (PHFA) to protect more than 20,000 residences in the Reading Prong, a uranium-rich area in Berks, Bucks, Lehigh, and Northampton counties, against radon. PHFA officials fear that if residents develop radon-related illnesses after their homes are radon-proofed with state financial aid, the agency could be sued. A PHFA spokesman has said that the agency does not plan to carry insurance against such litigation and that PHFA will not offer the loans until the state legislature passes a law granting the agency immunity.

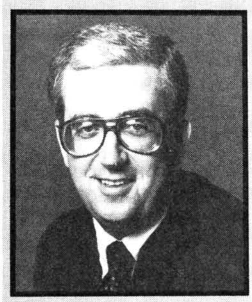

Carlson: Limit contaminant sources

The Illinois Environmental Protection Agency (IEPA) has proposed a groundwater protection plan that stresses prevention of problems rather than reaction to them. IEPA Director Richard Carlson said in January that the plan would give the agency authority to order potential contaminant sources set back specific distances from groundwater supplies. The plan also will give IEPA the power to require local governments to prepare and implement management plans for all existing and potential sources of contaminants within their jurisdictions. IEPA and other state agencies would assist communities in defining areas, called capture zones, from which groundwater users draw their supplies. The agency also will offer help to communities in devising ways to prevent contaminants from entering or spreading to these capture zones.

California's Department of Health Services is offering grants to promote innovation in the management of hazardous wastes. Grants for feasibility studies are awarded for up to 90% of the amount needed or $25,000, whichever is less. The amount obtainable for design is up to 70% of cost, to a maximum of $50,000 (90% for small businesses). Effectiveness evaluation studies are allowed up to 90% (100% for small businesses) of cost, to a maximum of $100,000, and construction gets up to 50% (80% for small businesses) to a top amount of $400,000. Guidelines for grant applications were issued March 1; awards will be made by July 1.

Although Wisconsin's rain is acid, fish in many of the state's lakes should not be damaged for at least 100 years, according to James Bockheim of the University of Wisconsin—Madison. In January, he said that soils and forests surrounding most lakes are "unexpectedly rich in weatherable, acid-adsorbing minerals." Bockheim adds that his calculations suggest that under current conditions "it would take 100–1000 years for the soils to take up enough hydrogen ions from rain to wear down the soils' buffering capacity." Also, many of Wisconsin's lakes get their water from groundwater that has seeped through the soil and has had much of its acidity removed. By comparison, lakes strongly affected by acid rain, such as those in New York's Adirondack Mountains, lie on bedrock rather than soil.

AWARD

Bruce Ames, developer of the Ames test, received the 1985 Kenneth A. Spencer Award in Kansas City, Mo., Feb. 20, 1986. Sponsored by the American Chemical Society, the award is presented annually to a scientist who has made a significant contribution to the field of agriculture and food chemistry. Ames is professor and chairman of the department of biochemistry at the University of California at Berkeley. The Ames test is a simple, inexpensive test that uses bacterial strains to detect dangerous chemicals that cause mutation of DNA—a likely cause of cancer.

SCIENCE

The high incidence of liver cancer in some parts of China may be ascribable to naturally occurring aflatoxins, suggested Fun Sun Chu of the University of Wisconsin—Madison in January. In those regions of China, liver cancer causes 50 of every 100,000 deaths—10 times the death rate found in the United States. Aflatoxins are poisons generated by molds, especially *Aspergillus flavus* and *A. parasiticus,* that grow on nuts, grains, and seeds under certain conditions of weather and food storage. Problems with aflatoxins have been known since the 1960s when a number of turkeys died after eating moldy peanuts. The poisons have been difficult to detect until now; Fun recently developed a means of detecting minute amounts of aflatoxins in food and urine. He says that his method is quicker and more sensitive than the test now used by the U.S. Food and Drug Administration.

TECHNOLOGY

An in situ test for carbamate and organophosphate pesticides uses the enzyme cholinesterase to detect these compounds. Developed by MRI Ventures (Kansas City, Mo.), the test yields results within minutes and costs less than $5. By comparison, conventional tests for pesticides cost $100–$300/sample and require several days. A pesticide sample is placed on a polyethylene ticket and pressed for three minutes against a laminated plastic foil with disks containing the enzyme and a substrate. The enzyme disk is then peeled off and examined for color. A blue tint confirms the absence of pesticides; white shows that pesticides are present or that the ticket is not working. According to MRI, pesticides can be detected to levels as low as 1–10 ppm.

Fluidized-bed combustion (FBC) of culm, with limestone shows promise as a source of energy to produce electric power. Culm is the low-sulfur carbonaceous waste product from anthracite mining in eastern Pennsylvania. Large piles of the refuse, some of them containing millions of tons, scar the countryside and contribute heavily to local air and water pollution. The Economic Development Council of Northeastern Pennsylvania and other organizations envision the construction of a $131-million FBC culm-burning power plant in Frackville, Pa., that would provide steam and electrical power to customers in the area.

Insect pests can be monitored and trapped with pheromone bait, according to Consep Membranes (Bend, Ore.). Pheromones lure insects into traps and prevent them from mating. Consep has developed a system known as BioLure, which helps pest managers locate infestations, estimate their severity, define the target pest species, and plan controls. The pheromone slowly diffuses through a membrane on the lure, which is a small disk-shaped reservoir. It contains a sticky substance that traps the insects. Lures are placed in fields or orchards or around bins or storage areas two to three weeks before the expected emergence of the pests. Consep spokesmen say that the lure can attract more than 30 species of insects, thereby reducing the need for chemical pesticides.

An acid hydrolysis reactor for converting wood lignocellulose to renewable fuels is being developed by the Solar Energy Research Institute (SERI, Golden, Colo.). Its function is to convert lignocellulose to glucose and, in turn, to ethanol fuel. Wood chips are loaded into a reactor at either end of the reactor chain. Air is purged from the reactor, and the chips are heated with steam. Water is then forced into the chips for the prehydrolysis stage at 150 °C. Next, hydrolysis with aqueous acid is carried out to decompose the lignocellulose to glucose. After hydrolysis, any waste material is dumped. SERI engineers believe that the use of a set of reactors configured in series can increase glucose yield by 20% over methods currently in use.

Laser technology can be used to detect the presence of toxic contaminants in groundwater, says Wayne Chudyk of Tufts University (Medford, Mass.). The detector uses an ultraviolet (UV) laser focused onto the tip of a fiber about 0.6 mm wide. The fiber can carry the UV laser up to 25 m inside a test well. The water does not show fluorescence, but many organic contaminants such as benzene and other aromatic compounds do. The fluorescence is shown as voltage readings by which the presence and amount of the contaminants can be evaluated. This quick and relatively inexpensive test procedure is useful for determining whether more expensive laboratory tests will be needed, according to Chudyk.

Acid hydrolysis reactor

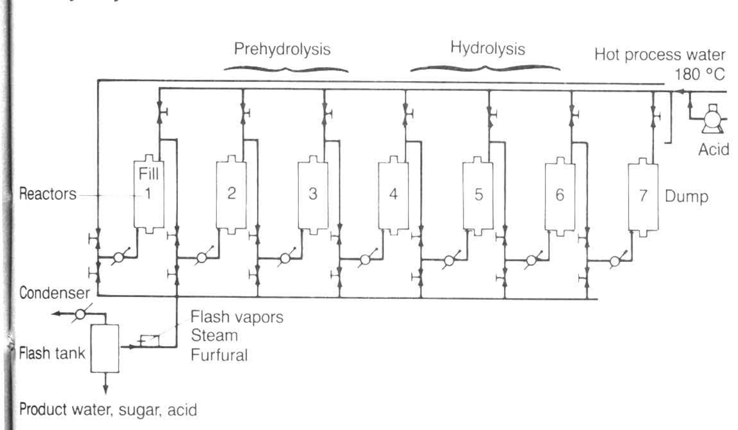

Source: SERI *In Review*, December 1985

BUSINESS

The Department of Energy has awarded a contract to Roy F. Weston (West Chester, Pa.) to provide technical support services to the department's Office of Civilian Radioactive Waste Management, which is charged with managing the nation's spent fuel and radioactive waste. The contract carries a term of two years with options to extend the contract annually for three years. The total value of the contract is in excess of $70 million. The office was created by the Nuclear Waste Policy Act of 1982. Beginning in 1998, the office will be responsible for preparing deep-mined geological repositories.

The use of mediation and negotiation to resolve environmental disputes has grown exponentially since 1973, says Gail Bingham of the Conservation Foundation (Washington, D.C.). In that year, mediators helped to settle a long-standing dispute over a proposed flood control dam in the state of Washington. By the end of 1977, nine disputes had been mediated. By mid-1984, the number of disputes settled through mediation had risen to more than 160. This record of dispute resolution will be presented in a book, *Resolving Environmental Disputes: A Decade of Experience,* to be published by the Conservation Foundation later this year.

FMC Corporation (Schaumberg, Ill.) has designed, built, and is operating a flue gas desulfurization demonstration system in Colorado Springs, Colo. The system is based on dry sorbent injection and will demonstrate the ability of the technology to reduce by 70% SO_2 emissions from a 223-MW low-sulfur coal-fired utility boiler. The flue gas is routed into two ducts, each leading to a fabric filter that removes particulate matter from half of the gas emitted. Next, the gas is treated with dry, pulverized sodium sesquicarbonate, which reacts with SO_2 to form sodium sulfite and sulfate. It is hoped that the dry injection system will be a viable alternative to more complex and costly means of SO_2 removal at low-sulfur coal-fired boilers. Future dry injection tests will use sodium bicarbonate and raw trona (sodium ore).

Late last year, Consolidation Coal (Pittsburgh, Pa.) pledged $75,000 to support a study on the effects of acid rain on spruce forests. The study is being conducted by the U.S. Department of Agriculture's Northeast Forest Experiment Station. A company spokesman says that "although considerable research has gone into the question of forest damage from acid rain, much more is needed. Since forest effects may take years to develop and detect, and perhaps years to reverse, we cannot afford to overlay this important ecological problem with political bickering and narrow-interest agendas." Consolidation Coal is publishing a series of newsletters that will digest information published in current scientific literature, according to the spokesman.

Representatives of electric utilities in the United States, France, West Germany, Japan, and Switzerland have signed an agreement to carry out joint research to develop "more efficient, reliable, and environmentally attuned" coal plants to provide world energy in the twenty-first century. About $15 million is being provided by U.S. electric utilities through the Electric Power Research Institute (Palo Alto, Calif.). Other participants and contractors in the program will furnish $10 million. The main categories of work will include boiler technology and turbine technology.

ES&T FEATURES

Hazardous waste destruction

Thermal techniques will be increasingly used as legal restrictions on land disposal take effect

E. Timothy Oppelt
Environmental Protection Agency
Cincinnati, Ohio 45268

The thermal destruction of hazardous waste involves the controlled exposure of waste to high temperatures (usually 900 °C or greater) in an oxidizing environment. Thermal destruction processes include thermal oxidation, starved-air, or pyrolytic incineration systems; high-temperature industrial processors such as boilers, cement kilns, and industrial furnaces in which hazardous waste is burned as a fuel; and various emerging high-temperature processes such as molten salt or plasma or electric furnaces.

Properly designed and operated thermal destruction systems offer the prospect of destroying the hazardous organic components of waste streams and reducing waste volume. In some instances, these systems can recover energy or materials such as hydrochloric or sulfuric acid. As a result, thermal destruction systems have become recognized over the past decade as an increasingly desirable alternative to the more traditional methods of disposing of hazardous wastes in landfills, lagoons, and injection wells.

The improper design, operation, or use of such systems, however, may pose a threat to public health through emissions of potentially hazardous components of the wastes or their combustion byproducts. The recognition of the inherent environmental advantages of the thermal destruction of waste, balanced against the potential problems of improper practice, led EPA to develop performance standards and permit requirements for thermal destruction systems under the terms of the Resource Conservation and Recovery Act of 1976 (RCRA). Incinerator standards have been in place since June 1982 (*1*) and more are currently under development for the disposal of hazardous wastes in industrial processes.

Thermal destruction is expected to gain greater acceptance as EPA responds to its congressional mandate to restrict land disposal of many hazardous wastes. It is also seen as a way of cleaning up abandoned and uncontrolled disposal sites as required by the terms of the Comprehensive Environmental Response, Compensation and Liability Act of 1980 (CERCLA, or Superfund).

Current practice

The most recent comprehensive data on the practices of thermal destruction of hazardous wastes come from surveys of industrial activity conducted by EPA in 1981 (*2*). It is estimated that the United States generated 264 million metric tons (mt) of waste that year, a large portion of which consisted of nonhazardous materials (water) contaminated with smaller amounts of hazardous materials (*2*). More than 5.5 mt was thermally destroyed, 1.7 mt was disposed of in 240 incineration facilities, and 3.8 mt was disposed of in 1300 industrial boilers and furnaces. EPA estimates that as much as 25 mt of the waste generated in 1981 could have been destroyed thermally (*3*).

Hazardous waste incineration practice is more extensively documented than is waste disposal in industrial boilers and furnaces. Incinerators have been the subject of EPA research for nearly 12 years. Regulation, notification, and permit requirements also have produced a large amount of information on incinerators. The practice of using wastes as fuel in industrial boilers and process furnaces will not be fully regulated until late 1986.

In the United States, the incineration technique most commonly used in 1981 was liquid injection (*4*). Liquid incinerators, which are most frequently used to dispose of waste at the site of generation, are employed almost exclusively to destroy pumpable liquid waste. They are usually simple refractory-lined cylinders (either horizontal or vertical) equipped with one or more waste burners. Liquid wastes are injected through the burner, atomized to fine droplets, and burned in suspension. Auxiliary fuel burners and separate waste injection nozzles can be oriented for axial, radial, or tangential firing.

Fixed-hearth incinerators, including excess-air and starved-air or pyrolytic incinerators, are the second most common technology for hazardous waste incineration. Starved-air incinerators, which were first marketed in the early 1960s, have seen rapid growth in use, particularly for the on-site disposal of solid wastes.

Hazardous waste incineration practices as of 1981

Ownership
80% private
20% commercial and military

Waste
77% of facilities handle on-site wastes only
79% of units handle liquids only
11% of units handle bulk wastes (solids and liquids)
10% of units handle special-purpose wastes, such as explosive wastes

Equipment
48% are liquid injection units
19% are fixed-hearth units
6% are rotary kiln or combination units
27% are other (weapons decommissioning or fluidized-bed combustion)
45% have air pollution control systems
22% employ heat recovery

Operations
Median: 1800 °F at 2 s residence time (gas)
Range: 1200–2300 °F; 0.1–6.5 s residence time; most operate on an intermittent schedule

Capacity
Median: liquids, 150 gal/h; solids, 650 lb/h
Range: 0.3 – 142 × 10^6 = Btu/h

Manufacturing
57 companies actively market incinerators
28 companies have sold units
Most units have been installed since 1970
32–40 units are under construction

Starved-air incinerators typically involve two-stage combustion processes by which liquid or solid waste is fed into a primary chamber operated at 50–80% of the stoichiometric air requirement. Vaporized and partially destroyed combustion products are then directed to an afterburner where excess air is added to complete the destruction, usually at a higher temperature than that in the primary chamber.

Rotary kiln incinerators are the third most common incinerator design. They are the most versatile incinerators in that they can destroy solid wastes, slurries, and containerized wastes in addition to liquids. These units are therefore most frequently incorporated into commercial off-site incineration facility designs. The waste is volatilized and partially destroyed in the rotating kiln, a cylindrical refractory-lined shell mounted on a slight incline. Combustion gases then pass through a high-temperature afterburner to complete the destruction process.

The typical air pollution control systems for hazardous waste incinerators include a combustion gas quench, a venturi scrubber (for particulate control), a packed-bed or tray tower acid gas adsorber for acid gas removal, and a mist eliminator. It is interesting to note, however, that more than half of the incinerators in 1981 used no air pollution control systems at all. Perhaps this was because these facilities handled low-ash, low-halogen-content liquid waste streams for which such control measures are not usually necessary.

Many wastes unidentified

There is little precise information on the exact kinds of waste going to thermal destruction facilities. Many facilities operate intermittently and handle mixtures of wastes that are difficult to describe in terms of EPA standard waste codes. A 1983 EPA study examined data on 413 waste streams going to 204 of the 240 incineration facilities in the United States (*5*). The major waste streams incinerated were spent, nonhalogenated solvents (EPA waste code F003) and corrosive and reactive wastes contaminated with organics (EPA waste codes D002 and D003). These materials accounted for 44% of the waste incinerated. Other important wastes included hydrocyanic acid (P063), acrylonitrile bottoms (K011), and contaminated water (D001).

Hazardous wastes also are burned as fuels in many industrial applications. In 1981 such practices disposed of more than twice the amount of waste that was incinerated without being used as fuel. Hazardous waste is burned as fuel in industrial boilers, cement kilns, ironmaking furnaces, and lightweight aggregate and asphalt plants. The principal attractions of this approach consist of cost savings in fuel, waste transportation, and disposal.

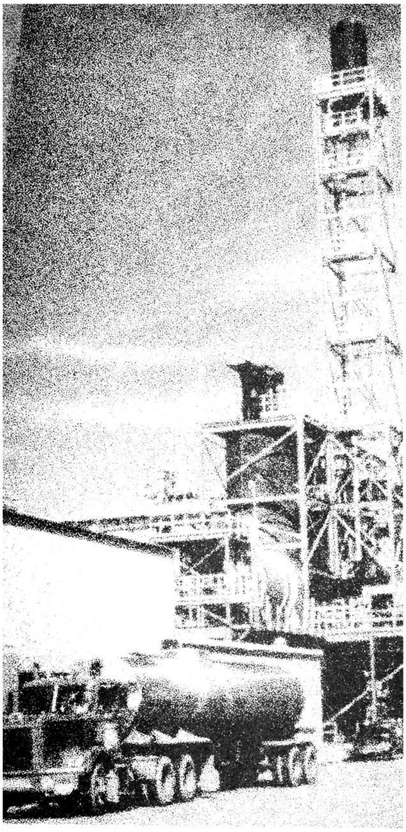

Versatile rotary kiln incinerators destroy many varieties of waste

The most recent source of information on waste fuel use in industrial processes was compiled for EPA in 1984 (*6*). The study presents results of a national questionnaire on waste fuel and waste oil use in 1983. It reveals that more than 1300 facilities used hazardous-waste-derived fuels (HWDF) that year, accounting for a total of 230 million gal.

The chemical industry (Standard Industrial Classification [SIC] 28) accounted for 67% of this fuel and waste oil use, although it operated only 12.4% of the facilities using HWDF. Other industries included SIC 26 (paper), SIC 29 (petroleum), SIC 32 (stone, clay, glass, concrete), and SIC 33 (primary metals). Sixty-nine percent of the waste was burned in large quantities by facilities that make up only 1.6% of the 1300 facilities. These included facilities with medium and large industrial boilers, cement and aggregate kilns, and iron-making furnaces.

Although data specific to the individual waste codes are not readily available, recent information shows that in 1983, 30% consisted of organic solvents and 45% was made up of other hazardous organics (*6*). Most of this waste was generated on site, and 74% of the balance arrived directly from off-site generators rather than through intermediaries.

Thermal destruction devices

Until recently, only limited data were available on the performance of thermal destruction devices in destroying waste and curbing pollutant emissions. EPA and others conducted performance tests during the 1970s that used a variety of trace organic pollutant sampling and analysis techniques. These techniques often were geared to measuring overall combustion and destruction efficiencies rather than the ability of an incinerator to comply with the rigid performance requirements mandated by RCRA today (*7*).

Since 1981, EPA has conducted a program of performance testing at thermal destruction facilities. The program was designed to provide information on the ability of processes to destroy hazardous wastes to the degree required by the 1982 incinerator performance standards (*1*). Before obtaining operating permits, operators must demonstrate that the facilities can meet the following requirements:

- at least 99.99% destruction and removal efficiency (DRE) for each principal organic hazardous constituent (POHC) in the waste feed;
- at least 99% removal of hydrogen chloride from the exhaust gas if hydrogen chloride stack emissions are greater than 4 lb/h; and
- particulate emissions not exceeding 0.08 grains/dry standard cubic foot (dscf), corrected to 7% oxygen in the stack gas.

EPA's performance evaluation program encompassed the testing of many commercial and industrial thermal destruction devices and designs, sizes of facilities, and varieties of wastes. Testing procedures used standard EPA sampling and analysis methods, including the volatile organic sampling train (VOST), a sampling technique specially developed for detecting low concentrations of volatile POHCs in emissions (*8, 9*).

Test protocols included waste and base fuel analysis for hazardous constituents; stack gas sampling and analysis for hazardous constituents, particulate matter, hydrogen chloride, metals, and criteria pollutants (NO_x, SO_2); ash and scrubber water analysis; and appropriate process monitoring and control data (CO, CO_2, O_2, temperature at critical points, flows, and pressures).

The evaluations usually were conducted under operating conditions normally used at the facility; the objective was to determine whether typical performance met incineration emission standards. Normally, operating conditions were not intentionally varied to assess changes in performance. In many tests, however, various compounds, such as carbon tetrachloride, trichloroethylene, and chlorobenzene, were added to the waste feed to facilitate comparison of performance results among facilities. In cases of industrial processes using a hazardous waste as supplemental fuel, baseline tests also were conducted to determine background levels of emissions with only the conventional fuel.

Tables 1–3 describe the facilities and wastes studied by the test program and summarize destruction and emission control performance data (*10–13*). These test results are significant because they reveal that a well-operated incinerator, industrial boiler, or process kiln can achieve a DRE of 99.99%. All of the incinerators tested achieved this level of performance for candidate POHC compounds in concentrations >1000 ppm in the waste feed. Candidate POHC compounds at concentrations <500 ppm frequently were not destroyed to the extent of 99.99%.

This phenomenon, which also was observed in tests of other thermal destruction devices, was unexpected. A number of possible explanations have been advanced. At the low stack emission concentrations necessary to demonstrate 99.99% DRE for <500 ppm POHCs, sampling and analysis techniques may be limiting factors. Also at these low emission levels, sufficient amounts of POHC candidate compounds may actually be formed as incomplete combustion or recombination byproducts of other materials in the wastes to cause the DRE to fall below 99.99%.

EPA is conducting research to assess this concentration phenomenon. From a regulatory standpoint, however, it is not currently perceived as a problem, because few if any of the low-concentration compounds in the wastes identified in the EPA test program actually would have been selected as POHCs in trial burns had existing EPA guidelines on POHC selection been employed.

The waste at each site typically contained many hazardous compounds that were candidates for being selected as POHCs. All of the compounds that could be measured were measured, and DRE values were calculated. Under current EPA permit guidelines, however, only two or three compounds, usually the highest in concentration, were selected as POHCs to measure DRE attainment.

Industrial boilers, particularly the larger water tube units, were acceptable devices for waste destruction. Cement kilns, lime kilns, and lightweight aggregate kilns with adequate combustion

TABLE 1
Incineration facilities tested

Facility	Control device	Waste	DRE[a] (number of nines)[b]	HCl control (average)	Average particulate emissions (g/dscf)
Commercial rotary kiln–liquid incinerator (87 million Btu/h)	Packed-tower adsorber; ionizing wet scrubber	Drummed, aqueous, liquid organic waste with carbon tetrachloride, TCE[c], perchloroethylene, toluene, phenol	5.3	99.4%	0.67
Commercial fixed-hearth, two-stage incinerator (25 million Btu/h)	Electrified gravel bed filter; packed-tower adsorber	Liquid organic and aqueous waste with chloroform, carbon tetrachloride, TCE, toluene, perchloroethylene	4.4	98.3%	0.178
On-site two-stage liquid incinerator (6 million Btu/h)	Packed-tower adsorber	Liquid organic waste with carbon tetrachloride, dichlorobenzene, TCE, chlorobenzene, chloromethane, aniline, phosgene	4.4	99.7%	0.027
Commercial fixed-hearth two-stage incinerator (2 million Btu/h)	None	Liquid organic waste with TCE, carbon tetrachloride, toluene, chlorobenzene	4.7	>4 lb/h[d]	0.089
On-site liquid injection incinerator (4.8 million Btu/h)	None	Liquid organic waste with aniline, diphenylamine, mono- and dinitrobenzene	6.7	>4 lb/h[d]	0.092
Commercial fixed-hearth two-stage incinerator (10 million Btu/h)	None	Aqueous and organic liquid waste with carbon tetrachloride, TCE, benzene, phenol, perchloroethylene, toluene, methylethyl ketone	4.8	>4 lb/h[d]	0.40
On-site rotary kiln with liquid injection (35 million Btu/h)	Venturi scrubber with cyclone separators and packed-tower adsorbers	Liquid organic, paint waste and filter cakes with methylene chloride, chloroform, benzyl chloride, hexachloroethane, toluene, TCE, carbon tetrachloride	5.3	99.9%	0.01
Commercial fixed-hearth two-stage incinerator (75 million Btu/h)	Venturi scrubber	Aqueous and organic liquids and solid waste with methylene chloride, chloroform, carbon tetrachloride, hexachlorocyclopentadiene, toluene, benzene, TCE	4.6	98.3%	0.075

[a]Destruction and removal efficiency (mass weighted average for all POHCs >100 ppm in waste feed). [b]For example, 99.995% DRE = 4.5 nines. [c]TCE = trichloroethylene. [d]No HCl control device; waste is low in total organic chlorine content.

TABLE 2
Industrial boiler facilities tested

Facility	Control device	Waste	DRE[a] (number of nines)[b]
Watertube stoker, wood-fired (10 million Btu/h)	Multiclone	Creosote sludge with phenol, pentachlorophenol, and naphthalene	3.8
Packaged firetube, gas-fired (8.5 million Btu/h)	None	Alkyd wastewater with toluene	4.1
Field-erected watertube, gas- or oil-fired (230 million Btu/h)	None	Phenol waste	5.6
Converted stoker, oil-fired (90 million Btu/h)	None	Methanol, toluene, and chlorinated organics including perchloroethylene	4.8
Packaged watertube, oil-fired (110 million Btu/h)	None	Methyl methacrylate byproducts with carbon tetrachloride, chlorobenzene, and TCE[c]	4.5
Converted watertube, oil-fired (60 million Btu/h)	None	Paint solvents with carbon tetrachloride, TCE, toluene, and chlorobenzene	3.8
Modified firetube, waste-fired (40 million Btu/h)	Two scrubbers in series	Highly chlorinated organics including carbon tetrachloride	4.8
Tangentially fired watertube, coal-fired (250 million Btu/h)	Electrostatic precipitator	Methyl acetate, carbon tetrachloride, trichloroethane, chlorobenzene	4.1
Packaged watertube, gas-fired (62 million Btu/h)	None	Aniline waste with nitrobenzene, carbon tetrachloride, TCE, benzene, toluene	4.8
Packaged watertube, waste-fired (10 million Btu/h)	None	Toluene, chlorinated organics including carbon tetrachloride and TCE	5.0
Packaged watertube, oil-fired (60 million Btu/h)	None	Blended waste with light oil and carbon tetrachloride, benzene, TCE, and toluene	5.7

[a]Destruction and removal efficiency (mass weighted average for all POHCs >100 ppm in waste feed). [b]For example, 99.995% DRE = 4.5 nines. [c]TCE = trichloroethylene.

TABLE 3

Industrial kiln facilities tested

Facility	Control device	Waste	DRE[a] (number of nines)[b]
Wet process cement kiln; nonatomized waste; 140 million Btu/h, oil-fired	Fabric filter	Waste liquids including methylene chloride, chloroform, carbon tetrachloride	2.8
Wet process cement kiln; atomized waste; 170 million Btu/h, coal-fired	Electrostatic precipitator	Waste liquids including methylene chloride, MEK[c], trichloroethane, toluene, Freon 113	4.2
Dry process cement kiln; nonatomized waste; 228 million Btu/h, coal- or coke-fired	Electrostatic precipitator	Waste liquids including methylene chloride, Freon 113, MEK, toluene, trichloroethane	4.1
Dry process cement kiln; atomized waste; 300 million Btu/h, coal- or coke-fired	Fabric filter	Waste liquids including trichloroethane, trimethylbenzene, xylene, methylene chloride	>4
Lime kiln; atomized waste; 50 million Btu/h, coke- or gas-fired	Fabric filter	Waste liquids including methylene chloride, MEK, TCE[d]	4.7
Shale aggregate kiln; atomized waste; 35 million Btu/h, coal-fired	Scrubber	Waste liquids including perchloroethylene, MEK	>5
Clay aggregate kiln, 20 million Btu/h, coal-fired	Scrubbers	Waste liquids including MEK, perchloroethylene, toluene	4.8
Clay products kiln; atomized waste; 37.5 million Btu/h, oil-fired	Fabric filter	Waste liquids, waste oil, Freon 113, perchloroethylene, carbon tetrachloride, benzene, TCE, toluene	3.5

[a]Destruction and removal efficiency (mass weighted average for all POHCs >100 ppm in waste feed). [b]For example, 99.995% DRE = 4.5 nines. [c]MEK = methylethylketone. [d]TCE = trichloroethylene.

control and waste atomization all met or exceeded the 99.99% DRE requirement. It is also important to note that for all of the incinerators and industrial processes tested, the DREs observed have been attributable to actual destruction rather than to removal or capture of hazardous organic compounds. Ash, scrubber water, and air pollution control device residues were typically below detection limits for POHCs and organics in general.

All incinerators and industrial process kilns tested met or approached the RCRA removal standard for hydrogen chloride. Industrial boilers typically have no existing controls for hydrogen chloride, but none exceeded the 4 lb/h emission standard, because wastes with low net chlorine content were burned. In some cases the kilns failed by very small margins to meet the standard for hydrogen chloride. Minor changes in their operation, however, could readily overcome that problem.

Achieving the particulate emission standard was a problem with a number of the incinerators tested (*10–13*). Four of the eight units failed to meet the RCRA standard. Two of those facilities were marginally above the emission limit and probably could have met the standard with minor operating adjustments. The remaining two facilities appeared to need significant design and operating changes. This general trend is consistent with the results of RCRA permit trial burns conducted for other incineration facilities over the past two years.

No significant changes in particulate emissions were observed for industrial boilers and some of the industrial process kilns at which waste fuels were burned. Some increased emissions were observed in kilns employing electrostatic precipitators for particulate control. These increases were attributed to changes in the electrical resistivity of the particles caused by the presence of increased chloride levels. Adjustments in precipitator operation should correct this shortcoming in most cases.

Analysis of the pooled data from the incinerator test program revealed that there was no absolute level of mean combustion temperature, mean gas-phase residence time, or carbon monoxide emission concentration that could be correlated with the achievement of 99.99% DRE. Residence times ranged from 0.1 s to 6.5 s in the facilities tested. Temperatures ranged from 648 °C to 1450 °C. Carbon monoxide levels were as high as 600 ppm, but at most plants they ranged from 5 ppm to 15 ppm.

The relationships between DRE and these characteristics are, in all likelihood, specific to the facility in question. Waste characteristics, waste atomization, and mixing in the combustion chamber are equally important to achieving high DRE. Timing, funding, and facility constraints did not allow the collection of enough performance data under varying conditions at each site tested to quantify these relationships. EPA continues to obtain test results and information from trial burns and from tests at EPA pilot scale research facilities. This information is added to the data base in an effort to improve the predictability of DRE of incineration processes.

It is not yet possible to specify absolute levels of process operating parameters that will guarantee in advance that an incinerator will meet the 99.99% DRE standard for a particular waste. Therefore, efforts are being made to identify easily monitored process emissions which may be real-time indicators of the onset of a process's failure to achieve acceptable DRE. In other words, continuous monitoring for specific absolute levels of emissions of carbon monoxide, oxygen, and total halogenated organic carbon cannot guarantee that a 99.99% DRE is being attained.

The objective of EPA's research is to identify and quantify engineering relationships between potential incinerator process failures, such as inadequate waste atomization and overfeeding, and process performance indicator emissions, such as carbon monoxide, total unburned hydrocarbon, oxygen, and emissions of potentially difficult-to-incinerate tracer compounds (sulfur hexafluoride, various freons) that could be "spiked" into the incinerator feed. Such relationships could be quantified during trial burns at each facility and could be used for process control by operators and for compliance assessment by regulators.

This research is being conducted in bench scale and pilot scale thermal destruction research facilities in Cincinnati, Ohio; Research Triangle Park, N.C.; and at EPA's Combustion Research Facility near Pine Bluff, Ark. Additional full-scale facility testing is being conducted to assess non-steady-state or upset combustion conditions on DRE and indicator emissions (rapid, usually short-lived departures from normal operation, such as temperature increases or decreases and increases in carbon monoxide emissions).

Incinerability

EPA researchers have also examined the test data to try to define DRE values for POHCs as a function of the various approaches that have been suggested for determining a POHC's incinerability or its difficulty in being thermally destroyed (*14*). EPA guidelines for conducting a trial burn suggest that a compound's incinerability and concentration in the waste are important criteria for selecting it as a POHC (*15*).

The various methods that have been considered for the incinerability ranking of hazardous wastes have been a matter of some scientific debate over the past several years. EPA has recommended using a compound's heat of combustion as a criterion. Other suggestions include the use of bond energies derived from theoretical kinetics, autoignition temperatures, and laboratory data on thermal decomposition to approximate compound incinerability. Analysis of pooled field test data indicated that no strong correlation could be found for DRE as opposed to any of the ranking methods. Research data, however, suggest the use of an incinerability ranking based on gas-phase thermal stability data collected in laboratory experiments under oxygen-deficient conditions (*14*).

Comparison of these stability data with appropriate field test data indicates that field thermal stability rankings could be predicted from the laboratory data in 70% of the cases evaluated. Additional research is being conducted to expand the number of compounds for which comparisons can be made.

Incomplete combustion products

The current RCRA standards regulate destruction and removal only for the major hazardous compounds in the waste. Under poor combustion conditions, many compounds may decompose only partially to form products of incomplete combustion (PICs), which are also hazardous compounds of concern if they are emitted. For the purposes of the EPA test program, compounds are considered PICs if they are regulated organic compounds (listed in the *Code of Federal Regulations,* Title 40, Part 261, Appendix VIII, revised July 1, 1985) detected in stack emissions but not present in the waste feed at concentrations >100 ppm. The PICs most frequently identified in the EPA testing of incinerators and industrial boilers have been benzene, chloroform, and tetrachloroethylene (*11, 16*). As of June 1985, detailed PIC analyses had been completed for three cement kiln tests. The most common PICs identified during the kiln tests were benzene, benzaldehyde, toluene, and various naphthalenes (*12*).

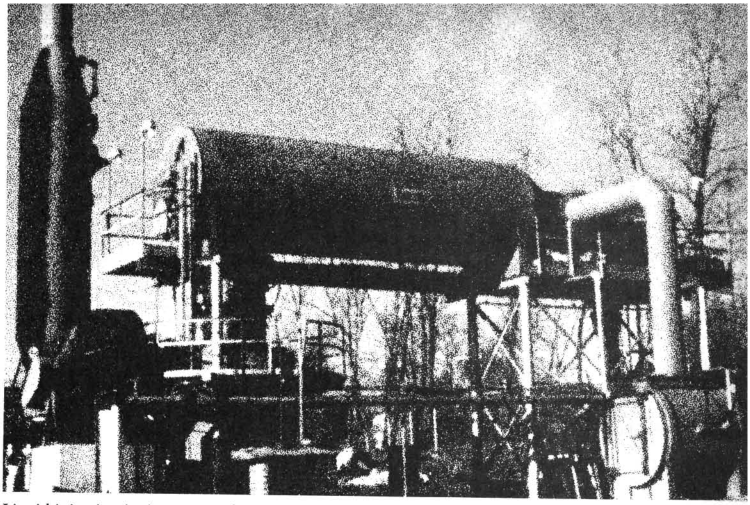

Liquid injection incinerators often are used to dispose of liquid wastes

EPA is conducting research to assess the nature and magnitude of PIC emissions from the thermal destruction of hazardous waste. Current data suggest that for thermal destruction facilities where high degrees of DRE have been achieved for POHCs, PIC emissions are also low and not of environmental concern. Consequently, EPA does not plan to regulate PICs under RCRA. EPA is conducting research, however, to determine whether there are problems with PICs in untested waste–facility combinations not included in the test program or under marginal thermal destruction conditions (for example, the failure to meet DRE standards). Knowledge of the mechanisms of PIC formation and of PIC abatement through the control of combustion conditions is therefore important to EPA.

Thermal destruction prospects

Prospects for the increased use of thermal destruction of hazardous wastes are good. Incineration is a proven, commercially available technology that has been demonstrated to be suitable for handling a wide variety of wastes. Industrial high-temperature processes also can be modified to destroy certain hazardous wastes (particularly combustible liquids) and allow for the recovery of energy.

Thermal destruction is currently used to dispose of only 2% of the 264 mt of hazardous wastes generated annually. Many of the remaining wastes are still directly disposed of on land. However, the recently promulgated Hazardous and Solid Waste Amendments of 1984 (the RCRA amendments), with their sweeping provisions to restrict the land disposal of many wastes, will prompt increased consideration of thermal destruction as an option. Many waste generators already are placing emphasis on this option in the interest of resolving long-term liability issues through destruction rather than through uncertain land-based containment techniques.

It also is virtually certain that increased Superfund cleanup activities will generate wastes and on-site treatment residues that will be managed by thermal destruction. Most of these wastes will be more appropriate for destruction in large commercial incinerators or in multipurpose mobile incinerators, which are now under development for use on site.

For the near future, perhaps the next five years, there appears to be sufficient thermal destruction capacity. An EPA study completed in 1984 estimated that on-site and commercial incineration capacity use is somewhere between 37% and 74% (*17*). Another assessment estimated incinerator capacity use at 47% for 1981.

There also are more than 43,000 industrial boilers in the United States, of sizes and designs that could achieve acceptable waste destruction (*18*). Of this number, 5500 boilers are located in the chemical, petroleum refining, and paper industries. About 70% of the total hazardous waste generated and more than 95% of all potentially combustible hazardous waste could be disposed of in these boilers. Although only 10 industrial process kilns currently are being used to dispose of hazardous waste, the operators of as many as 600 kilns across the United States might consider this option (*18*).

Restriction on land disposal

EPA has estimated the amount of hazardous waste that might be redirected to commercial incineration as a result of restrictions on disposal in landfills, lagoons, and injection wells (*17*). These restrictions are expected to result in an excess of demand over existing capacity of commercial incineration facilities of 215–306% for liquid wastes alone. Translated into facility capacity, this percentage converts to as many as 26 land-based incinerators (disposing of 20,000 t each), or 10 incinerator ships (50,000 t each). Solid hazardous waste and Superfund cleanup residues would further increase the shortfall.

Although many boiler and kiln facilities could dispose of waste, much that will become available for feeding into these facilities is likely to be increasingly less attractive to their operators. This waste will tend to be much less combustible because it is higher in solid, ash, and water content and therefore more suitable for conventional commercial incineration.

Permitting and siting difficulties are significant impediments to the development of commercial incinerator capacity and to the use of industrial kilns for waste disposal. Consequently, little growth of available commercial incineration capacity may be expected over the short term. A three- to five-year delay is possible before significant new capacity could be available.

Many believe that the use of self-contained mobile incinerators or larger but transportable units is one way of mitigating the public opposition that frequently plagues the construction of permanent centralized incineration facilities. Although a number of mobile systems have been proposed, most are still in development. Little actual field testing has been done beyond that under way on an EPA-owned mobile rotary kiln incinerator (*19*). This unit has been tested for the efficiency of polychlorinated biphenyl and carbon tetrachloride destruction. It is currently being tested for its ability to incinerate dioxin-contaminated soils in Missouri.

More wastes burned

Thermal destruction is an effective and broadly applicable technique for the destruction of organic hazardous wastes. Performance tests conducted by EPA indicate that incinerators and many high-temperature industrial processes are capable of achieving RCRA performance and emissions standards. Although only a small percentage of the hazardous waste managed annually in the United States is currently destroyed thermally, significant increases in the use of these processes is anticipated because of the 1984 RCRA amendments and increased Superfund remedial actions. Permit and siting difficulties may, however, delay the installation of new incinerator capacity, particularly for commercial facilities.

Test burns of hazardous waste

To determine how well incineration works, EPA has been conducting a series of test burns at its combustion research facility near Pine Bluff, Ark. One objective is to learn how well incineration destroys hazardous waste, especially dioxin-contaminated liquids and leachate sludges. Another is to test the effectiveness of emissions sampling equipment and techniques.

The first test burn, completed last autumn, involved the incineration of 300 gal of wastes from the production of 2,4,5-trichlorophenol and the herbicide 2,4,5-T. These wastes, which were highly contaminated with dioxins, were obtained from a Superfund site near Jacksonville, Ark. Results of preliminary analyses indicate that no dioxins were present in the stack emissions.

EPA plans to conduct similar test burns for residues from a number of Superfund sites in the United States. These tests are expected to begin in April 1986 and will involve

• PCB-contaminated sludges and soils from the Bridgeport Rental and Oil Services site in Bridgeport, N.J.,

• contaminated soils from the Stringfellow Landfill in Riverside County, Calif., and

• dioxin-contaminated soils, stream sediments, sludges, and activated carbon from Love Canal in Niagara Falls, N.Y.

Acknowledgment

This document has been reviewed in accordance with EPA policy and approved for publication. Mention of commercial products does not constitute endorsement or recommendation for use.

Before publication, this article was reviewed for suitability as an *ES&T* feature by Selim M. Senkan, Illinois Institute of Technology, Chicago, Ill. 60616; and Barry Dellinger, University of Dayton Research Institute, Dayton, Ohio 45469.

References

(1) *Fed. Regist.* **1982,** *47,* 27516–35.
(2) "National Survey of Hazardous Waste Generators and Treatment, Storage and Disposal Facilities Regulated under RCRA in 1981," U.S. Government Printing Office Order No. 055000-00239-8; EPA: Washington, D.C., 1984.
(3) "Draft Regulatory Analysis for Proposed RCRA Regulations on Burning of Hazardous Wastes"; EPA: Washington, D.C., 1984.
(4) "A Profile of Existing Hazardous Waste Incineration Facilities and Manufacturers in the United States," PB-84-157072; EPA: Washington, D.C., 1984.
(5) Vogel, G. et al. "Composition of Hazardous Waste Streams Currently Incinerated," Mitre Corporation Report; EPA: Washington, D.C., 1983.
(7) Background Document, RCRA Section 264.34, Final Standards for Hazardous Waste Incineration; EPA: Washington, D.C., 1981.
(8) "Test Methods for Evaluating Hazardous Waste," Report SW-846; EPA: Washington, D.C., 1980.
(9) "Sampling and Analysis Methods for Hazardous Waste Combustion," EPA-600/8-84-002, PB-84-155-545; EPA: Washington, D.C., 1984.
(10) "Performance Evaluation of Full-Scale Hazardous Waste Incineration," PB-85-1295000; EPA: Washington, D.C., 1984; Vols. 1-5.
(11) "Engineering Assessment Report—Hazardous Waste Co-firing in Industrial Boilers," PB-85-197838/A05, PB197838/A08; EPA: Washington, D.C., 1984; Vols. 1, 2.
(12) Mournighan, R. E. et al. In *Proceedings of the International Conference on New Frontiers for Hazardous Waste Management,* EPA-600/9-85/025; EPA: Washington, D.C., 1985; pp. 533–49.
(13) "Evaluation of Hazardous Waste Incineration in Aggregate Kilns," Florida Solite Corporation Report, PB-85-189/066 AS; EPA: Washington, D.C., 1985.
(14) Dellinger, B. et al. In *Proceedings of the Eleventh Annual Research Symposium: Incineration and Treatment of Hazardous Waste,* EPA-600/9-85-028; EPA: Cincinnati, Ohio, 1985; pp. 160–70.
(15) "Guidance Manual for Hazardous Waste Incinerator Permits," Report SW-966; EPA: Washington, D.C., 1983.
(16) Trenholm, A. et al. In *Proceedings of the Tenth Annual Research Symposium: Incineration and Treatment of Hazardous Waste,* EPA-600/9-84-022; EPA: Cincinnati, Ohio, 1984; pp. 84–95.
(17) "Assessment of Incineration as a Treatment Method for Liquid Organic Hazardous Wastes—Background Report III: Assessment of the Commercial Hazardous Waste Incineration Market," U.S. Government Printing Office Order No. 1985-526-778/30376; EPA: Washington, D.C., 1985.
(18) Olexsey, R. A. In *Proceedings of the Tenth Annual Research Symposium: Incineration and Treatment of Hazardous Waste,* EPA-600/9-84-022; EPA: Cincinnati, Ohio, 1984; pp. 162–77.
(19) Yezzi, J. et al. In *Proceedings of the 1984 Waste Processing Conference;* American Society of Mechanical Engineers: New York, N.Y., 1984; pp. 514–34.

***E. Timothy Oppelt** is chief of the Thermal Destruction Branch, Alternative Technologies Division, Hazardous Waste Engineering Research Laboratory at EPA. He directs a national research program in the treatment and destruction of hazardous waste. Oppelt received a B.S. in civil engineering and an M.S. in sanitary engineering from Cornell University and an M.B.A. from Xavier University. He is a member of the American Institute of Chemical Engineers and of the Air Pollution Control Association.*

Supercritical fluid processing

Separations and reactions are applications that point to a bright future for this environmental control technology

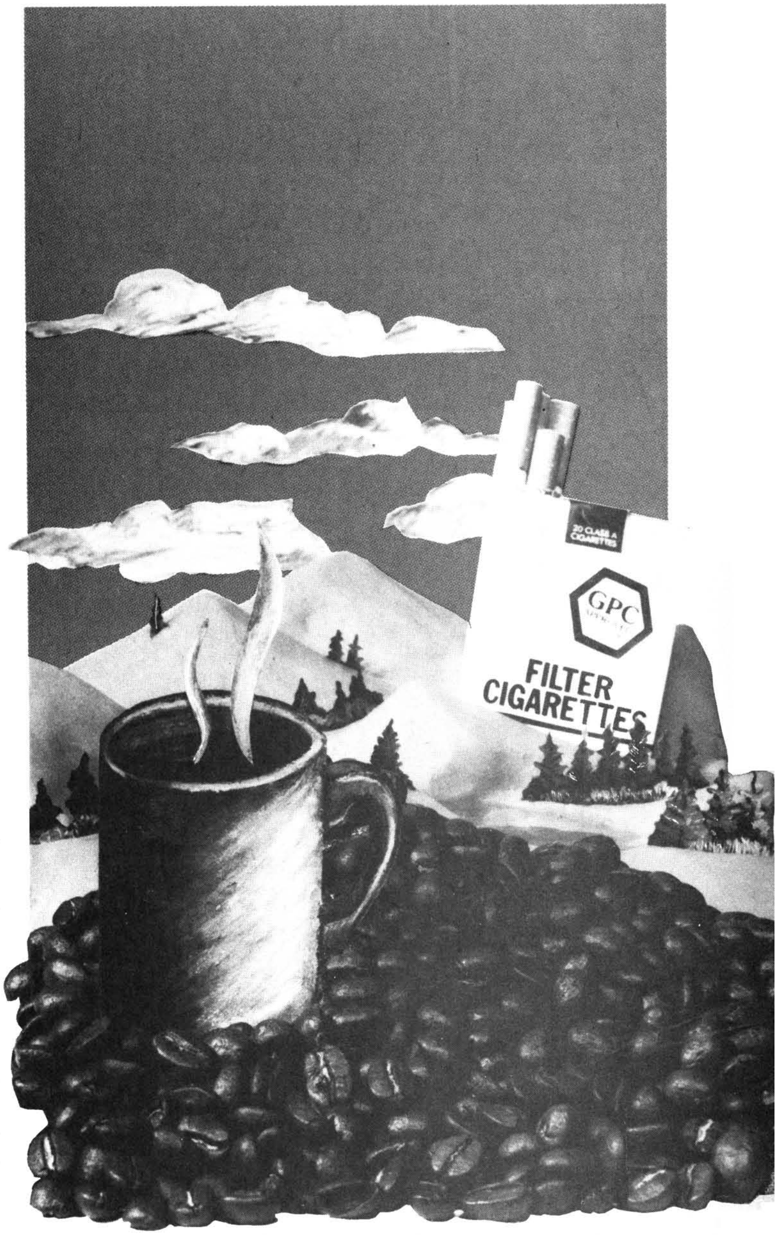

Charles A. Eckert
John G. Van Alsten
Thomas Stoicos
University of Illinois
Urbana, Ill. 61801

Separations and detoxification reactions often can be run advantageously using supercritical fluids (SCFs) as processing media. The use of a supercritical solvent frequently permits extraction of very dilute toxic species, either directly or in a two-step process. SCF solvents not only increase reactivity but offer the potential for simultaneous separation and detoxification.

Supercritical fluids offer excellent potential as process solvents in chemical and environmental engineering applications. An SCF is a substance that has been heated above and compressed beyond its critical temperature and critical pressure. As such, it exists as a single fluid phase, with some characteristics of gases and liquids, as well as some particular properties of its own. Figure 1 shows that it is possible to move directly from a liquid to a gas without phase separation simply by taking a path through the SCF region of the phase diagram.

By operating in the supercritical region, it is possible to take advantage of a variety of interesting and useful properties. In the vicinity of the critical point, density is an extremely strong function of pressure; in fact, at the critical point compressibility becomes infinite. Densities also become quite high at relatively moderate pressures—at only 200 bar and 35 °C the density of CO_2 is close to 0.8 g/cc.

The special properties of fluids near a critical point make them ideal media for mass transfer. Primarily, very high density means that there is a corre-

0013-936X/86/0920-0319$01.50/0

FIGURE 1
Pressure–temperature diagram of a pure material[a]

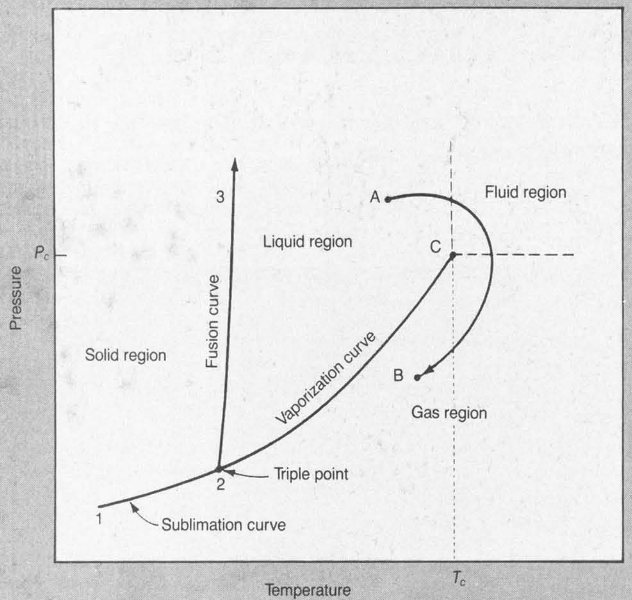

[a]Line A–B is the path for changing a liquid to a vapor without two separate phases being present
P_c = critical pressure; T_c = critical temperature

FIGURE 2
Desorption of trichlorophenol[a]

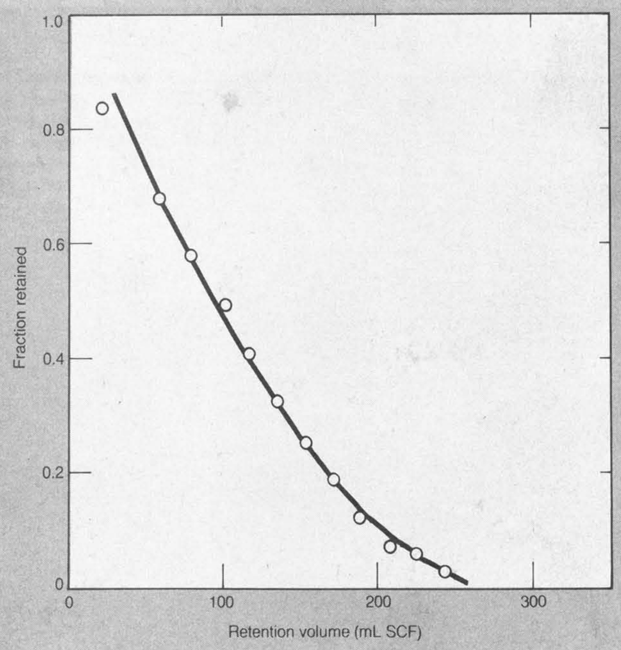

[a]From diatomaceous soil by supercritical ethylene at 50 °C

spondingly high capacity for solutes. In fact, the solubility varies exponentially with the solvent density. The high compressibility means that within this critical region, these properties undergo large changes with relatively small changes in operating conditions. For example, the solubility of the solute phenanthrene in supercritical ethylene undergoes a 10^3 change in solubility with only a 150-bar change in operating pressure. This makes solubility programming possible; a desired solute solubility is set by proper selection of system temperature and pressure.

Furthermore, the transport properties of SCFs are most favorable. Molecular diffusivity of SCFs is substantially higher—by one to two orders of magnitude—than that for normal liquids. Moreover, the viscosity is almost as low as that for gases, facilitating both pumping and natural convection.

Many common substances have critical temperatures near ambient, making them especially attractive as process fluids. These include carbon dioxide (30 °C), ethylene (10 °C), ethane (32 °C), fluoroform, (45 °C), and sulfur hexafluoride (46 °C). At higher temperatures, one might consider aliphatic or aromatic hydrocarbons, or polar and protic compounds such as alcohols, ammonia, or even water.

Carbon dioxide has been especially attractive for use in the food, pharmaceutical, and pollution control industries because it is relatively hazardless and nontoxic. Other solvents, however, especially tailored mixtures, frequently have superior properties.

A significant cost factor for many separation processes is the recovery of the extracting solvent. This is usually an energy-intensive step. In this case, however, the solvent is in the supercritical state and therefore can be recovered by reducing the pressure and changing the temperature. From the process engineering point of view, it is desirable to design a temperature-controlled separation with only minimum pressure drop requirements.

Application of SCF technology

Many of the early investigations of SCFs as solvents were reported in the patent literature and have resulted in a number of applications that are either already in commercial use or are under intensive investigation (*1*, *2*). In Kerr McGee's ROSE (residuum oil supercritical extraction) process, supercritical pentane is used to remove valuable petroleum components from still bottoms. Decaffeination of coffee is accomplished by soaking the beans in water and then immersing them in supercritical CO_2; the water is essential for mass transfer of the caffeine from

DEPEND ON IT! ES&T

All forward thinking environmental scientists depend on ES&T. They get the most authoritative technical and scientific information on environmental issues—and so can you! Have *your own* subscription delivered directly to you each month!

☐ **YES!** Enter my own subscription to *ENVIRONMENTAL SCIENCE & TECHNOLOGY* at the rate I've checked below:

Published Monthly One Year Rate	U.S.	Canada & Mexico	Europe	All Other Countries
ACS Members*	☐ $ 28	☐ $ 36	☐ $ 44	☐ $ 51
Nonmembers—Personal*	☐ $ 42	☐ $ 50	☐ $ 58	☐ $ 65
Nonmembers—Institutional	☐ $164	☐ $172	☐ $180	☐ $187

☐ Payment Enclosed (Payable to American Chemical Society)
☐ Bill Me ☐ Bill Company Charge my ☐ MasterCard ☐ VISA
☐ Diners Club/Carte Blanche

Card No. ____________________

Expires __________ Interbank No. __________ (MasterCard only)

Signature ____________________

Name ____________________

Title __________ Employer __________

Address ☐ Home ☐ Business ____________________

City, State, Zip ____________________

Employer's Business: ☐ Manufacturing, type __________

☐ Academic ☐ Government ☐ Other __________

***Subscriptions at these rates rates are for personal use only.**
Subscriptions outside the US, Canada, & Mexico are delivered via air service. Foreign payment must be made in US currency by international money order, UNESCO coupons, US bank draft, or order through your subscription agency. For nonmember rates in Japan, contact Maruzen Co., Ltd.
Please allow 45 days for your first copy to be mailed. Redeem until December 31, 1986. **1986**

MAIL THIS POSTAGE-PAID CARD TODAY!

3491X

CALL TOLL FREE
(800) 424-6747 (U.S. only)

NO POSTAGE
NECESSARY
IF MAILED
IN THE
UNITED STATES

BUSINESS REPLY MAIL
FIRST CLASS PERMIT NO. 10094 WASHINGTON, D.C.

POSTAGE WILL BE PAID BY ADDRESSEE

American Chemical Society
Marketing Communications Department
1155 Sixteenth Street, N.W.
Washington, D.C. 20036-9976

within the bean. Among the processes still in the experimental stage are the removal of active ingredients from hops and spices and the removal of nicotine from tobacco. This latter process holds considerable advantages over conventional liquid extraction because the supercritical solvent leaves the essential aromas in the leaves and maintains them in a physically unaltered state.

An area of particular interest to analytical chemists is that of supercritical chromatography. By using an SCF as the mobile phase, capacity ratios (retention times) may be reduced by more than 1000 times, compared with those that result from standard gas chromatography (*3*). As with high-performance liquid chromatography, SCF chromatographs can be programmed by pressure rather than temperature to speed elution times. This in turn reduces the possibility of destroying thermally labile compounds.

Of most interest, however, are the rapidly developing possibilities for using this new technology in various aspects of environmental control. Basically, there are three categories of processes for such applications of SCF technology:

- *One-step separation.* The SCF is put into direct contact with another phase and is used to remove a contaminant. Ultimate purification and recovery of the material removed may or may not be economical.
- *Two-step separation.* The contaminated phase is put into contact with a second intermediate phase, not the SCF, such as an adsorbent. The contaminant is first transferred to the intermediate phase, most often at ambient pressure, and removed by an SCF in a separate, second step at an elevated pressure. Again the subsequent processing of the contaminant is immaterial.
- *Reactive separation.* The SCF is put into direct contact with the contaminated material. It simultaneously dissolves the material and serves as a reaction medium for a specific chemical change, such as a detoxification reaction.

The one-step separation is most applicable when the concentration of the material to be removed is relatively high. For example, a number of processes for recovering alcohols from aqueous solutions with supercritical CO_2 have been proposed (*4, 5*). Certainly, one can envision comparable extraction of many other organics, such as higher alcohols, aromatics, esters, ketones, and aldehydes, from water or other solvents by similar means. Such an SCF extraction would be especially advantageous for the removal and subsequent separation of a series of multiple, hard-to-separate species. Ringhard and Kopfler have reported good results for extracting fairly dilute contaminants from water in a one-step process (*6*).

Botanical Resources has patented a process that uses supercritical CO_2 to remove pyrethrin—a naturally occurring insecticide—from pyrethrum flowers (*7*). Pyrethrin is highly toxic to insects but almost totally nontoxic to warm-blooded animals. An additional advantage is that it decomposes with time and does not accumulate in the environment. As a consequence, the insects do not develop a resistance to the substance. The capital and operating costs of this SFC extraction process are about one-half those of the conventional multistep organic solvent method.

Another example of the single-step separation is the decontamination of solids by extraction with an SCF. Knopf and co-workers have removed DDT from soil samples using supercritical CO_2 (*8*). At the University of Illinois we have studied the removal from soil of chlorinated aromatics, such as trichlorophenol, as model compounds for polychlorinated biphenyls (PCBs) and dioxins. Figure 2 shows the results of a semibatch flow experiment in which supercritical ethylene is used to remove virtually all trichlorophenol from a soil sample.

In the vast majority of separation studies using either the one-step or two-step process, pure CO_2 was used as the only SCF. But other solvents, especially tailored solvent mixtures, almost always offer significant technical and economic advantages. The soil decontamination study mentioned above is just one of many examples that demonstrate this point.

The two-step process offers significant advantages in the concentration of very dilute contaminants. By the use of a properly chosen intermediate phase, contaminants in part-per-million or even part-per-billion concentrations in a gas or liquid stream can be greatly concentrated in the additional step either for recovery or detoxification.

Perhaps the most interesting application proposed for the two-step process is in the augmentation of current methods of wastewater treatment that use either activated carbon or synthetic resinous adsorbents for the purification of industrial waste streams. In these systems, the solvent is used to regenerate beds of adsorbent that have become saturated with contaminant, allowing the adsorbent to be recycled.

Current methods, such as steam stripping and thermal regeneration, are energy intensive and therefore expensive to use. Researchers at Arthur D.

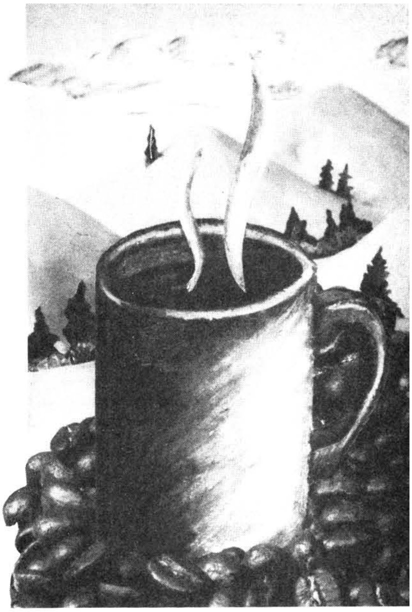

Little (ADL) have made several studies comparing supercritical and conventional methods and have found that SCF stripping can indeed be economically attractive (*9, 10*). A typical flow sheet for one such process is shown in Figure 3. In one study, the compounds atrazine and dinitrobutylphenol (contaminants in the waste stream of a pesticide plant) were successfully removed from activated carbon at an estimated cost of 14 to 29 cents per pound of carbon, which compares favorably with thermal regeneration at 29 to 36 cents per pound.

This technology has also been applied to the regeneration of resinous adsorbents. Although these special adsorbents are often far more efficient and have far greater selectivity than activated carbon, they are temperature sensitive and therefore expensive to recycle because thermal regeneration cannot be used. Typically, the resin is regenerated using a solvent wash-and-distillation process, which is highly energy intensive. Because SCFs can operate at moderate temperatures and can be far more readily recycled than liquid solvents can, SCFs appear ideal for this process. ADL found that using a resin followed by supercritical washing saves 71–83% of the cost of running a conventional process that uses carbon adsorbent followed by thermal regeneration for such diverse compounds as alachlor, phenol, and acetic acid.

Removal and concentration of trace contaminants from gas streams by the two-step SCF process also are possible. Eppig and co-workers report advantageous regeneration efficiencies and economics for activated-carbon regeneration after treating air streams that

FIGURE 3
Arthur D. Little process for regenerating an adsorbent from wastewater purification

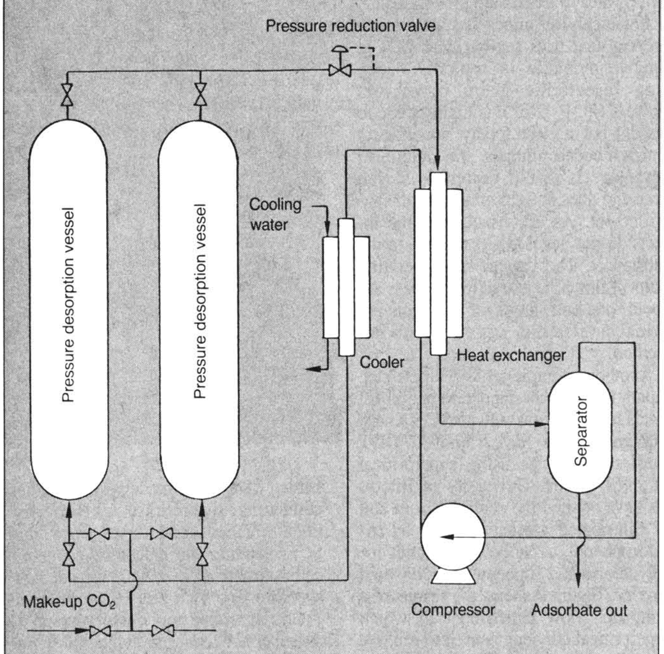

FIGURE 4
Modar process for oxidative detoxification of waste streams

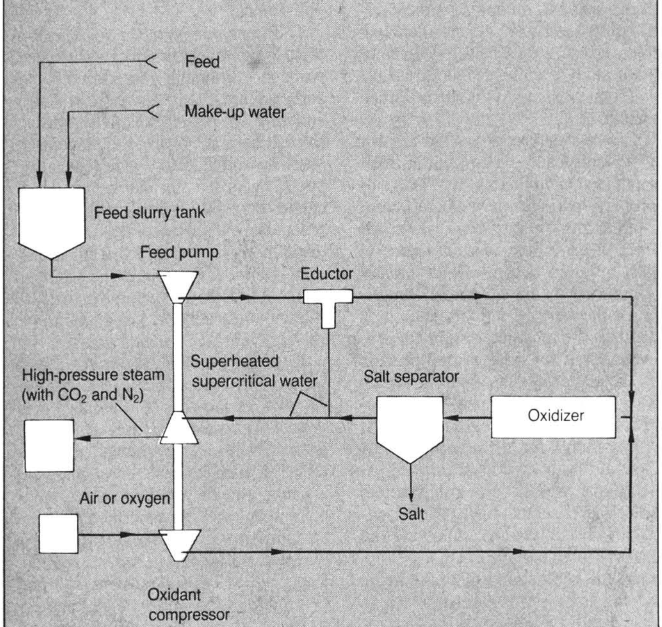

contain traces of gasoline, alcohols, or ketones (*11*). Especially noteworthy is the ability of the SCF (CO_2) to give complete regeneration over many cycles without showing any apparent loss of adsorbent activity.

Finally, reactive separation is another area of great potential utility. One example is in the direct destruction of organic waste streams by supercritical water (SCW) oxidation, as proposed by Modar (*12*). In the process illustrated in Figure 4, the wastes are slurried and then mixed with oxygen and SCW. Because water has a very high critical temperature (374 °C), hydrogen bonding is virtually nonexistent, and the fluid becomes an excellent organiclike solvent—this gives the fluid complete miscibility with the organic feed stream.

In this process the organics are rapidly oxidized to light gases (CO_2, N_2, and CO), and any halides present can be precipitated as salts (the SCW is a poor solvent for ions). This mixture of products and solvent, now at a much higher temperature (550 °C) due to the exothermic oxidation reactions, flows through a salt separator and then is split into two streams, one of which is used to bring the feed mixture of water and waste up to supercritical conditions. The other stream is used to run a turbine to pressurize the feed oxygen to the elevated level needed for injection.

Modar has conducted numerous test runs on a bench scale SCW oxidation system and reports complete and rapid destruction of a variety of model contaminants. These include DDT, biphenyl, trichloroethane, ethylene dichloride, and two PCBs. In all cases, the conversion of these compounds to light gases and salts was reported as greater than 99.99%.

Modar claims a processing cost of \$10–\$30/gal of organics for a 50-gal/d mobile unit (*13*). For a 2500–25,000-gal/d unit the company estimates processing costs of \$0.10–\$2.00/gal. These costs are much lower than those for incinerating chemical wastes, which can run as high as \$2000/t, mostly for fuel. The supercritical water process burns fuel only at startup.

Another application of the reactive SCF technology is in the precombustion desulfurization of high-sulfur coals (*14*). In this process, supercritical alcohol (generally ethanol) is used as both an extractant and a reactant to remove organic sulfur constituents from coal. There may also be some removal of nitrogen and chlorine compounds. The high temperatures involved and the gaslike nature of the fluid enable it to penetrate the porous solid to break down the coal matrix. In this manner, organic sulfur compounds are reduced to products such as ethyl disulfide, ethyl sulfide, thioacetal, and thiophene. Significantly, only trace quantities of hydrogen sulfide are formed. The sulfur content of feed coal has been reduced by as much as 48%.

Phase equilibria

Supercritical fluid processing is a powerful tool for separations and reactions, but the development of technically and economically feasible applications depends largely on a sound qualitative and quantitative understanding of the pertinent solution thermodynamics. Modern phase equilibrium engineering can now reliably and accurately correlate, model, and often predict phase equilibria for many SCFs, and this is in fact the key to useful applications of SCF technology.

The purpose of this paper is not to review all of the detailed methods of characterizing SCF thermodynamics for a phase equilibrium specialist; typical data and theory are available elsewhere (*15–25*). Rather, the purpose of this paper is to encourage environmental researchers concerned with a specific application to consider SCFs and to communicate fruitfully with separations experts, who can in turn calculate the detailed phase equilibria.

Solvent and solute mixtures

For the first time, sufficient data are available to researchers who wish to examine solvent effects and mixed solutes. We have been able to determine the effects of the chemical nature of the solute and solvent, and we have used the results to design solvent mixtures tailored to specific applications. Let us review some results for mixed solutes, because these data give information on selectivity, which is most important in any separation effort and generally more crucial in practice than is loading or solubility.

The first study in this area was by Kurnik and Reid, who investigated the potential of pure SCFs in the separation of chemically similar solids (*26*). Their results were most dramatic; the two solute species appeared to enhance one another's solubility so that the solubility of each component in the ternary system (two solutes, one solvent) was greater than that component's solubility in the binary system (one solute, one solvent) under the same conditions.

An example of their results for a system of naphthalene, benzoic acid, and CO_2 is illustrated in Figure 5, where the solubilities of the solutes in the ternary system are compared with their solubilities in the binary system. The increase in solubility of benzoic acid is 280%; that for naphthalene is 107%. The discovery of this synergism has important implications to theory (in addition to its obvious implications for practice) because it indicates that solute–solute interactions, heretofore assumed to be negligible in these relatively dilute solutions, may in fact be quite substantial in SCFs.

Schmitt recently studied the system of acridine, anthracene, and CO_2 and found no synergism. The solute solubilities in the ternary system are identical to those in the acridine–CO_2 and anthracene–CO_2 systems (*27*). This is in marked contrast to other ternary systems he investigated. One possible explanation for this observed deviation is that in the system of acridine, anthracene, and CO_2 the solubilities are very small, roughly a few ten-thousandths mole fraction. This solubility range may in fact be too dilute for the solute species to "see" one another in solution and therefore to be enhanced in solubility by one another.

Further evidence comes from the work of Kwiatkowski et al., in which

FIGURE 5
Synergistic effects for mixed solutes in CO_2[a]

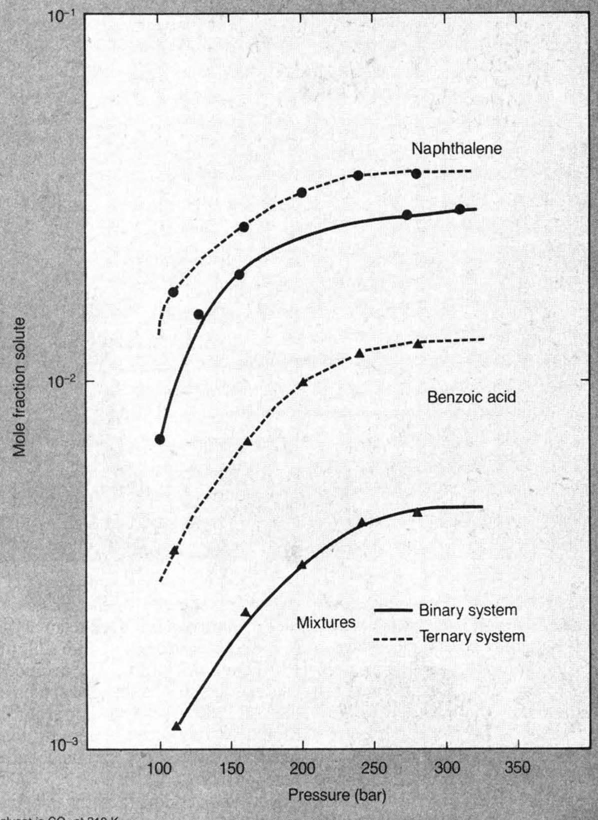

[a]Solvent is CO_2 at 318 K

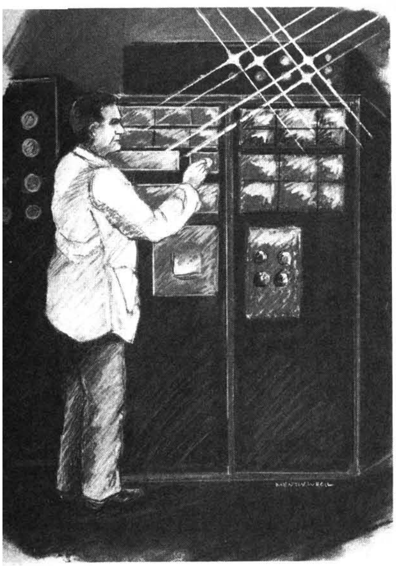

the system of anthracene, phenanthrene, and CO_2 was investigated (*28*). Here, the solubility of anthracene was found to be promoted by the presence of phenanthrene but not vice versa. In this system the phenanthrene is in greater concentration, by about a factor of fifteen, and so allows the anthracene molecules to see the phenanthrene. The phenanthrene, however, cannot see the anthracene in solution. Spectrosopic measurements are needed to confirm these hypotheses.

One consequence of the studies on solute mixtures is the realization that pure SCFs do not exhibit good selectivities as solvents, at least for solutes of reasonably similar size and shape. No differentiation based on functionality of the solutes has been noted (other than that due to solute vapor pressure, which is strictly a property of the condensed phase). This is of great importance to any separation process (*21*) because commonly used fluids, such as CO_2 and ethylene, are nonfunctional themselves and so can interact with solute species only through nonspecific van der Waals forces. It is apparent that to induce some greater differentiability to the solvent, its composition must be modified by the addition of some substance that will act as an entrainer, to promote the solute's solubility in the SCF.

The effect of adding a small quantity of entrainer to the SCF can be quite dramatic. Figure 6 illustrates the increase in solubility of the solute acridine in entrained solutions relative to its solubility in a solution of pure CO_2 (this is the entrainer effect). The addition of one mole percent methanol can increase the solubility several hundredfold. Moreover, this increase appears to be selective to species of certain chemical functionality.

FIGURE 6
Entrainer effects for solutes in methanol-doped CO_2[a]

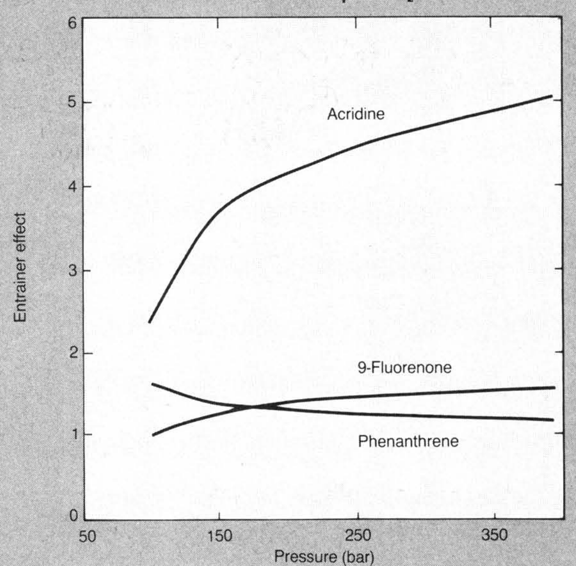

[a]Doped (1%) CH_3OH at 50 °C

Note that acridine (a nitrogen heterocycle, capable of acting as a hydrogen bond acceptor) is strongly promoted in solution, whereas 9-fluorenone (a bridged carbonyl compound) and phenanthrene (a much less polar compound) show little effect. The doped supercritical solvent now exhibits a selectivity not seen when it is used as a pure fluid, giving it far greater potential as a separation solvent. A more complete discussion of entrainer effects on separations is given elsewhere (*29*).

As an example of the potential of entrained supercritical solvents to real applications, we have applied our results from solubility measurements to the work of deFilippi and Robey, who performed a cost analysis on the supercritical desorption of various contaminants from beds of granular activated carbon and polymeric adsorbents (*9*). The cost of performing such an operation may be reduced by 50–90% by optimizing the supercritical solvent used. Based on deFilippi and Robey's results, this would decrease the cost of the operation to below that of conventional thermal regeneration as it is used today. Thus, SCF technology is a powerful tool that has a bright future in environmental engineering applications.

Acknowledgment

This project has been financed in part with federal funds as part of the program of the Advanced Environmental Control Technology Research Center of the University of Illinois at Urbana–Champaign, which is supported under cooperative agreement CR 806819 with EPA. The contents do not necessarily reflect the views and policies of EPA, nor does the mention of trade names or commercial products constitute endorsement or recommendation for use. Additional funding was provided by the Department of Energy, under grant DOE DEFG22-84 PC70801, and by the Illinois Coal Research Board, through the Center for Research on Sulfur in Coal.

Before publication, this article was reviewed for suitability as an *ES&T* feature by John Seinfeld, California Institute of Technology, Pasadena, Calif. 91125; and Michael Paulaitis, University of Delaware, Newark, Del. 19716.

References

(1) *Angew. Chem. Int. Ed. Engl.* **1978,** *17*(10), 701–9.
(2) Gearhart, J. A.; Garwin, L. Presented at the 1976 National Petroleum Refiners Association, San Antonio, Tex., March 1976.
(3) Gouw, T. H.; Jentoft, R. E. *J. Chromatogr.* **1972,** *68,* 303–23.
(4) Paulaitis, M. E.; Gilbert, M. L.; Nash, C. A. Presented at the 2nd World Congress of Chemical Engineering, Montreal, Que., Canada, October 1981.
(5) Kuk, M. S.; Montagna, J. C. In *Chemical Engineering at Supercritical Fluid Conditions;* Paulaitis, M. E. et al., Eds.; Ann Arbor Science: Ann Arbor, Mich., 1983; pp. 101–11.
(6) Ringhard, P. H.; Kopfler, F. C. Presented at the 186th National Meeting of the American Chemical Society, Washington, D.C., September 1983.
(7) Sims, M. *Chemical Engineering* Jan. 25, 1982, pp. 50–51.

(8) Knopf, F. C.; Brady, B.; Groves, F. R. *CRC Crit. Rev. Environ. Control* **1985,** *15*(3), 237–74.
(9) deFilippi, R. P.; Robey, R. J. "Supercritical Fluid Regeneration of Adsorbents," Project Summary, EPA-600/52-83-038; EPA: Washington, D.C., 1983.
(10) Pricht, R. D. et al. *AIChE Symp. Ser.* **1982,** *78,* 136–49.
(11) Eppig, C. P.; deFilippi, R. P.; Murphy, R. A. "Supercritical Fluid Regeneration of Activated Carbon Used for Volatile Organic Compound Vapor Adsorption," EPA-600/2-82-067; EPA: Washington, D.C., 1981.
(12) Modell, M. et al. "Destruction of Hazardous Wastes Using Supercritical Water," Modar, Inc.
(13) *Chemical Week* April 21, 1982, p. 26.
(14) Muchmore, C. B. et al. Presented at the St. Louis Section Symposium of AIChE, April 1984.
(15) Eckert, C. A. et al., submitted for publication in *AIChE J.*
(16) Paulaitis, M. E. et al. *Rev. Chem. Eng.* **1982,** *1,* 179–250.
(17) Tsekhanskaya, Y. V.; Iomtev, M. B.; Mushkin, E. V. *Russ. J. Phys. Chem.* **1962,** *36,* 1177–81.
(18) Johnston, K. P.; Ziger, D. H.; Eckert, C. A. *Ind. Eng. Chem. Fundam.* **1982,** *21,* 191–97.
(19) Kurnik, R. T.; Holla, S. J.; Reid, R. C. *J. Chem. Eng. Data* **1981,** *26,* 47–51.
(20) Van Leer, R. A.; Paulaitis, M. E. *J. Chem. Eng. Data* **1980,** *25,* 257–59.
(21) Van Alsten, J. G.; Hansen, P. C.; Eckert, C. A. Presented at the AIChE Annual Meeting, San Francisco, Calif., November 1984.
(22) Johnston, K. P.; Eckert, C. A. *AIChE J.* **1981,** *27,* 773–79.
(23) Hansen, P. C.; Ellison, T. K.; Eckert, C. A., submitted for publication in *Fluid Phase Equilib.*
(24) Gilbert, S. W.; Eckert, C. A. Presented at the AICHE Annual Meeting, Chicago, Ill., November 1985.
(25) Eckert, C. A. et al. *J. Phys. Chem.*, in press.
(26) Kurnik, R. T.; Reid, R. C. *Fluid Phase Equilib.* **1982,** *8,* 93–105.
(27) Schmitt, W. J. Ph.D. Thesis, Massachusetts Institute of Technology, Cambridge, Mass., 1984.
(28) Kwiatkowski, J.; Lisicki, Z.; Majewski, W. *Ber. Bunsenges. Phys. Chem.* **1984,** *88,* 865–69.
(29) Van Alsten, J. G.; Eckert, C. A. *Fluid Phase Equilib.*, in press.

***Charles A. Eckert** is department head and Alumni Professor of chemical engineering at the University of Illinois at Urbana–Champaign. He is a leading authority in solution thermodynamics and kinetics in applications to separation processing. He received a B.S. and an M.S. from MIT and a Ph.D from the University of California at Berkeley, all in chemical engineering. Eckert has received the Coburn Award of the AIChE, and the Ipatieff Prize of the ACS. He is a member of the National Academy of Engineering.*

***John G. Van Alsten** (l.) did his undergraduate work at Hope College, where he majored in chemistry and physics. He completed his M.S. and Ph.D. in chemical engineering at the University of Illinois, conducting thesis research in supercritical solution thermodynamics. Van Alsten is currently a research chemical engineer at the Shell Westhollow Research Center in Houston, Tex.*

***Thomas Stoicos** (r.) did his undergraduate work in chemistry at Kenyon College in Gambier, Ohio, and received an M.S. and a Ph.D. from the University of Illinois at Urbana–Champaign in chemical engineering. Stoicos spent three years as a senior research chemical engineer in a separations group at Signal-UOP Research Center in Des Plaines, Ill., and one year at the University of Illinois as a visiting assistant professor. He is an authority on separation processes, especially under extreme conditions.*

Banning land disposal of hazardous wastes

Richard M. Dowd

The 1984 Hazardous and Solid Waste Amendments to the Resource Conservation and Recovery Act and the implementing regulations proposed by EPA in the Jan. 14, 1986, *Federal Register* are designed to prohibit land disposal of hazardous wastes *unless* the EPA administrator finds that land disposal of certain wastes is "protective of human health and the environment."

One of the more significant departures from previous statutes governing waste disposal is that the new law unambiguously shifts the burden of proof to disposers and generators of hazardous wastes. The statute makes it clear that unless EPA has strong evidence to the contrary—and that evidence must be provided by an interested party in a petition to the agency—any type of land disposal of the untreated wastes must be banned.

EPA has two primary responsibilities: first, to promulgate exceptions to the statutory prohibitions in the form of treatment standards that will ensure minimization of long-term and short-term threats to human health and the environment, and second, to grant exceptions from the statutory prohibitions through approval of petitions demonstrating that continued land disposal of specific wastes is "protective of human health and the environment."

In establishing the treatment standards for exceptions to the ban, EPA may set maximum concentrations for the chemical constituents either in the leachate or in the waste itself. Alternatively, it can establish specified treatment methods to be applied to wastes instead of or prior to land disposal.

EPA has made it clear that it prefers to adopt the concentration route, using "screening levels," that is, levels of measurement at which action must be taken. If a technology is unavailable, a waste that in itself meets the screening levels—for example, contaminated soil from Superfund cleanups—will be deemed to protect human health and the environment.

Upcoming decisions

The statute's philosophy of imposing total bans if EPA and interested petitioners have not acted by certain dates imposes tremendous burdens on the agency and on waste disposers and generators. Over the coming five years, agency officials must arrive at a number of decisions:

- They must decide by Nov. 8, 1986, whether it is necessary to prohibit treatment or require alternative treatment for spent solvents and dioxin- and furan-containing wastes, including 23 hazardous constituents.
- They must decide by July 8, 1987, whether to ban landfill disposal of wastes on the "California list," which includes liquids with chlorinated solvents and eight metals.
- By Aug. 8, 1988, they must rule on disposal of specified process wastes, including approximately 110 specific hazardous waste constituents.
- They must decide by June 8, 1989, on 22 specified process wastes and 125 hazardous constituents.
- Finally, by May 8, 1990, agency officials must decide on 13 specified process wastes and approximately 100 hazardous waste constitutents.

Each of these decisions will require an enormous amount of work.

Budgetary constraints

Agency staff levels have not risen to meet this statutory requirement, and the current budgetary climate does not encourage hope for increased resources. The Gramm–Rudman–Hollings cuts may lead to as much as a 25% reduction in available resources in fiscal year 1987, more in 1988 and 1989.

If EPA fails to set standards for specific wastes, in the form of alternative technologies or of standard screening levels, the statutory prohibitions take effect. EPA can make decisions regarding exemptions or extensions only for a series of legislatively explicit reasons, including the finding of a lack of alternative technologies. Extensions or exemptions cannot be based simply on the fact that the agency was unable to complete its work by the deadlines.

The petition

The petition is the *only* forum for consideration of site-specific information. To ensure that the data in a petition have a reasonable degree of scientific certainty—enabling the waste to be disposed of on land—EPA has identified four categories of information that must be presented:

- the exposure potential, through fate and transport;
- a population analysis, which is required if the constituent concentration at the point of exposure will exceed EPA's standards;
- toxicological data on site conditions; and
- the leachate concentration.

For this information, EPA will require a substantial quality assurance and quality control (QA–QC) program that the petitioner must certify to undertake. Such programs can include audits of data collection and even independent monitoring and modeling of the site.

Although many QA–QC procedures are straightforward—for example, analytical quality control—others, such as data collection quality control, are in their infancy. If the data cast doubt on the approvability of the petition, EPA will reject the petition at that stage.

All of these steps add time to petition preparation, thus reducing the amount of time available for review and making efficient petition approval a difficult task.

Richard M. Dowd, Ph.D., is a Washington, D.C., consultant to Environmental Research & Technology, Inc.

ES&T VIEWS

Ozone in the stratosphere

Continuation of the Pimentel report

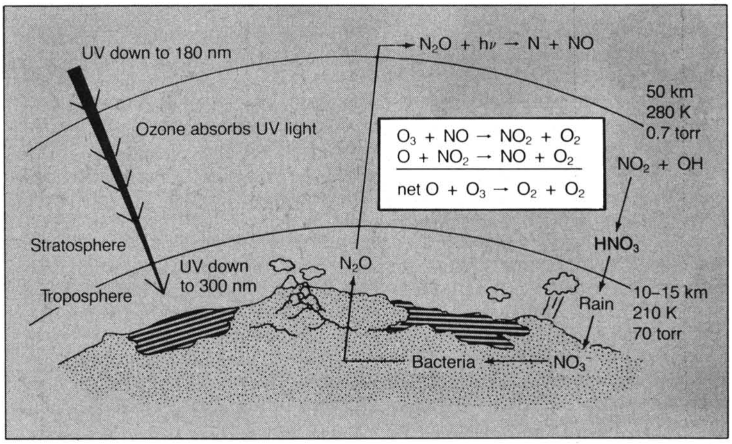

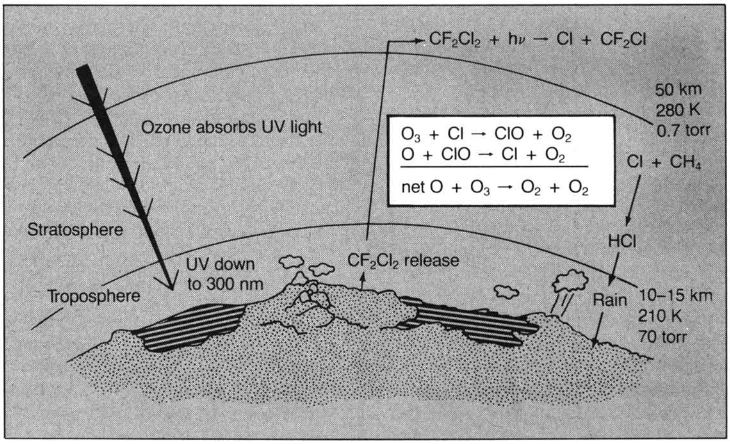

The possibility of polluting the stratosphere to the point of partially depleting the protective ozone layer was first raised only about a dozen years ago. This seemingly improbable notion found much scientific support, and it is now one of the best examples of a potentially serious environmental problem of global extent. It is a problem, furthermore, that exemplifies chemistry's central role in its understanding, analysis, and solution.

Why do we need to worry about stratospheric chemistry? Ozone in the stratosphere is the natural filter that absorbs and blocks the sun's short wavelength ultraviolet radiation that is harmful to life. The air in the stratosphere—a cloudless, dry, cold region at altitudes between about 10 to 50 km—mixes slowly in the vertical direction, but rapidly in the horizontal. Consequently, harmful pollutants, once introduced into the stratosphere, might remain there for periods as long as years, and, if so, they will rapidly be distributed around the earth across borders and oceans, making the problem truly global. A large reduction of our ozone shield would result in an increase of potentially dangerous ultraviolet radiation at the earth's surface.

To understand how easily the ozone layer might be perturbed, it is useful to recognize that ozone is actually only a trace constituent of the stratosphere; at its maximum concentration ozone makes up only a few parts per million of the air molecules. If the diffuse ozone layer were concentrated into a thin shell of pure ozone gas surrounding the earth at atmospheric pressure, it would measure only about 3 millimeters (1/8 inch) in thickness. Furthermore, ozone destruction mechanisms are based on chain reactions in which one pollutant molecule may destroy many thousands of ozone molecules before being transported to the lower atmosphere, chemically transformed, and removed by rain.

Chemistry's crucial role in understanding this problem has emerged through the identification and measurement of several ozone-destroying chain processes. Fifty years ago, the formation of an ozone layer in the midstratosphere was qualitatively described in terms of four chemical and photochemical reactions involving pure oxygen species (O, O_2, and O_3). Today, we know that the rates of at least 150 chemical reactions must be considered in order to approach a quantitative model for simulating the present stratosphere and predicting changes resulting from the introduction of various pollutants. The chemistry begins with absorption of solar ultraviolet radiation by O_2 molecules in the stratosphere. Chemical bond rupture occurs, and ozone, O_3, and oxygen atoms, O, are produced. Then, if nitric oxide, NO, is somehow introduced into the stratosphere, an important chemical chain reaction takes place.

The NO and NO_2 reactions together

furnish a true catalytic cycle in which NO and NO_2 are the catalysts. Neither species is consumed, because each is regenerated in a complete cycle. Each cycle has the net effect of destroying one oxygen atom and one ozone molecule (collectively called "odd oxygen"). This catalytic cycle is now believed to be the major mechanism of ozone destruction in the stratosphere. In the natural atmosphere, the oxides of nitrogen are provided by biogenic emissions at the Earth's surface by soil and sea bacteria of nitrous oxide, N_2O. This relatively inert molecule slowly mixes into the stratosphere where it can absorb ultraviolet light and then react to form NO and NO_2.

Of course, oxides of nitrogen directly introduced to the stratosphere are expected to destroy ozone as well, and this was the basis of the first perceived threat to the ozone layer—larger fleets of supersonic aircraft flying in the stratosphere and depositing oxides of nitrogen via their engine exhausts. Nuclear explosions also produce copious quantities of oxides of nitrogen, which are carried into the stratosphere by the buoyancy of the hot fireballs. A significant depletion of the ozone layer in the event of a major nuclear war was forecast in a 1975 study by the National Academy of Sciences, although this environmental effect of nuclear war may pale in comparison with the recently suggested potential of a "nuclear winter." Both effects underscore the delicacy of the atmosphere and its sensitivity to chemical transformations.

Then, in 1974, just as the possible impact of stratospheric planes was reaching the analysis stage, concern was raised about other man-made atmospheric pollutants. Halocarbons, such as $CFCl_3$ and CF_2Cl_2 (chlorofluoromethanes, or CFMs), had become popular as spray-can propellants and refrigerant fluids, mainly because of their chemical inertness. The absence of reactivity meant absence of toxicity or other harmful effects on terrestrial life. Ironically, this meant that there was no place for the CFMs to go but up—up into the stratosphere where ultraviolet photolysis could occur. Chemists then recognized that if this occurred, the resultant chlorine species, Cl and ClO, could enter into their own catalytic cycle, destroying ozone in a manner exactly analogous to the destruction caused by the oxides of nitrogen.

Once this possibility had been recognized, analysis of the whole stratospheric ozone chemistry began in earnest. An international committee of scientific experts assembled by the National Academy of Sciences examined in detail the state of our knowledge of every aspect of the problem. It became clear that the additional chemistry introduced to the stratosphere added not just these two catalytic chemical reactions to the roster, but a total of about 40 new reactions involving such species as Cl, ClO, HCl, HOCl, $ClONO_2$, the halocarbons, and several others. Most of these reactions had never before been studied in the laboratory.

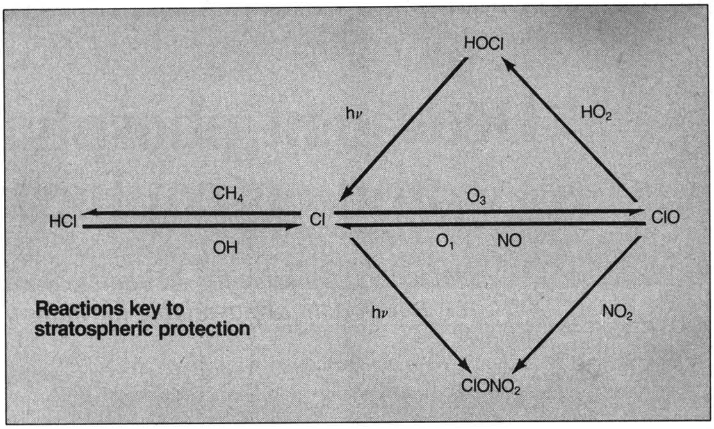

Laboratory kineticists and photochemists responded to the challenge by providing reliable rate constants and absorbances for the proposed processes using the growing arsenal of modern experimental methods. Recent progress in the experimental accomplishments of this field has been remarkable. It has become possible, for example, to generate nearly any desired reactive molecular species in the laboratory in a variety of ways, to bring them together with other reactive species, and to measure their rates of reaction under known, controlled conditions. Such direct measurements of these extremely rapid reactions were only a distant goal a decade ago, but they are now a reality.

Finally, field measurements of minor atmospheric species have been revolutionized by some of the recent advances in analytical chemistry. Methods originally developed for ultrasensitive detection of extremely reactive species in laboratory studies have been modified and adapted to measure such constituents as O, OH, Cl, ClO, and others at parts-per-trillion concentrations in the natural stratosphere. This has been accomplished recently in experiments in which a helium-filled balloon carries an elaborate instrument package to the top of the stratosphere where the package is dropped while suspended by a parachute. As the instrument traverses the stratosphere, it measures concentrations of several important trace chemical species and telemeters the information to a ground station. Very recently, the first successful reel-down experiment was performed in which the instrument package was lowered 10 to 15 km from a stationary balloon platform and reeled back up again like a giant yo-yo. This method results in a huge increase in the amount of data that can be obtained in a single balloon flight. It will also allow for the first time a study of the time evolution and variability of the stratosphere.

Much has been accomplished in the past 10 years. Many of the needed 100 to 150 photochemical and rate processes have been measured in the laboratory, and many of the trace species measured in the atmosphere. Yet, research remains to be done. For example, two of the important chemical species containing chlorine, HOCl and $ClONO_2$, have yet to be measured anywhere in the stratosphere. Refinements in the reaction rates for many of the important processes are still required, and exact product distributions for many of the reactions are still lacking. Nevertheless, the original NAS study, the research programs it spawned, and the subsequent follow-up studies provided a firm and timely basis for legislative decisions about regulation of CFM use. Industrial chemists produced alternative, more readily degradable substances to replace the CFMs in some applications. Monitoring programs are in place so that trends in the stratospheric composition can be watched. The stratospheric ozone issue provides a showcase example of how science can examine, clarify, and point to solutions for a potential environmental disturbance. Premature initiation of regulation was avoided because the problem was recognized early enough to permit deliberate, objective analysis and focused research to narrow the uncertainty ranges. From first recognition on, chemists played a lead role.

This is the third in a seven-part series.

Detergent phosphate bans and eutrophication

Data were available for 40 bodies of water in 1978; today, data are available for more than 400

By G. Fred Lee and R. Anne Jones

The guest editorial by Werner Stumm ("Clean shirts and clean water," *ES&T*, November 1985, p. 1013) is critical of an earlier editorial by Russell Christman ("Phosphate here, phosphate there . . ." *ES&T*, June 1985, p. 467). Christman had commented that in some situations detergent phosphate bans may produce "no noticeable improvement in water quality."

This editorial exchange is typical of those that have taken place over the past 20 years. It basically reflects the controversy that has existed over whether every bit of phosphate control helps to manage eutrophication or whether a certain amount of phosphate must be controlled before a water body will show a discernible improvement in water quality.

Recently, Maki and colleagues have concluded that the detergent phosphate bans enacted in various regions and states in the United States have not produced measurable improvements in water quality (*1*). The reason for this is that insufficient phosphate control was achieved by the bans to bring about a measurable reduction in phosphorus. Christman's position is strongly supported by this research.

In his editorial Stumm stated that "our power to predict the effect of phosphate loadings on lakes (of different morphology and hydraulic residence time) is remarkably quantitative and suited to generalization." We strongly agree. R. Vollenweider and the Organization for Economic Cooperation and Development (OECD) conducted eutrophication studies during the mid-1970s and we did follow-on studies that showed it is possible to predict with a high degree of reliability the effects of altering the phosphorus load to a water body (*2–6*).

G. Fred Lee

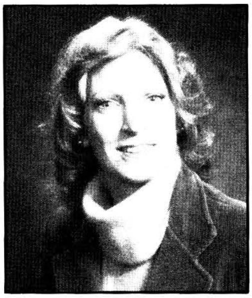

R. Anne Jones

The Vollenweider-OECD eutrophication model has been expanded to approximately 400 lakes (*5*). It is clear that it is indeed possible to make a quantitative prediction of the effects of a detergent phosphate ban and thereby to ascertain the potential benefits of such a ban.

Recently, we developed a general relationship (Figure 1) that can be used to evaluate the potential benefits of a detergent phosphate ban (*7*). It is based on the finding that a reduction of approximately 20% in the phosphorus load to a water body must be achieved to produce a discernible effect on water quality. This 20% value is independent of the trophic state. It is based on our experience and has been corroborated by many colleagues. It was developed from the phosphorus load–chlorophyll relationship that was developed in the Vollenweider–OECD eutrophication studies (*2–5*). It is also demonstrated in Table 1 (*7*).

Figure 1 is read as follows: If 40% of the phosphorus in domestic wastewater were due to detergents, and if the domestic wastewater discharge represented 30% of the total phosphorus load to the lake, the removal of detergent phosphate would result in no detectable change in water quality of the water body. On the other hand, if the domestic wastewater discharge represented 60% of the total phosphorus load to the lake, removal of detergent phosphate would result in a detectable improvement in water quality. An even greater improvement would result from the removal of detergent phosphate if the domestic wastewater represented 100% of the total phosphorus load to the lake.

In order to assess the effect of a detergent phosphate ban on water quality it is necessary to know the percentage of phosphorus in the domestic wastewater that enters the water body, either directly or indirectly, and the percentage of the total phosphorus load that is derived from domestic wastewater. These are, respectively, the ordinate and the abscissa in the figure. The stippled area in the figure is the region in which a discernible change in water quality would be expected as a result of changing the phosphorus load. The density of stippling indicates the magnitude of the change expected.

Those water bodies that derive most of their phosphate from detergent phosphate in domestic wastewater should show the greatest change as a result of a detergent phosphate ban. It is important

0013-936X/86/0920-0330$1.50/0

coordinates just entering the stippled area, the change in water quality would be just detectable.

The relationship in the figure can be used to explain why Maki and colleagues concluded that detergent phosphate bans have not in general produced measurable improvements in water quality (*1*). Few water bodies have a high enough detergent-derived phosphorus load to show more than a 20% change in the total phosphorus load as a result of a detergent phosphate ban.

In the early 1970s detergent formulations in the United States contained a much higher percentage of phosphorus than they do today. At that time it was generally agreed that 50–60% of the phosphorus in domestic wastewater derived from detergent formulations. Today, however, in Michigan and Wisconsin, for example, where detergent phosphate bans have been enacted, studies have shown that 20–25% of the phosphorus is derived from detergent formulations. If only 20% of the phosphorus in a domestic wastewater effluent is derived from detergents, then it is unlikely that there would be any water body in which a detergent phosphate ban would result in a significant improvement in water quality, even if domestic wastewater were the only source of phosphorus for the body of water.

Almost all water bodies other than sewage ponds receive phosphorus from other sources, and detergent bans in the United States will have little or no effect on eutrophication-related water quality. In the early 1970s there was a possibility that such bans would affect water quality; however, this would have been for water bodies that had approximately half of their total phosphorus load derived from domestic wastewater.

This discussion does not consider a situation in which phosphorus is removed at wastewater treatment plants by iron or aluminum precipitation or by enhanced biological uptake. Ninety percent of the phosphorus in domestic wastewater can be readily removed by these methods at a per capita cost of less than one cent each day for populations exceeding 10,000.

It is obvious that where there are excessive fertilization problems in water receiving domestic wastewater discharges, the most effective way to control the phosphorus input is by iron or aluminum precipitation at the treatment plant. Stumm stated, "Phosphate removal in treatment plants is necessary but insufficient because some wastes unavoidably escape treatment; not all households are connected to treatment plants and storm water overflows."

TABLE 1
Perceptible changes in eutrophication-related water quality[a]

Trophic state	Annual average chlorophyll (μg/L)	Detectable change[b]
Oligotrophic	<2	0.5
Mesotrophic	4–10	1–2
Hypereutrophic	45	10

[a]Based on the Vollenweider–OECD phosphorus load–eutrophication relationship: A 20% change in the total phosphorus load is needed to produce a detectable change in water quality
[b]Based on chlorophyll (μg/L)

FIGURE 1
Effect of detergent phosphate on eutrophication-related water quality

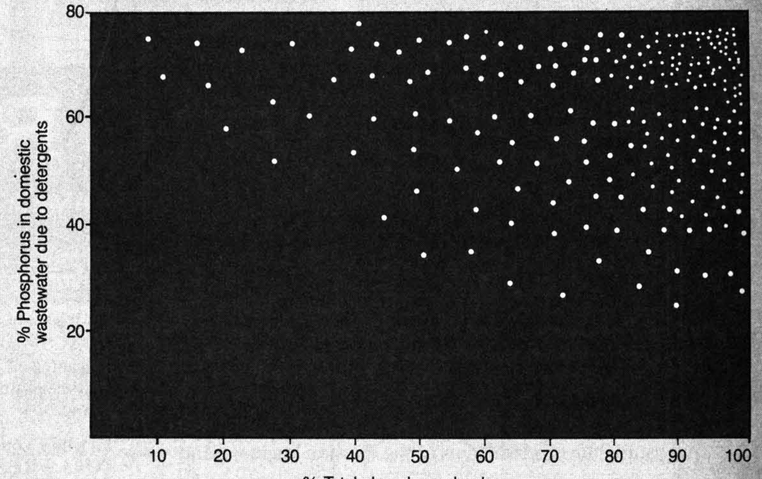

Source: Reference 7

Figure 1 can be used to determine on a site-specific basis whether septic tank systems, combined sewer overflows, and wastewater bypasses are the source of sufficient phosphorus to justify a detergent phosphate ban in addition to phosphorus control at the wastewater treatment plant. If these sources contribute more than 20% of the total phosphorus load to the water body, then enactment of a ban will likely produce a marginally detectable improvement in eutrophication-related water quality. It is important to note, however, that most septic tank wastewater disposal systems do not contribute significant amounts of phosphate to surface water (*8*).

We agree in part with both Stumm and Christman in that although detergent phosphate bans generally will not result in an overall improvement to water quality, there may be some situations in which eutrophication-related water quality would be improved by a ban. These situations are probably rare and would be characterized by a high percentage of the phosphorus entering the water body being derived from domestic wastewaters and a substantial percentage of the phosphorus in the domestic wastewaters being derived from detergents. These situations can be readily identified from the information available today.

References

(1) Maki, A. W.; Porcella, D. B.; Wendt, R. H. *Water Res.* **1984,** *18,* 893–903.
(2) Lee, G. F.; Rast, W.; Jones, R. A. *Environ. Sci. Technol.* **1978,** *12,* 900–908.
(3) Organization for Economic Cooperation and Development. *Eutrophication of Waters, Monitoring, Assessment, and Control;* OECD: Paris, France, 1982.
(4) Jones, R. A.; Lee, G. F. *Water Res.* **1982,** *16,* 503–15.
(5) Jones, R. A.; Lee, G. F. *World Health Organization Water Quality Bulletin,* in press.
(6) Rast, W.; Jones, R. A.; Lee, G. F. *J. Water Pollut. Control Fed.* **1983,** *55,* 990–1003.
(7) Lee, G. F.; Jones, R. A. *Lake Line Newsletter* January 1986, pp. 8–11.
(8) Jones, R. A.; Lee, G. F. *J. Water Pollut. Control Fed.* **1979,** *51,* 2764–75.

G. Fred Lee is distinguished professor and R. Anne Jones is an associate professor in the Department of Civil and Environmental Engineering at the New Jersey Institute of Technology in Newark, N.J.

professional consulting services directory

CLASSIFIED SECTION

INDEX TO THE ADVERTISERS IN THIS ISSUE

Emissions and Particle-Size Distribution of Some Metallic Elements of Two Peat/Oil-Fired Boilers

Ahti O. Itkonen[*†] **and Matti J. Jantunen**[‡]

Department of Environmental Hygiene, University of Kuopio, SF-70211 Kuopio, Finland, and Department of Environmental Hygiene and Toxicology, National Public Health Institute, Box 95, SF-70701 Kuopio, Finland

■ Two peat/oil-fired power plants—plant A, 100-MW_t pulverized peat fired, electrostatic precipitator (ESP) equipped, and plant B, 7-MW_t fluidized bed fired, multicyclone (MC) equipped—were studied to determine emissions of particles and 11 elements. Particulate samples were collected and fractionated before and after the fly ash collectors by the University of Kuopio modified Bird & Tole five-stage cascade centripeters, weighed, and analyzed by use of atomic absorption spectrometry. In pulverized peat firing the aerodynamic size distributions of particles were bimodal both before and after the ESP. The mass median aerodynamic diameter (MMAD) of the particulate matter was reduced in the ESP from 17 to 9.6 μm. In fluidized bed peat firing the particle size distribution showed only one mode. After the MC the MMAD was 2.3 μm. The studied elements were nonvolatile (Fe, Ca, Mg, and Co), slightly volatile (Cu and Ni), and volatile (As, Cd, Pb, and Zn). The concentrations of these elements in the fly ash, as well as the enrichment of the volatile elements on the smallest particles, showed no difference from pulverized coal combustion results. The volatile elements were further enriched in the ESP, because it collects large particles better than smaller ones and spherical molten ash particles better than complex, nonmolten ones. The latter resulted in concentration enrichment even within each particulate size class.

Introduction

During the last decade the objects of the Finnish energy policy have been to conserve and replace imported fuels with domestic ones, most importantly peat. Since 1970 the use of peat for fuel has increased rapidly. In 1980 about two million tons of peat was used in 11 municipal and industrial boilers. Most of these plants are fired with pulverized milled peat together with 5–60% oil.

The quality of peat varies considerably due to its moisture content (40–60%), sulfur content (0.1–0.4%), organic consistency, and degree of humification. As a fuel it is comparable to lignite. In the carbonizing chain peat is a prestage of brown coal. Because of the low heat value (6–12 MJ/kg) and density (300–400 kg/m^3) of milled peat, its use is economical only in the vicinity of the sources.

[†] Department of Environmental Hygiene, University of Kuopio, SF-70211 Kuopio, Finland.

[‡] Department of Environmental Hygiene and Toxicology, National Public Health Institute, Neulaniementie 4, Box 95, SF-70701 Finland.

Peat contains 2–10% ash. This incombustible mineral matter results from decayed plants, airborne dust, and waterborne matter that is washed or dissolved from the nearby mineral soils. Peat ash contains most of the known elements at least in trace quantities (*1*). Their concentrations vary significantly between bogs and even within the same bog (*2–4*).

The use of fossil fuels has attained widespread interest in environmental research. Environmental consequences of large-scale peat combustion have been studied only since 1978, and only a few publications of their results have appeared so far (*5–7*).

Peat combustion is known to produce plenty of particulate emissions, but increased efficiencies in solid fuel combustion and modern fly ash collectors have reduced the emissions of soot and fly ash.

The results presented in this publication are a part of a larger study made for the Finnish Ministry of Trade and Industry (*7*).

Materials and Methods

Plant Description. Plant A is a municipal power plant in Kuopio, Central Finland. Its operation began in 1972, and it is the first large peat-fired boiler plant in Finland. At capacity it produces 30 MW of electric power and 62 MW of district heat. The pulverized peat- and oil-fired boiler is equipped with two beater mills and four front-wall oil and peat burners. During our sampling the plant was run at 52–92% of the maximum load, and on the average 67% (39–84%) of the heat input was produced by peat. The combustion temperature was 1500–1600 K, and the flue gas temperature before the electrostatic precipitator was 430–450 K.

Plant B is located in Suonenjoki, 50 km from Kuopio. It produces district heat by burning milled peat and oil in a fluidized bed combustor (FBC). Its operation began in 1979. In a pyroflow FBC most of the bed material follows the hot flue gases. The hot cyclone adjancent to the boiler removes most of this material and returns it into the bed. The final fly ash collector is a multicyclone (MC) (*8*). During our sampling the plant was run at 33–53% of the maximum load, and on the average 66% (52–75%) of the heat was produced by peat. The combustion temperature was 970–1070 K, and the flue gas temperature was 390–410 K.

Sampling and Analysis. Particulates were collected before and after the ESP and the MC by modified Bird & Tole, five-stage cascade centripeter samplers. The cut

Table I. Calibrated and Repaired Cut Sizes of Cascade Centripeter

sampler stage	particle diam, μm calibration dry air, 297 K	plant A, 430 K	plant B, 400 K
1	>45	>52	>48
2	13-45	15-52	13-48
3	3.8-15	4.6-15	4.1-13
4	1.4-3.8	1.6-4.6	1.5-4.1
5	<1.4	<1.6	<1.5

sizes of this sampler type in calibration and their conversion to flue gas sampling conditions are published elsewhere (*9–11*) and presented in Table I. At plant A, the results of the total fly ash emission are based on 61 samples (9 soot blowing) collected before the ESP, and 22 samples (6 soot blowing) collected after the ESP. Sampling times were 10–20 min before and 1-2 h after the ESP, and the samples were taken during 97 h. Seventeen samples collected before and six collected after the ESP during a 24-h period were chosen for elemental analyses. Ten combined peat samples from this same period were used for fuel analyses.

At plant B, 16 fly ash samples (5 soot blowing) were collected after the MC collector. Sampling before the MC was impossible due to the plant construction. Sampling times ranged from 5 to 30 min, and the samples were collected during 23 h.

At plant A, peat samples were collected from the two beater mills every hour. For preparation and analysis these samples were combined to represent 5-h periods. At plant B, two peat samples were taken from the conveyor before the fuel silo for fuel analyses. Normal hourly operating records were obtained from the personnel at both plants. The plants were operated normally irrespective of the measurements and sampling program.

The vapor-phase elements were collected by a cryogenic trap; three 250-mL xylene bubblers in series in an ice bath, with a flow rate of 25 mL/s.

The fly ash samples were dried and weighed. The peat samples were dried at 378 K, weighed and ashed at 748 K, and weighed again. These together with the vapor-phase samples were analyzed by means of atomic absorption spectrometry using flame and graphite furnace techniques (Perkin-Elmer 460 + HGA 500) for the concentrations of Ca, Fe, Mg, Mn, Zn, Cu, Cd, Co, Ni, Pb, and As. The morphological studies of the fly ash samples were performed by use of scanning electron microscopy (SEM) (JEOL JSM-35).

Results and Discussion

The results have been converted to mass per input fuel energy units (ng/J), because this is the most stable emission parameter. This was done for each sample by computing the amount of flue gas produced by the combustion of 1 J worth of the analyzed peat with the air excess computed from the plant O_2 analyzer record.

Total Fly Ash Emissions. In plant A the average size distributions of fly ash before and after the ESP during soot blowing and normal operation are presented in Figure 1. The aerodynamic size distributions of particulates were bimodal both before and after the ESP. Before the ESP the modes occurred at $D_A < 1.6$ μm and $15 < D_A < 52$ μm. The mass median aerodynamic diameter (MMAD) of particulate matter was 17 μm, and its geometric dispersion (S_g) was 3.6. In the ESP the MMAD is reduced to 9.6 μm. The taller mode of the bimodal particle size distribution has moved to $4.6 < D_A < 15$ μm, and the smaller mode at

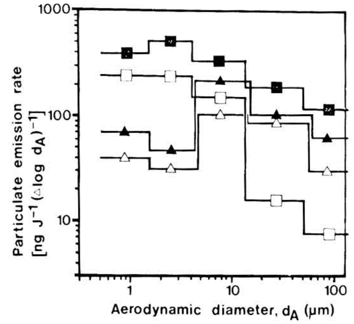

Figure 1. Emitted particle size distribution during soot blowing and normal operation at the two peat fired boilers: plant A, 100-MW$_t$ pulverized peat/oil-fired, ESP fly ash collector; plant B, 7-MW$_t$ peat/oil-fired FBC, MC fly ash collector.

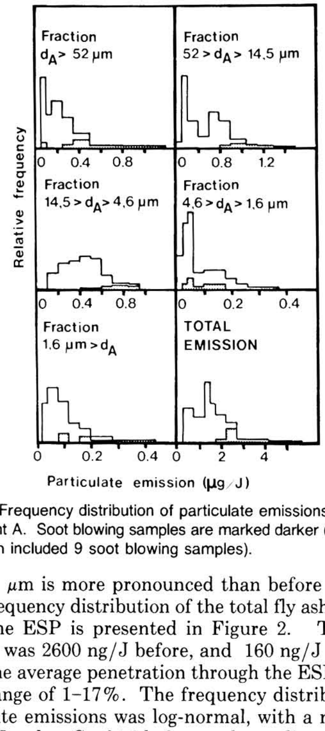

Figure 2. Frequency distribution of particulate emissions before the ESP at plant A. Soot blowing samples are marked darker (61 samples during 96 h included 9 soot blowing samples).

$D_A < 1.6$ μm is more pronounced than before the ESP.

The frequency distribution of the total fly ash emission before the ESP is presented in Figure 2. The mean emission was 2600 ng/J before, and 160 ng/J after, the ESP. The average penetration through the ESP was 6% with a range of 1–17%. The frequency distributions of particulate emissions was log-normal, with a median of 1500 ng/J and an S_g of 1.8 before, and a median of 90 ng/J and an S_g of 1.7 after, the ESP.

Morphologically, see Figure 3; the particulates can be categorized as follows: dense spherical molten ash particles, 2–15 μm in diameter, typical for coal combustion; typical sponge-like spherical particulates from oil combustion, 5–80 μm in diameter; remnants of botanical cell structures, very irregular in shape, and 8–40 μm in length; and tarlike condensed material on the backup filter.

In plant B the average size distributions of fly ash during soot blowing and normal operation are presented in Figure 1. This particle size distribution is unimodal. The mode

Table II. Comparison of Fly Ash Particle Size Distributions Measured from Solid-Fuel-Fired Boiler Plants

	combustion method	fly ash collector, penetration, %	particle size distribution parameters: MMAD, μm	S_g	measured range (D_A), μm	modes (D_A), μm
		Coal				
Ondov et al. (1979)[a] A	pulverized	ESP 0.3	1.6	1.57	0.2–20	1, 4
B	pulverized	ESP 2.5	8.6	2.2	0.2–20	7
Carpenter et al. (1980)	fluidized bed	CYC + BGH 0.8–1.5				
before collector[b]			3.9–6.1		0.6–10	
after collector[b]			2.3–2.4		0.6–10	
Shendrikar et al. (1983)	pulverized	BGH <0.5				
before collector					0.02–10	<0.8, 3, >10
after collector					0.02–10	<0.08, 1.5, >10
Jantunen et al. (1980)A	chain grate	MC 11	1.1	5.5	1–50	1
B	pulverized	ESP 0.4	2.9	3.0	1–50	2
		Lignite				
Carpenter et al. (1980)	fluidized bed	CYC + BGH[c] 2				
before collector[b]			4.5–4.8		0.6–10	
after collector[b]			2.8		0.6–10	
		Peat (This Study)				
Plant A	pulverized	ESP 6.1				
normal, before collector			16	3.3	1–50	1, 20
normal, after collector			9.2	3.4	1–50	1, 12
soot blowing, before collector			19	3.5	1–50	1, 20
soot blowing, after collector			11	3.5	1–50	1, 9
TWA,[d] before collector[d]			17	3.6	1–50	1, 17
TWA, after collector			9.6	3.6	1–50	1, 10
Plant B	fluidized bed	MC 25				
normal, after collector			2.3	3.7	1–50	1
soot blowing, after collector			4.1	5.4	1–50	2.5
TWA			2.4	2.8	1–50	

[a] After the fly ash collector, if not mentioned otherwise. [b] Top of the fluidized bed combustor. [c] Leaks reported in the baghouse (BGH). [d] Time-weighted average (TWA).

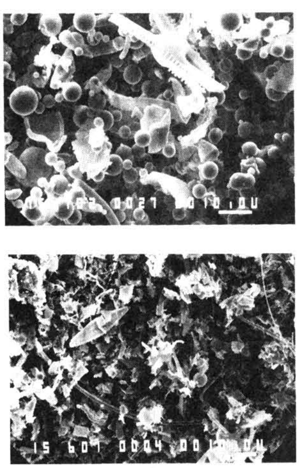

Figure 3. Scanning electron photomicrographs of fly ash particles collected at the ESP inlet (top) and outlet (bottom).

is at $1.6 < D_A < 4.6$ μm. The mean emission was 900 ng/J, and the emission frequency distribution was log-normal with a median of 710 ng/J and an S_g of 1.8.

In the morphological study of the fly ash the low combustion temperature became evident. There were no molten ash particles; remnants of botanical cell structures were abundant, and particles were mostly irregular agglomerates. The less abundant spherical particles were <3 μm in diameter.

Comparable studies of the particle size distributions of fly ash from coal-fired boilers have been reported in numerous papers (*9*, *12–15*). Table II summarizes the particle size distributions from these studies. This table indicates no interdependence between MMAD and S_g, fly ash collector type, or efficiency. The total fly ash penetration through the ESP depends strongly on the particle size. McElroy (*14*) gives a penetration vs. aerodynamic particle size curve for the ESP of a 520-MW coal-fired boiler. Figure 4 presents a comparison between penetration and particle size in this and our study. The ESP studied by McElroy is clearly more efficient than the one in this study, and this moves the peak penetration toward smaller particle size (1.2 μm vs. 2–4 μm).

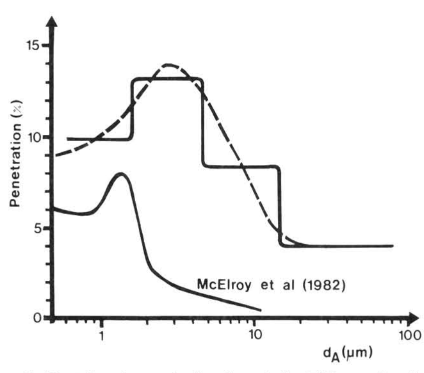

Figure 4. Peat fly ash penetration through the ESP as a function of particle size. Overall penetration varied 0.9–17% and averaged 6.1%, 61 samples before the ESP and 22 samples after it during a 96-h period.

Emissions of the 11 Elements. The concentrations of Ca, Fe, Mg, Mn, Co, Cu, Ni, As, Cd, Pb, and Zn in

Table III. Concentrations of 11 Elements of Peat in Ash

element	plant A mean, μg/g	plant A std deviation,[a] %	plant B mean, μg/g
Ca	59 000	13	40 000
Fe	90 000	8	62 000
Mg	11 000	4	5 300
Mn	2 100	19	600
Co	40	11	9
Cu	100		100
Ni	65	18	62
As	19	28	8
Cd	2	19	1
Pb	44	41	52
Zn	180	42	240

[a] Standard deviation is given as % of mean.

laboratory-ashed peat differed for the fuels of the two boiler plants; the fuels came from different bogs. Because several fuel samples were taken from plant A, and analyzed separately, both mean concentrations and their standard deviations can be given. They represent statistics of 5-h combined samples and are presented in Table III. The concentrations given for peat ash at plant B are means of two analyzed combined samples. They are also presented in Table III.

The above-mentioned 11 elements occur in peat mostly as oxides. In coal combustion many of these oxides evaporate partly and condense later on fly ash particles and boiler surfaces. The smallest fly ash particles possess the highest concentrations of these condensing elements. (*12, 14–20*).

Plant A. The maximum furnace temperature was 100–200 K lower than in common pulverized coal firing. Figure 5 presents the size-dependent emissions of the 11 elements before and after the ESP. For the nonvolatile (Fe, Ca, Mg, and Co) elements—the so-called matrix elements—the emission curves have the same shape as for the total fly ash emissions. Cu and Ni show slightly volatile behavior, and As, Cd, Pb, and Zn are volatile; i.e., they concentrate on the two smallest particle size fractions ($D_A < 4.6$ μm).

The enrichments of various elements in coal fly ash particles have been presented by Coles and co-workers (*19*). They defined the enrichment factor for element X for a given D_A as the concentration ratio of element X and Ce in fly ash particles of D_A divided by the same concentration ratio in coal. McElroy and co-workers (*14*) defined enrichment as the concentration ratio of element X and Fe in fly ash particles of D_A divided by the same concentration ratio for D_A = 10 μm. Because both Ce and Fe are matrix elements, Coles' and McElroy's enrichment factors are equal if Coles' enrichment factor for matrix elements is 1.0 for D_A = 10-μm particles. In fact, Coles' enrichment factors for matrix elements were (Mg excluded) 0.8–1.1 for D_A 6.0- and 18.5-μm particles.

We did not analyze Ce, so Fe was chosen for the reference element to keep the results as comparable as possible to those of Coles and McElroy. The enrichment factors in this study are computed for element X for given D_A as the concentration ratio of element X and Fe in fly ash of D_A divided by the same concentration ratio in laboratory ashed peat. This method lies between the ones used by Coles and McElroy.

Our enrichment factors before and after the ESP fly ash collector are presented in Table IV together with the enrichment factors given by Coles and co-workers (*19*), after the fly ash collector, and those computed from the data presented by McElroy and co-workers (*14*), before any fly

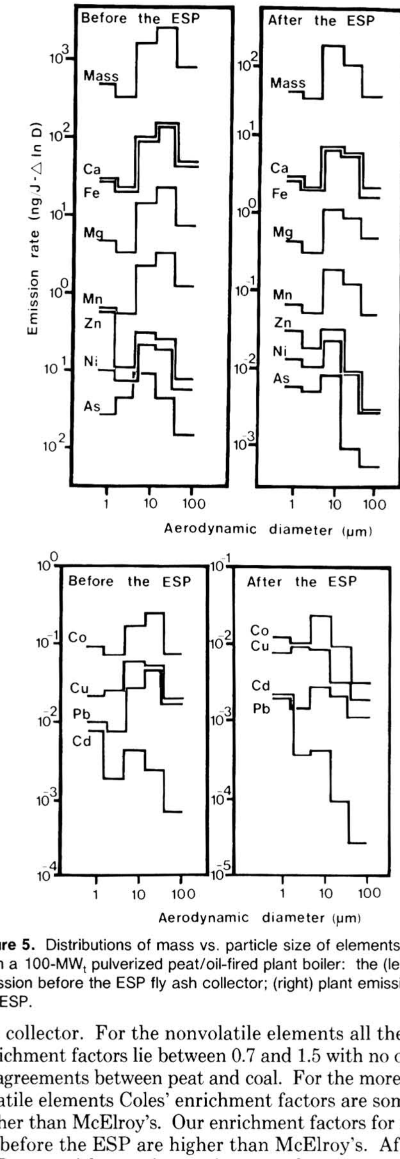

Figure 5. Distributions of mass vs. particle size of elements emitted from a 100-MW_t pulverized peat/oil-fired plant boiler: the (left) boiler emission before the ESP fly ash collector; (right) plant emission after the ESP.

ash collector. For the nonvolatile elements all the listed enrichment factors lie between 0.7 and 1.5 with no obvious disagreements between peat and coal. For the more or less volatile elements Coles' enrichment factors are somewhat higher than McElroy's. Our enrichment factors for As and Zn before the ESP are higher than McElroy's. After the ESP our enrichment factors for most elements are similar to those presented by Coles. No major disagreements appear between the two fuels and three studies. We conclude that the volatility of mineral elements in peat firing is similar to coal firing.

When comparing our enrichment factors before and after the ESP, one notices that the volatile elements for a given D_A are further enriched in the fly ash collector. This phenomenon is quite prominent for the strongly volatile As, Cd, Pb, and Zn in the two smallest particle size fractions, where the enrichment factors after the ESP are roughly twice the factors before it.

The amount of a condensing element that a given particle can collect in relation to its own mass is dominated by its surface-to-mass ratio; i.e., the smaller and more irregular the particle is, the higher its final concentration of, e.g., Cd will be. Fly ash from pulverized peat com-

Table IV. Enrichment Factors of 11 Elements vs. Aerodynamic Particle Size in Our Study of Peat Fly Ash and Two Studies of Coal Fly Ash

	D_A > 52, μm[a]		D_A = 15–52 μm[a]		MMAD = 18.5 μm[b]	D_A = 4.6–15 μm[a]		MMAD = 6.0 μm[b]	D_A = 3 μm[c]	MMAD = 3.7 μm[b]	D_A = 1.6–4.6 μm[a]		MMAD = 2.4 μm[b]	D_A = 1.0 μm[c]	D_A < 1.6 μm[a]		D_A = 0.3 μm[c]
	B[d]	A[e]	B	A	A	B	A	A	B	A	B	A	A	B	B	A	B
Ca[f]	1.5	0.97	1.4	1.2	0.9	1.5	1.2	0.9		0.9	1.4	1.3	0.9		1.3	1.1	
Mg[f]	1.4	1.7	1.2	1.2	0.5	1.3	1.2	0.6		0.6	1.3	1.2	0.6		1.3	1.1	
Mn[f]	1.3	0.82	1.0	0.91	0.8	1.1	1.2	0.8		1.0	1.2	1.1	1.2		1.0	0.98	
Co[g]	0.87	1.1	0.71	0.70	1.0	0.67	0.73	1.9		2.1	0.78	1.3	2.1		0.78	1.3	
Cu[g]	1.5	1.0	1.5	1.2	1.1	1.6	2.4	1.6		1.8	2.9	3.7	2.4		2.7	3.2	
Ni[g]	1.1	1.0	1.1	1.2	1.0	1.9	2.4	1.9	2.0	2.2	2.8	3.9	2.1	2.2	3.0	3.4	2.5
As[h]	1.5	1.0	1.4	0.63	1.2	4.5	4.7	4.0	1.7	7.0	9.6	10	11	2.0	4.1	8.1	3.5
Cd[b]	1.1	0.69	1.2	0.86	0.4	3.2	3.2	1.6		2.8	5.9	10	4.7		18	42	
Pb[h]	1.0	1.7	0.81	1.0	1.4	2.3	2.3	3.1		4.1	4.8	8.2	5.2		2.1	5.1	
Zn[h]	1.0	0.78	0.98	0.83	1.0	2.0	2.4	2.6	2.7	4.0	2.9	4.8	8.1	3.1		5.6	6.4

[a] This study enrichment factor = $([X]/[Fe])D_A/([X]/[Fe])_{\text{peat ash}}$. [b] Coles et al. (1982) enrichment factor = $([X]/[Ce])D_A/([X]/[Ce])_{\text{coal}}$. [c] McElroy et al. (1982) enrichment factor = $([X]/[Fe])D_A/([X]/[Fe])_{10\mu m}$. [d] B, Before the fly ash collector. [e] A, After the fly ash collector. [f] Matrix elements, litophilic behavior. [g] Intermediate elements. [h] Volatile, strong small particle association.

Table V. Emissions and Penetrations of 11 Elements in Pulverized Peat/Oil Combustion

	fuels		fly ash			penetration, %[a]	
	peat[b]	oil[c]	before ESP	after ESP	vapor phase	particulate	total
no. of samples	10		17	6	1 (24 h)		
total particulates, ng J^{-1}	3100	8–45	2900	170		6.0	6.1
Ca, ng J^{-1}	200		180	12	1.7	6.7	7.6
Fe, ng J^{-1}	260	0.1	170	12	0.7	7.1	7.6
Mg, ng J^{-1}	33	<0.1	27	1.9	0.2	7.0	7.8
Mn, ng J^{-1}	5.8	0.00	4.0	0.3	0.1	7.3	10
Co, pg J^{-1}	120	1.0	60	5.3	0.0	9.5	9.5
Cu, pg J^{-1}	310		330	39	49	12	27
Ni, pg J^{-1}	190	130	300	32	0.2	9.4	11
As, pg J^{-1}	60	0.45	110	11	0.1	9.9	10
Cd, pg J^{-1}	4.0	2.4×10^{-3}	8	1.7	0.0	21	21
Pb, pg J^{-1}	120	1.5	90	16.8	0.3	18	18
Zn, pg J^{-1}	460	4.5	620	65	250	10	51

[a] Computed from data after ESP vs. before ESP. [b] Concentration in peat ash is computed per joule of heat value and weighted by the portion of energy derived from peat during the sampling period (69%). [c] Concentration in oil ash is computed per joule of heat value and weighted by the portion of energy derived from residual oil during the sampling period (31%). Oil trace elements and other properties are obtained from the Technical Research Center of Finland.

Table VI. Emissions of 11 Elements in Milled Peat/Oil Combustion in FBC

	fuels		Fly ash after MC time-weighted average	vapor phase	penetration, %
	peat[a]	oil[b]			
no. of samples	2		15	1 (23 h)	
Ca, ng J^{-1}	76		23	0.3	30
Fe, ng J^{-1}	120	0.1	27	0.04	23
Mg, ng J^{-1}	10	0.1	2.7	0.3	25
Mn, ng J^{-1}	1.3	0.00	0.3		23
Co, pg J^{-1}	18	1.1	5.7		30
Cu, pg J^{-1}	190		63	4.3	33
Ni, pg J^{-1}	120	140	95		37
As, pg J^{-1}	15	0.5	11		
Cd, pg J^{-1}	2	0.003	5.4		
Pb, pg J^{-1}	106	1.6	94		
Zn, pg J^{-1}	470	5.0	5700[d]	116	

[a] See Table V (67%). [b] See Table V (33%). [c] Computed from time-weighted average emission vs. contribution of fuels. Due to the small number of fuel samples, smallest concentrations lead to impossible results. [d] Incomprehensible data; see text and figure.

bustion consists of spherical and irregular particles (see Figure 3A). The ESP collects spherical particles more efficiently than irregular ones, which is obvious from the theory of field charging and charged particle collection (*21*). Irregular particles are also more likely to re-entrain from the collector plates. As a result, the irregular particles in the fly ash are enriched in the ESP (see Figure 3A, B). Our conclusion is that the enrichment factors of the volatile elements are increased in the ESP within the smallest particle size fractions because of this phenomenon. Figure 6 presents the concentration of the most volatile studied element, Cd, in each particle size fraction before and after the ESP. As a result of the volatile element enrichment into the most penetrating particles, their penetrations are

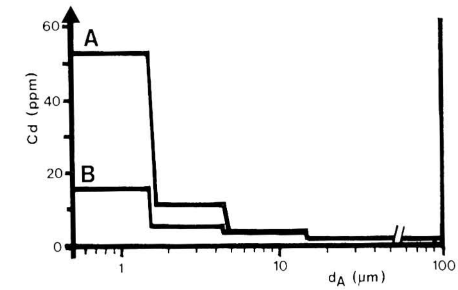

Figure 6. Concentration of Cd in each fly ash particle size category before (B) and after (A) the ESP (100-MW$_t$ pulverized peat/oil-fired boiler).

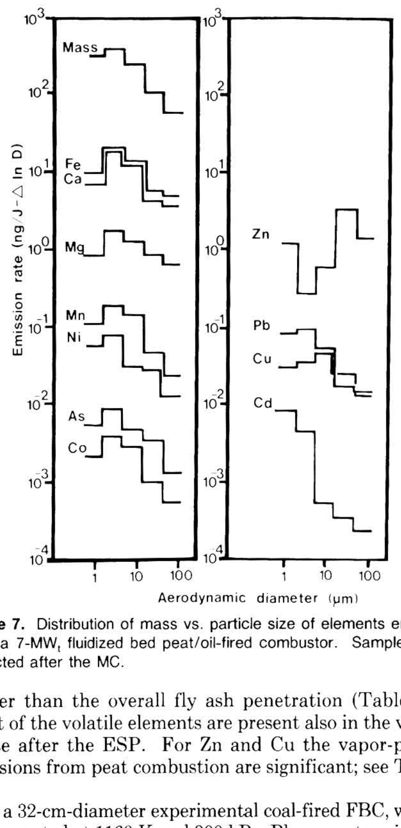

Figure 7. Distribution of mass vs. particle size of elements emitted from a 7-MW$_t$ fluidized bed peat/oil-fired combustor. Samples are collected after the MC.

higher than the overall fly ash penetration (Table V). Most of the volatile elements are present also in the vapor phase after the ESP. For Zn and Cu the vapor-phase emissions from peat combustion are significant; see Table V.

In a 32-cm-diameter experimental coal-fired FBC, which was operated at 1160 K and 900 kPa, Pb was not enriched, but Cd showed some enrichment (*22*). Little or no enrichment of volatile elements into the smallest particles was found in another small (46-cm-diameter) experimental coal-fired FBC, which was operated at 1070–1270 K and atmospheric pressure (*20*). Bi, Hf, and Pb were slightly enriched in 0.7–1.1-μm particles compared to 1.9–4.1-μm particles.

In our study of the FBC-fired plant B both Pb and Cd were enriched into the smallest particles, as can be seen from Figure 7. Both enrichments are much higher than found in the coal-fired FBC studies. The enrichments of other elements are either nonexistent or unclear because of our small number of samples. The stranger behavior of Zn (Table VI and Figure 7) cannot be explained from any data collected in this study or found in the literature. Zn seems to concentrate on the largest particles, and its total amount is increased by an order of magnitude from peat to fly ash. The abnormally high Zn emissions occurred during soot blowing. There is a possibility that large Zn-rich particles are entrained by corrosion from some combustor materials.

For Fe and Ca, the emission curve in Figure 7 is similar to the total mass except for the smallest particle size, where much of the particulate matter was presumably soot.

Acknowledgments

We gratefully acknowledge H. Lihtamo and T. Savolainen for their assistance in the collection and analyses of the samples. We also express our appreciation to the personnel of both power plants as well as the Department of Environment Hygiene at the University of Kuopio without whose assistance and cooperation this study could not have been accomplished.

Registry No. Ca, 7440-70-2; Fe, 7439-89-6; Mg, 7439-95-4; Mn, 7439-96-5; Co, 7440-48-4; Cu, 7440-50-8; Ni, 7440-02-0; As, 7440-38-2; Cd, 7440-43-9; Pb, 7439-92-1; Zn, 7440-66-6.

Literature Cited

(1) Lautkoski, R.; Pohjola, V.; Savolainen, I.; Vuori, S. Laboratory of Nuclear Power Technology, Report 55, Helsinki, 1980; 135 pp (in Finnish).
(2) Metso, J.; Niinistö, L.; Yliruokanen, I. *Kem. Kemi* **1976**, *3*(9), 409–412.
(3) Jantunen, M. J.; Lihtamo, H.; Itkonen, A.; Roponen, R. Department of Environmental Hygiene, University of Kuopio: Kuopio, Finland, 1981; 39 pp.
(4) Huttunen, S.; Karhu, M. Statens Naturvårdsverket Report 1495, Stockholm, Sweden, 1981; 104 pp.
(5) Rudling, L.; Löfroth, G. Statens Naturvårdsverket Report 1449, Stockholm, Sweden, 1981; 88 pp (in Swedish).
(6) Pohjola, V.; Hahkala, M.; Häsänen, E. Technical Research Centre of Finland, Research Reports 231, Helsinki, 1983; 125 pp, Appendix 131 pp (in Finnish).
(7) Jantunen, M. J.; Itkonen, A.; Lihtamo, H.; Savolainen, T. Ministry of Trade and Industry, Department of Energy, Series D:41, Helsinki, 1983; 69 pp (in Finnish).
(8) Yip, H. H.; Bengtsson, L.; Engström, F.; Lahtinen, S. "Proceedings of the 2nd World Congress of Chemical Engineering"; Montreal, Oct 4–9, 1981; pp 36–41, Vol II.
(9) Jantunen, M. J.; Itkonen, A.; Lihtamo, H.; Savolainen, T. Project Coal—Health-Environment Technical Report 53, Vällingby, Sweden, 1983; 44 pp.
(10) Hounam, R. F.; Sherwood, R. J. *Am. Ind. Hyg. Assoc. J.* **1965**, *26*, 122–131.
(11) O'Connor, D. T. Report AHSB (RP) R 108, United Kingdom Atomic Energy Authority, Harwell, Didcot, Berkshire, 1971; 11 pp.
(12) Ondov, J. M.; Ragaini, R. C.; Biermann, A. H. *Environ. Sci. Technol.* **1979**, *13*(8), 946–953.
(13) Carpenter, R. L.; Newton, G. J.; Rothenberg, S. J.; DeNee, P. B. *Environ. Sci. Technol.* **1980**, *14*(7), 854–859.
(14) McElroy, M. W.; Carr, R. C.; Ensor, D. S.; Markowski, G. R. *Science* **1982**, *215*(4528), 13–19.
(15) Shendrikar, A. D.; Ensor, D. S.; Cowen, S. J.; Woffinden, G. J.; McElroy, M. W. *Atmos. Environ.* **1983**, *17*(8), 1411–1421.
(16) Davison, R. L.; Natusch, D. F. S.; Wallace, J. R. *Environ. Sci. Technol.* **1974**, *8*(13), 1107–1113.
(17) Kaakinen, J. W.; Jorden, R. M.; Lawasani, M. H.; West, R. E. *Environ. Sci. Technol.* **1975**, *9*(9), 862–869.
(18) Lindberg, S. E.; Andren, A. W.; Raridon, R. J.; Fulkerson, W. *EHP, Environ. Health Perspect.* **1975**, *12*, 9–18.
(19) Coles, D. R.; Raganini, R. C.; Ondov, J. M.; Fisher, G. L.; Silberman, D.; Prentice, B. A. *Environ. Sci. Technol.* **1979**, *13*(4), 455–459.

(20) Natusch, D. F. S. *EHP, Environ. Health Perspect.* **1978**, *22*, 79–90.
(21) White, H. J. "Industrial Electrostatic Precipitation"; Addison-Wessley: Reading, MA, 1963.
(22) Murthy, K. S.; Howes, J. E.; Nack, H. *Environ. Sci. Technol.* **1979**, *13*(2), 197–204.
(23) Weissmann, S. H.; Carpenter, R. L.; Newton, G. J. *Environ. Sci. Technol.* **1983**, *17*(2), 65–71.

Received for review November 19, 1984. Accepted September 16, 1985. We are indebted to the Finnish Ministry of Trade and Industry and the Maj and Tor Nessling Foundation for the funding of this study.

Singlet Oxygen in Surface Waters. 3. Photochemical Formation and Steady-State Concentrations in Various Types of Waters

Werner R. Haag[‡] and Jürg Hoigné*

Swiss Federal Institute for Water Resources and Water Pollution Control (EAWAG), 8600 Dübendorf, Switzerland

■ For prediction of the rate with which organic compounds are oxidized and photoproducts formed in the aquatic environment by the $^1O_2$ route, the steady-state concentrations of $^1O_2$ in various waters were determined by using furfuryl alcohol as a trapping agent. Under noon, summer sunlight (Switzerland) in lake, river, and wastewaters, surface concentrations were $(0.3\text{–}3) \times 10^{-14}$ M $^1O_2$ per mg of DOC/L. The more highly colored waters actually tend to produce less $^1O_2$ for a given amount of adsorbed light. Separation of natural aquatic organic compounds by gel permeation chromatography resulted in fractions showing little correlation between $^1O_2$ production efficiency and molecular weight, indicating that large macromolecular structures are not a prerequisite for the sensitization of $^1O_2$ formation. Application of the specific $^1O_2$ concentration data to the estimation of lifetimes of environmental pollutants yields half-lives as short as several hours only for a few especially reactive types of compounds but orders of magnitude longer for most of the compounds expected to be found in the aquatic environment.

Introduction

Certain types of compounds become transformed in sunlight more rapidly in colored natural waters than in distilled water (*1–12*). One pathway by which this can occur is the reaction with electronically excited, singlet molecular oxygen ($^1O_2$), formed when dissolved organic materials absorb sunlight and transfer energy to dissolved oxygen (*1–3, 5–9*). Since $^1O_2$ is rapidly quenched back to the ground state by water, it is present only in low steady-state concentrations ($[^1O_2]_{ss} < 10^{-12}$ M) and only during sunshine (*1*).

In order to be able to predict the half-lives of organic compounds in the aquatic environment when they are determined by a $^1O_2$ reaction, knowledge of both the reaction-rate constant for $^1O_2$ with the specific compound and the concentration, $[^1O_2]_{ss}$, is required. At present neither area of knowledge is well established: (i) Although rate constants for reactions with $^1O_2$ have been determined for many compounds (*13*), the measurements were mostly performed in organic solvents, and the accuracy of these and their applicability to aqueous systems are limited. (ii) Although Zepp et al. (*1*) developed the fundamental concepts and a practical method for measuring $[^1O_2]_{ss}$, using 2,5-dimethylfuran (DMF) as a trapping agent, others (*2*) did not obtain comparable results.

In part 1 of this series of papers (*7, 8*), it was demonstrated that furfuryl alcohol (FFA) is a suitable and convenient $^1O_2$-selective trapping agent in natural waters. In the present study it was of interest to see what concentrations of $^1O_2$ might be expected in Swiss lake and river waters and to compare them with those determined in wastewater, seawater, and humic acid solutions. An effort was made to identify the molecular weight of the $^1O_2$-producing sensitizers by determining $[^1O_2]_{ss}$ on fractions of surface waters or humic acid solutions separated by gel permeation chromatography. An additional purpose was to see if the results reported by Zepp et al. (*1*) for surface waters, using DMF, could be verified in similar waters when FFA was used.

Theoretical Section

In an irradiated water sample, the processes of importance with respect to oxidation of an acceptor compound A by $^1O_2$ may be summarized by eq 1–4 where S and S*

$$S \xrightarrow[I_a]{h\nu} S^* \xrightarrow[\Phi^1O_2]{O_2} {}^1O_2 + S \qquad (1)$$

$$^1O_2 \xrightarrow{k_d} O_2 \text{ (physical quenching by } H_2O) \qquad (2)$$

$$^1O_2 + A \xrightarrow{k_q} O_2 + A \text{ (physical quenching by A)} \qquad (3)$$

$$^1O_2 + A \xrightarrow{k_r} \text{products (chemical reaction with A)} \qquad (4)$$

are the ground-state and excited-state sensitizer (the dissolved organics), respectively, I_a is the rate of sunlight absorption in einstein L^{-1} s^{-1}, and Φ^1O_2 is the quantum efficiency of $^1O_2$ production. (For further theoretical background see part 1 of ref 7 and Zepp et al. (*9*)). It should be noted that physical quenching of $^1O_2$ by A (eq 3) occurs for many compounds and does not lead to loss of A; only chemical reaction (eq 4) does. The rate of oxidation is then

$$-\frac{d[A]}{dt} = I_a\Phi^1O_2\left(\frac{k_r[A]}{k_d + k_A[A]}\right) \qquad (5)$$

where $k_A = k_r + k_q$.

From eq 5 it can be seen that, when $k_A[A] \ll k_d$, loss of A will be first order in A, given a constant light intensity and sensitizer concentration. On the other hand, when $k_A[A] \gg k_d$, loss of A will be zero order in A. For determinations of $[^1O_2]_{ss}$ (see below) it is important to limit the trapping agent to low enough concentration ($[A] = 0.1k_d/k_A$) to avoid repressing $[^1O_2]_{ss}$ and to keep the loss of A first order. For furfuryl alcohol, the upper concentration limit therefore is about 2×10^{-4} M, since $k_d = 2.5 \times 10^5$ s^{-1} (*14*) and $k_A = k_r = 1.2 \times 10^8$ M^{-1} s^{-1} (*7*). This is also often the practical concentration limit for compounds

[‡] Present address: SRI International, Menlo Park, CA 94025.

having a lower k_A when the oxygen concentration in water ($\sim 3 \times 10^{-4}$ M at 20 °C when equilibrated with air) should not be exceeded.

The rate of loss of acceptor may also be formulated as

$$-\frac{d[A]}{dt} = k_r[^1O_2]_{ss}[A] \quad (6)$$

If the illumination intensity is constant and $k_A[A] \ll k_d$, then $[^1O_2]_{ss}$ is also constant and may be calculated for substrates with known k_r values from the slope of a plot of log [A] vs. t, i.e., from k_{exptl}

$$-\frac{d[A]}{dt} = k_{exptl}[A] \quad (7)$$

$$[^1O_2]_{ss} = \frac{k_{exptl}}{k_r} \quad (8)$$

When solutes such as azide (N_3^-) or D_2O are added that increase or decrease, respectively, the overall quenching rate of $^1O_2$ (*13*), $[^1O_2]_{ss}$ is affected correspondingly,

$$[^1O_2]_{ss}' = \frac{k_d}{k'_d}[^1O_2]_{ss} \quad (9)$$

Here the superscript indicates conditions of added solute. The k'_d value can be calculated from $k^{D_2O}_d = 1.6 \times 10^4\ s^{-1}$ (*14*) and $k_{N_3^-} = 9 \times 10^8\ M^{-1}\ s^{-1}$ (*13*) (both constants are based on $k_d = 2.5 \times 10^5\ s^{-1}$). For mixed solvents the overall effects can be considered to be proportional to the mole fractions of the participating solvents.

Under sunlight, $[^1O_2]_{ss}$ varies over the course of a day since the incident light intensity varies. Thus, it is convenient to measure the exposure dose, D, in terms of energy per unit area over a broad wavelength band. Plots of log [A] are then linear not with time but with sunlight exposure dose, i.e.,

$$-\frac{d[A]}{dD} = k^D_{exptl}[A] \quad (10)$$

where k^D_{exptl} is the experimentally determined slope of a plot of log [A] vs. D. Dividing eq 6 by eq 10 and rearranging give

$$[^1O_2]_{ss} = \frac{k^D_{exptl}}{k_r} \cdot \frac{dD}{dt} \quad (11)$$

Thus $[^1O_2]_{ss}$ may be evaluated for any exposure dose rate (dD/dt, or sunlight intensity) from the measured k^D_{exptl} and known k_r. For our measurements we have chosen to use the maximum, noon, summer Swiss (47.5° N) sunlight intensity as the reference condition for dD/dt, and so all results are normalized to this value. We found this maximum, total sunlight intensity (280–2800 nm) at the water surface to be about 1000 W m^{-2}. Note, however, that absolute intensities need not be known for normalization to the reference condition since the calibration factor cancels out when multiplying k^D_{exptl} by dD/dt.

Experimental Section

Chemicals were as described previously (*7*). pH adjustments were made by using NaOH or phosphate buffers (normally 5 mM). Preparative gel permeation chromatography was performed by F. Fuchs at the Engler-Bunte-Institut in Karlsruhe, FRG, using a TSK-HW40(S) column and pH 7 phosphate buffer elution. For this purpose, he pretreated Greifensee water by passing it through a cation exchanger to convert salts to their H^+ form, by concentrating on a rotoevaporator, and desalting by electrodialysis (*15*). The DOC was measured on a Dohrman DC-80 Carbon Analyzer.

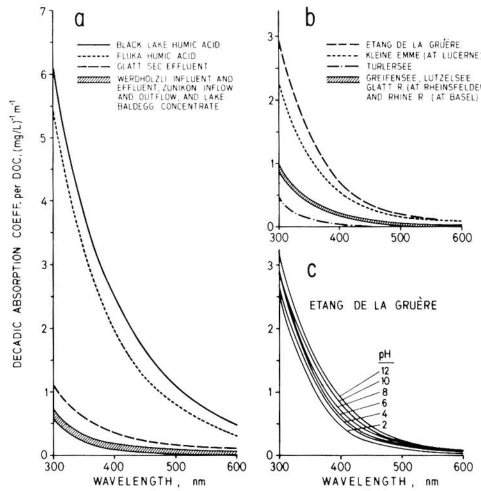

Figure 1. Absorption spectra of filtered waters used for $[^1O_2]_{ss}$ determinations: (a, b) waters at their natural pH, humics in pH 7 phosphate buffer; (c) water from Etang de la Gruère adjusted to various pH levels using NaOH or H_3PO_4.

Water Samples. Water sources with high DOC concentrations were chosen to maximize the observable effects. The lakes studied are eutrophic, pre-Alpine lakes; Etang de la Gruère is a humic-rich moor. The Long Island seawater had a salinity of 3.3%. The isolated humic acids and the Lake Baldegg DOC concentrate have been described previously (*7*).

The secondary effluent from the Wastewater Treatment Plant Glatt (City of Zürich) had undergone activated sludge treatment (partially nitrifying; average sludge age $\sim$3 days) including clarification but without iron precipitation. It was not filtered before use. The Werdhölzli Wastewater Treatment Plant's influent was taken following the preclarification step and treated in the laboratory with a nitrifying activated sludge (average sludge age also $\sim$3 days) to yield the equivalent of a secondary effluent. The Zünikon Waste Stabilization Pond serves a town of 120 people and has a surface capacity of about 15 m^2/person. There are no other significant water inputs to the pond, which is 1–2 m deep and has an average residence time of 40–50 days. It is also highly eutrophic.

Samples from lakes were normally taken from about 15 cm below the surface, filtered through 0.45-μm pore-size membranes, and stored at 4 °C in the dark. Storage and $[^1O_2]_{ss}$ measurements were performed at the natural water pH. The river waters were filtered through 8-μm pore-size membranes and used within a few days. Absorption spectra of the waters tested are given in Figure 1. Iron and manganese concentrations were measured in the lake waters by atomic absorption spectrometry and found to be $\leq$20 μg/L except for Etang de la Gruère, which had 120 μg/L iron (after filtration). Other water quality data are listed in Table I.

$[^1O_2]_{ss}$ measurements were based on eq 7, using FFA as the trapping agent. Water samples were made 10^{-4} M in FFA with minimal dilution, placed into a 1.5 cm i.d. × 25 cm quartz tube, stoppered, irradiated, and analyzed. No effort was made to avoid headspace since FFA is not volatile from water. Aliquots were removed at various time intervals and kept in the dark. No loss of FFA was observed in the dark or when irradiated in distilled water.

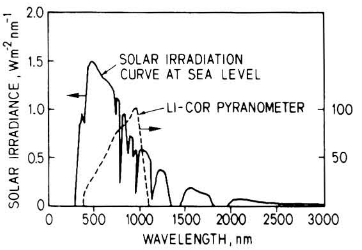

Figure 2. LI-200SB Pyranometer spectral response compared with the energy distribution in the solar spectrum (data supplied by the manufacturer).

FFA was quantitated by reverse-phase HPLC as described previously (*7*).

Irradiations were performed either in sunlight, on a rack that held the tubes at about 15° from the horizontal, or in a water-cooled merry-go-round reactor (MGRR) with a Hanau TQ 718 high-pressure Hg lamp filtered through solidex borosilicate glass. Although the output spectra of these two sources are not at all similar, a fairly consistent factor of 12.3 ± 2.4 (95% confidence limit) was found for the ratio of $[^1O_2]_{ss}$ in the MGRR to that in the sunlit tubes corrected for a flat water body in sunlight at 1000 W m^{-2} (for corrections of geometry effects, see below) for four different water samples (a lake water, a wastewater, and two humic acids). In both cases the temperature was 25 ± 5 °C. Sunlight intensity (in W m^{-2}) was estimated with a LI-COR Model LI-200SB pyranometer, which measures both direct and diffuse irradiation reaching a flat surface. Although the detector responds only to light of 400–1100 nm (see Figure 2), it is calibrated by the manufacturer using an Eppley PSP pyranometer to give total sunlight intensity (280–2800 nm).

For samples exhibiting a significant absorbance, the measured $[^1O_2]_{ss}$ value was converted to a surfce value, $[^1O_2]_{ss}{}^{\circ}$, by dividing by the light screening factor, S_λ (*6, 16*), given by

$$S_\lambda = (1 - 10^{-\alpha_\lambda l})/2.3\alpha_\lambda l \qquad (12)$$

where l is the light pathlength, taken to be 1.5 cm in the tubes, and α_λ is the decadic absorption coefficient of the water at the wavelength of maximum $^1O_2$ production in sunlight or the MGRR. The choice of wavelength was not of critical importance since the corrections were less than 30%.

Similarly, average concentrations assuming a well-mixed, upper layer of a natural water body were estimated by using

$$[^1O_2]_{ss}{}^{l} = S_\lambda[^1O_2]_{ss}{}^{\circ} \qquad (13)$$

whereby S_λ was calculated at 410 nm. This wavelength was found to give the best approximation when $[^1O_2]_{ss}{}^{l}$ was calculated independently from quantum yields as a function of wavelength for a few humic acids (*8*).

Results and Discussion

Tests for $^1O_2$ Intermediacy. Figure 3 gives the results of some kinetic tests for the intermediacy of $^1O_2$ in the photooxygenation of FFA in solutions of natural humic materials. The linearity of the semilog plots of residual [FFA] vs. time is in agreement with theoretical expectation (*9*) as presented above. The greatly reduced rates in both distilled and deoxygenated natural water demonstrate that both sensitizer and oxygen, respectively, are required for the reaction. The slight loss of FFA observed upon de-

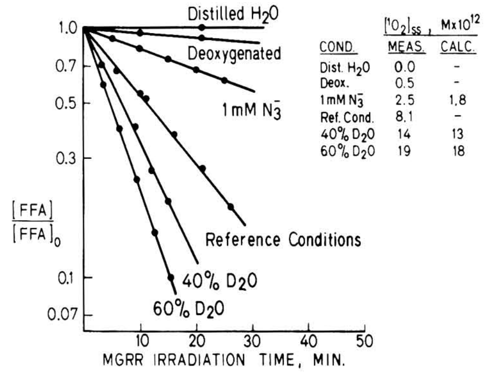

Figure 3. Loss of 10^{-4} M furfuryl alcohol sensitized by Fluka humic acid (DOC = 16 mg/L) at pH 7 irradiated in the MGRR. The distilled H_2O solution contained no humic acid, and the deoxygenated solution had been purged with N_2 for 25 min.

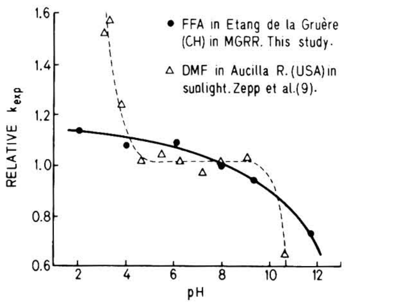

Figure 4. Effect of pH on the photooxygenated rates of FFA and DMF in natural waters. Relative rates within each system are defined as unity at pH 8.

oxygenation could be due to a direct reaction between FFA and humic acid triplets; however, this loss was not considered significant since O_2 exclusion was not rigorous. Azide ion and D_2O caused a decrease and increase, respectively, in the slopes by the amounts expected from eq 9, strongly supporting a $^1O_2$ mechanism. Product studies using Black Lake Humic acid as a sensitizer also support the intermediacy of $^1O_2$ (*7*). Similar results, i.e., the requirements of light, oxygen, and sensitizer and the formation of the same major HPLC product peak, were found in this study for natural waters in sunlight. Thus, the photooxygenation of FFA under visible and near-UV light in the presence of natural dissolved organics occurs predominantly via $^1O_2$.

Calibration of Geometry Effects. Sunlight photolysis rates measured in test tubes are greater than those for flat water bodies because of the lens effect of the curved glass walls and because tubes are exposed to light from all sides (*17*). Comparison of photooxygenation rates in tubes with those in bottom-blackened, flat, crystallizing dishes was made for three water samples that photooxygenated rapidly (which avoided evaporation of water or FFA). The dishes were set in a flat water bath with a water level equaling that of the solution inside the dishes. The resulting factor of 1.5 for the ratio of rates in tubes to rates in dishes was subsequently used to convert all results to those corresponding to flat water bodies. This factor is significantly lower than those observed by Dulin and Mill (*17*), also determined on solutions of low absorbance, but for direct photolyses.

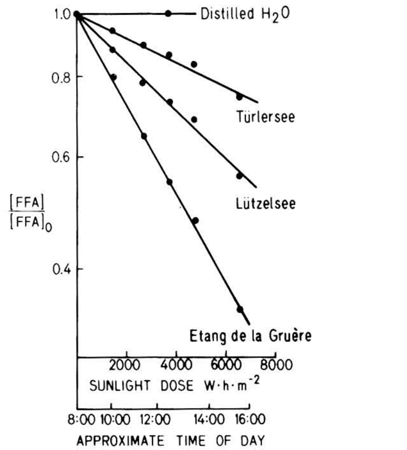

Figure 5. Sunlight photooxygenation of FFA in some lake waters in 1.5-cm-i.d. quartz tubes.

pH Effects. Figure 4 shows the effect of pH on the rate of photooxygenation of FFA in water from Etang de la Gruère. The results corroborate the conclusions of Zepp et al. (*9*) that despite noticeable increases in absorbance with increasing pH (see Figure 1c), $^1O_2$ concentrations are not significantly affected by pH in the natural water pH range. The fact that there are differences at the pH extremes between our results and those of Zepp et al. (*9*) suggests that the shape of the curves results from changes in sensitizing efficiencies of the dissolved organics rather than from effects common to all $^1O_2$ reactions, such as quenching of $^1O_2$ by OH^-. The waters used in the present study had pH values between 6.5 and 9.4.

$[^1O_2]_{ss}$ of Various Waters Exposed to Sunlight. *Natural Waters and Humics.* Figure 5 gives examples of first-order plots of FFA loss in natural waters as a function of sunlight exposure dose. The linearity of the plots over a wide range of sunlight intensities shows that simple photometric dosimetry is adequate and verifies the suggestion of Zepp et al. (*9*) that rate constants for sensitized reactions may be calibrated based on total sunlight (polychromatic) exposure dose measurements. This is presumably due to the fact that, unlike many direct photolyses, the action spectra of aquatic humics exhibit a rather broad overlap with the sunlight spectrum (*8, 9*), and therefore photooxygenation rates are insensitive to the relatively small changes in the solar spectrum (mostly near 300 nm) associated with daily and seasonal variations in the solar zenith angle. Correspondingly, we found little difference (±25%) between summer and winter rate constants for a given water sample when these were based on the total energy of the sunlight exposure dose measured photometrically. Furthermore, the constancy of the ratio of rates in the MGRR to those in sunlight (see Experimental Section) shows that even measurements using light sources with spectra considerably different from the sun can be used to predict rates of DOC-sensitized reactions in the environment.

Table I presents the results of some $^1O_2$ concentration measurements in various waters exposed to sunlight. The $^1O_2$-producing efficiencies of the different waters can be compared by normalizing to the DOC or absorptivity. This is possible because for a given water $[^1O_2]_{ss}{}^0$ is proportional to the concentration of its DOC, and therefore to absorbance, when these are varied by dilution of a given water. This is shown in Figure 6 and ref 9. The lack of decrease

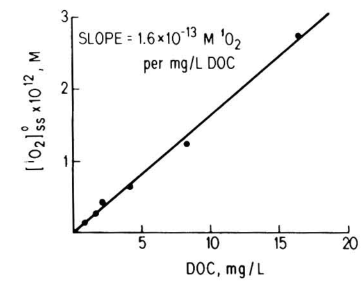

Figure 6. Maximum surface $[^1O_2]_{ss}$ under Swiss sunlight as a function of DOC, using humic acid from Black Lake, USA, buffered to pH 7. The data were normalized to a flat water body and corrected for light attenuation using the absorption coefficient at 410 nm (maximum of $^1O_2$ production by this humic acid in sunlight) and assuming a path length of 1.5 cm in the tubes.

in slope at high DOC values in Figure 6 demonstrates that quenching of $^1O_2$ by the DOC, if it occurs, is insignificant compared to quenching by water. Thus, the DOC itself does not affect the lifetime of $^1O_2$ even at the highest concentration (DOC = 16 mg/L) studied. The DOC-normalized values in Table I are a function of both the absorptivities and the quantum efficiencies of the dissolved organics, whereas the absorptivity-normalized values reflect the quantum efficiencies alone.

It may be pointed out that the DOC value of 13 mg/L for the Etang de la Gruère is among the highest found in Swiss natural waters, and therefore the corresponding surface $^1O_2$ concentration of 3×10^{-13} M can be considered an upper limit for Swiss waters. The high DOC-normalized values of the humic acids are due to their much greater absorptivities than natural waters (see Figure 1); their quantum efficiencies are about the same or slightly lower than those of natural waters (*6, 8*). For these humic acids, the good agreement between the measured values and those calculated from their independently determined quantum yields (*8*) confirms the validity of the present measurement method.

The results for natural waters show that while absorptivities (α_{366}) can vary considerably, DOC-normalized and absorptivity-normalized $[^1O_2]_{ss}$ values vary within a much smaller range. This results in the absorptivity being the dominant water quality parameter controlling the surface $^1O_2$ concentration. However, the absorptivity-normalized values and therefore the quantum efficiencies tend to be lower in the more colored waters. For example, the Türlersee has low absorptivity but a high quantum efficiency, whereas the Etang de la Gruère has a high absorptivity but a low quantum efficiency. This trend appears to be general: the data in Figure 7 show a similar tendency for the various U.S. waters studied by Zepp et al. (*1, 6, 18*). This effect cannot be due to quenching of $^1O_2$ by the DOC, as mentioned above, but may result from differences in the type of DOC or to small interferences by some other oxidative processes. It is notable that the waters that have relatively low absorptivity and high quantum efficiency are generally those whose DOC is of aquatic origin (autochthonous), whereas those with relatively high absorptivity and low quantum efficiency are more often associated with DOC of terrestrial origin.

Due to light attenuation, concentrations of $^1O_2$ can be orders of magnitudes greater at the surface than even at only 1 m depth. Therefore, in Table I (last column) the average $^1O_2$ concentration in an assumed mixed surface layer of 1 m depth is also presented (calculations based on eq 13). For most of the waters studied nearly all the

Table I. $[^1O_2]_{ss}$ in Various Waters Under Maximum, Noon, Summer Sunlight (~1000 W m^{-2}) in Switzerland (47.5° N)

water source	month taken	pH	DOC, mg/L	α_{366}, m^{-1}	measured $t_{1/2}$ FFA, h^{a}	$[^1O_2]_{ss}{}^{\circ} \times 10^{14}$ M^{a}	$[^1O_2]_{ss}{}^{\circ}$/DOC $\times 10^{14}$ M per mg/L^{a}	$[^1O_2]_{ss}{}^{\circ}/\alpha_{366}$ $\times 10^{14}$ M per m^{-1} ^{a}	$[^1O_2]_{ss}{}^{1m}$ $\times 10^{14}$ M^{a,b}	%A
prealpine eutrophic lakes										
Türlersee	7.83	8.5	8.3	0.8	24	6.7	0.8	8.3	4.4	61
Greifensee	10.82	8.4	3.5	1.1	20	8.0	2.3	7.4	4.6	71
Lützelsee	7.83	8.5	7.9	2.2	12	13	1.7	5.9	5.1	90
Etang de la Gruère	7.83	7.7	13	15.4	6^{d}	28^{d}	2.2^{d}	1.8^{d}	1.5	100
rivers^{c}										
Rhine (at Basel)	7.83	8.1	3.2	0.87	27	5.9	1.8	6.8	3.6	65
Kleine Emme (Emmenbr.)	7.83	8.2	3.2	2.9	16	10	3.2	3.4	2.7	97
Glatt (Rheinsfelden)	7.83	8.4	4.1	1.4	15	11	0.8	8.0	5.2	89
municipal wastewaters										
Glatt (secondary effluent)	11.83	7.3	8.6	4.2	11	14	1.1	3.3	2.7	99
Werdhölzli										
(influent)	4.84	7.8	31	8.1	15^{e}	11^{e}	0.3^{e}	1.4^{e}	0.8^{e}	100
(secondary effluent)	4.84	8.2	15	3.1	14^{e}	11^{e}	0.8^{e}	3.5^{e}	2.2^{e}	99
Zünikon Waste Stabilization Pond										
(inflow)	7.84	8.3	20	3.2	11	15	0.7	4.7	4.2	97
(outflow)	7.84	8.4	14.	3.0	13	12	0.9	4.0	3.4	97
seawater										
Long Island (USA)	7.83	7.7	≤1.5	0.28	≥70	≤2				
dyes (5 mg/L) in buffered distilled water										
rose bengal		8	1.2	44^{f}	0.009^{d}	14 000^{d}	12 000^{d}	320^{d,f}	140^{f}	100
methylene blue		8	3.0	106^{f}	0.006^{d}	20 000^{d}	6 700^{d}	190^{d,f}	80^{f}	100
isolated DOC										
Lake Baldegg concentrate		9.4					1.5^{d}	7.1^{d}		
Fluka humic acid		7					7.1^{d}	2.5^{d}		
Black Lake (USA) humic acid		7					16^{d}	5.4^{d}		
calculated from quantum yields (8) assuming no light attenuation										
Lake Baldegg concentrate		7					1.8	8.6		
Fluka humic acid		7					6.6	2.3		
Black Lake humic acid		7					17	5.6		
literature comparison										
Zepp et al. (*1*), surface and coastal waters		4.1–8.7	4–77	1.2–123		6–71^{g,h}	0.7–2.9^{g,h}	1.3–6.1^{d,g,h}		
Zepp et al. (*6*), surface waters and humic acids				25		25–94^{i}		1.0–3.8^{i}		
Zafiriou (*5*), coastal waters				0.3–1.2		1.6–3.8^{g,h,j}		2.8–7.1^{g,h,j}		
Wolff et al. (*2*), surface waters			8–21			0.4–7.6^{h}	0.22^{h}			

[a] Corrected to flat water body values using the factor 1.5. [b] Calculated using eq 12 and 13 with α_{410}. Values are percent of 410-nm light absorbed in 1 meter. [c] Switzerland. [d] Corrected for light attenuation. [e] Measured in the MGRR and converted to sunlight, flat water body values using the factor 12.3. [f] Using α_{λ} at the maximum in the visible wavelength region. [g] Normalized to flat water body values by dividing by an estimated factor of 2.0. [h] Measured using DMF, corrected in this work for the updated value of k_r for DMF (*7, 13*) ($k_r = 6.3 \times 10^8$ M^{-1} s^{-1}) by dividing by 1.6. Values correspond to a sunlight intensity of about 800 W m^{-2}. [i] Measured using DMF assuming $k_r = 7.8 \times 10^8$ M^{-1} s^{-1} and corrected for sunlight attenuation by the original authors. Values correspond to average yearly sunlight intensity at 40° N. [j] Sunlight intensity not given.

effective light is absorbed in this layer. Therefore, in contrast to surface $^1O_2$ concentrations, these depth-averaged concentrations are determined predominantly by the quantum efficiencies rather than absorptivities. The result is that highly colored waters that exhibit the highest $^1O_2$ surface concentrations actually tend to have the lowest concentrations averaged over a meter, since the quantum efficiencies decrease somewhat with absorptivity. Thus,

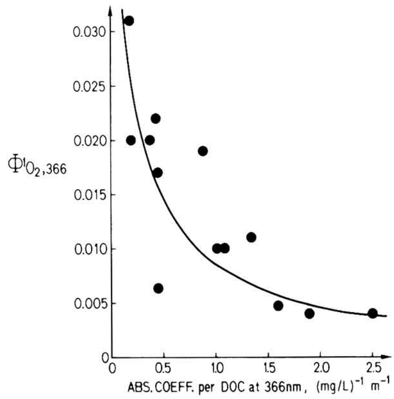

Figure 7. Quantum efficiencies of $^1O_2$ production as a function of absorption coefficient at 366 nm for various natural waters and humics. Data are taken from Zepp et al. (*1, 6, 18*).

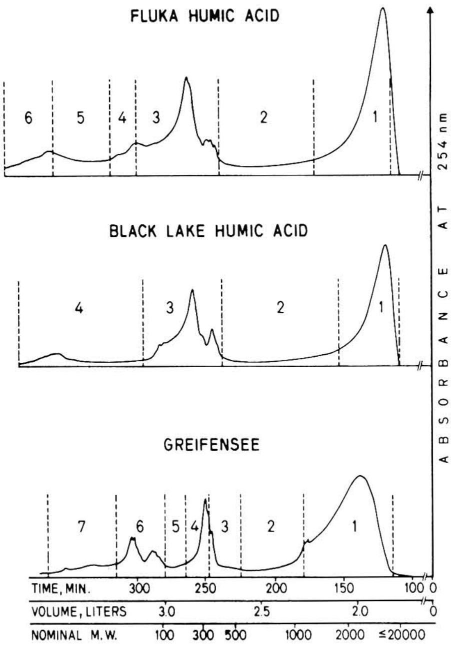

Figure 8. Preparative gel permeation chromatograms of various waters showing fractions collected (*15*).

comparing surface concentrations in different waters can give a distorted view of the relative importance of $^1O_2$ for the transformation of dissolved organics.

For practical purposes we are interested in quantifying the photochemical effect taking part over a given mixed depth in a water body (absorbing a significant portion of the light) rather than just at the surface. Although empirical measurements on samples of short optical path lengths exposed to sunlight (as are generally applied and are used here) are easy to perform and yield $^1O_2$ concentrations directly, they are of limited usefulness because they do not give the quantum yield information necessary for exact calculations of $[^1O_2]_{ss}$ as a function of depth, since the light is polychromatic. A better approach for this purpose would therefore be to measure absorbances and quantum yields for $^1O_2$ formation as a function of wavelength (*8*).

Wastewaters. Surprisingly, the highly absorbing wastewater samples gave surface concentrations of $^1O_2$ only similar to natural surface waters. In the Werdhölzli samples, the constancy of $[^1O_2]_{ss}$ before and after activated sludge treatment, which decreased the DOC value by a factor of 2, suggests that either $^1O_2$-producing organic material is present initially and is resistant to microbiological degradation or the materials present initially are weak $^1O_2$ producers and are being transformed to more active compounds. In either case, the average quantum efficiency appears to increase as a result of biological transformation, since the absorptivity decreases (along with the DOC) while $[^1O_2]_{ss}$ remains constant.

Organic Dyes as Sensitizers. The values for rose bengal and methylene blue were included in Table I as examples of organic dyes having very high absorptivities and quantum yields of $^1O_2$ production. Addition of such dyes and subsequent sunlight exposure has been suggested as a method of treating wastewaters (*19, 20*). While the concentrations of $^1O_2$ formed in sunlit wastewaters by themselves are adequate to remove only certain types of micropollutants, the concentrations generated upon addition of such dyes are considered by some authors to be sufficient to oxidize much of the DOC and destroy coliforms at reasonable rates (*19, 20*). (It should be noted here that the observed effects may be partly due to direct reactions with the excited-state sensitizer or to peroxides or radicals whose formation is only initiated by $^1O_2$.) However, questions of dye stability or of how to remove the dye following treatment (in the case of polymer-supported sensitizer) need clarification before this method can be considered further.

Comparison with Earlier Studies. The results of previous workers are summarized at the bottom of Table I for comparison. Note that except in one case (*6*), these authors did not correct the data to flat water body values (*21*) and used a k_r value for DMF that had been measured in methanol. Therefore we have adjusted the results assuming a typical flat water body correction factor of 2 (*17*) and the recently measured k_r for DMF in water (6.3×10^8 $M^{-1}\ s^{-1}$ (*7, 13*)) yielding $[^1O_2]_{ss}$ values about a factor of 3 lower than those originally published (*1, 2, 5*). The DOC- and absorptivity-normalized results of this study are in the same range as those found by Zepp et al. (*1, 6*) and Zafiriou (*5*), thereby reaffirming the validity of the DMF $^1O_2$ measurement technique. The Dutch waters studied by Wolff et al. (*2*) yielded significantly lower values than found in the Swiss or U.S. waters, but the former results are in some doubt because of a discrepancy in the oxygen and DMF consumptions. However, such lower values could also be expected if the highly eutrophic waters studied had undergone less biological transformations (see above).

Fractionation by Molecular Weight. In an initial attempt to gain some understanding of the types of compounds that might be responsible for sensitizing the formation of $^1O_2$, we measured the $^1O_2$-producing efficiencies of individual gel permeation chromatographic fractions of Greifensee water and Black Lake and Fluka humic acids. Figure 8 shows the chromatograms for the three waters indicating the fractions collected, and Table II gives the contribution of each fraction to the total $^1O_2$ production of a given water. Comparison of the sum of the contents of the individual fractions to those of the source waters shows that for the two samples of humic acids only 30% of the DOC was recovered. This only accounted for 20% of the total $^1O_2$-producing capacity. In contrast, for the

Table II. Contribution of Various Molecular Weight Fractions to Total DOC-Normalized $^1O_2$ Concentration in Various Waters Under Maximum, Noon, Summer Sunlight in Switzerland[a]

water source and fraction no. (Figure 8)	nominal MW	absorbance coeff. at 366 nm, (mg C/L)$^{-1}$ m^{-1}		C in fraction/C injected	$[^1O_2]_{ss}/\alpha_{366} \times 10^{14}$ M per m^{-1}	$[^1O_2]_{ss}$/DOC in fraction × 10^{14} M per mg/L	$[^1O_2]_{ss}$/total DOC, % of source water
Fluka humic acid							
1	≳20 000–1300	2.7		0.090	2.0	5.4	6
2	1300–480	0.9		0.037	4.1	3.5	1.5
3	480–100	1.6		0.088	5.4	8.6	9
4	<100	2.0		0.013	4.2	8.4	1.5
5	<100	1.5		0.022	3.6	5.4	1.5
6	<100	1.5		0.021	3.8	5.7	1.5
			total recovered	0.271			21
source water		2.8		1.00	2.9	8.1	100
Black Lake humic acid							
1	≳20 000–1700	2.5		0.094	3.6	8.9	5
2	1700–430	0.6		0.083	6.9	4.1	2
3	430–100	2.0		0.076	12	25	12
4	<100	0.8		0.061	6.4	5.1	2
			total recovered	0.314			21
source water		3.3		1.00	4.8	16	100
Greifensee							
1	≳20 000–1100	0.26		0.442	6.5	1.7	34
2	1100–540	0.24		0.067	7.1	1.7	5
3	540–370	0.25		0.040	6.0	1.5	3
4	370–230	0.24		0.051	8.8	2.1	5
5	230–100	0.16		0.029	11	1.7	2
6	<100	0.26		0.100	9.2	2.4	11
7	<100	0.29		0.072	10	3.0	10
			total recovered	0.801			70
source water		0.31		1.00	7.2	2.3	100

[a] Measured in the MGRR and converted to sunlight, flat water body values by dividing by 12.3. Includes corrections for light attenuation using the wavelengths of maximum $^1O_2$ production in the MGRR of 366 nm for Fluka, 410 nm for Black Lake, and 340 nm for Greifensee samples.

Greifensee water the 80% recovered DOC accounted for 70% of the total $^1O_2$ production. The fact that the DOC- and absorptivity-normalized values for the source waters lie in the ranges observed for the separate fractions indicates no major changes in $^1O_2$-producing abilities as a result of the chromatography.

The percentage contribution of the individual fractions is given in the last column in Table II. It was not possible to find a single molecular weight fraction that far outweighed the others in total $^1O_2$ production. The fractions in the molecular weight range 100–500 seemed to exhibit somewhat higher efficiencies (DOC- or absorptivity-normalized values), but this is counterbalanced by the fact that they did not contain a major portion of the total DOC. In the Greifensee water, the high molecular weight material contained a large portion of the DOC, but its efficiency was relatively low. One may nevertheless conclude that, because the low molecular weight material is as good or better at producing $^1O_2$ than is the high molecular weight material, macromolecular conformational structures are not important for the sensitization of $^1O_2$ formation by aquatic humus.

Application of Results. Once $[^1O_2]_{ss}$ has been measured and corrected for the depth of the mixed layer of a waterbody to be considered, eq 6 may be used to calculate the half-life (or rate of product formation) by the $^1O_2$ route of any compound for which k_r in water is known. This has been done in Table III, assuming $[^1O_2]_{ss} = 4 \times 10^{-14}$ M, the average value in the top meter of the natural waters studied here. It is important to use k_r rather than k_A in such computations since, as noted in the Theoretical Section, k_A includes physical quenching of $^1O_2$ by the substrate, which does not result in loss of substrate.

Table III. Comparison of the k_A and k_r Values Known for Compounds in Water[a] and Estimates of Sunlight Half-Lives by the $^1O_2$ Route Assuming $[^1O_2]_{ss} = 4 \times 10^{-14}$ M[b]

compound	k_A, M^{-1} s^{-1}	k_r, M^{-1} s^{-1}	$t_{1/2}$, h
9,10-dimethylbenzanthracene	6.3×10^9	6.3×10^9 [c]	0.8
bilirubin	4.3×10^9	7.5×10^8	6
2,5-dimethylfuran (DMF)	6.3×10^8	6.3×10^8	8
tyramine (pH 10)	2.8×10^8	2.4×10^8	20
imidazole (pH 7)	1.5×10^8	1.5×10^8 [c]	32
furfuryl alcohol (FFA)	1.2×10^8	1.2×10^8	40
azide ion	5×10^8	$\lesssim 10^8$	≳50
histidine (pH 8)	$\sim 10^8$	$\sim 10^8$ [c]	~50
methionine (pH 6–11)	$\sim 3 \times 10^7$	$\sim 3 \times 10^7$ [c]	~200
lysozyme (pH 6)	2×10^8	1×10^7	≥500
arginine, adenine, thymine	$\leq 10^6$		≥5000

[a] All kinetic data were taken from Wilkinson and Brummer (*13*) except for azide ion, which is from Lindig and Rodgers (*22*), bilirubin which is from Galliani et al. (*23*), and FFA which is from Haag et al. (*7*). All data were normalized to $k_d = 2.5 \times 10^5$ s^{-1} (14). [b] Mean value in the top meter of the surface waters presented in Table I. [c] Maximum value assuming $k_r = k_A$. For histidine and methionine this assumption is by analogy to the observations made in D_2O by Matheson and Lee (*24*).

Unfortunately, k_r in water is known for relatively few compounds (see Table III). Of the nearly 700 compounds for which rate data for reactions with $^1O_2$ were reviewed by Wilkinson and Brummer (*13*), only about 30 were measured in water, and of these, k_r are distinguished from

k_A in only 6 cases. In some of the other cases we can assume that $k_r \approx k_A$ by chemical analogy to compounds for which this is known to be true (such as small furans). But for other cases it must be assumed that k_r is much lower than k_A (mostly for large molecules). In addition, it is difficult to apply the data obtained in organic solvents to aqueous systems because the rates measured in different solvents can differ by orders of magnitude, the relative proportions of physical quenching and chemical reaction can be shifted, and some compounds will ionize in water, which affects their rates (*25*, *26*).

Nevertheless, one may conclude from the literature data that $^1O_2$ is such a selective oxidant that at the concentrations found in natural waters it will present an important degradation pathway for only a few types of compounds. Such compounds include those with specific structural components such as Diels–Alder reaction centers, those containing highly electron rich double bonds, or those having functional groups that are easily oxidizable, such as alkyl sulfides and thiones or some types of phenolate ions (*26*). However, this conclusion should not be taken to preclude that indirect phototransformations in natural waters can also involve other processes such as radical reactions or direct interactions between the substrate and excited state humics (*6*, *10–12*).

Acknowledgments

We wish to thank Martin Jekel and Friedrich Fuchs of the Engler-Bunte-Institute in Karlsruhe for performing the gel permeation chromatography. Our appreciation goes to Frank Scully, André Braun, and Richard Zepp for many discussions and for reviewing the manuscript. We thank limnologists H. Ambühl and R. Ribi for the light photometry measurements. Portions of this paper were presented at the Conference on Gas-liquid Chemistry of Natural Waters, Brookhaven National Laboratory, Upton, NY, 1984, and at the Fifth Conference on Water Chlorination: Environmental Impact and Health Effects, Willimsburg, VA, 1984.

Registry No. DOC, 7440-44-0; DMF, 625-86-5; FFA, 98-00-0; O_2, 7782-44-7; Rose Bengal, 11121-48-5; Methylene Blue, 61-73-4; 9,10-dimethylbenzanthracene, 58429-99-5; bilirubin, 635-65-4; tyramine, 51-67-2; imidazole, 288-32-4; histidine, 71-00-1; methionine, 63-68-3; lysozyme, 9001-63-2; arginine, 74-79-3; adenine, 73-24-5; thymine, 65-71-4.

Literature Cited

(1) Zepp, R. G.; Wolfe, N. L.; Baughman, G. L.; Hollis, R. C. *Nature (London)* **1977**, *267*, 421–423.
(2) Wolff, C. J. M.; Halmans, M. T. H.; van der Heijde, H. B. *Chemosphere* **1981**, *10*, 59–62.
(3) Baxter, R. M.; Carey, J. H. *Freshwater Biol.* **1982**, *12*, 285–292.
(4) Ross, R. D.; Crosby, D. G. *J. Agric. Food Chem.* **1973**, *21*, 335–337.
(5) Zafiriou, O. C. In "Chemical Oceanography"; Riley, J. P., Chester, R., Eds.; Academic Press: London, 1983, pp 339–379, Vol. 8.
(6) Zepp, R. G.; Schlotzhauer, P. F.; Sink, R. M. *Environ. Sci. Technol.* **1985**, *19*, 74–81.
(7) Haag, W. R.; Hoigné, J.; Gassmann, E.; Braun, A. M. *Chemosphere* **1984**, *13*, 631–640.
(8) Haag, W. R.; Hoigné, J.; Gassmann, E.; Braun, A. M. *Chemosphere* **1984**, *13*, 641–650.
(9) Zepp, R. G.; Baughman, G. L.; Schlotzhauer, P. F. *Chemosphere* **1981**, *10*, 119–126.
(10) Mill, T.; Hendry, D. G.; Richardson, H. *Science* **1980**, *207*, 886–887.
(11) Draper, W. M.; Crosby, D. G. *J. Agric. Food Chem.* **1981**, *29*, 699–702.
(12) Skurlatov, Y. I.; Zepp, R. G.; Baughman, G. L. *J. Agric. Food Chem.* **1983**, *31*, 1065–1071.
(13) Wilkinson, F.; Brummer, J. G. *J. Phys. Chem. Ref. Data* **1981**, *10*, 809–999.
(14) Rodgers, M. A. J.; Snowden, P. T. *J. Am. Chem. Soc.* **1982**, *104*(20), 5541–5543.
(15) Fuchs, F.; Raue, B. *Vom Wasser* **1981**, *57*, 95–106.
(16) Zepp, R. G. In "The Handbook of Environmental Photochemistry"; Hutzinger, O., Ed.; Springer-Verlag: Berlin, 1982; pp 19–41, Vol. 2, Part B.
(17) Dulin, D.; Mill, T. *Environ. Sci. Technol.* **1982**, *16*, 815–820.
(18) Zepp, R. G.; Schlotzhauer, P. F. *Chemosphere* **1981**, *10*, 479–486.
(19) Acher, A. J.; Rosenthal, I. *Water Res.* **1977**, *11*, 559–562.
(20) Acher, A. J.; Juven, B. I. *J. Appl. Environ. Microbiol.* **1977**, *33*, 1019–1023.
(21) Zepp, R. G., U.S. Environmental Protection Agency, Athens, GA, personal communication, 1984.
(22) Lindig, B. A.; Rodgers, M. A. J. *Photochem. Photobiol.* **1981**, *33*, 627–634.
(23) Galliani, G.; Manitto, P.; Monti, d. *Isr. J. Chem.* **1983**, *23*, 219–222.
(24) Matheson, I. B. C.; Lee, J. *Photochem. Photobiol.* **1979**, *29*, 879–881.
(25) Sluyterman, L. A. *Recueil Trav. Chim. Pays-Bas* **1961**, *80*, 989–1002.
(26) Scully, F.; Hoigné, J. Swiss Federal Institute for Water Resources and Water Pollution Control (EAWAG), Dübendorf, Switzerland, 1984, submitted for publication, 1986.

Received for review December 21, 1984. Accepted September 3, 1985. This work was supported in part by the research foundation of the chairman of the board of the Swiss Federal Institute of Technology (Project: Abiotic Photolytic Oxidations in Natural Waters).

A Unified Physicochemical Description of the Protonation and Metal Ion Complexation Equilibria of Natural Organic Acids (Humic and Fulvic Acids). 1. Analysis of the Influence of Polyelectrolyte Properties on Protonation Equilibria in Ionic Media: Fundamental Concepts

Jacob A. Marinsky* and James Ephraim

Chemistry Department, State University of New York at Buffalo, Buffalo, New York 14214

■ The high sensitivity of the potentiometric properties of weakly acidic polyelectrolytes (gel or linear) to medium ionic strength has been quantitatively explained. Advantage can be taken of this highly useful assessment to facilitate a valid physical chemical description of protonation phenomena encountered with natural organic polyacids such as humic and fulvic acids.

I. Introduction

Elucidation of the protonation properties of humic substances is complicated by two factors, their polymeric nature and their heterogeneity. The first of these is responsible for the strong dependence of their potentiometric properties on the neutral salt concentration level of the aqueous medium. The second is due only to the presence of a mixture of functional groups of different acid strength in a typical humic substances molecule.

In order to be able to quantify the acidic properties of a particular humic substance, the contribution of each factor to the observed potentiometric properties must be separated. The only possible way to accomplish this is through a capability for assessing accurately the contribution of polymeric properties to the potentiometric properties measured experimentally. Once this is accomplished the heterogeneity factor, which is unaffected by the neutral salt concentration level, is accessible for refinement through specific heterogeneity estimates.

In the various attempts that have been made to model the proton binding by humic substances, this need for separate consideration of the polyelectrolyte effect prior to consideration of the effect on hydrogen binding exerted by the presence of a mixture of acidic groups of different acid strength has not been appreciated. Indeed, in most of the models accommodation of the observed properties is sought in only one of the two factors.

For example, in the site-binding model, one of the several most often employed, intrinsic pK values and abundances are assigned to the smallest number of monoprotic acids that reproduce the potentiometric data (*1–4*). However, because of neglect of electrolyte concentration effects, the parameters so obtained are not applicable to data obtained at salt concentration levels different from those used in their studies.

In other attempts to interpret the potentiometric behavior of humic substances continuum models have been applied. In this approach polyelectrolyte perturbations become an intrinsic component of the distribution function (*5–9*). The existence of a continuum of binding sites that is implied in these distribution models is believed by us to overestimate the complexity of the problem as well. In nature there is the tendency to resist the statistical, undirected distribution of structural components in the course of the development of a product. There are vectors (e.g., environmental) that influence the path to the eventual natural product. This natural course must limit somewhat the site distribution in humic substances to narrower boundaries than provided by the continuum approach. The fact that there are differences between humic substances from different sources (aquatic, marine, soil) is attributable to the environmental vectors alluded to above.

Finally in the third kind of model (*9–18*) generally employed all deviations are attributed to the polyelectrolyte nature of the humic substances. However, Posner (*17*), as early as 1964, recognized that this kind of model could not account for the effect of ionic strength on the potentiometric properties. He correctly concluded that the observed potentiometric properties were additionally complicated by the presence of different acidic functional groups in the humic substances molecule.

It is the purpose of this paper to present the carefully documented basis, already developed (*19*), for a well-defined experimental approach to the quantitative separation of the contribution of simple neutral salt concentration levels to the potentiometric properties of the weakly acidic polymer substances. This earlier research led to the development of procedures for determining the flexibility and salt permeability characteristics of such substances. Methods have also been developed to use such characterization of weakly acidic polymeric substances for quantitative estimate of their effect, as a function of excess salt, on the computed values of the apparent pK at any degree of neutralization. These methods, described in the course of their documentation in the text that follows, have been shown to be applicable to fulvic acids (*20*).

II. Fundamental Concepts

In the development of this section of the manuscript the two different properties, salt permeability and salt impermeability, assignable to weakly cross-linked gels are discussed and analyzed. The sensitivity of potentiometric properties to electrolyte concentration levels as a consequence of electrolyte penetration or repulsion by the matrix and the method for identifying experimentally which of the two matrix properties is applicable to the particular polymeric substance under investigation are then presented. Finally all the concepts and procedures shown to be applicable to the cross-linked weakly acidic polyelectrolyte gels are demonstrated to be equally applicable to their linear analogues as well. This result documents the applicability of all concepts developed to any charged polymeric molecule no matter whether its existence in the system as a separated phase is physically discernable or not.

A. Sensitivity of the Potentiometric Properties of Weakly Acidic Gels to the Presence of Neutral Salt. *1. Salt-Permeable Matrix.* The Donnan model and its use in the development of the concepts under discussion in this section of the manuscript have been presented in great detail in earlier publications (*19, 21–24*) by one of us (JAM). As a consequence only its essential features are outlined in the presentation that follows: Consider the disposition of diffusible components, MX and HX, be-

0013-936X/86/0920-0349$01.50/0

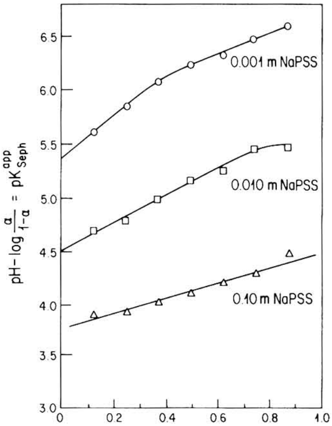

Figure 1. Potentiometric properties of the flexible Sephadex CM50-120 gel measured at three different sodium polystyrenesulfonate concentration levels (Donnan potential term neglected).

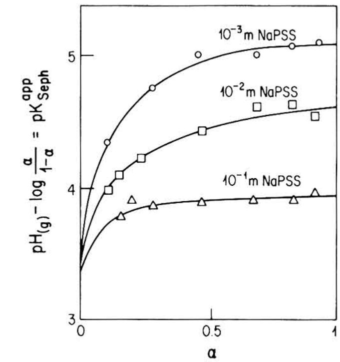

Figure 2. Potentiometric data of Figure 1 analyzed with Donnan potential term.

tween solution and gel phases during each step of the potentiometric titration of a weakly acidic (or weakly basic) gel, $(HA)_\nu$, in the presence of simple electrolyte, MX. With equilibrium established during each step of the neutralization the chemical potential, μ, of each component is identical in both phases over the course of the titration with standard base. By choosing the standard state of each component to be the same in both phases, as well, the equilibrium distribution of HX and MX between the two phases is expressed by eq 1 given: In this equation π is

$$\ln\left[(a_{HX}\bar{a}_{MX})/(\bar{a}_{HX}a_{MX})\right] = \frac{\pi}{RT}(V_{HX} - V_{MX}) \quad (1)$$

the osmotic pressure of the water component in the gel phase; V and a refer, respectively, to the partial molar volume and activity associated with HX and MX; and the bar, placed directly above the a, is used to identify the gel phase. Since the term $\pi/RT(V_{MX} - V_{HX})$ is very small even in highly constrained gels (when π = 200 atm, $V_{MX} - V_{HX}$ = 0.0012 L, with the employment of a Na^+ salt and $(\pi/RT)(V_{MX} - V_{HX})$ is <0.005 at room temperature (*25*)), eq 1 may be simplified as shown without introduction of significant error

$$\log\left(a_{HX}\bar{a}_{MX}/\bar{a}_{HX}a_{Mx}\right) = 0 \quad (2)$$

By cancelling the activity, a_{X^-}, of the common coion, X^-, in eq 2 the following useful equation is obtained:

$$pH - pM = p\bar{H} - p\bar{M} \quad (3)$$

In the examination of potentiometric data obtained for the kind of system under discussion it is standard procedure to plot the apparent pK, evaluated with the Henderson–Hasselbalch equation given below, vs. α, the degree of dissociation,

$$pH - \log\frac{\alpha}{1-\alpha} = pK^{app}{}_{(HA)_\nu} \quad (4)$$

Such treatment of potentiometric data results in the automatic inclusion of the Donnan term, pM − p$\bar{M}$, in the computed value of $pK^{app}{}_{(HA)_\nu}$. As a consequence the apparent pK is a sensitive function of the ionic strength of the system under examination, plots of $pK^{app}{}_{(HA)_\nu}$ vs. α tending to separate as shown in Figure 1. As the concentration level of M^+ is decreased from 0.10 to 0.010 and 0.0010 M the curves are displaced upward.

The validity of this interpretation of the displacement of apparent pK with ionic strength has been documented in our earlier studies (*22–24*) by showing that the intrinsic pK of the repeating functional unit of a weakly acidic gel (e.g., Sephadex (carboxymethyldextran) and a cross-linked polymethacrylic acid gel) is resolved by use of the gel-phase p$\bar{H}$ in the Henderson–Hasselbalch equation

$$p\bar{K}^{app}{}_{(HA)_\nu} = p\bar{H} - \log\frac{\alpha}{1-\alpha} =$$
$$pH + p\bar{M} - pM - \log\frac{\alpha}{1-\alpha} = pK^{app}{}_{(HA)_\nu} + (p\bar{M} - pM) \quad (4a)$$

Only the values of pH and pM were experimentally accessible, while the value of p$\bar{M}$ had to be computed to achieve this documentation. The method for accomplishing this has been detailed in an earlier paper (*22*) as well. For each molecular unit of HA dissociated one molecule of positive ion must be accessible to the gel phase to preserve its electroneutrality. Since $\bar{M}^+ \gg \bar{H}^+$, the total quantity of $\bar{M}^+$ in the gel phase can be taken to be essentially equal to the quantity of acid dissociated in the course of its neutralization with standard base. With measurement of the gel-phase water content at each point of the neutralization the molality of $\bar{M}^+$ becomes calculable.

By substituting $p\bar{C}_M$ for p$\bar{M}$ in eq 4a to permit reanalysis of the data presented for the very flexible Sephadex CM-50-125 through plots of $p\bar{K}^{app}{}_{(HA)_\nu}$ vs. α at the three different ionic strength levels employed, the three separated curves in Figure 1 are replaced by three curves that converge to a common point as α approaches zero (Figure 2). This dependence of $p\bar{K}^{app}{}_{(FA)_\nu}$ on α at different ionic strength levels is duplicated by carboxymethyldextran, the gel's linear polyelectrolyte analogue, in Figure 3, the curves converging once again to the same common point (*26*). This property of convergence to a common point as α approaches zero is attributable to removal of charge from the polymeric molecule surface as α approaches zero. If one presumes all nonideality to be attributable to the potential field emanating from the charged surface of the molecule the common point of convergence, 3.3 ± 0.05, at α = 0 in Figures 2 and 3 corresponds to the intrinsic pK of the repeating monomer unit. Compelling support for this analysis of Figures 2 and 3 comes from the fact that a pK of 3.3 is reported in the literature for methoxycarboxylic acid, the weakly acidic molecule that resembles very closely the acidic unit repeated throughout the car-

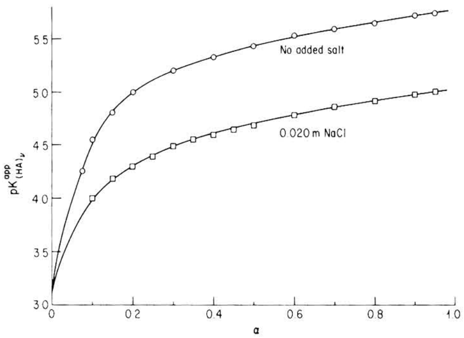

Figure 3. Dependence of potentiometric properties of carboxymethyldextran, the linear polyelectrolyte analogue of Sephadex, on salt medium concentration (*26*).

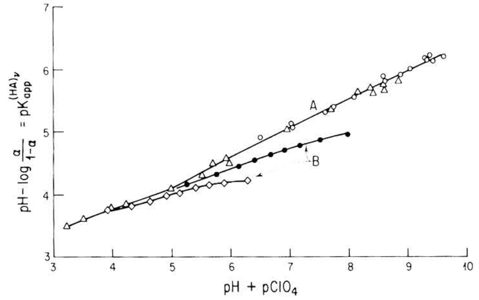

Figure 4. (A) Uniqueness of the $pK^{app}{}_{(HA)_\nu}$ function plotted vs. ($pH + pClO_4$) using potentiometric data obtained with the rigid Sephadex Gel (CM-25) over a $NaClO_4$ concentration level ranging from (△) 0.0010 to (O) 0.10 M. (B) Removal of the $pK^{app}{}_{(HA)_\nu}$ function uniqueness in a flexible Sephadex gel (CM-50): (●) 0.010 M $NaClO_4$ (◇) 0.10 M $NaClO_4$.

boxymethyldextran molecule (*27*).

a. Implications of the Donnan Model. If the gel is *rigid* and if the concentration of M^+ in the gel phase is *much greater* than its concentration in the solution phase $\bar{C}_M$ has to be a uniquely defined quantity at each α value encountered no matter what the neutral salt (MX) concentration level is. As α approaches zero the accompanying reduction in $\bar{C}_{M^+}$ has to result eventually in some dependence of $\bar{C}_{M^+}$ on ionic strength at the reduced α values. However, over the α range where uniqueness of $\bar{C}_{M^+}$ prevails the $\bar{C}_{H^+}$ must also be uniquely defined at each α value by the free energy of dissociation of the repeating acidic units. As a consequence $p\bar{H} - p\bar{M}$ is independent of the external neutral salt concentration level as long as $\bar{C}_M \gg C_M$ and the gel is rigid. The consequence of this is that plots of $pK^{app}{}_{(HA)_\nu}$ vs. α at two different salt concentration levels, 1 and 2, are displaced from each other by $pX_1 - pX_2$, in two separate potentiometric examinations of the neutralization of a rigid, weakly acidic gel with standard base.

Most important, however, is the fact that a plot of $pK^{app}{}_{(HA)_\nu}$ vs. (pH + pX) will provide unambiguous evidence for a *rigid* gel matrix that is *permeable* to diffusible components (HX, MX, and H_2O) when the salt concentration level is varied over a range in which $\bar{C}_M > C_M$. When these conditions are met the single unique curve that is resolved is unaffected by the presence of different quantities of salt in the system.

Such a plot of potentiometric data obtained with the rigid Sephadex CM-25 at several different concentration levels of $NaClO_4$ (0.10–0.0010 M) uniquely resolves the top curve presented in Figure 4 to illustrate this.

The two lower curves of Figure 4 show that with the highly flexible C-50 Sephadex gel the uniqueness of the plot is lost, the data obtained at each ionic strength yielding curves that eventually separate as the neutralization reaction proceeds.

2. *Salt-Impermeable Matrix.* One can expect Poisson–Boltzmann statistics, used as shown in eq 5a and 5b given below, to express accurately the effective concentration of counterions at the surface of the matrix of a salt-impermeable gel. In these equations

$$(\vec{M}^+) = (M^+)\exp(-\epsilon\psi_{(a)}/kT) \quad (5a)$$

$$(\vec{H}^+) = (H^+)\exp(-\epsilon\psi_{(a)}/kT) \quad (5b)$$

the symbol → placed above the letter representation of H^+ and M^+ identifies the effective concentration of these counterions at the charged gel surface relative to their effective average macroscopic concentrations measured potentiometrically; ϵ represents the unit charge of the ion; $\psi_{(a)}$ corresponds to the potential at the surface of the charged gel molecule; k is Boltzmann's constant; and T is the absolute temperature of the system. At equilibrium the ratio of the activities of H^+ and M^+ in the solution is equal to their ratio at the surface of the gel

$$\frac{(\vec{M}^+)}{(\vec{H}^+)} = \frac{(M^+)\exp(-\epsilon\psi_{(a)}/kT)}{(H^+)\exp(-\epsilon\psi_{(a)}/kT)} = \frac{M^+}{H^+} \quad (6)$$

and eq 3 applies once again

$$pH - pM = p\vec{H} - p\vec{M} \quad (3a)$$

In a rigid, salt-impermeable gel the value of $\vec{M}^+$ is uniquely defined at each α value as it is in the rigid salt-permeable gel. This in turn uniquely defines $\vec{H}^+$ as before, since the free energy of dissociation of the functional units that constitutes the rigid gel matrix cannot be a variable function of X in the constant environment of the molecular surface. As a consequence the uniquely defined ratio of $(\vec{M}^+)/(\vec{H}^+)$ must also be mimicked in the aqueous solution with the salt-impermeable gel, as long as $(\vec{M}^+)$ is equal to or greater than (M^+). When $(\vec{M}^+)$ becomes equal to or smaller than M^+ as α approaches zero the $(\vec{M}^+)/(\vec{H}^+)$ ratio can no longer control the $(\vec{M}^+)/(H^+)$ ratio in solution. In this instance the charge on the surface of the molecule has to be close to zero, and $(\vec{H}^+)$ approaches (H^+) in value.

a. Implications. On the basis of the above analysis potentiometric data compiled during neutralization of a rigid, weakly acidic, salt-impermeable gel with standard base should yield $pK^{app}{}_{(HA)_\nu}$ vs. α plots separated by the logarithmic ratio of the ionic strength employed in each potentiometric examination just as is observed with the salt-permeable gels.

In addition, plots of $pK^{app}{}_{(HA)_\nu}$ vs. pH should, in the salt-impermeable case, provide a unique description of the system that is independent of the concentration level of salt employed.

That this is indeed the case has been shown by the important research of Paterson and Rahman (*28*). In their investigation of the anionic capacity of crystalline analogues of hydrous oxides they have found, for example, that the Cl^- capacity of β-FeOOH is a single-valued function of (pH + pX) when the neutral salt employed is NaCl but becomes a single functional value of pH alone when $NaClO_4$ is used to vary the ionic strength of the system. In the presence of $NaClO_4$, the anion exchange capacity becomes uniquely pH dependent because perchlorate ion is excluded by its size from entering the pore structure of the β-FeOOH.

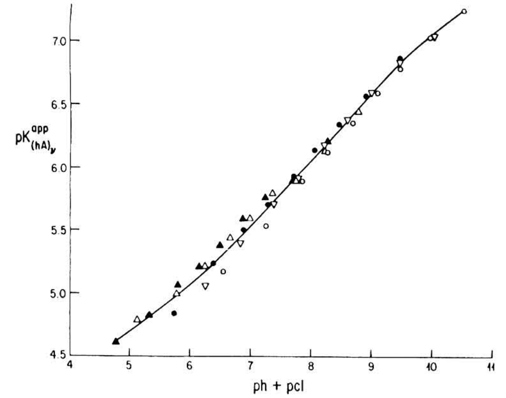

Figure 5. Apparent pK values obtained for poly(acrylic acid) at five different sodium chloride concentrations plotted vs. (pH + pCl). The $pK^{app}_{(HA)_\nu}$ values are interpolated from the potentiometric titration curves presented in Figure 4 of ref 29. NaCl concentrations (O) 0.00500, (▽) 0.0100, (●) 0.0200, (△) 0.0500, and (▲) 0.100 N.

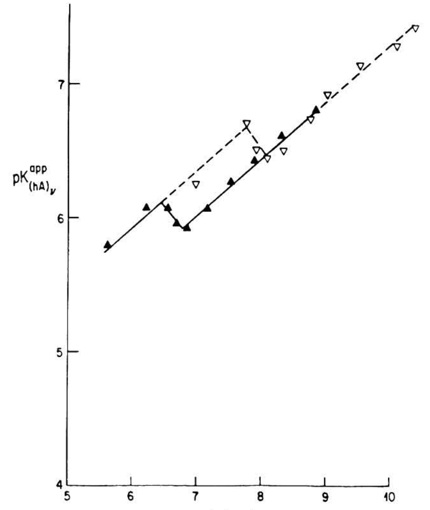

Figure 6. Apparent pK values obtained for isotactic poly(methacrylic acid) in (▲) 0.100 and (▽) 0.0100 N NaCl plotted vs. (pH + pCl). The pK^{app} values are interpolated from the potentiometric titration curves presented in Figure 5 of ref 29.

III. Application of Fundamental Concepts

The fact that potentiometric data obtained with weakly acidic (basic) gels yield apparent pK values that are either uniquely a function of (pH + pX) when the gel is rigid and permeable to simple salt or uniquely a function of pH alone when rigid and impermeable to simple salt is of sizeable importance and value. Its importance and value are remarkably magnified, however, by the fact that these criteria can be usefully applied to the examination of potentiometric data obtained with the linear polyelectrolyte analogues of their weakly acidic (basic) cross-linked gels. This result, published earlier (*19*), is summarized briefly below in Figures 5–10. In these figures $pK^{app}_{(HA)_\nu}$ is plotted vs. (pH + pX) for the polyelectrolytes poly(acrylic acid), poly(methacrylic acid) (*29*), poly(D,L-glutamic acid), and poly(L-glutamic acid) (*30*); for polyethylenimine and poly(vinylamine) (*31*), the apparent pK is plotted vs. pH

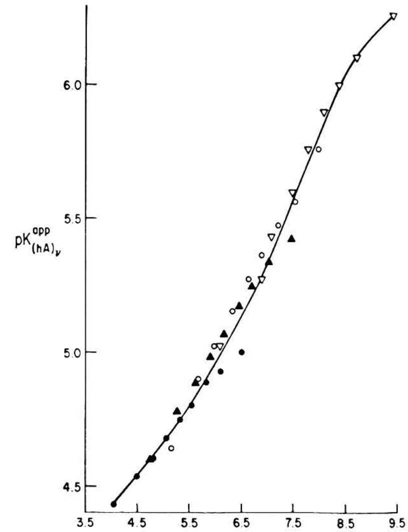

Figure 7. Apparent pK values obtained for poly(D,L-glutamic acid) at four different sodium chloride concentrations plotted vs. (pH + pCl). The $pK^{app}_{(HA)_\nu}$ values are interpolated from the potentiometric titration curves presented in Figure 1 of ref 30. NaCl concentrations (▽) 0.010, (O) 0.10, and (O) 0.050, (▲) 0.10, and (●) 0.40 N.

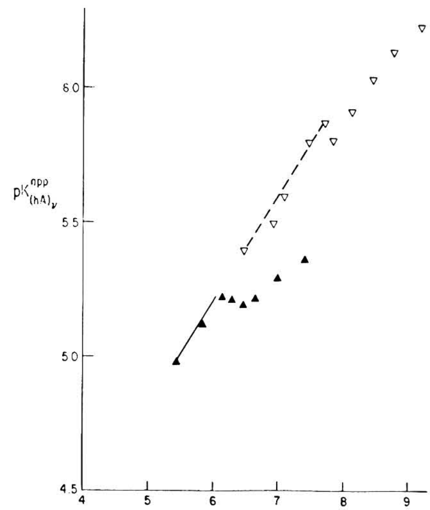

Figure 8. Apparent pK values obtained for poly(L-glutamic acid) in (▽) 0.010 and (▲) 0.10 N NaCl plotted vs. (pH + pCl). The $pK^{app}_{(HA)_\nu}$ values are interpolated from the potentiometric titration curves presented in Figures 2 and 4 of ref 30.

alone. Anion activity coefficients employed to evaluate pX for use in the ordinate term were obtained from the single ion activity coefficient values based upon computation due to Kielland (*32*) up to an ionic strength of 0.10, the upper range of their projected validity. Above this ionic strength the mean molal activity coefficient published for the uni-univalent salt was employed.

A single unique curve is obtained for poly(acrylic acid) (Figure 5) and poly(D,L-glutamic acid) (Figure 7) to show that these linear polyelectrolytes are rigid and imperme-

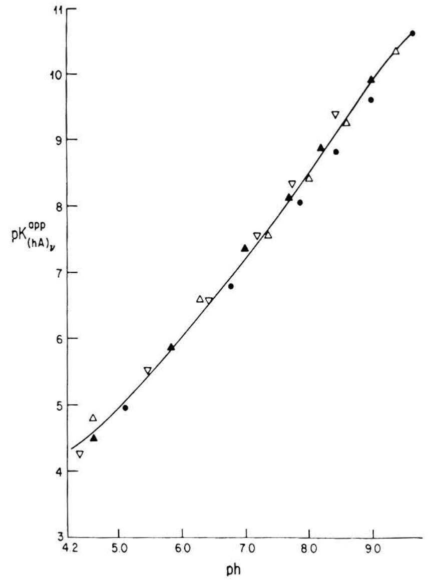

Figure 9. Apparent pK values obtained for polyethyleneimine in (▽) 0.0010, (▲) 0.010, (△) 0.10, and (●) 1.0 N NaCl plotted vs. the experimental pH. The p$K^{app}{}_{(hA)_\nu}$ values are interpolated from the potentiometric titration curves presented in Figure 1 of ref 31.

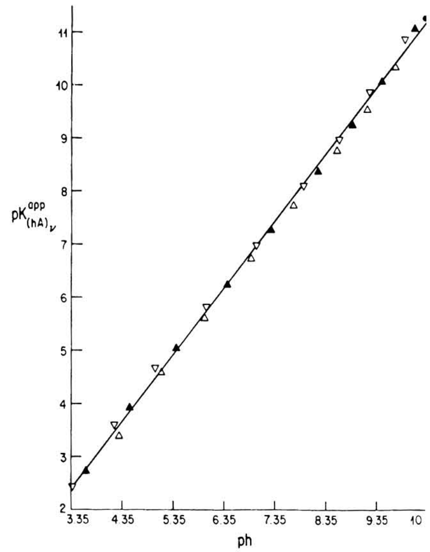

Figure 10. Apparent pK values obtained for poly(vinylamine) in (▽) 0.050, (△) 0.10, and (▲) 1.0 N NaCl plotted vs. the experimental pH. The p$K^{app}{}_{(hA)_\nu}$ values are interpolated from the potentiometric titration curves presented in Figure 3 of ref 31.

able to salt. The divergence in p$K^{app}{}_{(HA)_\nu}$ from the otherwise uniquely resolved curve in Figure 6 arises from the discontinuity originating from conformational change in the poly(methacrylic acid) molecule from a compact to random coil configuration. This molecule is thus rigid and permeable to salt in both forms. With the poly(L-glutamic acid) molecules there is, using data due to Olander and Holtzer (*30*), in Figure 8 a unique description of p$K^{app}{}_{(HA)_\nu}$ as a function of pH + pX only in the helix region. There is a divergence of curves after passing the discontinuities due to the transition from the α-helix to its single strand conformation. From this result we can conclude that the α helix configuration is inflexible and permeable to salt; the single-stranded molecule is on the other hand apparently quite flexible and hydrophilic.

Finally, the resolution of a single unique curve when p$K^{app}{}_{(HA)_\nu}$ is plotted vs. pH alone for the polyethylenimine and the poly(vinylamine) assigns rigidity and salt impermeability to these hydrophobic polyelectrolytes.

IV. Conclusions

There is no question that a method has been devised for the elucidation of the nature of charged polymeric molecules no matter whether they exist as a separate gel phase or are completely dissolved in the aqueous medium employed. Their rigidity or lack of rigidity and their permeability or impermeability to simple salt can be deduced with certainty from plots of apparent pK vs. (pH + pX) and pH alone. In addition the displacement of plots of p$K^{app}{}_{(HA)_\nu}$ vs. α as a function of ionic strength can be used to provide a basis for correction of the electrostatic disturbance of this term (*21–24*).

We can see from this that the protonation equilibria encountered with natural organic acids (humic and fulvic) should be susceptible to analysis by the above approach. The fact that it is is fully documented in the next paper of this series where corrections for nonideality due to the charged surface of the rigid, hydrophobic fulvic acid molecule have been resolved. Correction for this source of nonideality has then permitted a reasonable resolution of the heterogeneity factor, which leads to the residual salt-independent variation of p$K^{app}{}_{(HA)_\nu}$ with α in the fulvic acid molecule (*20*).

Literature Cited

(1) Sposito, G.; Holtzelaw, K. M. *Soil Sci. Am. J.* **1977**, *41*, 330–336.

(2) Sposito, G.; Holtzclaw, K. M.; Keech, D. A. *Soil Sci. Soc. Am. J.* **1977**, *41*, 1119–1125.

(3) Paxeus, N.; Wedborg, M. Chalmers Institute, Gothenburg, Sweden, private communication, 1985.

(4) Eberle, S. H.; Feuerstein, W. *Naturwissenschaften* **1979**, *66*, 572–578.

(5) Gamble, D. S. *Can. J. Chem.* **1970**, *48*, 2662–2669.

(6) Gamble, D. S. *Can. J. Chem.* **1972**, *50*, 2680–2690.

(7) Burch, R. D.; Langford, C. H.; Gamble, D. S. *Can. J. Chem.* **1978**, *56*, 1196–1201.

(8) Shuman, M. S.; Collins, G. J.; Fitzgerald, P. J.; Olson, D. L. In "Aquatic and Terrestrial Humic Materials"; Christman, F. R., Gjessing, E. G., Eds.; Ann Arbor Sci.: Ann Arbor, MI, 1983; pp 349–370.

(9) Perdue, E. M.; Lyttle, C. R. *Environ. Sci. Technol.* **1983**, *17*, 654–660.

(10) Choppin, G. R.; Kulberg, J. *J. Inorg. Nucl. Chem.* **1978**, *40*, 651–657.

(11) Takamatsu, T.; Yoshida, T. *J. Soil Sci.* **1978**, *125*, 377–382.

(12) Plechanov, N.; Josefsson, B.; Dyrssen, D.; Lundquist, K. In "Aquatic And Terrestrial Humic Materials"; Christman F. R., Gressing, E. T., Eds.; Ann Arbor Sci.: Ann Arbor, MI, 1983; pp 387–401.

(13) Dempsey, B. A.; O'Medlia, C. R. In "Aquatic and Terrestrial Humic Materials"; Christman F. R., Gjessinger, E. T., Eds.; Ann Arbor Sci.: Ann Arbor, MI, 1983; pp 239–273.

(14) Pommer, A. M.; Breger, I. A. *Geochim. Cosmochim. Acta* **1960**, *i0*, 30–44.

(15) Huizenga, D. K.; Kester, D. R. *Limnol. Oceanogr.* **1979**, *24*, 145–450.

(16) Varney, M. S.; Mantoura, R. F. C.; Whitfield, M.; Turner, D. R.; Riley, J. P. In "Trace Metals in Sea Water"; Proceedings of the NATO Conference, 1981; pp 751–772.

(17) Posner, A. M. In "Proceedings of the 8th International Congress of Science"; Bucharest, Roumania, 1964; Part II.
(18) Wilson, D. E.; Kinney, P. *Limnol. Oceanogr.* **1977**, *22*, 281-289.
(19) Marinsky, J. A. *J. Phys. Chem.* **1985**, *89*, 5294-5303, 5303-5307.
(20) Marinsky, J. A.; Ephraim, J.; Mathuthu, A.; Alegret, S.; Bicking, M. J.; Malcolm, R. *Environ. Sci. Technol.*, following paper in this issue.
(21) Marinsky, J. A.; Lim, F. G.; Chung, C. *J. Phys. Chem.* **1983**, *87*(16), 3139-3145.
(22) Marinsky, J. A.; Slota, P. In "Ions in Polymers", Advances in Chemistry Series; American Chemical Society: Washington, DC, 1980, pp 311-325.
(23) Marinsky, J. A.; Merle, Y. *Talanta* **1984**, *31*, 199-204.
(24) Marinsky, J. A.; Alegret, S.; Escalas, M. T. *Talanta* **1984**, *31*, 683-687.
(25) Mukerjee, P. *J. Phys. Chem.* **1961**, *65*, 740-746.
(26) Gekko, K.; Noguchi, H. *Biopolymers* **1975**, *14*, 2555-2561.
(27) Sillen, L. G.; Martell, A. "Stability Constants of Metal Ion Complexes", The Chemical Society, Burlington House: London, England, 1964.
(28) Paterson, R.; Rahman, H. *J. Colloid Interface Sci.* **1984**, *97*, 428-429.
(29) Nagasawa, M.; Murase, T.; Kondo, K. *J. Phys. Chem.* **1965**, *69*, 4005-4012.
(30) Olander, D. S.; Holtzer, A. *J. Am. Chem. Soc.* **1968**, *90*, 4549-4556.
(31) Bloy von Treslong, C. J.; Staverman, A. J. *Recl. Trav. Chim. Pays-Bas* **1974**, *93*, 171-177.
(32) Kielland, J. *J. Am. Chem. Soc.* **1973**, *59*, 1675-1681.

Received for review January, 18, 1985. Revised manuscript received November 25, 1985. Accepted December 12, 1985.

A United Physicochemical Description of the Protonation and Metal Ion Complexation Equilibria of Natural Organic Acids (Humic and Fulvic Acids). 2. Influence of Polyelectrolyte Properties and Functional Group Heterogeneity on the Protonation Equilibria of Fulvic Acid

James Ephraim,[†] Salvador Alegret,[‡] Andrew Mathuthu,[†] Margaret Bicking,[†] Ronald L. Malcolm,[§] and Jacob A. Marinsky*,[†]

Chemistry Department, State University of New York at Buffalo, Buffalo, New York 14214, Analytical Chemistry Department, Autonomous University of Barcelona, Bellaterra (Barcelona), Spain, and U.S. Geological Survey, Mail Stop 107, Denver Federal Center, Denver, Colorado 80225

■ Potentiometric studies of the neutralization of several fulvic acid sources with standard base in aqueous and nonaqueous media have been conducted. Analysis of the results with a recently developed unified physicochemical model has shown that the protonation behavior of these fulvic acid sources is a reflection of (1) their polyelectrolyte nature and (2) their heterogeneity. It has been possible to ascribe the polyelectrolyte properties observed to a rather inflexible fulvic acid molecule whose variably charged surface is impermeable to simple electrolyte.

I. Introduction

Humic substances, including peat and highly organic soils, comprise a large segment of the world's surface organic carbon. Their geochemical properties, in particular their acid–base characteristics and metal ion binding reactions, have a major importance in areas such as agriculture, water quality, and geochemistry (*1–3*). These chemical properties appear to provide humic substances their capability to control soil and water quality. For example, they can buffer acidic input and they can bind, transport, and redistribute potentially toxic metal ions released by accelerated weathering from acid rain. Recent research has emphasized the important relationship between acid precipitation and metal ion concentration (*4, 5*).

The importance of understanding the fundamental chemical interactions that regulate the distribution of metal ions such as aluminum in areas affected by acid deposition is evident from the following observations. The association of large amounts of aluminum with organic matter has been reported by several workers (*6–8*). Subsurface soils from Virginia have less exchangeable aluminum than surface soils because of differences in their organic matter content (*9*). Acid soils containing large amounts of organic material yield low aluminum concentrations in the soil solution, and soils, such as volcanic ash soils, with a high aluminum content are useful in croplands because of organic matter accumulation (*10*).

Although humic substances have been studied for over a century, only in recent years has it become clear that they exhibit properties similar to weak acid polyelectrolytes having a range of apparent molecular weights, solubilities, and acid strengths (*11, 12*). Schnitzer and co-workers have shown that humic substances consist of a three-dimensional array of aromatic rings that have numerous functional groups and side chains (*13*). The low-MW fractions are small polydisperse polyelectrolytes that may, in many instances, aggregate. The high-MW fractions are gels.

Characterization of the impact of environmental factors on humic materials must center on the role of proton and metal ion binding in these systems. At least two types of metal ion–humic reactions have been identified (*11, 12*), an electrostatic binding due to polyelectrolyte effects (charged polymer surfaces) (*14*) and inner sphere complex formation (*15, 16*) including chelation (*15*). Their polyelectrolyte nature and the heterogeneity of their composition are the important sources of complication in the interpretation of the various equilibra encountered.

As was pointed out in the first paper of this series (*17*) one or the other of these factors has been ignored in the numerous investigations that have been carried out to interpret the protonation and metal ion binding equilibria encountered with these natural organic acids (*18*). As a consequence the numerous publications that have appeared relating metal ion binding to humic substances present a complicated spectrum of contradictions (*19–22*).

[†] State University of New York at Buffalo.
[‡] Autonomous University of Barcelona.
[§] U.S. Geological Survey.

 0013-936X/86/0920-0354$01.50/0

Also, few publications provide data from which the various equilibria (ion exchange, complexation, and chelation) encountered can be expressed (23).

It is quite apparent that only a scheme which accommodates the main sources of complication can lead to the development of a uniform physicochemical description of these systems. In the course of our earlier research with gels and their polyelectrolyte analogues (24–33) an approach that provides the capability for resolving complexities arising from the polyelectrolyte nature of a molecule has been developed (25). With this capability transferred to the analysis of the potentiometric properties of natural organic acids it is believed that patterns of disturbance originating in their polyelectrolyte nature can be taken into account to permit a precise analysis of the contribution of their functional group heterogeneity to the residual potentiometric pattern.

It has been the objective of this research program to examine whether such quantitative resolution of functional group heterogeneity effects encountered in the potentiometric examination of different fulvic acid samples can indeed be facilitated through deductions of polyelectrolyte behavior provided by our model.

To achieve this goal, it was decided to examine the potentiometric properties of several different fulvic acid (FA) sources via titrations carried out at different salt (KNO_3 and $NaNO_3$) concentration levels (0.0010–0.10 M) and with varying amounts of FA. These data were to be analyzed by examining the dependence of $pK^{app}_{(HA)_\nu}$ on α, the degree of dissociation, on the ($pH + pNO_3$) term, and on pH. The correlations obtained were expected to show whether polyelectrolyte effects are contributed by a variable charge on the FA molecule surface and whether the macromolecule behaves like a hydrophilic (permeable) three-dimensional volume element or a hydrophobic (impermeable) two-dimensional surface (25). With this information available assessment of charged surface effects to the experimental potentiometric pattern was expected to facilitate resolution of the contribution of functional group heterogeneity to the protonation properties of the fulvic acid.

Evidence for the existence of different functionality groups in the particular FA source deduced in this way was to be supplemented by the potentiometric examination of the protonation of FA in nonaqueous media and through the potentiometric examination in aqueous media of FA in the presence of excess heavy metal ion (Eu^{3+} and Cu^{2+}). By this approach, chelation by bi- or trifunctional chelating units of the FA molecule was expected to liberate H^+ not otherwise detectable by the earlier potentiometric examination procedure in aqueous medium.

II. Experimental Section

(a) Chemicals and Their Preparation for Use. All chemicals used in the experimental program were reagent grade. Sterile, deionized, triply distilled water was made CO_2 free by boiling prior to use in the preparation of all solutions. Standard sodium and potassium hydroxide solutions prepared from carbonate-free Dilut-It analytical concentrates (J. T. Baker Chemical Company) were stored in polyethylene bottles inside a desiccator containing ascarite to maintain a CO_2 free atmosphere. Periodic standardizations of base were made with potassium hydrogen phthalate by determining the equivalence point potentiometrically or with phenolphthalein indicator. Burets employed to dispense the standard base were fitted with ascarite-filled tubes to minimize dissolution of CO_2. When small quantities of fulvic acid were employed in the program ultraprecision micrometer burets (accuracy 0.1 μL) were used to dispense the titrant.

The Armadale Horizons Bh fulvic acid used in the research program was obtained from the Chemistry Department of Concordia University in Montreal, Quebec (34). The Suwannee River fulvic acid source was kindly supplied by the U.S. Geological Survey in Denver (35). Its examination was of added interest because of its selection by the International Humic Substances Society (IHSS) as the aquatic fulvic acid reference standard. A fulvic acid isolated by N. Paxeus and M. Wedborg (30) from natural waters in Sweden was the third natural organic acid examined in the course of the research. Each fulvic acid source upon receipt was vacuum dried at 40 °C to assure uniform sampling in every experiment. They were stored at 5 °C in closed containers.

Tetra-*n*-butylammonium hydroxide, 25% w/w in CH_3OH and available in 100-g quantities as reagent V 362-5 from Baker Chemical, was used in the potentiometric titrations carried out in nonaqeous media. It was prepared for use by dilution with anhydrous 2-propanol. The resultant solution was blanketed with N_2 prior to storage in a glass-stoppered vessel. It was standardized, prior to use, with benzoic acid dissolved in *N,N′*-dimethylformamide.

(b) Apparatus, Methods, and Procedures. All electrochemical measurements were made with an Orion Research microprocessor analyzer, Model 901 (digital pH meter), using a saturated calomel electrode (Radiometer K401) as the reference electrode. The pH was measured with a glass electrode (Radiometer G202B) and a Radiometer combination electrode (GK 2321 C).

Prior to the pH measurements the glass electrode was calibrated with standard buffer solutions over the experimental pH range encountered in a particular study. A precise adjustment of the calibration was assured in a number of instances by measuring the pH of standard solutions (0.0100–0.000 100 M) of HNO_3 in potassium (sodium) nitrate solutions at the ionic strength of the fulvic acid systems scheduled for poteniometric study. The measurements were made on the solution by placing the polyethylene cell into a double-walled beaker designed to accommodate circulation of thermostated water. A Precision Scientific Model 154 constant-temperature bath was used to maintain the temperature of the cell at 25.0 ± 0.1 °C. The polyethylene cell was fitted with a plastic lid with inlets for the electrodes, nitrogen gas, and the buret. To avoid any evaporation of the sample, the N_2 gas that was used to ensure a CO_2-free atmosphere over the sample was presaturated with water vapor by bubbling it through a solution at the same ionic strength as the sample under study.

In a limited number of these potentiometric titrations of FA, Cu(II) or Eu(III) was added to produce mixtures with different molar ratios of FA to metal ion. By use of this approach it was possible to deduce the presence, in the fulvic acid molecule, of very weakly acidic groups not detectable in the standard titration procedure described above. The extra appearance of hydrogen ion in the system was measurable from comparison with the observed release of hydrogen ion in the metal-ion-free, but otherwise equivalent, system. The potentiometric pattern of both Eu(III) and Cu(II) during titration with standard base is easily discernable, so the quantity of metal ion bound strongly to the FA molecule could be assessed with reasonable accuracy to show it to be comparable with the capacity of the FA measured earlier in aqueous media.

Potentiometric examination of the neutralization of FA with standard base was also conducted in nonaqueous medium in order to distinguish between the presence of

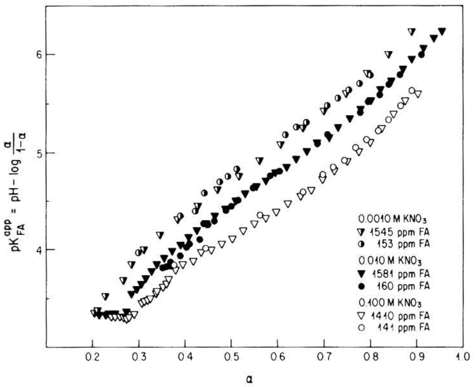

Figure 1. Variation of $pK^{app}{}_{FA}$ in Armadale Horizons Bh fulvic acid with degree of dissociation at three different ionic strength levels: ionic medium, KNO_3.

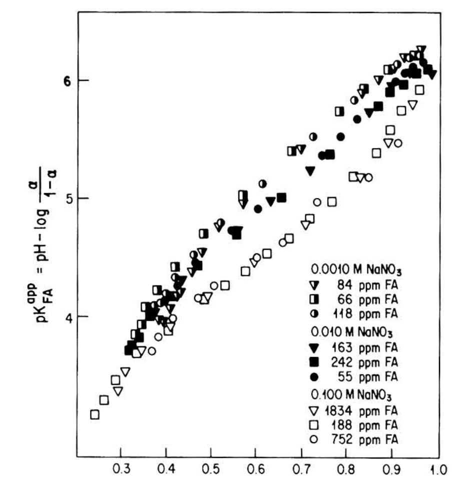

Figure 2. Variation of $pK^{app}{}_{FA}$ in Armadale Horizons Bh fulvic acid with degree of dissociation at three different ionic strength levels: ionic medium, $NaNO_3$.

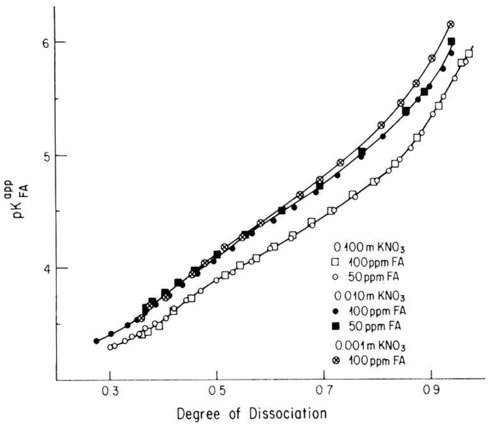

Figure 3. Variation of $pK^{app}{}_{FA}$ in Suwannee River fulvic acid at three different ionic strengths: ionic medium, KNO_3.

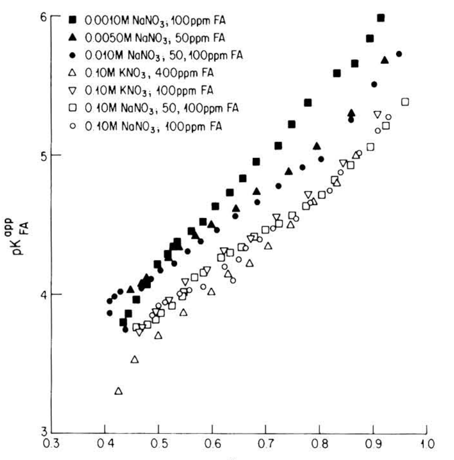

Figure 4. Variation of $pK^{app}{}_{FA}$ in aquatic fulvic acid from Sweden at three different ionic strength levels: ionic medium, $NaNO_3$ and KNO_3.

COOH and OH moieties constituting the FA molecule. In a particular set of experiments the potentiometric properties of dimethylformamide solutions of *p*-hydroxybenzoic acid (PHBA) with and without FA present, were measured under a nitrogen atmosphere during titration with standard tetrabutylammonium hydroxide dissolved in 2-propanol to achieve this objective. In the FA-free system the two inflections in the plot of potential (E in mV) vs. volume of base (VTBAH) were equally spaced to demonstrate the validity of the measurement. In the presence of FA the two inflections, still very well-resolved, permitted computation of the separate contribution of carboxylic and OH acidity in the FA (*37*).

To facilitate these potentiometric measurements, it was necessary to replace the saturated KCl of the calomel reference electrode with aqueous 1 M tetra-*n*-butylammonium chloride (TBACl). The electrode, when not in use, was stored in the TBACl solution.

III. Results

(a) Potentiometric Properties of Fulvic Acid in Aqueous Media. (*i*) *Protonation Properties of FA as a Function of Ionic Strength and FA Concentration.* Representative potentiometric data obtained during titration with standard base (NaOH, KOH) of the three FA sources present at different concentration levels in the bulk electrolyte ($NaNO_3$, KNO_3) used to define the different ionic strengths, from 0.10 to 0.0010, employed in this study are presented in Figures 1–4. In these figures apparent pK ($pK^{app}{}_{FA}$ = pH − log [$\alpha/(1-\alpha)$]) is plotted vs. α, the degree of dissociation, for the FA–Na(K)NO_3 systems studied. The points obtained at each ionic strength with FA at a particular concentration level are differentiated by the identifying symbols noted in each figure. The data in the three systems are similar. The potentiometric curves tend to converge as α approaches zero. The separation of the potentiometric curves as α increases is noticeably a function of ionic strength, the divergence being greatest at the lowest ionic strength employed. We learn from this pattern of behavior that a variably charged surface in the FA molecule must be operative. The sensitivity of divergence to ionic strength is, however, much less than in a typical high-molecular-weight polyelectrolyte such as poly(methacrylic acid); this result is consistent with end effects introduced as a result of the relatively small poly-

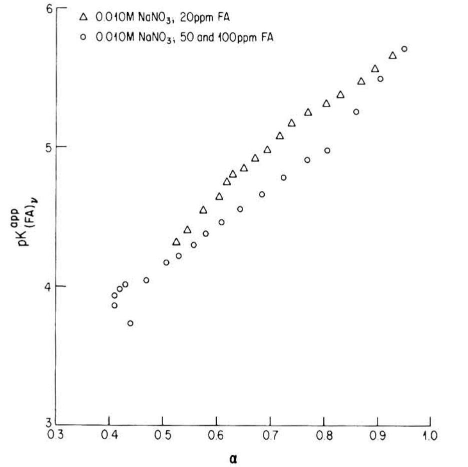

Figure 5. Effect on the $pK^{app}{}_{FA}$ function of lowering FA concentration levels from >50 ppm to 20 ppm at a fixed ionic strength (I = 0.010): Swedish fulvic acid.

meric molecules associated with the low-molecular-weight FA molecule (~1000). The sizeable increase in apparent pK with α at every ionic strength (>4 pK units) that is observed is greater than in a typical linear polyelectrolyte and has to be an artifact arising from the heterogeneity of functionality in the FA molecule itself.

There are differences between the parallel sets of data obtained with the three FA source as well. The vertical separation of the curves obtained as a function of ionic strength in the Suwannee River FA system is significantly smaller than in the Armadale and Swedish FA systems. This difference in the pattern of $pK^{app}{}_{FA}$ dependence on ionic strength has to be due to the fact that the potential field defined by the variably charged surface operative in the Suwannee River FA molecule is somewhat lower than in other FA molecules. Since the quantity of acidic groups per gram is the same (5.6 mequiv), within experimental error, in each fulvic acid source, this result suggests that the Suwannee River FA molecule is smaller, on the average, than the two other FA molecules. With low-molecular-weight molecules the effect of surface charge is a sensitive function of the degree of polymerization because of greater importance of end effects.

Portions of the potentiometric data obtained with the Swedish sample at I = 0.10 (400 ppm; $0.425 \geq \alpha \leq 0.75$), I = 0.010 (50, 100 ppm; $0.41 \geq \alpha \leq 0.55$)e, and I = 0.0050 (50 ppm; $0.45 \geq \alpha \leq 0.55$) yield patterns of behavior that differ significantly from those obtained with the other FA sources. Whereas the potentiometric properties of the Armadale Horizons Bh and Suwannee River FA were found to be insensitive to a fulvic acid concentration level varying from 55 ppm upward, the potentiometric properties of the Swedish FA at I = 0.10 remained unaffected only in the 50–100 ppm range. When the fulvic acid concentration level was raised to 400 ppm the $pK^{app}{}_{FA}$ was lowered considerably at low α values and did not merge with $pK^{app}{}_{FA}$ values obtained at the 50 and 100 ppm concentration levels until an α value of 0.75 was reached. In the lower α regions the $pK^{app}{}_{FA}$ values obtained with I = 0.0010 and 0.0050 did not tend to merge with the $pK^{app}{}_{FA}$ values obtained at the higher I as they did in the Armadale and Suwannee River FA systems.

The sensitivity of the $pK^{app}{}_{FA}$ vs. α plot to the concentration level of FA over the 50–100 ppm range, lost on

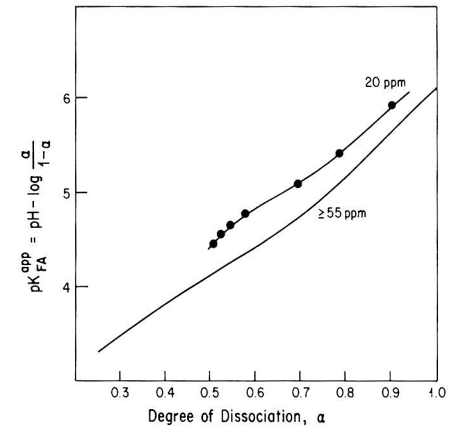

Figure 6. Effect on the $pK^{app}{}_{FA}$ function of lowering FA concentration levels to 20 ppm at a fixed ionic strength (I = 0.10 M): Armadale Horizons Bh fulvic acid.

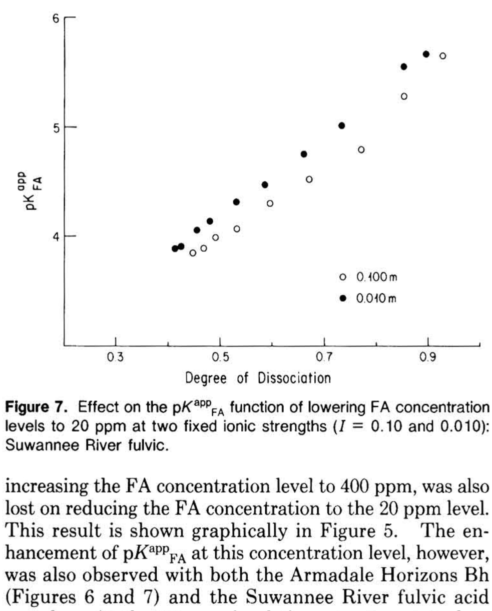

Figure 7. Effect on the $pK^{app}{}_{FA}$ function of lowering FA concentration levels to 20 ppm at two fixed ionic strengths (I = 0.10 and 0.010): Suwannee River fulvic.

increasing the FA concentration level to 400 ppm, was also lost on reducing the FA concentration to the 20 ppm level. This result is shown graphically in Figure 5. The enhancement of $pK^{app}{}_{FA}$ at this concentration level, however, was also observed with both the Armadale Horizons Bh (Figures 6 and 7) and the Suwannee River fulvic acid samples. At the 20 ppm level the potentiometric data obtained with the Armadale FA are displaced upward as shown in Figure 6. Representative data that were compiled with the Suwannee River fulvic acid at the 20 ppm level in 0.10 and 0.010 M KNO_3 medium are presented in Figure 7. These two curves are each ~0.2 pK units higher than the corresponding curves in Figure 3 to illustrate the same sensitivity of $pK^{app}{}_{FA}$ to low-level concentrations (20 ppm) in the Suwannee River FA reference source.

(*ii*) *Resolution of the Permeability and Rigidity Properties of the Fulvic Acid Molecule.* Criteria have been developed from study of the potentiometric properties of weakly acidic polyelectrolyte gels and their linear analogues (*25*) that permit the assessment of (a) the permeability or impermeability to salt, acid, and water of the volume element associated with these polymeric molecules and (b) the rigidity or lack of rigidity of this volume element over a wide range of experimental conditions. The concentration of counterions in the polymer domain element is

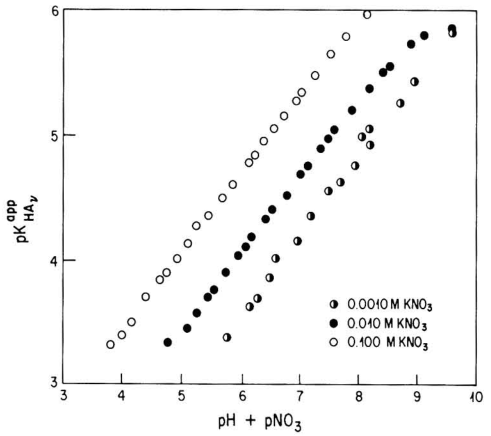

Figure 8. Variation of pK^{app}_{FA} with the (pH + pNO_3) term in Armadale Horizon Bh fulvic acid: ionic strength range from 0.0010 to 0.10.

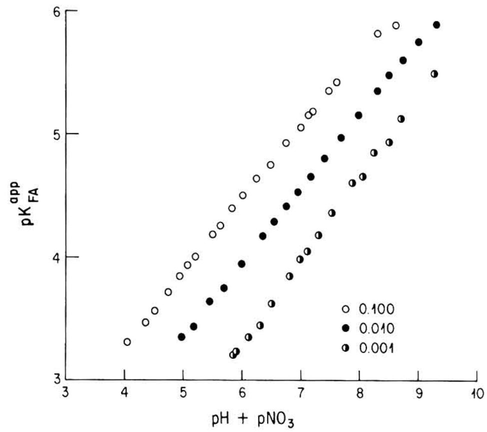

Figure 9. Variation of pK^{app}_{FA} with the (pH + pNO_3) term in Suwannee River fulvic acid: ionic strength range from 0.0010 to 0.10.

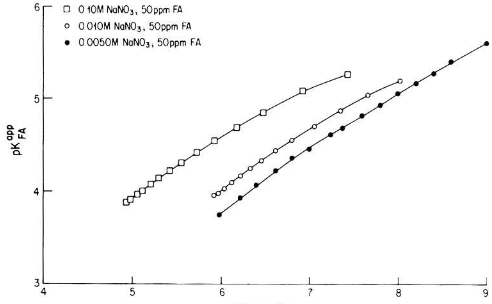

Figure 10. Variation of pK^{app}_{FA} with the (pH + pNO_3) term in Swedish fulvic acid source: ionic strength range from 0.0050 to 0.10.

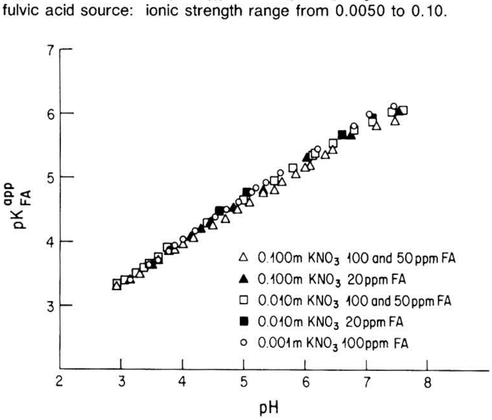

Figure 11. Variation of pK^{app}_{FA} with pH in Armadale Horizons Bh fulvic acid: ionic strength range from 0.0010 to 0.10.

sizably higher than in the bulk solution even at neutral salt concentration levels as high as 0.10 M until the lowest dissociation values are approached. If rigid and permeable to the diffusable components of the system (simple salt, acid, water) the concentration of the potential-determining counterions is uniquely a function of the degree of dissociation, invasion by salt being effectively restrained by the Donnan potential exerted at the boundary of the bulk solution. The concentration of hydrogen ion is reproducibly controlled as well at every degree of dissociation by the free energy of the functional group dissociation. As a consequence the concentration ratio of counterions in the rigid volume element of the polymer domain has to be uniquely defined by the degree of dissociation of the polyelectrolyte.

In a rigid polyelectrolyte that is impermeable to the diffusible components of the system such uniqueness of the concentration ratio is even more rigorously defined at every degree of dissociation. This is so because entry of extra counterion into the polymer domain volume element that is allowed to satisfy the Donnan equilibrium of salt and acid in the two phases of the permeable system is, of course, completely excluded in the impermeable polymer molecule.

Classical thermodynamic arguments have been used (*25–33*) to show that the ratio of the activities of the counterions in the polymer domain element, if permeable, must, at equilibrium, be equal to their ratio in the bulk solution. As a consequence one can expect the apparent p*K* of a rigid, weakly acidic polyelectrolyte molecule to be a unique function of the logarithmic term, pH + pX, at any ionic strength (*25*). If, on the other hand, the polyelectrolyte is rigid and impermeable to the diffusible components of the system, the apparent p*K* is expected to relate uniquely to the bulk solution pH at any ionic strength (*25*).

Some flexibility in the polymer molecule has to yield a change in the volume of the effective polymer domain when there is a change in the ionic strength of the system because of the accompanying change in the water activity of the external solution. This change in volume results in a change in the concentration and activity ratio of the counterions at a particular degree of dissociation. This is reflected in the divergence, with ionic strength, of plots of apparent p*K* vs. (pH + pX) in the permeable polymer system and vs. the pH alone in the impermeable polymer system (*25*).

The permeability and rigidity of the three fulvic acid sources are examined in plots of apparent p*K* vs. (pH + pNO_3) (Figures 8–10) and pH alone (Figures 11–13) with the potentiometric data complied at the different neutral salt concentration levels employed in this study. The curves in Figure 8–10 are separated from each other by the pX term, which, when removed in the plots of apparent p*K* vs. pH, essentially merge into a single curve for the Armadale and Suwannee River fulvic acids. This result

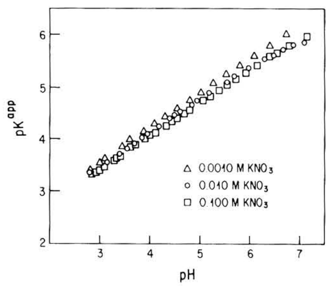

Figure 12. Variation of $pK^{app}{}_{FA}$ with pH in Suwannee River fulvic acid: ionic strength range from 0.0010 to 0.10.

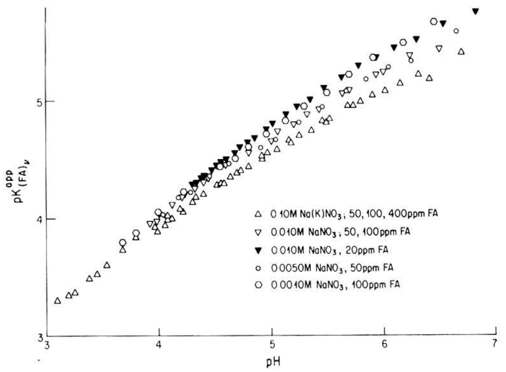

Figure 13. Variation of $pK^{app}{}_{FA}$ with pH in Swedish fulvic acid source: ionic strength range from 0.0010 to 0.10.

provides unambigous proof of the existence in aqueous medium of these fulvic acids as essentially rigid, impermeable polymeric molecules. With the Swedish fulvic acid source there is divergence into three separate curves at I = 0.10, 0.010 (0.0050), and 0.0010 with increasing pH to indicate that this fulvic acid molecule must be a good deal more flexible than the other two fulvic acid molecules. One result obtained with the Swedish fulvic acid source is clearly inconsistent with the pattern of behavior noted for the other FA sources. There is a shift upward of the curve obtained at I = 0.010 when the FA concentration level is lowered to 20 ppm. It was found with the Armadale and Suwannee River fulvic acids that the $pK^{app}{}_{FA}$ vs. pH curves were uniquely defined at a fixed ionic strength over the complete FA concentration range employed. The data obtained with the Swedish FA at I = 0.10, however, do not corroborate this observed independence of the $pK^{app}{}_{FA}$ vs. pH curve to FA concentration levels.

(b) Release of FA Protons by Chelation Reactions. The presence in FA of additional acidic functionality too weak to be detected in the standard titration procedure has been demonstrated through a comparison of the potentiometrically measurable acidity of FA alone and in the presence of varying quantities of Cu(II) and Eu(III). These data are presented graphically in Figures 14–19 and show that very weakly acidic groups intrinsic to the FA, but inaccessible in our earlier method of exploration, are deprotonated by chelation to the Cu(II) and Eu(III). In the presence of Cu(II) the extent of such extra release of protons is approximately 50%, in the Armadale and Swedish fulvic acids (Figures 14 and 16), and only 25–30%, in the Suwannee River fulvic acid (Figure 15), of the total acidity measurable earlier in aqueous medium. In the presence of Eu(III) the extra release of protons in all three

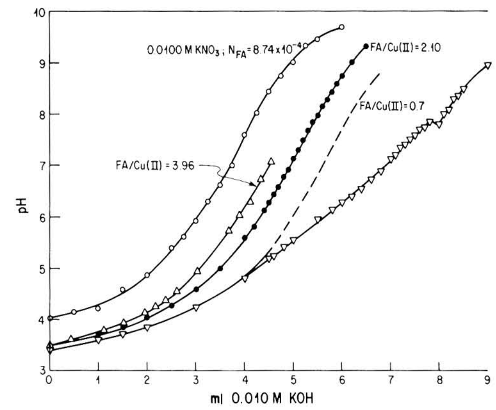

Figure 14. Proton release from Armadale Horizons Bh fulvic acid in the presence of Cu(II).

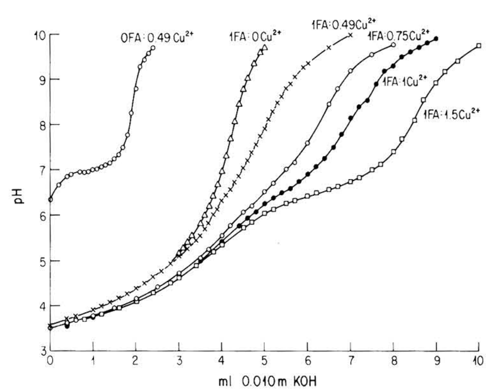

Figure 15. Promotion of the proton release from weakly acidic OH groups of Suwannee River fulvic acid in the presence of Cu(II).

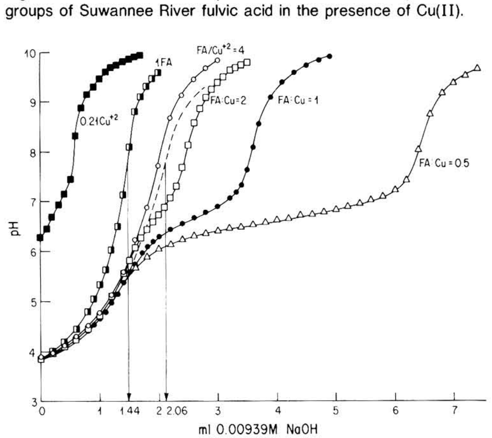

Figure 16. Proton release from weakly acidic OH groups of a Swedish fulvic acid in the presence of Cu(II).

fulvic acid sources amounts to 25–30% of the total acidity released in the earlier studies. The source of this acidity has been attributed to OH (phenolic) groups ortho to the stronger acidic groups that constitute the fulvic acid molecule.

From Figures 14–16 we see that when the quantity of FA present is insufficient to effectively remove the free

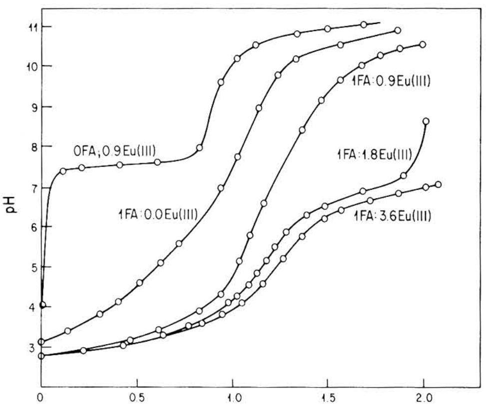

Figure 17. Proton release from weakly acidic OH groups of Armadale Horizons Bh fulvic acid in the presence of Eu(III).

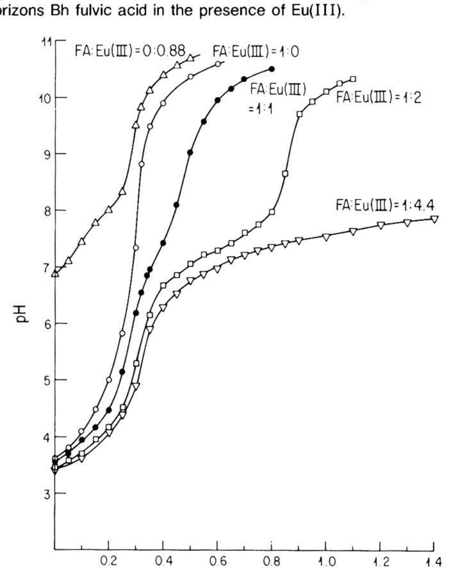

Figure 18. Proton release from Suwannee River fulvic acid in the presence of Eu(III).

Cu^{2+} ion from solution prior to its hydrolysis at a pH above 5 the potentiometric description of the complexation reactions between FA and Cu(II) is interfered with by the hydrolysis reaction of the free Cu^{2+} ion. The potentiometric profile uniquely attributable to the Cu(II)–FA complexation reactions, as a result, is interrupted before a sufficient fraction of the curve can be defined to provide a firm basis for the accurate projection of its shape to the equivalence point. To circumvent this difficulty, several experiments in which the binding capacity of the FA for Cu(II) was not exceeded were run for each fulvic acid source examined. By this approach the hydrolysis of Cu(II) was avoided, and the general shape of the potentiometric curve attributable to the spectrum of Cu(II) interactions with the various acidic groups of the fulvic acid was determined. The curves were found to be very similar in shape to the curve obtained with fulvic acid alone. For example in Figure 14 the shape of the potentiometric curve when the ratio of Cu(II) to fulvic acid is less than unity,

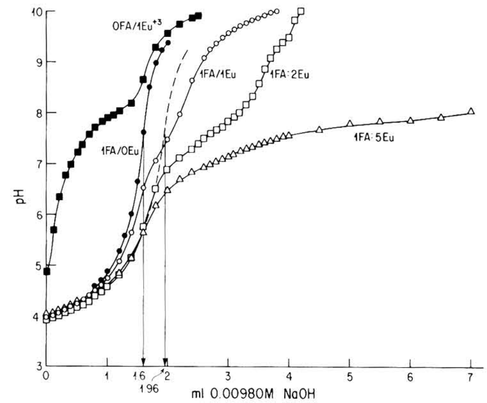

Figure 19. Proton release from Swedish fulvic acid in the presence of Eu(III).

on an equivalent basis, is the same as that obtained with the fulvic acid alone. Only the equivalence point is shifted to the right. It is on this basis that the potentiometric data obtained in excess Cu(II) have been extrapolated as shown to obtain the extra protonation estimate of about 25% and 50% in the three different fulvic acid molecules.

With the Eu(III) fulvic acid system it is easier to differentiate the sources of extra protonation. In the presence of excess Eu(III) the plateau that occurs at pH ~7 as a result of hydrolysis of the free Eu(III) is more sharply defined than in the buffered region attributable to copper(II) ion hydrolysis. This may be seen from the potentiometric response of Eu(III) alone to the addition of standard base that is also presented in Figure 17.

When standard base is added to the FA-free Eu(III) solution an immediate rise in pH from ~4 to ~7 occurs. The pH then remains essentially at this level with further addition of base until the ratio of base to rare earth, on a milliequivalent basis, is about unity. At this point the pH rises steeply once again with the addition of base to signal complete hydrolysis of the Eu(III). When FA and Eu(III) are present together in equal quantities, on a milliequivalent basis, however, no such plateau appears at pH ~7. In those instances where excess Eu(III) is present the quantity of base corresponding to the length of the pH plateau is equal to the difference in the equivalents of Eu(III) and FA initially present.

The difference in extra proton release between the Armadale and Swedish FA and the Suwannee River FA has been attributed to the accessibility of a very weakly acidic group in a position next to the stronger acidic group of the two bidentate chelating sites, present in approximately equal quantity, in the Armadale and Swedish FA source, while only one such chelating site is available in the Suwannee River FA source. The fact that the extra release of protons in the presence of Eu(III) is the same in all three fulvic acid sources tells us that the extra bidentate site in the Armadale and Swedish FA must form a much stronger chelate with Cu(II) than it does with Eu(III), while the bidentate site common to all FA sources must bind strongly to both Cu(II) and Eu(III). On this basis we have tentatively attributed the second chelating site of both the Armadale and Swedish fulvic acid molecule to a salicylic-acid-like moiety. The stability constant of Cu(salic) is 4.6×10^{10}, while the value reported for $Eu(salic)^+$ is only 2.75×10^4 (*38*), to lend credence to this estimate. The bidentate site that is strongly complexed by both Eu(III) and Cu(II) has, on the basis of results obtained in complexation studies with trace-level concentrations of $^{154}Eu^{3+}$ (*39*) and in the nonaqueous titration studies of these fulvic acids reported next, been assigned to a dihydroxyl functional group.

Further examination of the plots of pH vs. volume of base added that were obtained as a function of the molar ratio of FA to Cu for the three FA sources shows that Cu^{2+} and Eu^{3+} are removed more effectively from solution by the Armadale FA at equivalent FA/M^{n+} ratios. For example at a FA/Cu molar ratio of 2 about 20% of the Cu^{2+} added to the Swedish and Suwannee River FA samples is indicated to be accessible for hydrolysis by the length of the pH buffered region (Figures 15 and 16); the absence of such a buffered region in the Armadale FA system (Figure 14) shows that essentially all the Cu^{2+} has been effectively bound to the FA molecule at the FA/Cu ratio considered. In a similar situation with Eu(III) the pH-buffered region attributable to the first step in the hydrolysis of Eu(III) indicates that 40–50% of the Eu(III) remains unsequestered in the Suwannee River and 20% in the Swedish fulvic acids (Figures 18 and 19), while there is no evidence for the existence of free Eu(III) ion in the Armadale fulvic acid when the ratio of Eu to FA on a milliequivalent basis is unity (Figure 17).

The fact that the quantity of Cu(II) and Eu(III) bound to the Armadale Horizons Bh fulvic acid is approximately equal to the site capacity of the fulvic acid molecule is not consistent with mass action considerations. It is reasonable to expect some of the functional groups to be less than fully complexed when the ratio of metal to fulvic acid, on an equivalent basis, is about 1. In a system of this kind the distribution of the least strongly complexed species has to accommodate a greater percentage of free ligand and free metal ion than the more strongly complexes species so that saturation of sites, as observed, is puzzling. The binding property of the Suwannee River and the Swedish fulvic acid molecules is in much better agreement with expectation.

In a later, more quantitative study of the interaction of Cu^{2+} with the Armadale Horizons Bh fulvic acid this extra binding of Cu^{2+} was not predictable with the multiple-site model (*40*) developed for the anticipation of speciation in this system. The extra removal of Cu^{2+} had to be rationalized by assuming interaction between the hydrolyzed Cu(II), $CuOH^+$, and the surface-complexed Cu(II) species. Presumably a similar interaction occurs between $Eu(OH)^{2+}$ and the surface-complexed Eu(III) of the Armadale FA molecule.

The fact that the Suwannee River and Swedish FA sources behave similarly in their interaction with Cu^{2+} seems at first glance to be contradictory as well. The Swedish FA, since it contains one more chelating site than the Suwannee River FA, would, on this basis, be expected to bind Cu^{2+} more effectively in comparable experimental situations.

The source of this contradictory behavior in the binding of Cu^{2+} has, on the basis of the nitrogen content of these acids, been tentatively identified with an aminocarboxylic acid group whose presence in the Suwannee River FA is somewhat higher than in the Swedish FA. Because of the high affinity of this bidentate group for Cu^{2+} (*38*) and because the amino group associated with it has a relatively low pK (p$K_2 \sim 9$) compared with the pK of the phenolic group of the salicylic acid (p$K_2 \sim 13$) and the second hydroxyl group of the dihydroxyl chelate unit (p$K_2 \sim 11$) its second proton is released more easily. As a consequence the level of Cu^{2+} binding by the aminocarboxylic acid group can be comparable with its binding by the other two groups even though its abundance in the FA molecule is a good deal lower. The presence of more amino acid in the Suwannee River FA than in the Swedish FA is thus consistent with the fact that the removal of Cu^{2+} in both FA sources is comparable; the extra binding of Cu by the amino carboxylic acid compensates for the extra binding of Cu^{2+} by the salicylic-acid-like moiety in the Swedish FA.

The above explanation of the comparable binding tendencies exhibited by the Suwannee River and Swedish fulvic acid molecules for Cu^{2+} does not explain the difference in binding tendencies of these two fulvic acids for Eu(III). The Eu(III) has little affinity for the amino carboxylic acid moiety (*28*), and there is no sizeable differentiation in binding to be expected as a consequence of the presence or absence of a salicyclic acid unit in the fulvic acid molecule. As a consequence one would expect equivalent binding of the Eu(III) by the two fulvic acid molecules rather than the preferential binding of the Eu(III) by the Swedish fulvic acid (80% vs. 60%) when the ratio of Eu(III) to fulvic acid on an equivalent basis is unity.

Evidence for the presence in the Armadale Horizons Bh fulvic acid molecule of a chelating group, unaccessible, like the aminocarboxylic moiety, to detection with the potentiometric studies carried out, has been found (*39, 40*), and this group may be presumed to be present in different quantity in the Swedish and Suwannee River fulvic acid molecules as well. This functional group, an aldehyde or ketone, presumed to replace the weaker OH in the dihydroxyl unit (*39, 40*) could appear to a small but differing extent in the two FA molecules to yield the observed difference in binding properties of the two fulvic acid molecules.

Finally a comparison of the p$K^{app}{}_{FA}$ vs. α curves due to the three fulvic acids sources studied (Figures 1–4) shows that the curves can be displaced vertically by as much as 0.35 pK units from each other at each ionic strength examined. On this basis it is evident that one or more of the component acidic units of the three fulvic acid molecules are of different acidic strength. Since an inverse relationship has been shown to exist between the extent of Cu^{2+} complexation, i.e., the extent of (inner-sphere) covalency of the Cu–O bond, and the acid strength of the complexation site (*41*) the strength of binding to the more acidic sites of the three fulvic acids is expected to differ somewhat in each of the fulvic acid molecules to provide an additional rationalization of differences in the binding of Cu^{2+}, and perhaps Eu^{3+}, from that expected on the basis of the chelating sites considered to be accessible in each of the FA molecules.

(c) Potentiometric Properties of Fulvic Acid in Nonaqueous Media. (*i*) *Preliminary Research.* Resolution of functionality in the Armadale FA beyond that achieved in aqueous medium was next sought through employment of a nonaqueous medium. The first potentiometric examinations of FA dissolved in dimethylformamide, however, did not yield any better resolution of functionality than the earlier titrations in aqueous medium. Wright and Schnitzer (*42*) had failed similarly when they titrated some humic and fulvic acid preparations from the A and B horizons of Spodosol with sodiumaminethoxide in either pyridine, dimethylformamide (DMF) or ethylenediamine.

Resorting to the use of an internal standard, however, resulted in the enhanced resolution of acid functionality in the FA just as it had in earlier studies of lignin by Pobiner (*37*) and bitumen by Nakajima and Tanobe (*43*). Pobiner found that the addition of *p*-hydroxybenzoic acid

Table I. Functional Group Analysis of Armadale Horizons Bh Fulvic Acid (FA) Using *p*-Hydroxybenzoic Acid (PHBA) as an Internal Reference

PHBA, g	FA, g	equiv points, mL of TBAH[a] 1st	2nd	capacity, mequiv/g COOH	OH	total
0.0920	0.0	12.55	25.10	7.20	7.20	
0.0767	0.0	10.50	21.10	7.23	7.23	
0.0829	0.0	11.50	23.00	7.30	7.30	
0.02400	0.019 19	4.82	8.75	4.20[b]	1.76[b]	5.96
0.02413	0.019 30	4.82	8.80	4.13[b]	1.84[b]	5.97
0.01756	0.014 04	3.50	6.42	4.11[b]	1.93[b]	6.04
				4.15	1.84	5.99

[a] Molarity of TBAH = 0.0528 M. [b] After subtraction of PBHA contribution.

Table II. Functional Group Analysis of Suwannee River Fulvic Acid in DMF Using PHBA as an Internal Reference

PHBA, g	FA, g	equiv points, of mL TBAH[a] 1st	2nd	capacity, mequiv g COOH	OH	total
2.043×10^{-2}	0	3.60	7.20	7.24	7.24	
4.086×10^{-2}	0	7.20	14.40	7.24	7.24	
4.086×10^{-2}	0	7.20	14.40	7.24	7.24	
2.043×10^{-2}	1.17×10^{-2}	4.80	9.40	4.22[b]	1.41[b]	5.63
2.043×10^{2}	8.70×10^{-3}	4.60	9.10	4.26[b]	1.42[b]	5.68
				4.24[b]	1.42[b]	5.66[b]

[a] Molarity of TBAH = 0.0411. [b] After subtraction of PHBA contribution.

(PHBA) facilitated resolution of the carboxylic and phenolic components of his lignin samples. Nakajima and Tanobe added benzoic acid and phenol to their bitumen samples to facilitate differentiation of the potential response to weak and very weak acid components of the bitumen.

In order to select the internal reference most useful for our purposes, preliminary experiments using humic acid obtained from the Aldrich Chemical Company were conducted in the presence of *p*-hydroxybenzoic acid, benzoic acid, phenol, and a combination of benzoic acid and phenol. Two inflections in the potentiometric plot assignable to carboxylic and phenolic (or very weak carboxylic acid) moieties, respectively, were obtained only when *p*-hydroxybenzoic acid or the combination of benzoic acid and phenol was employed as the internal reference standard. The eventual selection of *p*-hydroxybenzoic acid as the internal reference in our potentiometric examination of FA in nonaqueous medium was based upon the better reproducibility and more effective resolution of the two inflections in the potentiometric response initially associated with neutralization of the PHBA alone and retained in the presence of the humic acid samples.

(*ii*) *Resolution of Acidic Functionality in Armadale Horizons Bh Fulvic Acid.* The capability for distinguishing between weakly acidic carboxylic and phenolic and/or alcoholic OH functionality provided by use of PHBA as an internal reference standard having been reasonably demonstrated in the preliminary studies with the Aldrich humic acid source, this approach was next employed to facilitate a similar analysis of functionality in the Armadale Horizons Bh FA samples. Representative potentiometric titration curves that were obtained with the internal reference standard alone and in the presence of FA are presented in Figure 20. The results of this phase of the experimental study are summarized in Table I. The carboxylic acid capacity of 4.15 ± 0.05 mequiv/g and the "phenolic (alcoholic)" capacity of 1.84 ± 0.1 mequiv/g that are deduced from these data yield a total capacity of 5.99 ± 0.15 mequiv/g, exceeding the total acidity measurable in aqueous media (Figures 1 and 2) by 0.35 mequiv/g.

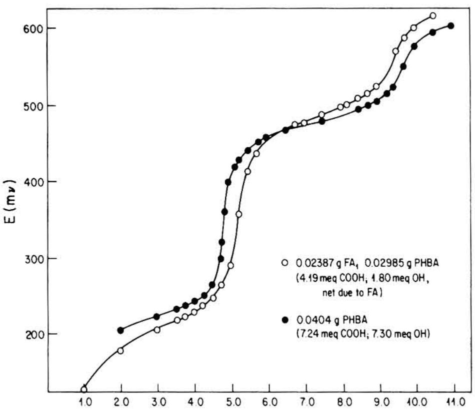

Figure 20. Potentiometric titration in DMF of PHBA in the absence and presence of Armadale Horizons Bh fulvic acid.

These results are believed to indicate that most of the hydroxyl functionality discernable in the DMF cannot be attributable to phenolic OH, which is too weakly acidic to be measurable in aqueous medium. It has been assigned to an acidic alcohol (enol) with only 74% of the acidity measurable in aqueous medium being attributed to carboxylic acid functionality. The extra titratable proton may indicate the presence of phenolic functionality sufficiently acidic to be detectable in the DMF ($9 > pK < 11$) while not being measurable in aqueous medium.

(*iii*) *Resolution of Acidic Functionality in Suwannee River Fulvic Acid.* Representative potentiometric data that were obtained during titration with standard tetrabutylammonium hydroxide in 2-propanol of the internal reference standard, *p*-hydroxybenzoic acid, alone and in the presence of fulvic acid dissolved in dimethylformamide, are plotted vs. the volume of standard base used in Figure 21. The results of this phase of the study are summarized in Table II. The carboxylic acid capacity of 4.24 ± 0.02

Table III. Functional Group Analysis of Swedish Fulvic Acid in DMF Using PHBA as an Internal Reference

masses of acids used, g		equiv points, mL of TBAH[a]		capacities, mequiv/g		
PHBA	FA	1st	2nd	COOH	OH	total
3.6685×10^{-2}		5.486	10.972	7.35	7.35	
3.6685×10^{-2}		5.486	10.972	7.35	7.35	
1.8343×10^{-2}		2.947	5.894	7.35	7.35	
3.6685×10^{-2}	2.00×10^{-2}	7.30	13.25	4.40[b]	1.14[b]	5.54
3.6685×10^{-2}	2.01×10^{-2}	7.33	13.31	4.44[b]	1.15[b]	5.59
				av 4.42[b]	1.145[b]	5.57

[a] Molarity of TBAH = 0.04841. [b] After subtraction of PHBA contribution.

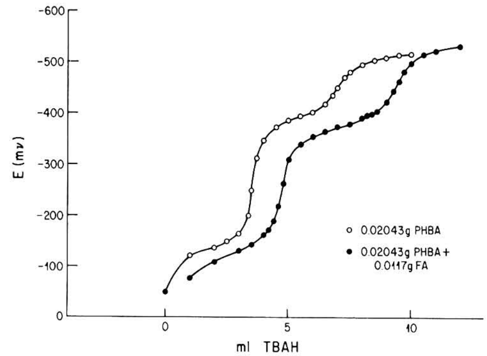

Figure 21. Potentiometric titration in DMF of PHBA in the absence and presence of Suwannee River fulvic acid.

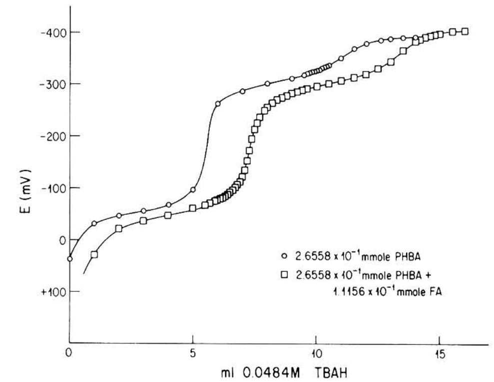

Figure 22. Potentiometric titration in DMF of PHBA in the absence and presence of Swedish fulvic acid.

mequiv/g and acidic OH capacity of 1.41 ± 0.02 mequiv/g that are resolved from these data yield a total capacity of 5.66 ± 0.05 mequiv/g fulvic acid in good agreement with the 5.60 ± 0.04 mequiv/g capacity obtained from the data presented in Figure 3.

With these results we substantiate the existence of a weakly acidic hydroxyl functionality in the Suwannee River fulvic acid that is assigned to an acidic alcoholic (enol) just as it was in the Armadale study. The excess acidity, observed in the Armadale study and attributed to phenolic functionality ($9 < pK > 11$), is apparently not present in the Suwannee River fulvic acid.

(*iv*) *Potentiometric Properties of Swedish Fulvic Acid in Nonaqueous Media.* Representative potentiometric data that were obtained during titration with standard tetrabutylammonium hydroxide in 2-propanol of the internal reference standard, *p*-hydroxybenzoic acid, alone and in the presence of fulvic acid dissolved in dimethylformamide, are plotted vs. the volume of standard base used in Figure 22. The results of this phase of the study are summarized in Table III. The carboxylic acid capacity of 4.42 ± 0.05 mequiv/g and the alcoholic OH capacity of 1.15 ± 0.05 mequiv/g that are resolved from these data yield a total capacity of 5.57 ± 0.05 mequiv/g fulvic acid in good agreement with the 5.60 ± 0.04 mequiv/g capacity obtained from the data presented in Figure 4.

With these results we substantiate the existence of a weakly acidic hydroxyl functionality in the Swedish fulvic acid as well. It also is assigned to an acidic alcohol (enol). The 7% excess acidic capacity observed for the Armadale FA in nonaqueous medium and attributed to phenolic functionality ($9 > pK < 11$) is apparently not present in the Swedish fulvic acid as well.

(d) Model for the Interpretation of Protonation Equilibria of Fulvic Acid in Aqueous Media. (*i*) *Contribution of Polyelectrolyte Properties to Protonation Equilibria.* The potentiometric criteria developed in an earlier paper (*25*) and briefly outlined in the first paper of this series (*17*) show that the three fulvic acid molecules studied are impermeable to simple salt (Figures 11–13) with two (Armadale and Suwannee River) of the three quite rigid as well. These properties in the FA molecule produce a ratio of $Na^+(K^+)$ to H^+ at the molecule surface that is uniquely defined by α, the degree of dissociation. This ratio is mimicked in the aqueous solution, and as long as the activity of $Na^+(K^+)$ in the solution is lower than its activity at the molecular surface the apparent pK will be affected by ionic strength.

We see from this that increasing the salt concentration of a fulvic acid–$Na(K)NO_3$ system must eventually reduce the discrepancy between surface and solution activities of $Na^+(K^+)$ to zero thereby removing the dependence of apparent pK on ionic strength.

The reduction of α toward zero must have this effect, as well, on the sensitivity of apparent pK to ionic strength. As α approaches zero the surface charge must eventually be lowered sufficiently, even at the lowest ionic strength levels, to reach a point where the activity of $Na^+(K^+)$ at the molecule surface and in the solution proper is the same. Below this point apparent pK has to be insensitive to ionic strength once again.

To test these predictions, potentiometric data were complied at higher salt concentration levels than those presented in Figures 1–4. These data, obtained at $I = 1.0$ and 5.0 M with the Armadale Horizons Bh fulvic acid are plotted in Figure 23 together with the earlier $pK^{app}{}_{FA}$ vs. α plots compiled at lower I values (Figures 1 and 2). Both of the model-based predictions are found to prevail. First, the curves obtained at the two highest salt concentration levels are nearly identical to show that the predicted removal of the differences between the activity ratio of the $Na^+(K^+)$ ion at the surface of the fully dissociated fulvic acid molecule and in the solution proper, the factor pro-

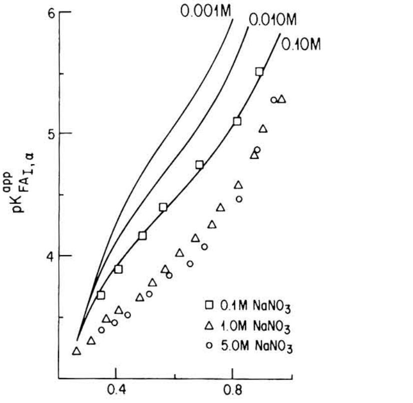

Figure 23. Insensitivity of $pK^{app}{}_{FA_{I,\alpha}}$ to ionic strength at high neutral salt concentration levels: Armadale Horizons Bh fulvic acid.

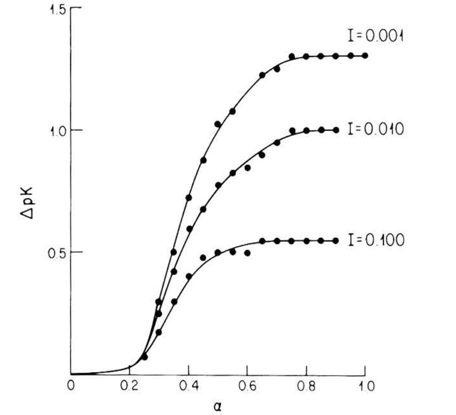

Figure 24. Variation of electrostatic deviation term (ΔpK) at three different ionic strength levels: Armadale Horizons Bh fulvic acid.

posed by the model to be responsible for the sensitivity of apparent pK to ionic strength, has been reached at a salt concentration level of 1.0 M. Second, the curves merge as α is lowered to support fully this model-based prediction.

The model, however, also predicts that a 10-fold change in the ionic strength of the excess salt medium on going from I = 1.0 to 0.10, from I = 0.10 to 0.01, and from I = 0.010 to 0.0010 should have produced parallel curves displaced by one pK unit in Figure 23 as long as the activity of the $Na^+(K^+)$ at the molecule surface remains at least 10 times greater than the critical value of about unity reached at I = 1.0 M. Instead the curves are separated eventually by 0.55, 0.45, and 0.2, respectively.

The discrepancy observed between experiment and theory can be attributed to the fact that the fulvic acid molecule is small. For example, the Armadale Horizons Bh FA has been determined to have an average molecular weight of ~1000. Because of this, end effects become important in the linear molecule, the functional sites nearest the two ends of the molecule tending to behave like a normal monomeric molecule. One can, on this basis, envisage the extent of departure from predicted behavior to depend on the relative contribution of the FA molecule extremities and its rigid, impermeable, charged surface to the potentiometric properties.

This modification of the model explains the small but increasing negative displacement of the $pK^{app}{}_{FA_{I,\alpha}}$ vs. α curves with each 10-fold increase in the concentration of the neutral salt medium until I_c, the critical, limiting neutral salt concentration level of 1.0 M, is reached.

In the revised model, I_c, the ionic strength beyond which $pK^{app}{}_{FA_{I,\alpha}}$ is no longer a sensitive function of the neutral salt concentration level, is used to assign the activity of the $Na^+(K^+)$ ion in 1.0 M $Na(K)NO_3$ solution to its activity, a_{I_c}, at the surface of the fully dissociated Armadale Horizons Bh fulvic acid molecule. On this basis the surface activity of $Na^+(K^+)$ at any α value is $a_{I_c}\alpha$, neglecting the change in activity coefficient with surface concentration during the neutralization process.

With this revised model the variation of $K^{app}{}_{FA_{I,\alpha}}$, the apparent dissociation constant of the fulvic acid molecule, with α and I, when I < 1.0 M, is directly related to the fractional, (x) and $(1 - x)$, contribution of end and charged surface effects in the molecule as shown below in eq 1.

$$K^{app}{}_{FA_{I,\alpha}} = K^{app}{}_{FA_{I/c,\alpha}}[(x) + (1 - x)(a_I/a_{I_c}\alpha)] \quad (1)$$

The experimental potentiometric plot obtained at and beyond I_c, the critical ionic strength, provides $K^{app}{}_{FA_{Ic,\alpha}}$ for use in eq 1 whose range of utility is restricted to the experimental situation where $a_I/a_{I_c\alpha} < 1$. One can expect this condition to be met only after an α value large enough to produce a noticeable surface charge effect is reached. Before this limiting α value is reached $a_I/a_{I_c\alpha} = 1$ and

$$K^{app}{}_{FA_{I,\alpha}} = K^{app}{}_{FA_{I/c,\alpha}} \quad (1a)$$

That this is indeed the case may be seen in Figure 24 where the vertical displacement of the $pK^{app}{}_{FA_I}$ vs. α curves (I = 0.10, 0.010, and 0.0010 M) from the I = 1.0 and 5.0 M curves presented in Figure 23 is plotted vs. α. The curves diverge at α = 0.2 to define the point at which the charged molecular surface is sufficiently developed to lead to $a_I/a_{I_c\alpha}$ values smaller than unity. By use of values of $K^{app}{}_{FA_{I,\alpha}}$ and $K^{app}{}_{FA_{Ic,\alpha}}$ interpolated from Figure 24 and the $a_I/a_{I_c}\alpha$ term developed with the model, eq 1 has been used to estimate the fractional contribution of end effects to the reduced displacement of $pK^{app}{}_{FA_{I,\alpha}}$ curves with ionic strength in the high α region (from 0.5 to 1.0): For the three different salt concentration levels (0.0010, 0.010, and 0.10 M) the fractional contribution of end effects is about 0.06, 0.09, and 0.17, respectively.

The slow increase with ionic strength in the estimated fractional contribution of end effects from this interpretation of the displacement of the $pK^{app}{}_{FA}$ curves is believed to indicate that head-to-tail interaction between FA molecules may be promoted with dilution of the neutral salt medium.

(ii) Contribution of Functional Heterogeneity to Protonation Equilibria. The sizeable rise in the value of apparent pK ($pK^{app}{}_{FA_{Ic,\alpha}}$) with α that still characterizes the potentiometric properties of the Armadale Horizons Bh fulvic acid molecule when charged surface effects are no longer operative is observable in the lowest curve presented in Figure 23. The positive slope of this $pK^{app}{}_{FA_{Ic,\alpha}}$ vs. α curve, because of the absence of any polyelectrolyte effect, has its origin exclusively in the functional group heterogeneity of the fulvic acid molecule. Our program to quantify site heterogeneity estimates has used this lower curve to assist in selection of the most reasonable assignment of abundance and intrinsic pK values to the mixture of acidic functional groups present in the fulvic acid molecule. The final choice of these parameters was based on the capability they provided for the accurate reproduction of the experimental curve by computation.

Table IV. Comparison of Experimentally Based Overall Degree of Dissociation, α_0^e, of Armadale Fulvic Acid with Summation of Computed Contributions of Four Separate Acidic Sites to Overall Degree of Dissociation, α_0^c [a]

pH	α_1	α_2	α_3	α_4	α_0^e	α_0^c
2.982	0.938	0.276	0.057	0.002	0.300	0.327
3.181	0.960	0.377	0.087	0.003	0.350	0.370
3.349	0.973	0.471	0.124	0.004	0.400	0.410
3.513	0.981	0.565	0.171	0.006	0.450	0.452
3.700	0.992	0.765	0.340	0.016	0.550	0.555
4.126	0.995	0.842	0.458	0.026	0.600	0.608
4.344	0.997	0.898	0.582	0.042	0.650	0.657
4.568	0.998	0.936	0.700	0.069	0.700	0.702
4.827	0.999	0.964	0.809	0.118	0.750	0.746
5.127	1.000	0.982	0.894	0.211	0.800	0.791
5.478	1.000	0.992	0.950	0.375	0.850	0.844
5.904	1.000	0.997	0.981	0.615	0.900	0.907
6.504	1.000	0.999	0.995	0.864	0.950	0.968

[a] Acid site 1, $pK_1^{int} = 1.8$; acid site 2, $pK_2^{int} = 3.4$; acid site 3, $pK_3^{int} = 4.2$; acid site 4, $pK_4^{int} = 5.7$. Abundance, A, of sites: $A_1 = 0.245$, $A_2 = 0.304$, $A_3 = 0.224$, $A_4 = 0.227$; $\alpha_1 A_1 + \alpha_2 A_2 + \alpha_3 A_3 + \alpha_4 A_4 = \alpha_0^c$

First estimates of these parameters were facilitated by the insight gained both from the potentiometric studies in the presence of excess Cu^{2+} and Eu^{3+} and in nonaqueous medium and from a study of the complexation of trace-level concentrations of $^{154}Eu^{3+}$ by the fulvic acid molecule under varying conditions of pH, fulvic acid concentration, and the presence of excess simple salt (*39*).

From the extra release of protons observed in the chelation studies two acidic units in approximately equal quantity and constituting about 50% of the total acidity measurable in the standard titration of fulvic acid with base were considered to be associated with weakly acidic phenolic groups in an ortho position to them. The fact that Cu^{2+} was strongly attached to the two chelate sites whereas Eu^{3+} was attached to only one was, as we have mentioned earlier, the basis for identifying one of the sites with a salicyclic-acid-like group.

The pK_a of 3.0 associated with the salicylic acid molecule and an abundance assignment of 25% were used in the first estimate of pK and abundance assignments made to resolve the functional group heterogeneity of the Armadale Horizons Bh fulvic acid molecule. The second acidic group, with an abundance also equal to approximately 25%, was, on the basis of the trace $^{154}Eu^{3+}$ complexation studies (*39*), assignable to a weakly acidic group characterized by an intrinsic pK of approximately 5.7. This weakest measurable acidic group was identified with the OH group shown by the nonaqueous potentiometric studies to constitute about 25% of the normally titratable acidity. The remaining 45–50% of the acidity had to be divided approximately equally between two more acidic groups, one relatively strong (pK $\sim$ 1.8) and the other relatively weak (pK $\sim$ 4.3) to provide a computed $pK^{app}{}_{FA_{lc,a}}$ vs. α curve that mimicked the shape of the lowest titration curve presented in Figure 23.

The optimum pK and abundance, A, assignments eventually resolved with the above first estimates are $pK_1 = 1.8$, $A_1 = 0.245$; $pK_2 = 3.2$, $A_2 = 0.304$; $pK_3 = 4.2$, $A_3 = 0.024$; and $pK_4 = 5.7$, $A_4 = 0.227$. The good to excellent agreement between computation and experiment that use of these parameters effects can be seen from careful inspection of Table IV. In this table we have shown that the overall degree of dissociation measured for fulvic acid (60 ppm and greater) at each experimental pH during its neutralization with standard base can be reproduced by computations based upon the above assignments of intrinsic pK and abundance values to the four separate functional units proposed. The sums of $A_1\alpha_1$, $A_2\alpha_2$, $A_3\alpha_3$, and $A_4\alpha_4$ computed at each fixed pH over the neutralization range examined in Figure 23 are in excellent agreement with the overall experimental α values as shown in Table IV to justify the proposed dissection of the fulvic acid molecule.

IV. Summary and Conclusions

Potentiometric studies of the neutralization of three different fulvic acid molecules, Armadale Horizons Bh FA, Suwannee River reference standard FA, and an aquatic FA from Sweden, with standard base in aqueous and nonaqueous media have been conducted. Analysis of the results has shown that the protonation behavior of fulvic acid is always a reflection of (1) its polyelectrolyte nature and (2) its functional group heterogeneity. The spectrum of functional units (carboxylic and OH) that comprise a fulvic acid molecule are sufficiently different in acid strength to dominate the large change in apparent pK ($pK^{app}{}_{FA}$) with degree of neutralization (α). These studies have also shown that each fulvic acid molecule is impermeable to simple salt (hydrophobic) with the Armadale Horizons Bh and the Suwannee River fulvic acid molecules a good deal more rigid than the Swedish fulvic acid molecule.

The capability for estimate of nonideality contributions to the apparent pK with increasing charge on the fulvic acid molecule surface during neutralization with standard base has permitted resolution of functional group heterogeneity in the fulvic acid molecule through abundance and pK assignments. Additional insight has been gained with respect to the carboxylic and OH content of the fulvic acid molecule from the potentiometric examination in nonaqueous medium of the neutralization of the fulvic acid in the presence of an internal reference standard, *p*-hydroxybenzoic acid, and from the protonation enhancement in aqueous medium affected by the addition of both Eu(III) and Cu(II) to the fulvic acid sample. Such studies have facilitated the elucidation of the multidentate character of these functional sites as well. The different degree of proton release enhancement from two of the three fulvic acid molecules in the presence separately of an excess of Cu^{2+} or Eu^{3+} has indicated that the Armadale Horizons Bh fulvic acid and the Swedish fulvic acid molecules contain both salicylic-acid-like and dihydroxyl bidentate groups while the Suwannee River fulvic acid molecule contains only the weak acidic dihydroxyl group.

Comparison of the potentiometric profiles of the three different fulvic acid molecules in the presence separately of excess Cu(II) and Eu(III) has also provided some evidence for (1) the variable presence of small quantities of an aminocarboxylic acid group and (2) the possibility of different degrees of fractional involvement of a carbonyl group with the weakly acidic dihydroxyl moiety. The much enhanced removal of these metal ions by the Armadale Horizons Bh fulvic acid at high pH and in the presence of excess metal ion has been attributed to reaction of the copper and europium complexed surface of the fulvic acid molecule with $Cu(OH)^+$ or $Eu(OH)^{2+}$ to form R(Cu–O–Cu) and R(Eu–O–Eu). Such selective reaction of the Armadale fulvic may occur as a result of the greater dipole density of this more highly aromatic fulvic acid molecule.

The reasonableness of the functional group arrangement deduced for the fulvic acid molecules has been tested with some success. By use of stability constants from the literature for Cu^{2+} complexed species most closely resembling the uni- and bidentate complexes presumed to be formed with these sites and by correcting for nonideality introduced by the potential field emanating from the charged surface of the fulvic acid molecule at the different experimental conditions, it has been possible to predict the Cu^{2+} ion binding characteristics of the Armadale Horizons Bh fulvic acid. The computed complexation behavior compares favorably with the experimentally observed complexation behavior of the Cu^{2+} ion *(40)*.

Registry No. Cu, 7440-50-8; Eu, 7440-53-1.

Literature Cited

(1) Stevenson, F. J. *BioScience* **1972**, *22*, 643–650.
(2) Greiner, J. W. *Econ. Geol.* **1922**, *17*, 407–415.
(3) Graham, E. R. *Soil Sci.* **1941**, *52*, 291–303.
(4) Cronan, C. S.; Schofield, C. L. *Science* **1979**, *204*, 304–315.
(5) Beamish, R. J.; Van Loon, J. C. *J. Fish. Res. Board Can.* **1977**, *34*, 649–660.
(6) McLean, E. O.; Reicosky, D. C.; Lakschamanan, C. *Proc. Soil. Sci. Soc. Am.* **1965**, *29*, 374–381.
(7) Rienke, H. B.; Corey, R. B. *Proc. Soil. Sci. Soc. Am.* **1967**, *31*, 749–762.
(8) Reeve, N. G.; Summer, M. E. *Proc. Soil Soc. Am.* **1971**, *35*, 38–43.
(9) Coleman, N. T.; Thomas, G. W. In "Soil Acidity and Liming"; Pearson, R. W., Adams, F., Eds.; American Society of Agronomy: Madison, WI, 1967; No. 9, pp 1–41.
(10) Evans, C. E.; Kamprath, E. J. *Proc. Soil Soc. Am.* **1970**, *34*, 893–898.
(11) Gamble, D. S. *Can. J. Chem.* **1972**, *50*, 2680–2690.
(12) Gamble, D. S. *Can. J. Chem.* **1973**, *51*, 3217–3222.
(13) Schnitzer, M.; Khan, S. U. "Humic Substances in the Environment"; Marcel Dekker, Inc.: New York, 1972.
(14) Marinsky, J. A. "Ion Exchange"; Marinsky, J. A., Ed.; Marcel Dekker, Inc.: New York, 1966; Chapter 9.
(15) Eger, C.; Anspach, W. M.; Marinsky, J. A. *J. Inorg. Nucl. Chem.* **1968**, *30*, 1911–1924.
(16) Marinsky, J. A.; Anspach, W. M. *J. Phys. Chem.* **1975**, *79*, 433–439.
(17) Ephraim, J.; Marinsky, J. A. *Environ. Sci. Technol.* **1986**, *20* (4).
(18) Perdue, E. M. In "Humic Substances in Soil, Sediment and Water"; Aiken, G. R., McKnight, D., Weshaw, R. L., MacCarthy, P., Eds.; Wiley: New York, 1985; Chapter 20, pp 493–526.
(19) Florence, T. M.; Batley, G. E. *CRC Crit. Rev. Anal. Chem.* **1980**, *9*, 219–296.
(20) Jackson, K. S.; Jonasson, T. R.; Skippen, G. B. *Earth Sci. Rev.* **1978**, *14*, 97–146.
(21) Ryan, D. K.; Weber, J. H. *Anal. Chem.* **1982**, *54*, 986–990.
(22) Stevenson, J. J. "Humus Chemistry"; Wiley: New York, 1982; 443 pp.
(23) Davies, R. I. Cheshire, M. V.; Graham-Bryce, I. J. *J. Soil Sci.* **1969**, *20*, 65–73.
(24) Gamble, D. S.; Marinsky, J. A.; Langford, C. H. "Advances in Ion Exchange and Solvent Extraction, Humic-Trace Metal Ion Equilibria in Natural Waters"; Marinsky, J. A., Marcus, Y., Eds.; Marcel Dekker, Inc.: New York, 1985; Chapter 7, Vol. 9, pp 373–481.
(25) Marinsky, J. A. *J. Phys. Chem.* **1985**, *89*, 5294–5303, 5303–5307.
(26) Marinsky, J. A.; Wolf, A.; Bunzl, K. *Talanta* **1980**, *27*, 461–468.
(27) Marinsky, J. A.; Gupta, S.; Schindler, P. *J. Coll. Interface Sci.* **1982**, *89*, no. 2, 401–411.
(28) Marinsky, J. A.; Lim, F. G. *J. Phys. Chem.* **1983**, *87*(16), 3139–3145.
(29) Marinsky, J. A.; Slota, P. "An Electrochemical Method for the Determination of the Effective Volume of Charged Polymers in Solution" (Ions in Polymers Symposium), Advances in Chemistry Series #187; American Chemical Society: Washington, DC, 1980; pp 311–325.
(30) Marinsky, J. A.; Merle, Y. *Talanta* **1984**, *31*, 199–204.
(31) Alegret, S.; Marinsky, J. A.; Escaleas, M. T. *Talanta* **1984**, *31*, 683–687.
(32) Marinsky, J. A.; Reddy, M. M. *Org. Geochem.* **1984**, *7*, 207–214.
(33) Marinsky, J. A.; Reddy, M. M. *Org. Geochem.* **1984**, *7*, 215–221.
(34) Gamble, D. S. *Can. J. Chem.* **1970**, *48*, 2662–2669.
(35) Thurman, D. M.; Malcolm, R. L. "Structural Study of Humic Substances, New Approaches and Methods"; Christman, R. F., Gjessing, E. T., Eds.; Ann Arbor Sci.: Ann Arbor, MI, 1983; pp 1–23.
(36) Paxeus, N.; Wedborg, M. "Acid–Bose Properties of Aquatic Fulvic Acid and its Low Molecular Weight Fraction", International Humic Substance Society Second International Conference, The University of Birmingham England, July 22–28, 1984.
(37) Pobiner, H. *Anal. Chim. Acta* **1983**, *155*, 57–65.
(38) Sillen, L. G.; Martell, A. Stability Constants of Metal Ion Complexes, The Chemical Society: Burlington House: London, England, 1964.
(39) Ephraim, J.; Cramer, S. J.; Marinsky, J. A., 1985 unpublished data.
(40) Ephraim, J.; Marinsky, J. A. *Environ. Sci. Technol.* **1986**, *20* (4).
(41) Wright, J. R.; Schnitzer, M. *Trans. Int. Congr. Soil Sci. 7th* **1960**, *2*, 112–118.
(42) Nakajima, T.; Tanobe, C. J. *Inst. Pet.* **1973**, *59*, 32–37.

Received for review January 19, 1985. Revised manuscript received November 25, 1985. Accepted December 12, 1985. We acknowledge financial support of this research by the National Science Foundation and the Nuclear Fuel and Waste Management Company in Stockholm, Sweden.

Environ. Sci. Technol. 1986, 20, 367–376

A Unified Physicochemical Description of the Protonation and Metal Ion Complexation Equilibria of Natural Organic Acids (Humic and Fulvic Acids). 3. Influence of Polyelectrolyte Properties and Functional Heterogeneity on the Copper Ion Binding Equilibria in an Armadale Horizons Bh Fulvic Acid Sample

J. Ephraim and J. A. Marinsky*

Chemistry Department, State University of New York at Buffalo, Buffalo, New York 14214

■ The objective of this research, the development of a model that permits the interpretation of metal ion binding to a fulvic acid source in every conceivable experimental situation, has been reached. The model corrects, in a quantitative way, for deviations in the potentiometric properties that arise from two disruptive factors intrinsic to any fulvic acid source, a variable electric field, emanating from the surface of the fulvic acid molecule as a consequence of its increasing charge during nuetralization with standard alkali, and site heterogeneity. In the research conducted the complexation of Cu^{2+} by an Armadale Horizons Bh fulvic acid sample was studied to facilitate the program. The use of literature-based stability constants for the Cu^{2+} ion complexed species formed with the different sites deduced from the design of the experimental program led to a capability for predicting the binding of macro quantities of Cu(II) to Armadale Horizon Bh fulvic acid as a function of degree of neutralization, ionic strength, and metal ion and fulvic acid concentration. The predictive quality provided by such assignment of binding parameters is felt to provide strong corroborative support for the deduced site assignments and thus for the model itself.

I. Introduction

The goal of our research program has been to develop a fundamentally sound approach to the interpretation of hydrogen and metal ion binding to humic substances in every conceivable situation (*1–4*). To facilitate reaching this goal, the protonation equilibria of three different fulvic acid sources were examined first (*5*). A scheme for successful rationalization of their protonation equilibria was developed. With this scheme it has been possible (1) to account for nonideality due to the variable electric field emanating from the surface of the fulvic acid molecule as a consequence of its increasing charge during neutralization with standard alkali and (2) to account for site heterogeneity in the sample. After cancellation of nonideality effects it has been possible as well to assign intrinsic pK values to the various acidic sites together with their relative abundances in the fulvic acid molecule. The quantitative estimate of the chelation potential of the fulvic acid molecule provided by the release, during its neutralization with base, of extra H^+ in the presence of Cu^{2+} and Eu^{3+} combined with the capability for distinguishing between carboxylic and hydroxyl acidity provided by neutralization studies in nonaqueous media using *p*-hydroxybenzoic acid as an internal reference standard, has facilitated the judicious use of the site heterogeneity assignments for the deduction of functional site sequences in the fulvic acid molecule. Additional advantage provided by the model developed has been the provision of a capability for recognition of the fact that the fulvic acid molecule is impermeable to simple salt and for estimation of its degree of rigidity (*4*).

It has been the objective of this phase of the research to develop a multisite model that can be used to predict the metal ion binding behavior of fulvic acids. In the research that has been performed for this purpose in this portion of the study program, the binding of macro quantities of Cu^{2+} to the Armadale Horizons Bh fulvic acid molecule has been carefully examined as a function of degree of neutralization, ionic strength, and metal ion and fulvic acid concentration. The free Cu^{2+} measured in each instance has been used to compute the binding of Cu^{2+} by the sequence of sites deduced from the earlier protonation study (*5*) through employment of the literature-based formation constant for the metal ion complexed species presumed to be formed with each of these tentatively identified sites. The extent of agreement between the computed and experimentally determined Cu^{2+} binding values has been used as the basis for evaluating the reasonableness of the model.

II. Experimental Section

(a) Chemicals and Their Preparation for Use. All chemicals ($NaNO_3$, KNO_3, NaOH, KOH, and $Cu(NO_3)_2$) used in the experimental program were reagent grade. Sterile, deionized, triply distilled water was made CO_2 free by boiling prior to use in the preparation of all solutions. The standard sodium and potassium hydroxide solutions, prepared from carbonate-free Dilut-It analytical concentrates (J. T. Baker Chemical Company) were stored in polyethylene bottles inside a dessiccator containing ascarite to maintain a CO_2-free atmosphere. Periodic standardizations of base were made with potassium hydrogen phthalate by determining the equivalence point potentiometrically or with phenolpthalein indicator. Burets employed to dispense the standard base were fitted with ascarite-filled tubes to minimize dissolution of CO_2. When small quantities of fulvic acid were employed in the program ultraprecision micrometer burets (accuracy 0.1 μL) were used to dispense the titrant.

The Certified ACS cupric nitrate reagent (Fisher Scientific Company), used as the source of Cu^{2+} in the program, was standardized with ethylenediaminetetraacetic acid by determining the equivalence point either potentiometrically or from the color change of the indicator.

Armadale Horizons Bh fulvic acid from the Chemistry Department of Concordia University in Montreal, Quebec, was used in the research program. The fulvic acid, vacuum-dried at 40 °C to assure uniform sampling in every experiment, was stored at 5 °C in a closed container.

(b) Apparatus, Methods, and Procedures. All electrochemical measurements were made with an Orion Research microprocessor analyzer, Model 901 (digital pH meter), using a saturated calomel electrode (Radiometer-K401) as the reference electrode. The pH was measured with a glass electrode (Radiometer G202B) and a Radiometer combination electrode (GK 2321 C). The Cu^{2+}

concentration was measured with a Cu^{2+} selective electrode (Orion 94-29A) purchased from the Orion Corporation.

Prior to the sequence of pH and Cu^{2+} concentration measurements the electrodes were calibrated. The glass electrode was calibrated with standard buffer solutions over the experimental pH range encountered in a particular study. A precise adjustment of the calibration was ensured in a number of instances by measuring the pH of standard solutions (0.0100–0.000 100 M) of HNO_3 in potassium (sodium) nitrate solutions at the nitrate concentration level of the fulvic acid systems scheduled for potentiometric study. The Cu^{2+} selective electrode was calibrated in the presence of nitrate ion at the different bulk electrolyte concentration levels employed in the experimental program by measuring the potential of standard solutions prepared to cover the metal ion concentration range expected to be encountered.

The measurements were made by placing the polyethylene cell holding the solution into a double-walled beaker designed to accommodate circulation of thermostated water. A Precision Scientific Model 154 constant-temperature bath maintained the temperature of the cell at 25.0 ± 0.1 °C. The polyethylene cell was fitted with a plastic lid with inlets for the electrodes, nitrogen gas, and the buret. To avoid any evaporation of the sample, the N_2 gas used to ensure a CO_2-free atmosphere over the sample was presaturated with water vapor by bubbling it through a solution at the same ionic strength as the sample under study. Because the Cu^{2+} selective electrode is sensitive to light the sample cell was always shielded when the Cu^{2+} measurement was made.

Two kinds of experiments were conducted in the course of this study. In the first, standard KOH(NaOH) was added in regular increments to the fulvic acid–KNO_3-($NaNO_3$) system with the molar ratio of FA to $Cu(NO_3)_2$ fixed at a specified value. In the second kind of experiment standard $Cu(NO_3)_2$ was added in small, regular increments to the fulvic acid–KNO_3($NaNO_3$) system with the fulvic acid at a fixed degree of neutralization.

III. Development of Site-Binding Model for Anticipation of Cu^{2+} Binding to Armadale Horizons Bh Fulvic Acid

On the basis of the earlier study of the protonation properties of the Armadale Horizons Bh fulvic acid (5) it was estimated that of the total acidity measurable in aqueous solutions of Armadale fulvic acid 24.5% is attributable to a fairly strong carboxylic acid component characterized by an intrinsic pK of 1.8 (site I), 30.4% to a somewhat weaker carboxylic acid with an intrinsic pK of 3.4 (site II), and 22.4% to a still weaker carboxylic acid characterized by an intrinsic pK of 4.2 (site III); the remaining 22.7% of the acidity measurable in aqueous media was assigned to an acidic alcohol (enol) with an intrinsic pK of 5.7 (site IV).

It was also deduced from the data that two of the four acidic units corresponding to approximately 50% of the total acidity measurable in aqueous media must be associated in a bifunctional mode with two moieties too weakly acidic to be detected in the titrations with standard base. The 25–30% increase in proton release from the fulvic acid in the presence of excess Eu(III) ion was believed to provide strong evidence for one of them, while the 50% increase in proton release in the presence of excess Cu(II) ion was taken to indicate the existence of the additional weakly acidic functionality.

The two acidic units that were considered to be in an ortho position to the weaker acidic units of the two bidentate moieties presumed to be involved in the chelation of the Cu^{2+} ion were the carboxylic acid with a pK of 3.4 (site II) and the acidic alcohol with a pK of 5.7 (site IV). In the first instance the chelating unit is salicylic-acid-like (p$K_2 \sim 13$), while in the second instance one could envisage two OH units with p$K_2 \sim 11$. This estimate was based on the expectation that both Cu^{2+} and Eu^{3+} form strong enough chelates to release both protons of the dihydroxyl ligand presumed to be a component site of the Armadale fulvic acid. In the salicylic-acid-like unit hypothesized, only the Cu^{2+} ion could be expected to form the chelate. The pK of Cu salicylate is sufficiently large (pK_{CuSal} = 10.67) to release the proton from the OH group ortho (pK = 13) to the carboxylic acid unit while the pK of the Eu salicylate$^+$ (p$K_{EuSal^+} \sim 4.4$) is not (*6*).

It was concluded that the highly selective binding, at low pH levels, of Cu^{2+} by the fulvic acid molecule, when Cu^{2+} was present in a small quantity, could best be accounted for by the presence of an aminocarboxylic acid site in relatively low quantity. An amine group was consequently assigned a position ortho to 23.3% of the second carboxylic acid site to form a bidentate moiety sufficiently like the β-carboxymethylaminopropionic acid molecule (*6*) to mimic its complexation of Cu^{2+}. This abundance assignment is consistent with the nitrogen content listed in the elemental analysis reported for the Armadale Horizons Bh fulvic acid.

Finally, it has been observed that the OH site (site IV) is more accessible to multivalent metal ions than can be reasonably accounted for in the proposed dihydroxyl chelation route. Rationalization of binding experiments with trace-level concentrations of each metal ion required an alternate, more easily accessible path to chelation with this moiety (*7*). This requirement has been met by proposing that approximately 10% of the very weakly acidic OH neighbor of the site IV hydroxyl group is replaced by a carbonyl group.

Without resorting to this device attempts to correlate trace metal–ion binding measurements compiled in ion-exchange distribution studies using $^{60}Co^{2+}$, $^{65}Zn^{2+}$, $^{113}Cd^{2+}$, and $^{154}Eu^{3+}$ (*7*) with the sequence of sites deduced from the earlier protonation studies (*5*) severely underestimated the observed results.

The above assignment of another chelating route to site IV was based on the following logic: First, the differences between the measured binding of trace-metal ion and estimates of this parameter, based on the use of literature-based stability constants for the complexed species presumed to be formed with the sequence of sites deduced from the earlier protonation studies (*6*), were evaluated. These quantities of metal ion, presumed to be bound to a site, S, not considered in the earlier computations, divided by the experimentally measured concentration of free metal ion and the unaccessible concentration, C_s, of the postulated site, were then equated with eq 1, given below, to the stability constant of the complex, $MA^{(Z-1)+}$, presumed to be formed. With this equation, the value of α_S, the degree of dissociation of the S site, was related to

$$\frac{(M_b^{\text{exptl}} - M_b^{\text{calcd}})}{(M_f^{Z+})\left(\exp\left(-\frac{Z\epsilon\psi(a)}{kT}\right)\right)(\gamma_{M^{Z+}})(\alpha_S C_S)} = \beta_{MA^{(Z-1)+}} \qquad (1)$$

each other in x sets of experiments through the solution of x simultaneous equations arrived at by equating the left-hand side of eq 1, which is invariant. This procedure eliminated the need for real values of C_S and $\beta_{MA^{(Z-1)+}}$, which cancel in the operations. The exponential term was available as described in the second paper of this series

(5), and $\gamma_{M^{z+}}$ was accessible from Kielland's computation of single ion activity coefficients (8).

With the relative magnitude of α_x made available in this way the Henderson–Hasselbalch equation, modified as shown in eq 2, could be used to identify the site involved in the extra binding of the trace multivalent metal ion. To

$$\mathrm{pH} - \log \frac{\alpha x}{1 - \alpha x} - \exp(-\epsilon\psi_{(a)}/kT) = \mathrm{p}K^{\mathrm{int}}{}_{\mathrm{HS}} \quad (2)$$

do this, it was only necessary to test the arbitrary assignments of an absolute α value for use in the evaluation of the additional $(x - 1)$ α values to be employed in eq 2. The eventual correct assessment of an initial x value, if our estimate of the problem is correct, had to lead to a sequence of $(x - 1)$ α values that resolved a constant value for $\mathrm{p}K^{\mathrm{int}}{}_{\mathrm{HS}}$ with eq 2. The constant value of 5.65 ± 0.02 that is eventually resolved through the most appropriate assignment of α showed (1) that our assessment of the situation was correct and (2) that S had to be identified with the OH functional group assigned in the earlier protonation studies to site IV.

The fact that (1) the extra binding of the trace-metal ion studies, when examined in eq 1, yields $\beta_{\mathrm{MS}^{(z-1)+}}$ values in agreement with the formation constant values published for the acetylacetonate complexes with these respective metal ions when C_S is taken to correspond to ~10% of the site IV abundance in the fulvic acid molecule and that (2) the extra proton release by excess macro concentrations of Eu^{3+} (5) has to continue to remain reasonably consistent with the abundance assigned to this site has influenced our decision to relate this extra binding to substitution of the phenolic OH neighbor of site IV by a carbonyl group 10% of the time.

With this picture of the fulvic acid molecule eight Cu^{2+}-bound species, four unidentate species at site I, II, III, and IV, and four chelated species were presumed to form by simultaneous interaction of Cu^{2+} with the acidic units considered to be accessible, the quantity of Cu^{2+} bound by each depending on site availability and the respective free energy of formation. To facilitate this approach, the formation constants of the Cu^{2+}-bound species presumed to be formed in the system were assigned the literature values reported for their formation with the molecules resembled (6).

Before proceeding with such examination of these equilibria it was necessary first to determine $\alpha_{\mathrm{eff}}{}^{\circ}$, the effective overall degree of dissociation of the fulvic acid. This was accomplished in a two-step procedure. First, the experimental pH was used to interpolate $\mathrm{p}K^{\mathrm{app}}{}_{\mathrm{FA}}$ from the plot of $\mathrm{p}K^{\mathrm{app}}{}_{\mathrm{FA}}$ vs. pH obtained in our earlier protonation studies (5). The value of α_0 was then resolved from a separate plot of $\mathrm{p}K^{\mathrm{app}}{}_{\mathrm{FA}}$ vs. α obtained for Armadale Horizons Bh at the ionic strength of the system under investigation.

The value of $\alpha_{\mathrm{eff}}{}^{\circ}$, so determined, yielded the appropriate correction for concentration enhancement $(\exp(-\epsilon\psi_{(a)}/kT))$ of the free mobile counerions at the surface of the charged molecule

$$\mathrm{p}K^{\mathrm{int}}{}_{(\mathrm{FA})_n} + \exp(-\epsilon\psi_{(a)}/kT) = \mathrm{pH} - \log \frac{\alpha_n}{1 - \alpha_n} \quad (2a)$$

This term, accessible from our earlier analysis of protonation data compiled in the second paper of this series (Figure 23 and 24 of ref 5), was then used in eq 2a to determine the fractional dissociation of the three carboxylic acid and enol groups at every experimental situation.

The subscript n in eq 2a refers to the particular acidic site under consideration. With α_n made available in this way and with reasonable estimates of the magnitude of stability parameters appropriate for analysis of the formation of Cu(II)-bound species most likely to be formed accessible from the literature the following sequence of computations was entered to compute the quantity of each species formed at a particular experimental pH and pCu.

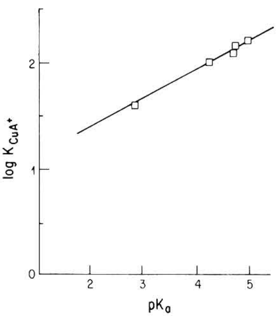

Figure 1. Linear relationship between log CuA^+ and pK of the corresponding monocarboxylic acid molecule.

To evaluate the quantity of unidentate species being formed in the course of our experiment at carboxylic acid sites I and III, the following equation was solved:

$$\beta_{\mathrm{CuR(COO)}_n{}^+} = \mathrm{CuR(COO)}_n{}^+/\mathrm{Cu_f}{}^+(\exp(-2\epsilon\psi a/kT)) \times (\gamma \mathrm{Cu}^{2+})(\alpha_n)[A_n(\mathrm{FA})_i - \mathrm{CuR(COO)}_n{}^+] \quad (3)$$

The formation constants of 2.5×10^1 and 1.7×10^2 assigned to $\beta_{\mathrm{CuR(COO)}_I{}^+}$ and $\beta_{\mathrm{CuR(COO)}_{\mathrm{III}}}$ were obtained from interpolation of the logarithmic plot of literature-based CuA^+ stability constants vs. the pK values of their corresponding monocarboxylic acid source, which are presented in Figure 1. This figure is based on the study of Lloyd who first demonstrated this linear relationship (9). There is a correction for Debyean long-range interaction of the Cu^{2+} with co-ions included in these equations to reduce the measured concentration to an effective concentration. This term, denoted by $\gamma_{Cu^{2+}}$, was obtained from Kielland's table of single ion activity coefficients (8). The $\exp(-\epsilon\psi_{(a)}/kT)$ term, extracted earlier from Figure 24 of the preceding paper (5) in this series to permit evaluation of α_n, is squared in eq 3 to correct for enhancement of the divalent Cu^{2+} at the site of reaction by the net electric field emanating from the charged surface of the fulvic acid molecule.

To evaluate the removal of Cu^{2+} from solution as both the salicylate-like chelate, $\mathrm{Cu(COO_{II})R(CO)}$, and the aminocarboxylic chelate, $\mathrm{Cu(COO_{II})RNH_2}^+$, and their competing unidentate species, $\mathrm{Cu(COO_{II})RCOH^+}$ and $\mathrm{Cu(COO_{II})RNH_3}^{2+}$, the following two sets of simultaneous equations were employed:

$$K_{\mathrm{Cu(COO_{II})R(CO)}} = (\mathrm{Cu(COO_{II})R(CO)}(a_{\mathrm{H}^+})/(\mathrm{Cu_f}^{2+}) \times (\exp(-\epsilon\psi_{(a)}/kT))(\gamma_{\mathrm{Cu}^{2+}})(\alpha_{\mathrm{II}})\{(A_{\mathrm{II}} - 0.07)(\mathrm{FA}_i) - (\mathrm{Cu(COO_{II})R(CO)} - (\mathrm{CuCOO_{II}})\mathrm{R(COH^+)}\} \quad (4)$$

$$\beta_{\mathrm{Cu(COO_{II})COH^+}} = (\mathrm{Cu(COO_{II})RCOH})^+/(\mathrm{Cu_f}^{2+}) \times (\exp(-2\epsilon\psi_{(a)}/kT))(\gamma_{\mathrm{Cu}^{2+}})(\alpha_{\mathrm{II}})\{(A_{\mathrm{II}} - 0.07)(\mathrm{FA}_i) - (\mathrm{Cu(COO_{II})RCO}) - \mathrm{Cu(COO_{II})RCOH^+}\} \quad (5)$$

and

$$K_{\mathrm{Cu(COO)_{II}RNH_2}^+} = (\mathrm{Cu(COO)_{II}RNH_2}^+)(a_{\mathrm{H}^+})/(\mathrm{Cu_f}^{2+}) \times (\exp(-\epsilon\psi_{(a)}/kT))(\gamma_{\mathrm{Cu}^{2+}})(\alpha_{\mathrm{II}})\{(A_{\mathrm{II}} - 0.23)\mathrm{FA}_i - \mathrm{Cu(COO)_{II}RNH_2}^+ - \mathrm{Cu(COO)_{II}RNH_3}^{2+}\} \quad (6)$$

and

$$\beta_{\mathrm{Cu(COO)_{II}RNH_3^{2+}}} = \mathrm{Cu(COO)_{II}RNH_3^{2+}}/(\mathrm{Cu_f^{2+}}) \times (\exp(-2\epsilon\psi_{(a)}/kT))(\gamma_{\mathrm{Cu^{2+}}})(\alpha_{\mathrm{II}})\{(A_{\mathrm{II}} - 0.23)\mathrm{FA}_i - \mathrm{Cu(COO)_{II}RNH_2^+} - \mathrm{Cu(COO)_{II}RNH_3^{2+}}\} \quad (7)$$

In the computations with eq 4–7 carboxylic acid site II is considered to be shared with the OH (23%) and NH_2 (7%) moieties, and its accessibility for formation of the bidentate and unidentate species designated above is expressed in these equations by $A_{\mathrm{II}} - 0.07$ and $A_{\mathrm{II}} - 0.23$ where $A_{\mathrm{II}} = 0.30$. The first of each of the two equations had to be expressed as it is because the concentrations of $\mathrm{(COO_{II})R(CO)^{2-}}$ and $\mathrm{(COO_{II})RNH_2^-}$ necessary for describing the formation of each chelate directly are not accessible. Instead we have described the following equilibria, which are more amenable to analysis:

$$\mathrm{Cu^{2+} + (HOC)R(COO_{II}^-) \rightleftarrows Cu(COO_{II})R(CO) + H^+} \quad (8a)$$

$$\mathrm{Cu^{2+} + H_3^+NR(COO_{II}^-) \rightleftarrows CuCOO_{II}RNH_2^+ + H^+} \quad (8b)$$

Because the K for these reactions, multiplied in the first instance by the formation constant of the phenolic group and in the second instance by the formation constant of the amine group, is equal to $\beta_{\mathrm{Cu(COO_{II})R(CO)}}$ and $\beta_{\mathrm{Cu(COO_{II})RNH_2^+}}$, respectively, we have assigned $K_{\mathrm{Cu(COO)RCO}}$ and $K_{\mathrm{Cu(COO_{II})RNH2^+}}$ values of 0.027 and 16. The pK of the phenolic group in salicylic acid is 13, and a K assignment of 0.027 corresponds to a β value of 2.7×10^{11}. The literature value of 4.7×10^{10} reported for this chelate in 0.1 M KCl reduces to the above value at zero ionic strength. Similarly, the pK of the amine in methylaminopropionic acid, selected as an appropriate representation of the aminocarboxylic acid site proposed, is 9.46 at $I = 0.1$, and the product $(K_{\mathrm{Cu(COO_{II})RNH_2^+}})(\beta_{\mathrm{COO_{II}RNH_3^+}}) = 4.6 \times 10^{10}$. The literature value of 2.8×10^{10} ($I = 0.1$) reported for this chelate is thus consistent with the assignment of 16 to $K_{\mathrm{Cu(COO_{II})RNH_2^+}}$. The stability constant employed for the unidentate species was 5.0×10^1, the β value corresponding, according to Figure 1, to a unidentate complex of Cu^{2+}, CuA^+, with a monocarboxylic acid moiety of approximately the same acid strength as site II. In eq 4 and 6 the squared $\exp(-\epsilon\psi_{(a)}/kT)$ term has been partially canceled by its simultaneous use to correct for enhancement of the univalent H ion concentration at the negatively charged surface of the fulvic acid molecule.

Evaluation of the simultaneous binding of Cu^{2+} in a unidentate mode to the acidic alcohol and in the chelates formed with the hydroxyl carbonyl and the dihydroxyl unit, respectively, used eq 9–11 in a manner paralleling the approach used in eq 4 and 5 and 6 and 7.

$$K_{\mathrm{Cu(CO_{IV}CRCO)}} = \mathrm{Cu(O_{IV}CRCO)} \times (a_{\mathrm{H^+}})/\mathrm{Cu_f^{2+}}(\exp(-\epsilon\psi_{(a)}/kT))\gamma_{\mathrm{Cu^{2+}}}(\alpha_{\mathrm{IV}})\{(A_{\mathrm{IV}})(0.9) \times (\mathrm{FA}_i) - \mathrm{Cu(O_{IV}CRCO)} - 0.9\mathrm{Cu(O_{IV}CRCOH)^+}\} \quad (9)$$

$$K_{\mathrm{Cu(CO_{IV}CRCO)^+}} = \mathrm{Cu(O_{IV}CRCO)^+}/(\mathrm{Cu_f^{2+}}) \times (\exp(-2\epsilon\psi_{(a)}/kT))(\gamma_{\mathrm{Cu}}{}^{2+})(\alpha_{\mathrm{IV}})\{A_{\mathrm{IV}}(0.1)(\mathrm{FA}_i) - \mathrm{Cu(O_{IV}CRCO)^+} - 0.1\mathrm{Cu(O_{IV}CRCOH)^+}\} \quad (10)$$

$$K_{\mathrm{Cu(O_{IV}CRCOH)^+}} = \mathrm{Cu(O_{IV}CRCOH)^+}/(\mathrm{Cu_f^{2+}}) \times (\exp(-2\epsilon\psi_{(a)}/kT))(\gamma_{\mathrm{Cu}}{}^{2+})\alpha_{\mathrm{IV}}\{A_{\mathrm{IV}}(\mathrm{FA}_i) - \mathrm{Cu(O_{IV}CRCO)} - \mathrm{Cu(O_{IV}CRCO)^+} - \mathrm{Cu(O_{IV}CRCOH)^+}\} \quad (11)$$

an equation directly expressing the formation constant of the dihydroxyl-based chelate could not be used once again because of inaccessibility of the concentration of the bidentate ligand site to computation. To circumvent this

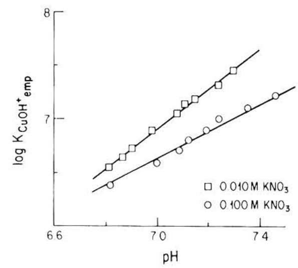

Figure 2. Hydrolysis of cupric ion.

difficulty as before, a K value of 2.0×10^{-2} was employed in eq 9. The product of this K value and the β value of $\sim 5 \times 10^{10}$ arbitrarily assigned to the weakly acidic hydroxyl group associated with the site IV enolate-bound Cu^{2+} leads to a β value of $\sim 1.0 \times 10^9$ for the chelate presumed to be formed. This β value is in reasonable accord with the formation constant values of oxygen-linked bidentate complexes of Cu^{2+} (*6*).

In eq 9 and 10 the abundance of the dihydroxyl group is reduced by 10% and 90% to account for the substitution with 10% frequency of a CO group for the neighboring phenolic group of this bidentate site. For an estimate of the quantity of Cu^{2+} bound by this substitute chelating group with eq 10 the formation constant of this chelate was also assigned a value of 10^9. In this instance there is experimentally based support for this assessment of the stability constant of $\mathrm{Cu(O_{IV}CRCO)}$ to lend additional credance to the selection of a β of 10^9 for both chelates. The tracer level studies mentioned earlier (7) yielded a β value of $\sim 10^6$ for the Co^{2+} and Zn^{2+} complexes formed with the postulated hydroxyl, carbonyl moiety. The literature-based stability contants of the analogous complexes of Co^{2+} (Zn^{2+}) and Cu^{2+} with acetylacetonate bear the ratio of 1:1000 that has been used to reach this value of 10^9.

The β value of 2.62×10^2 assigned to the unidentate complex formed with the fourth site was interpolated from Figure 1 once again.

In order to correct for hydrolysis of the Cu^{2+} ion in the high pH range, empirical relationships, based on potentiometric examination (pH, pCu) of dilute ($\leq 10^{-4}$ M) $Cu(NO_3)_2$ solutions in 0.10 and 0.010 M KNO_3 during the addition of standard base were compiled to describe the removal of Cu^{2+} from solution. These equations took the following form:

$$\mathrm{Cu_b} = (\mathrm{Cu_f})(\mathrm{OH})(K_{\mathrm{emp}}) \quad (12)$$

where K_{emp}, expressed as

$$K_{\mathrm{emp}} = \mathrm{Cu_b}/\mathrm{Cu_f}(\mathrm{OH}) \quad (13)$$

was available as a plot of log K_{emp} vs. pH (Figure 2).

In order to appreciate the need for this particular approach, let us examine the pH pattern obtained with a dilute $Cu(NO_3)_2$ solution to which standard base is slowly added. The system (see Figure 3) is buffered due to the hydrolysis of Cu^{2+} once a pH value between 5 and 6 is reached. This buffered region while primarily attributable to the formation of $Cu(OH)^+$ initially is complicated by the formation of $Cu(OH)_2$ and possibly by polymerization tendencies of the hydrolysis products. If we now compare this curve with the pH pattern obtained during neutralization of the FA in the presence of different quantities of $Cu(NO_3)_2$ (Figures 3, 14–16 in the preceding paper of this series (5)) we see that in excess $Cu(NO_3)_2$ the system is buffered in much the same way as it was in the absence

Table I. Binding of Cu^{2+} to Armadale Horizons Bh Fulvic Acid, Calculated vs. Experimental[a]

base, mL	pH	pCu	$Cu^{lit}_{b(calcd)}$	$Cu_{b(exptl)}$
A. Total FA = 0.4989 mmol; Total millimoles Cu^{2+} = 0.1044 mmol				
0.0000E+00	2.6720E+00	2.8180E+00	3.9933E-02	2.6852E-02
1.0000E-01	2.6840E+00	2.8370E+00	3.9888E-02	3.0026E-02
5.000E-01	2.7800E+00	2.8730E+00	4.3121E-02	3.5407E-02
8.0000E-01	2.8530E+00	2.8730E+00	4.6296E-02	3.5005E-02
1.0000E+00	2.9140E+00	2.8890E+00	4.8363E-02	3.7257E-02
1.2000E+00	2.9730E+00	2.9180E+00	4.9884E-02	4.1352E-02
1.4000E+00	3.0450E+00	2.9280E+00	5.2494E-02	4.2551E-02
1.6000E+00	3.1190E+00	2.9640E+00	5.4352E-02	4.7254E-02
1.8000E+00	3.1840E+00	2.9900E+00	5.6195E-02	5.0370E-02
2.0000E+00	3.2860E+00	3.0350E+00	5.9086E-02	5.5504E-02
2.2000E+00	3.3820E+00	3.0840E+00	6.1794E-02	6.0556E-02
2.4000E+00	3.4850E+00	3.1290E+00	6.5395E-02	6.4723E-02
2.6000E+00	3.5990E+00	3.2100E+00	6.8430E-02	7.1351E-02
2.8000E+00	3.7230E+00	3.2970E+00	7.2307E-02	7.7249E-02
3.0000E+00	3.8590E+00	3.3880E+00	7.7588E-02	8.2300E-02
3.2000E+00	3.9950E+00	3.4980E+00	8.6601E-02	8.7181E-02
3.4000E+00	4.1560E+00	3.6370E+00	8.5594E-02	9.1851E-02
3.6000E+00	4.3090E+00	3.7700E+00	8.5125E-02	9.5128E-02
3.8000E+00	4.5180E+00	3.9640E+00	8.4225E-02	9.8446E-02
3.9000E+00	4.5970E+00	4.0520E+00	8.3010E-02	9.9530E-02
4.0000E+00	4.6910E+00	4.1300E+00	8.3295E-02	1.0035E-01
4.2000E+00	4.9190E+00	4.3530E+00	8.2635E-02	1.0195E-01
4.4000E+00	5.1280E+00	4.5410E+00	8.3221E-02	1.0281E-01
4.6000E+00	5.3260E+00	4.7450E+00	8.2375E-02	1.0340E-01
4.8000E+00	5.6160E+00	4.9870E+00	8.5649E-02	1.0383E-01
4.9000E+00	5.7020E+00	5.0910E+00	8.4680E-02	1.0395E-01
5.0000E+00	5.8410E+00	5.1880E+00	8.8275E-02	1.0404E-01
5.1000E+00	5.9470E+00	5.3050E+00	8.8220E-02	1.0412E-01
5.2000E+00	6.1190E+00	5.4150E+00	9.4637E-02	1.0418E-01
5.3000E+00	6.2550E+00	5.5770E+00	9.4166E-02	1.0425E-01
5.4000E+00	6.4030E+00	5.6510E+00	1.0265E-01	1.0427E-01
5.5000E+00	6.5830E+00	5.8100E+00	1.0742E-01	1.0431E-01
5.6000E+00	6.7240E+00	5.9650E+00	1.0811E-01	1.0434E-01
5.7000E+00	6.9100E+00	6.0920E+00	1.1672E-01	1.0435E-01
5.8000E+00	7.0780E+00	6.2790E+00	1.1654E-01	1.0437E-01
B. Total FA = 0.3991 mmol; Total Cu^{2+} = 0.1570 mmol				
0.0000E+00	2.6040E+00	2.5820E+00	3.5782E-02	4.8345E-02
2.0000E-01	2.6680E+00	2.5850E+00	3.8175E-02	4.8573E-02
4.0000E-01	2.7190E+00	2.5880E+00	4.0022E-02	4.8803E-02
6.0000E-01	2.7810E+00	2.5950E+00	4.2131E-02	5.0025E-02
8.0000E-01	2.8400E+00	2.6050E+00	4.4022E-02	5.1963E-02
1.0000E+00	2.9080E+00	2.6150E+00	4.6271E-02	5.3869E-02
1.2000E+00	2.9840E+00	2.6190E+00	4.9141E-02	5.4334E-02
1.4000E+00	3.0730E+00	2.6430E+00	5.2049E-02	5.9398E-02
1.6000E+00	3.1570E+00	2.6730E+00	5.4769E-02	6.5488E-02
1.8000E+00	3.2550E+00	2.7140E+00	5.8066E-02	7.3346E-02
2.0000E+00	3.3350E+00	2.7270E+00	6.2217E-02	7.5438E-02
2.2000E+00	3.4560E+00	2.7680E+00	6.8393E-02	8.2444E-02
2.4000E+00	3.5540E+00	2.7950E+00	7.4817E-00	8.6618E-02
2.6000E+00	3.6840E+00	2.8490E+00	8.3469E-02	9.4563E-02
2.8000E+00	3.8490E+00	2.9060E+00	9.7906E-02	1.0199E-01
3.0000E+00	4.0080E+00	2.9810E+00	1.1807E-01	1.1050E-01
3.1000E+00	4.0700E+00	3.0150E+00	1.1916E-01	1.1391E-01
3.2000E+00	4.1580E+00	3.0720E+00	1.1975E-01	1.1913E-01
3.3000E+00	4.2320E+00	3.0990E+00	1.2284E-01	1.2133E-01
3.4000E+00	4.3350E+00	3.1970E+00	1.2012E-01	1.2847E-01
3.5000E+00	4.4150E+00	3.2280E+00	1.2336E-01	1.3038E-01
3.6000E+01	4.5550E+00	3.2960E+00	1.2754E-01	1.3419E-01
3.7000E+00	4.6570E+00	3.3530E+00	1.2980E-01	1.3695E-01
3.8000E+00	4.7920E+00	3.4380E+00	1.3182E-01	1.4048E-01
3.9000E+00	4.9160E+00	3.5190E+00	1.3352E-01	1.4326E-01
4.0000E+00	5.0640E+00	3.6200E+00	1.3539E-01	1.4609E-01
4.1000E+00	5.1740E+00	3.7560E+00	1.3093E-01	1.4900E-01
4.2000E+00	5.3560E+00	3.8740E+00	1.3520E-01	1.5089E-01
4.3000E+00	5.5260E+00	4.0200E+00	1.3683E-01	1.5263E-01
4.4000E+00	5.7060E+00	4.1820E+00	1.3930E-01	1.5398E-01
4.5000E+00	5.8640E+00	4.3610E+00	1.3913E-01	1.5500E-01
4.7000E+00	6.2690E+00	4.7100E+00	1.5235E-01	1.5610E-01
4.8000E+00	6.4210E+00	4.9030E+00	1.5172E-01	1.5642E-01
4.9000E+00	6.6370E+00	5.1190E+00	1.5574E-01	1.5665E-01
5.0000E+00	6.7850E+00	5.2780E+00	1.5702E-01	1.5675E-01
5.1000E+00	7.0010E+00	5.4910E+00	1.5981E-01	1.5685E-01
C. Total FA = 0.2883 mmol; Total Cu^{2+} = 0.02088 mmol				
0.0000E+00	2.7990E+00	3.6590E+00	1.3526E-02	1.2065E-02
2.0000E-01	2.8560E+00	3.6940E+00	1.4290E-02	1.2707E-02
4.0000E-01	2.9700E+00	3.7490E+00	1.6116E-02	1.3644E-02
6.0000E-01	3.0960E+00	3.8210E+00	1.8080E-02	1.4719E-02
8.0000E-01	3.2430E+00	3.9170E+00	2.0172E-02	1.5917E-02
1.0000E+00	3.4100E+00	4.0580E+00	2.1961E-02	1.7275E-02
1.2000E+00	3.6200E+00	4.2370E+00	2.3896E-02	1.8481E-02
1.4000E+00	3.8780E+00	4.4920E+00	2.5507E-02	1.9540E-02
1.6000E+00	4.1620E+00	4.8180E+00	2.6315E-02	2.0244E-02
1.8000E+00	4.4420E+00	5.1490E+00	2.6170E-02	2.0582E-02
2.0000E+00	4.7620E+00	5.4990E+00	2.6134E-02	2.0746E-02
2.2000E+00	5.0440E+00	5.8190E+00	2.5952E-02	2.0816E-02
2.4000E+00	5.5260E+00	6.3040E+00	2.6008E-02	2.0859E-02
2.6000E+00	5.9570E+00	6.7440E+00	2.6024E-02	2.0872E-02
2.7000E+00	6.2540E+00	7.0470E+00	2.6065E-02	2.0876E-02
2.8000E+00	6.5840E+00	7.4010E+00	2.6001E-02	2.0878E-02
2.9000E+00	6.9450E+00	7.7280E+00	2.6363E-02	2.0879E-02

[a] System: Cu^{2+}, FA, KNO_3: ionic strength = 0.10.

of FA. When the Cu^{2+} is already fully complexed by the FA no buffered region appears.

IV. Results and Discussion

(a) Test of Model. The results obtained from analysis of those experiments in which the ratio of Cu^{2+} to FA was fixed prior to stepwise addition of standard alkali are summarized in Table I (0.10 M KNO_3) and Table II (0.010 M KNO_3), while the results obtained in those experiments in which Cu^{2+} was added stepwise to the FA already at a fixed degree of neutralization are listed in Tables III (0.10 M KNO_3) and IV (0.010 M KNO_3). The predictions of bound Cu, computed as described above, are compared with the experimentally determined values in columns 4 and 5 of these tables.

Bias introduced into the estimates of bound Cu^{2+} by small error in the measurements of free Cu^{2+} was highly susceptible to experimental conditions. It was not in the computations of this parameter for comparison, even though both estimates were based on the same measurements. The nature of the computation was such that any error introduced was directly proportional to error in the measurement.

In those experiments where the ratio of Cu^{2+} to FA was fixed (Tables I and II) and base was added in small increments the first points were always compiled at relatively low pH values. As a consequence the extent of Cu^{2+} binding was usually quite low at the start; the initial estimates of bound Cu^{2+} listed in these tables are consequently the most susceptible to error. The precision of 1 mV in the measured potential that was achieved translates into an 8% uncertainty in the Cu^{2+} ion measurement. This level of uncertainty has to lead to a much larger uncertainty in the first experimentally based estimates of bound Cu^{2+}, since they are obtained from the small difference between two numbers very close to each other in magnitude.

Uncertainty in binding estimates approaches the 8% uncertainty level of the measurement itself when 40–80% of the Cu^{2+} initially present is bound to the fulvic acid molecule. With the last points compiled in these experiments almost all of the Cu^{2+} ion is eventually sequestered, and the estimate of bound Cu^{2+} is completely insensitive to error in the measurement.

In those experiments where the FA was initially at a fixed degree of neutralization and Cu^{2+} was added in small

Table II. Binding of Cu^{2+} to Armadale Horizons Bh Fulvic Acid, Calculated vs. Experimental[a]

base, mL	pH	pCu	$Cu^{lit}_{b(calcd)}$	$Cu_{b(exptl)}$
	A. Total FA = 0.04399 mmol; Total Cu^{2+} = 0.0522 mmol			
0.0000E+00	3.3950E+00	3.0880E+00	5.5355E-03	1.0963E-02
5.0000E-01	3.4640E+00	3.0580E+00	6.1033E-03	7.5759E-03
1.0000E+00	3.5630E+00	3.0810E+00	6.7328E-03	9.4627E-03
1.5000E+00	3.6680E+00	3.0850E+00	7.6829E-03	9.4434E-03
2.0000E+00	3.7820E+00	3.0880E+00	8.9784E-03	9.3294E-03
3.0000E+00	4.1270E+00	3.1420E+00	1.3797E-02	1.3621E-02
4.0000E+00	4.6230E+00	3.1880E+00	2.1827E-02	1.6849E-02
5.0000E+00	5.3230E+00	3.3220E+00	2.8873E-02	2.5758E-02
6.0000E+00	5.8100E+00	3.4060E+00	3.2917E-02	3.0016E-02
6.5000E+00	5.9890E+00	3.4670E+00	3.3099E-02	3.2752E-02
7.0000E+00	6.0910E+00	3.5440E+00	3.2433E-02	3.5769E-02
7.5000E+00	6.2330E+00	3.6400E+00	3.1801E-02	3.8913E-02
8.0000E+00	6.3470E+00	3.7320E+00	3.1020E-02	4.1357E-02
8.5000E+00	6.4750E+00	3.8620E+00	2.9893E-02	4.4093E-02
9.0000E+00	6.5760E+00	3.9880E+00	2.8848E-02	4.6083E-02
9.5000E+00	6.6920E+00	4.1680E+00	2.7483E-02	4.8125E-02
1.0000E+01	6.8300E+00	4.4280E+00	2.5860E-02	4.9942E-02
	B. Total FA = 0.04399 mmol; Total Millimoles Cu^{2+} = 0.03132 mmol			
0.0000E+00	3.4130E+00	3.3300E+00	4.8088E-03	7.7929E-03
1.0000E+00	3.6060E+00	3.3560E+00	5.6753E-03	8.7195E-03
1.5000E+00	3.7250E+00	3.3710E+00	6.3761E-03	9.2740E-03
2.0000E+00	3.8540E+00	3.3750E+00	7.4206E-03	9.2653E-03
3.0000E+00	4.2460E+00	3.4650E+00	1.1374E-02	1.3050E-02
4.0000E+00	4.8130E+00	3.5890E+00	1.8204E-02	1.7331E-02
4.5000E+00	5.2000E+00	3.6520E+00	2.2052E-02	1.9108E-02
4.6000E+00	5.2480E+00	3.6940E+00	2.1963E-02	2.0214E-02
4.8000E+00	5.4310E+00	3.7650E+00	2.3026E-02	2.1854E-02
5.0000E+00	5.5690E+00	3.8020E+00	2.4145E-02	2.2596E-02
5.5000E+00	5.9560E+00	3.9940E+00	2.5676E-02	2.5662E-02
5.8000E+00	6.1470E+00	4.1210E+00	2.5610E-02	2.7074E-02
6.0000E+00	6.2880E+00	4.2520E+00	2.5020E-02	2.8169E-02
6.2000E+00	6.4110E+00	4.4100E+00	2.4107E-02	2.9122E-02
6.6000E+00	6.7200E+00	4.7850E+00	2.2699E-02	3.0387E-02
6.8000E+00	6.8940E+00	5.1110E+00	2.1464E-02	3.0878E-02
7.0000E+00	7.1230E+00	5.4300E+00	2.0939E-02	3.1107E-02
7.1000E+00	7.1960E+00	5.6030E+00	2.0258E-02	3.1177E-02
	C. Total FA = 0.04399 mmol; Total Cu^{2+} = 0.01044 mmol			
0.0000E+00	3.4960E+00	3.8740E+00	3.8375E-03	3.7437E-03
1.0000E+00	3.7260E+00	3.9360E+00	4.4656E-03	4.5186E-03
1.5000E+00	3.8630E+00	3.9580E+00	4.8909E-03	4.7561E-03
2.0000E+00	4.0570E+00	4.0480E+00	5.4141E-03	5.7751E-03
2.5000E+00	4.2820E+00	4.1660E+00	6.0807E-03	6.8309E-03
3.0000E+00	4.6050E+00	4.3450E+00	7.1576E-03	8.0406E-03
3.5000E+00	5.0090E+00	4.6450E+00	7.9962E-03	9.2262E-03
4.0000E+00	5.5970E+00	5.1450E+00	8.3370E-03	1.0053E-02
4.2000E+00	5.8180E+00	5.3900E+00	8.0691E-03	1.0219E-02
4.4000E+00	6.1440E+00	5.6750E+00	8.3579E-02	1.0325E-02
4.5000E+00	6.2870E+00	5.8320E+00	8.3156E-03	1.0360E-02
4.6000E+00	6.4400E+00	5.9380E+00	8.7622E-03	1.0377E-02
4.7000E+00	6.5800E+00	6.1170E+00	8.5562E-03	1.0398E-02
4.8000E+00	6.7770E+00	6.2850E+00	8.9154E-03	1.0412E-02
4.9000E+00	6.9210E+00	6.4600E+00	8.7417E-03	1.0421E-02
5.0000E+00	7.1270E+00	6.6350E+00	9.0786E-03	1.0427E-02
	D. Total FA = 0.04075 mmol; Total Cu^{2+} = 0.00515 mmol			
0.0000E+00	3.5220E+00	4.3840E+00	2.6770E-03	3.0641E-03
2.0000E-01	3.5610E+00	4.3910E+00	2.7947E-03	3.0893E-03
4.0000E-01	3.6100E+00	4.4100E+00	2.9187E-03	3.1743E-03
6.0000E-01	3.6570E+00	4.4430E+00	3.0108E-03	3.3074E-03
8.0000E-01	3.7230E+00	4.4840E+00	3.1418E-03	3.4669E-03
1.0000E+00	3.7820E+00	4.5190E+00	3.2556E-03	3.51911E-03
1.2000E+00	3.8580E+00	4.5710E+00	3.3817E-03	3.7617E-03
1.4000E+00	3.9330E+00	4.6230E+00	3.4957E-03	3.9136E-03
1.6000E+00	4.0260E+00	4.6990E+00	3.6075E-03	4.1081E-03
1.8000E+00	4.1310E+00	4.7790E+00	3.7292E-03	4.2800E-03
2.0000E+00	4.2500E+00	4.8830E+00	3.8324E-03	4.4627E-03
2.2000E+00	4.3830E+00	5.0010E+00	3.9295E-03	4.6242E-03
2.4000E+00	4.5400E+00	5.1460E+00	4.0173E-03	4.7720E-03
2.6000E+00	4.7240E+00	5.3400E+00	4.0642E-03	4.9073E-03
2.8000E+00	4.9330E+00	5.5480E+00	4.1094E-03	4.9991E-03
3.0000E+00	5.1750E+00	5.8190E+00	4.0943E-03	5.0688E-03
3.2000E+00	5.4090E+00	6.0580E+00	4.0913E-03	5.1030E-03
3.4000E+00	5.7300E+00	6.4040E+00	4.0519E-03	5.1287E-03
3.6000E+00	6.0280E+00	6.7030E+00	4.0427E-03	5.1393E-03

Table II (Continued)

base, mL	pH	pCu	$Cu^{lit}_{b(calcd)}$	$Cu_{b(exptl)}$
3.8000E+00	6.2910E+00	6.9800E+00	4.0259E-03	5.1443E-03
4.0000E+00	6.7240E+00	7.3440E+00	4.1216E-03	5.1475E-03
4.2000E+00	7.0590E+00	7.7250E+00	4.0682E-03	5.1490E-03
	E. Total FA = 0.04075 mmol; Total Cu^{2+} = 0.002575 mmol			
0.0000E+00	3.5620E+00	4.7900E+00	2.0701E-03	1.7600E-03
2.0000E-01	3.6130E+00	4.8280E+00	2.1623E-03	1.8253E-03
4.0000E-01	3.6660E+00	4.8700E+00	2.2442E-03	1.8917E-03
6.0000E-01	3.7240E+00	4.9150E+00	2.3595E-03	1.9566E-03
8.0000E-01	3.7960E+00	4.9740E+00	2.4828E-03	2.0330E-03
1.0000E+00	3.8730E+00	5.0570E+00	2.5763E-03	2.1255E-03
1.2000E+00	3.9640E+00	5.1440E+00	2.7019E-03	2.2057E-03
1.4000E+00	4.0650E+00	5.2480E+00	2.8199E-03	2.2832E-03
1.6000E+00	4.1870E+00	5.3800E+00	2.9387E-03	2.3589E-03
1.8000E+00	4.3280E+00	5.5360E+00	3.0519E-03	2.4235E-03
2.0000E+00	4.4900E+00	5.7030E+00	3.1758E-03	2.4715E-03
2.2000E+00	4.6780E+00	5.9210E+00	3.2521E-03	2.5121E-03
2.4000E+00	4.8910E+00	6.1710E+00	3.3006E-03	2.5395E-03
2.6000E+00	5.1250E+00	6.4590E+00	3.3024E-03	2.5566E-03
2.8000E+00	5.3850E+00	6.7710E+00	3.2814E-03	2.5660E-03
3.0000E+00	5.6520E+00	7.1010E+00	3.2194E-03	2.5708E-03
3.2000E+00	5.9850E+00	7.4650E+00	3.1762E-03	2.5732E-03
3.4000E+00	6.2830E+00	7.8020E+00	3.2067E-03	2.5742E-03
3.6000E+00	6.6450E+00	8.1210E+00	3.1391E-03	2.5746E-03
3.8000E+00	6.9830E+00	8.4920E+00	3.0623E-03	2.5748E-03
4.0000E+00	7.4390E+00	8.9190E+00	3.0579E-03	2.5749E-03

[a] System: Cu^{2+}, FA, KNO_3; ionic strength = 0.010.

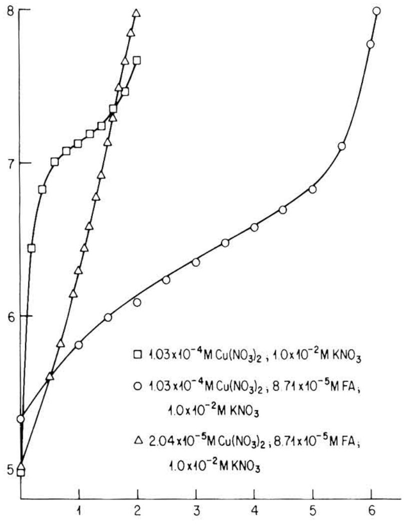

Figure 3. Comparison of the buffering properties of cupric ion in the absence and presence of fulvic acid.

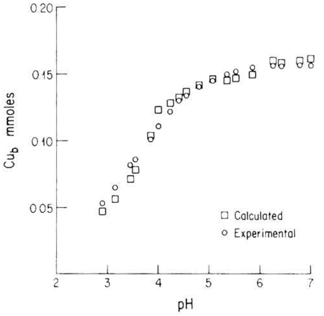

Figure 4. Comparison of the experimentally observed and model-predicted profile of cupric ion binding by fulvic acid (data from Table IB).

increments (Tables III and IV) the experimental estimates of bound Cu^{2+} were least susceptible to error at the start of the experimental run. Even as the end of these experiments was approached the difference between Cu^{2+} added to the system and the amount of Cu^{2+} remaining uncomplexed by the FA was large enough to maintain a precision level approaching 8%. Only in those instances where a large excess of Cu^{2+} was eventually added to make the difference between the initial and final concentrations of free Cu^{2+} small does the possibility of large uncertainty in the bound Cu^{2+} estimates become sizeable.

Examination of the 4th and 5th columns of Tables I–IV, while being careful to assign less weight to the bias-susceptible portions of column 5 in these tables, shows that agreement between the predicted and measured quantity of bound Cu^{2+}, using literature-based stability parameters, is, on the whole, quite good. In addition, the predictive quality is approximately the same at both ionic strengths employed in the research program to demonstrate unambiguously the validity of the electric field correction term. The graphical presentation of columns 4 and 5 from Table 1B in Figure 4 shows that the discrepancy between experiment and computation can be quite small.

One should note, however, that there is a tendency for the computation to underestimate seriously the binding of Cu^{2+} by the FA at a pH ≥5.5 in those experiments where the molar ratio of Cu^{2+} to FA approaches and exceeds unity (Table IIA, B). No rationalization of the data analysis procedure can account for the sizeable failure of the model to predict the experimental Cu^{2+} binding pattern when the ratio of Cu^{2+} to fulvic acid is high. From Table IIA, B we see that with a Cu^{2+} to fulvic acid ratio of 2.4 and 1.4 to 1 on a milliequivalent basis, calculation and experiment are in good agreement only in the lower pH range from 3.5 to ~6. Beyond this pH value compu-

Table III. Binding of Cu^{2+} of Armadale Horizons Bh Fulvic Acid at Fixed Initial Degree of Neutralization, Calculated vs. Experimental[a]

$Cu(NO_3)_2$, mL	pH	pCu	$Cu^{lit}_{b(calcd)}$	$Cu_{b(exptl)}$
	A. Total FA = 0.2520 mmol; Total Base = 0.250 mmol			
5.0000E−01	7.0940E+00	9.4100E+00	3.8370E−03	5.2200E−03
6.0000E−01	7.0280E+00	9.2110E+00	4.8422E−03	6.2640E−03
7.0000E−01	6.9680E+00	8.9650E+00	6.4999E−03	7.3080E−03
8.0000E−01	6.9260E+00	8.7910E+00	7.8139E−03	8.3519E−03
9.0000E−01	6.8710E+00	8.5840E+00	9.3985E−03	9.3959E−03
1.0000E+00	6.8260E+00	8.4100E+00	1.0742E−02	1.0440E−02
1.1000E+00	6.7780E+00	8.2290E+00	1.27073E−02	1.1484E−02
1.28000E+00	6.7310E+00	8.0840E+00	1.2992E−02	1.2528E−02
1.5000E+00	6.6030E+00	7.6570E+00	1.5421E−02	1.5659E−02
1.6000E+00	6.5630E+00	7.5560E+00	1.5849E−02	1.6703E−02
1.7000E+00	6.5210E+00	7.4260E+00	1.6441E−02	1.7447E−02
1.9000E+00	6.4450E+00	7.2370E+00	1.1762E−02	1.9834E−02
2.0000E+00	6.4130E+00	7.1210E+00	1.7696E−02	2.0877E−02
2.2000E+00	6.3400E+00	6.9400E+00	1.8381E−02	2.2963E−02
2.4000E+00	6.2700E+00	6.7660E+00	1.9074E−02	2.5049E−02
2.6000E+00	6.2020E+00	6.6100E+00	1.9700E−02	2.7134E−02
2.8000E+00	6.1380E+00	6.4470E+00	2.0489E−02	2.9218E−02
3.0000E+00	6.0870E+00	6.3240E+00	2.1124E−02	3.1301E−02
3.2000E+00	6.0130E+00	6.1430E+00	2.2202E−02	3.3379E−02
3.4000E+00	5.9570E+00	6.0520E+00	2.2555E−02	3.5460E−02
3.6000E+00	5.8950E+00	5.9080E+00	2.3555E−02	3.7533E−02
3.8000E+00	5.8320E+00	5.7480E+00	2.4943E−02	3.9598E−02
4.0000E+00	5.7950E+00	5.6790E+00	2.5428E−02	4.1673E−02
4.5000E+00	5.6670E+00	5.3930E+00	2.8342E−02	4.6810E−02
	B. Total FA = 0.1282 mmol; Total Base = 0.1034 mmol			
5.0000E−01	5.3170E+00	6.5550E+00	7.0014E−03	5.2084E−03
7.5000E−01	5.2110E+00	6.0930E+00	8.2950E−03	7.7963E−03
1.0000E+00	5.0820E+00	5.6420E+00	9.3091E−03	1.0344E−02
1.2500E+00	4.9720E+00	5.3260E+00	1.0068E−02	1.2851E−02
1.5000E+00	4.8710E+00	5.0070E+00	1.1154E−02	1.5242E−02
1.7500E+00	4.7710E+00	4.7430E+00	1.2318E−02	1.7497E−02
2.0000E+00	4.6740E+00	4.5070E+00	1.3658E−02	1.9542E−02
2.2500E+00	4.6010E+00	4.3300E+00	1.4938E−02	2.1467E−02
2.5000E+00	4.5260E+00	4.1530E+00	1.6483E−02	2.3042E−02
2.7500E+00	4.4650E+00	4.0070E+00	1.8021E−02	2.4405E−02
3.0000E+00	4.3990E+00	3.8610E+00	1.9736E−02	2.5260E−02
3.2500E+00	4.3510E+00	3.7570E+00	2.1104E−02	2.6187E−02
3.5000E+00	4.3070E+00	3.6600E+00	2.2525E−02	2.6804E−02
3.7500E+00	4.2780E+00	3.5980E+00	2.3485E−02	2.7857E−02
4.0000E+00	4.2370E+00	3.5250E+00	2.4538E−02	2.8326E−02
4.2500E+00	4.2140E+00	3.4620E+00	2.5770E−02	2.8752E−02
4.5000E+00	4.1850E+00	3.4030E+00	2.6830E−02	2.8991E−02
4.7500E+00	4.1630E+00	3.3440E+00	2.8101E−02	2.8870E−02
5.0000E+00	4.1440E+00	3.3200E+00	2.8389E−02	3.0183E−02

[a] System: FA, A^-, KNO_3; ionic strength = 0.10.

Table IV. Binding of Cu^{2+} to Armadale Horizons Bh Fulvic Acid at Fixed Initial Degree of Neutralization, Calculated vs. Experimental[a]

$Cu(NO_3)_2$, mL	pH	pCu	$Cu^{lit}_{b(calcd)}$	$Cu_{b(exptl)}$
1.0000E−01	5.9190E+00	8.5300E+00	1.4474E−03	1.0298E−03
2.0000E−01	5.7570E+00	7.5960E+00	2.6162E−03	2.0587E−03
3.0000E−01	5.5920E+00	6.9060E+00	3.3698E−03	3.0834E−03
4.0000E−01	5.4420E+00	6.3820E+00	3.7607E−03	4.0978E−03
5.0000E−01	5.2890E+00	5.9550E+00	4.0555E−03	5.0907E−03
6.0000E−01	5.1350E+00	5.5210E+00	4.4719E−03	6.0185E−03
7.0000E−01	5.0100E+00	5.1990E+00	4.9010E−03	6.8704E−03
8.0000E−01	4.9070E+00	4.9400E+00	5.3593E−03	7.6223E−03
9.0000E−01	4.8270E+00	4.7270E+00	5.8575E−03	8.2594E−03
1.0000E+00	4.7530E+00	4.5450E+00	6.3435E−03	8.7605E−03
1.1000E+00	4.7010E+00	4.4120E+00	6.7638E−03	9.2349E−03
1.2000E+00	4.6630E+00	4.3000E+00	7.1981E−03	9.6436E−03
1.3000E+00	4.6080E+00	4.1810E+00	7.5932E−03	9.8107E−03
1.5000E+00	4.5430E+00	4.0130E+00	8.3152E−03	1.0161E−02
1.7000E+00	4.4960E+00	3.8900E+00	8.9046E−03	1.0463E−02
1.9000E+00	4.4550E+00	3.7820E+00	9.4631E−03	1.0501E−02
2.0000E+00	4.4350E+00	3.7330E+00	9.7121E−03	1.0429E−02

[a] System: FA, A^-, KNO^3; ionic strength = 0.010.

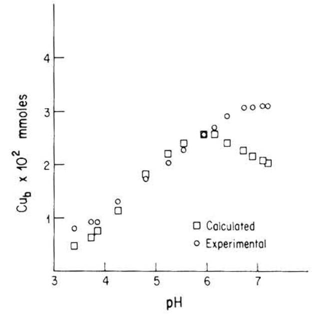

Figure 5. Discrepancy between calculation and experiment of bound copper (Table IIA).

tation predicts a maximum in the Cu^{2+} binding pattern, whereas additional removal of Cu^{2+} from solution continues to occur with increasing pH as shown in Figure 5. The prediction of a maximum contradicts mass-action-based expectations and has to be due to the unavailability in the

Table V. Resolution of K_{ov}[a]

base added, mL	pH	pCu	$Cu_{b(calcd)}$	$Cu_{b(exptl)}$	K_{ov}
		A. Total FA = 0.04399 mmol; Total Cu^{2+} = 0.0522 mmol			
7.00	6.091	3.544	3.253×10^{-2}	3.577×10^{-2}	1.827×10^{4}
7.50	6.233	3.640	3.180×10^{-2}	3.891×10^{-2}	2.879×10^{4}
8.00	6.347	3.732	3.102×10^{-2}	4.136×10^{-2}	3.352×10^{4}
8.50	6.475	3.862	2.989×10^{-2}	4.409×10^{-2}	3.892×10^{4}
9.00	6.576	3.988	2.885×10^{-2}	4.608×10^{-2}	4.416×10^{4}
9.50	6.692	4.168	2.748×10^{-2}	4.813×10^{-2}	5.377×10^{4}
10.00	6.830	4.428	2.586×10^{-2}	4.994×10^{-2}	7.09×10^{-4}
					av $(4.1 \pm 0.3) \times 10^{4}$
		B. Total FA = 0.04399 mmol; Total Cu^{2+} = 0.03132 mmol			
5.80	6.147	4.121	2.561×10^{-2}	2.707×10^{-2}	2.312×10^{4}
6.00	6.288	4.252	2.502×10^{-2}	2.817×10^{-2}	3.656×10^{4}
6.20	6.411	4.410	2.411×10^{-2}	2.912×10^{-2}	4.983×10^{4}
6.60	6.722	4.785	2.270×10^{-2}	3.039×10^{-2}	4.644×10^{4}
6.80	6.874	5.111	2.146×10^{-2}	3.088×10^{-2}	5.728×10^{4}
7.00	7.123	5.430	2.094×10^{-2}	3.111×10^{-2}	4.592×10^{4}
7.10	7.196	5.603	2.026×10^{-2}	3.118×10^{-2}	5.367×10^{4}
					av $(4.5 \pm 2) \times 10^{4}$

[a] System: Cu^{2+}, FA, KNO_3; ionic strength = 0.010.

model of an additional reaction path like the one proposed below.

We have presumed that with an excess of Cu^{2+} present there is a sufficient concentration of Cu^{2+} remaining in solution at pH >5 to form $Cu(OH)^+$, which may in turn interact with the Cu-complexed FA molecule while losing a proton. Let us consider the following sequence of reactions to apply (Ful = fulvate):

$$Cu^{2+} + OH^- \rightleftarrows CuOH^+ \quad (14)$$

$$CuOH^+ + CuFul \rightleftarrows CuOCuFul + H^+ \quad (15)$$

The net reaction is then

$$Cu^{2+} + OH^- + CuFul \rightleftarrows CuOCuFul + H^+ \quad (16)$$

and the overall equilibrium constant, K_{ov}, for the reaction can be expressed as

$$K_{ov} = (CuOCuFul)(H^+)^2/(Cu^{2+})(CuFul)K_w \quad (17)$$

To test the above possibility, the quantity of CuO-CuFul presumed to be formed at each experimental pH above 6.0 has been taken to be equal to the difference between the experimental and calculated amounts of bound copper. The quantity of CuFul was identified as the difference between the quantity of CuO-CuFul, so determined, and the quantity of FA initially present. The above stoichiometric estimate assumes that in the presence of a significant excess of Cu^{2+} the sites available for binding extra Cu are those functional units untouched by the interaction with $CuOH^+$.

The results of such treatment of the discrepancy observed between the calculated and experimentally measured binding of Cu^{2+} in the two runs where a Cu^{2+} excess was operative are presented in Table V. The K_{ov} values resolved from the two separate experiments, while fairly constant in the second set of computations, were not in the first. The average value of K_{ov} in both sets of computations, however, was essentially the same at 4×10^4. Even though the proposed reaction between $CuOH^+$ and CuFul cannot be claimed to have been substantiated, this result does indicate that the CuFul interacts with hydrolyzed species of the Cu^{2+} ion in a manner resembling the one postulated.

The eventual discrepancy between prediction and experiment in Table IIIA cannot be explained by the above. The essentially complete binding of Cu^{2+} by the fulvic acid with each addition of $Cu(NO_3)_2$, which is eventually not predictable with the model, cannot be attributed to the presence of $CuOH^+$ at the lower pH values where the discrepancy becomes sizable.

We do not consider this failure to be attributable to deficiencies in the model, however. Instead we believe that it is a consequence of the experiment itself which was initiated at pH >7. It seems reasonable to believe that at this pH level Cu(II) is present primarily as $CuOH^+$ and that this may result in irreversible interaction of the fulvic acid with hydrolyzed copper species. In the IIIB series of experiments where the model predicted the copper ion binding behavior so well such complication of the system was avoided by initiating the experiments at a low enough pH to eliminate hydrolysis of the Cu^{2+} ion as a complicating factor.

V. Conclusion

We can conclude from the above that the model we have developed is useful. It is able to accommodate disturbance to the measurable potentiometric properties that the presence of variable concentrations of excess salt introduces. It has been used successfully as well to reproduce the Cu^{2+} binding properties, over a pH range from 3 to 7, of a fulvic acid system while varying metal ion and fulvic acid concentration levels. Agreement between prediction and experiment in most instances has been good to excellent.

The model has failed, however, to anticipate the experimental binding properties of the Cu^{2+}–fulvic acid system beyond a pH level of 6 when the initial Cu^{2+} concentration exceeds, on a milliequivalent basis, the concentration of the fulvic acid. We believe that the explanation offered for this failure of the model is probably correct. Such extra binding of Cu^{2+} is not encountered under similar experimental conditions with the two other fulvic acid molecules (*10*) examined in our laboratory, as predicted by the model, and the postulated reaction may be considered to be a consequence of ion–dipole interaction facilitated by the more highly polar (aromatic) Armadale Horizons Bh fulvic acid molecule with $Cu(OH)^+$.

Finally, we belive that the model provides a meaningful profile of the growth and decay of Cu^{2+} complexes species as a function of experimental parameters. This capability is demonstrated admirably in Figure 6 where the quantity of each separate complexed species of Cu^{2+} projected to be formed by the model is plotted vs. the experimental pH of the particular system investigated. Careful study of this

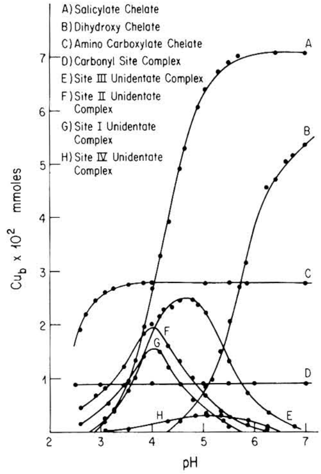

Figure 6. Predicted growth and decay of copper-complexed species in Armadale Horizons Bh fulvic acid as a function of pH.

figure shows that experiments can be designed to facilitate a knowledgeable spectroscopic study through enhancement of the presence of particular species for careful scrutiny. The capability of controlling the relative quantities of the various species that the model provides would also appear to simplify the route to direct resolution of the formation constants of these various species through the solution of sets of simultaneous equations. It is, in fact, these directions that our continuing research of fulvic acid plans to follow.

Registry No. Cu, 7440-50-8.

Literature Cited

(1) Gamble, D.; Marinsky, J. A.; Langford, C. H. In "Ion Exchange and Solvent Extraction"; Marinsky, J. A., Marcus, Y., Eds.; Marcel Dekker, Inc.: New York, 1985; Chapter VII, Vol. X, pp 373-482.
(2) Marinsky J. A.; Reddy, M. M. *Org. Geochem.* **1984**, *7*, No. 3/4, 207-214.
(3) Marinsky, J. A.; Reddy, M. M. *Org. Geochem.* **1984**, *7*, No. 3/4, 215-221.
(4) Marinsky, J. A.; Ephraim, J. *Environ. Sci. Technol.* **1986**, *20* (4).
(5) Ephraim, J.; Alegret, S.; Mathuthu, A.; Bicking, M.; Malcolm, R.; Marinsky, J. A. *Environ. Sci. Technol.* **1986**, *20* (4).
(6) Sillen, L. G.; Martell, A. E. "Stability Constants of Metal-Ion Complexes", The Chemical Society; Burlington House: London, 1964.
(7) Ephraim, J.; Mathuthu, A.; Alegret, S.; Cramer, S. J.; Marinsky, J. A., unpublished data, 1985.
(8) Kielland, J. *J. Am. Chem. Soc.* **1937**, *59*, 1675-1682.
(9) Lloyd, M.; V, Wycherley, V.; Monk, C. B. *J. Chem. Soc.* **1951**, 1786.
(10) Ephraim, J.; Mathuthu, A.; Bicking, M.; Marinsky, J. A., unpublished data, 1985.

Received for review May 16, 1985. Revised manuscript received November 25, 1985. Accepted December 12, 1985. We acknowledge financial support of this research by the National Science Foundation and the Swedish Nuclear Fuel and Waste Management Company in Stockholm, Sweden.

Determination of Linear Alkylbenzenesulfonates in Sewage Sludge by High-Resolution Gas Chromatography/Mass Spectrometry

James McEvoy* and Walter Giger

Swiss Federal Institute for Water Resources and Water Pollution Control (EAWAG), CH-8600 Dübendorf, Switzerland

■ Linear alkylbenzenesulfonates (LAS) were identified and quantitatively determined in anaerobically and aerobically stabilized sewage sludges. The analyses were accomplished by the formation of the sulfonyl chlorides and subsequent high-resolution gas chromatography (HRGC) with flame ionization detection and directly coupled mass spectrometry (HRGC/MS) employing both electron impact and chemical ionization modes. The total LAS concentrations ranged from 0.3 to 1.2% of dry sludge with only minor variations in the relative composition of LAS homologues and isomers. These concentrations are considerably larger than those of other pollutants that have been reported in sewage sludges. Although LAS are soluble in water, sorption of these amphiphilic chemicals onto suspended particles in sewage appears to be significant. In contrast to their biodegradability in the aqueous phase, LAS seem to be resistant to biodegradation during sludge treatment.

Introduction

Linear alkylbenzenesulfonates (LAS, i.e., 4-alkylbenzenesulfonates with linear alkyl substituents of 10–15 carbon atoms) comprise the majority of anionic surfactants currently manufactured by the chemical industry. The LAS production (USA, Western Europe, and Japan) for 1982 was estimated at 1 100 000 metric tons, accounting for 28% of all synthetic surfactants (*1*). As part of our investigations into the organic constituents of wastewaters (*2*) and sewage sludges (*3*) we have begun to study the behavior of LAS during wastewater and sludge treatment. Of particular concern was to determine, both qualitatively and quantitatively, any accumulation of LAS in digested sewage sludges that are largely applied to agricultural land.

It is known that LAS are present in significant quantities in primary sewage effluents (e.g., ref 4 and 5). Furthermore, it has been reported in several publications that LAS can make up a considerable portion of the fulvic acid fraction of sewage sludges (*6–8*) and can accumulate in soils to which sewage sludge is added. A wide variety of methods have been used to determine LAS in both commercial products and environmental samples (see recent review by Llenado and Neubecker, ref *9*). The majority of analytical methods for LAS determinations in wastewaters and waters employed ion pair formation of LAS with methylene blue and spectrophotometric determination (e.g., ref *10–13*). These determinations are not fully specific for LAS, however, as other organic and inorganic anions also form ion pairs with methylene blue (*13, 14*) nor is any information obtained on the distribution of indi-

0013-936X/86/0920-0376$01.50/0

Table I. Total Linear Alkylbenzenesulfonate Concentrations and Relative Distribution of Homologous Components in Digested Sewage Sludges and in Marlon A

origin of sludge sample	total LAS concn, g/kg of dry matter	distribution of homologous components, % no. of carbon atoms in aliphatic chain					
		10	11	12	13	14	15
(A) Affoltern	3.5	4	26	45	21	4	*a*
(B) Altenrhein	6.1	5	27	40	21	6	*a*
(C) Bassersdorf	5.4	4	35	42	16	3	*a*
(D) Eglisau	2.9	5	31	41	17	6	*a*
(E) Uster	4.5	4	30	42	19	5	*a*
(F) Wetzikon	11.9	2	27	40	25	5	1
(G) Winterthur	3.1	4	34	40	16	6	*a*
(H) Zürich-Glatt	7.1	3	28	44	20	5	*a*
(I) Helsinki-Herttoniemi, Finland	6.3	4	26	32	21	13	4
(J) Helsinki-Viikki, Finland	3.4	4	19	31	21	13	12
(K) Brooklyn, New York	6.9	2	16	34	32	16	*a*
(L) San Jose, California	5.2	4	24	38	27	7	*a*
(M) Marlon A		6	43	38	13	*a*	*a*
(N) Marlon A[b]		5	46	38	11	*a*	*a*

[a] Trace amount (<1%). [b] According to manufacturer's information.

vidual components present. It is characteristic of commercial surfactant products that they are complex mixtures of homologous and isomeric components (*9, 15*). For the specific characterization of individual LAS components, high-performance liquid chromatography (HPLC, *16*) or, after adequate alteration, high-resolution gas chromatography (HRGC) and gas chromatography/mass spectrometry (HRGC/MS) are required. Ion pair formation with methylene blue does allow the routine extraction of the LAS components from complex mixtures of organic compounds contained both in municipal wastewaters and sewage sludges. The extracts can then be cleaned up and prepared for HRGC and HRGC/MS analyses. The advantage of HRGC and in particular of HRGC/MS is that complex mixtures can be resolved into individual components. Frequently, LAS are recovered from methylene blue complexation on an ion-exchange column and then prepared for GC by either desulfonation to give alkylbenzenes (*17–19*) or derivatization to sulfonyl chlorides (*20–22*) or sulfonate esters (*20, 23, 24*).

It was concluded that LAS (and partially altered LAS) may play a significant part in the chemistry of soils to which sewage sludge has been added. Moreover, the contribution of carbon-bonded sulfur from LAS-type surfactants may be of concern as there are no common natural analogues (*6, 8*).

In this report, we present methods for the determination of LAS in stabilized sewage sludges in a rapid, specific, and quantitative manner. Our work was based on the microtechnique of Hon-nami and Hanya (*20*) who developed a gas chromatographic method for LAS determination by derivatization of the LAS to their methyl sulfonate esters *via* sulfonyl chlorides. However, analyses in our laboratory showed that HRGC of the methyl esters offered no advantages over that of the sulfonyl chlorides. Our analyses needed only small sample sizes (e.g., 0.05 g dry weight) and were rapid and routine.

Experimental Section

Samples and Materials. Sewage sludge samples were collected from 12 different municipal wastewater treatment plants, which are listed as samples A–L in Table I. Eleven sludge samples were collected from anaerobic digesters, and one sludge (sample D) had been aerobically stabilized. Eight sludges were from Switzerland (A–H in Table I), two from Finland (I and J), and two from the USA (K and L). The Swiss samples were collected from pipelines of mixed digesters during sludge transfer. The Finnish and American samples were mailed by air to Switzerland as aqueous suspensions without any conservation measures. All samples were stored for several months at 4 °C before analysis.

Marlon A, a commercial LAS surfactant was supplied in its protonated form (Marlon AS_3) by Chemische Werke Hüls AG, Marl, F.R.G. *p*-(Pentadec-3-yl)benzenesulfonate, as the sodium salt, for use as an internal standard was supplied by Unilever, Port Sunlight, Merseyside, U.K. Phosphorus pentachloride and methylene blue reagent were purchased from Merck, Darmstadt, F. R. G., and all solvents used were nanograde quality (Mallinckrodt, St. Louis, MO). Silica gel G thin-layer chromatography plates (20 × 20 cm, 0.25 mm) were obtained from Merck.

Extraction, Isolation, and Derivatization. Approximately 2 mg of Marlon A was dissolved in 15 mL of distilled water and added to a solution of methylene blue (2 mg) dissolved in 5 mL of water. The resulting blue aqueous solution was extracted in a separatory funnel several times with 5-mL portions of chloroform until most of the blue coloration had been removed from the aqueous phase. The chloroform extracts were combined and evaporated to dryness in a rotary evaporator. The residue was dissolved in dichloromethane and transferred to a 3-mL glass vial. The solvent was evaporated under a stream of nitrogen, and 0.5 mL of *n*-hexane and 0.05 g of phosphorus pentachloride were added. The vial was fitted with a tight-fitting, Teflon-lined screw cap, and the contents were heated on a hot plate (110 °C) for 20 min. The vial was allowed to cool, and 2 mL of *n*-hexane were added. The *n*-hexane solution was then evaporated to remove excess phosphorus pentachloride and the reaction byproduct phosphorus oxychloride ($POCl_3$) by volatilization and adsorption to the glass surface of the vial. The contents of the vial were taken up in *n*-hexane and transferred to another vial.

LAS were determined in sewage sludges using two methods: (A) a rapid screening analysis to see if LAS were present at all and (B) a confirmatory method, by which enriched LAS fractions were prepared for quantitative HRGC analyses.

Method A (Screening). Approximately 1 mL of wet sewage sludge was put in a 3-mL vial and dried in an oven at 105 °C until a constant dry weight had been reached. *n*-Hexane (0.5 mL) and phosphorus pentachloride (0.05 g) were added. Derivatization and extraction were carried out as described for the analysis of Marlon A.

Method B (Confirmatory). Fifty micrograms of the internal standard *p*-(pentadec-3-yl)benzenesulfonate dissolved in 50 μL of methanol was added to approximately 1 mL of aqueous sewage sludge in a 100-mL separatory funnel. Twenty milliliters of an alkaline (pH 10), aqueous solution of methylene blue was added and the contents were extracted with 15-mL portions of chloroform until the majority of the blue coloration had been extracted. An emulsion invariably formed in the chloroform layer upon shaking the funnel. The emulsion layer was drained into another separatory funnel. The aqueous phase was further extracted and the extracts added to the emulsion, which separated after several minutes. The chloroform layer was drained, and the remaining aqueous supernatant was again extracted with chloroform. The organic extracts were then combined and evaporated to dryness. The residue was dissolved in dichloromethane (0.5 mL) and purified by thin-layer chromatography (TLC) with dichloromethane as the mobile phase. The blue band corresponding to the methylene blue complexed components remained at, or very close to, the origin. This band was scraped off, and the components were eluted from the silica with methanol. The methanol extract was taken to dryness by rotary evaporation, redissolved in dichloromethane (1 mL), and transferred to a 3-mL vial. The solvent was completely evaporated under a stream of nitrogen. *n*-Hexane (0.5 mL) and phosphorus pentachloride (0.05 g) were added and reacted as described for the analysis of Marlon A.

High-Resolution Gas Chromatography (HRGC). HRGC analyses were made with a Carlo-Erba 2150 apparatus, equipped with a flame ionization detector (FID) and a split/splitless injector with septum flushing. The glass capillary column (19 m × 0.31 mm i.d.) had been deactivated by persilylation and coated with immobilized stationary phase (PS 255, (ref 23)). The injector temperature was 275 °C; samples were applied in *n*-hexane (0.5–1 μL) without stream splitting onto the column at ambient temperature. The split valve was opened after 30 s. After elution of the solvent, the oven temperature was raised at 4 °C/min from 50 to 300 °C for total extracts, and from 100 to 300 °C at 4 °C/min for samples that had been cleaned up by TLC. Hydrogen was used as carrier gas with a head pressure of 0.5 atm. Gas chromatographic peak areas were electronically integrated.

High-Resolution Gas Chromatography/Mass Spectrometry (HRGC/MS). A Finnigan mass spectrometer (Model 4021 C) with an INCOS 2000 data system was used for mass spectrometric identifications. A Carlo-Erba gas chromatograph (Model 4160) was connected to the mass spectrometer. A glass capillary column (PS 255 or SE-54) was directly coupled to the ion source by a fused silica capillary. Helium was used as carrier gas with a back pressure of 0.8 atm. Programming was from 60 to 270 °C at 4 °C/min. Splitless injection was used for all analyses. Typical operating conditions for electron impact ionization were with an ion source temperature of 250 °C, 40-eV ionizing energy, and a filament emission current of 350 μA. Spectra (m/z 50–500) were recorded every second. For chemical ionization, methane was used as the reagent gas, the ionization temperature was 150 °C, the ionizing energy 70 eV, and the pressure 0.37 torr. Spectra (m/z 100–400) were recorded every second.

Quantitation. Components were quantitatively determined in the confirmatory analyses by electronic integration of the HRGC/FID peak areas. The peak areas of the individual LAS components were related to that of the internal standard. It was assumed that the response factors of the individual LAS components are equal when analyzed by FID. In cases of coeluting compounds it was necessary to quantitate the individual constituents by HRGC/MS. The relative quantities of peaks belonging to the coeluting compounds were assessed by mass chromatographic comparison with homologues for which quantitation was straightforward. The internal standard occurred in all of the sludge samples but only in trace or minor quantities. To compensate for this co-occurrence, the following procedure was applied. In the screened samples, to which no internal standard was added, *p*-(pentadec-3-yl)benzenesulfonyl chloride was quantitated by mass chromatography relative to another isomer (*p*-(pentadec-4-yl)benzenesulfonyl chloride, see Table I), which eluted freely of all other LAS chlorides. In the confirmatory analyses of samples to which the internal

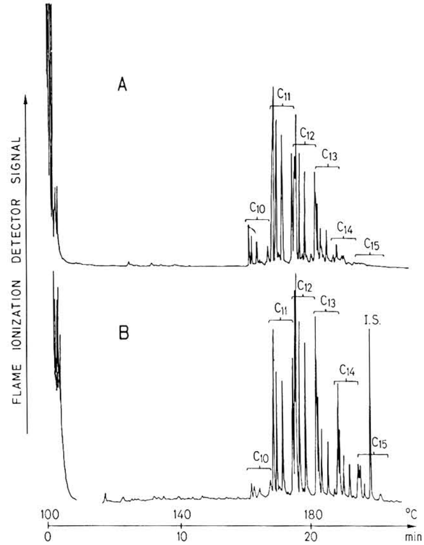

Figure 1. Gas chromatograms of linear alkylbenzenesulfonyl chlorides from (A) Marlon A and (B) sewage sludge from Helsinki–Herttoniemi (confirmatory analysis).

standard was added, a correction was then made for the amount of *p*-(pentadec-3-yl)benzenesulfonyl chloride already present in the sample as previously determined in the screening analysis.

The reproducibility of the determinations was measured by five replicate analyses of sample I in Table I by the confirmatory method. The results showed identical distributions of homologues and isomers, while the total concentrations were determined with a relative standard deviation of ±15%.

Results and Discussion

Isolation, Separation, and Identification of LAS Components. The separation and determination of LAS as their sulfonyl chloride derivatives were first performed with the commercial surfactant Marlon A, which was chosen as a representative of the many available technical LAS products. The aims of this analysis were to develop the isolation and separation of LAS and to provide a standard reference mixture of alkylbenzenesulfonyl chlorides for (i) HRGC/FID and HRGC/MS coinjection experiments with components extracted from sewage sludges and (ii) comparisons of the individual homologous and isomeric LAS components of this commercial surfactant with those present in the sludges. Furthermore, reference mass spectra of individual LAS compounds were recorded.

HRGC/FID of Marlon A. Figure 1A shows the high-resolution gas chromatogram of the LAS chlorides obtained from Marlon A. The peak pattern closely resembled that found by the HRGC analysis of the linear alkylbenzenes (LAB) that had been produced by the desulfonation of Marlon A (*18*). The relative percentage composition of the C_{10}–C_{13} homologues present in Marlon A was 6, 43, 38, and 13%, respectively. This is in good agreement with the average composition of Marlon A specified by the manufacturer (see Table I). The analyzed mixture consisted of all isomeric secondary substituted C_{10}–C_{13} benzenesulfonyl chlorides; primary substituted components were not detected. The elution of the various isomers for a given alkyl chain length depended upon the position of the attachment of the phenyl group to the alkyl

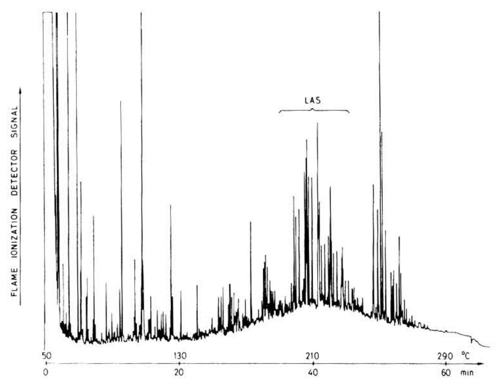

Figure 2. Gas chromatogram of the total extractables obtained from Helsinki-Herttoniemi sewage sludge after reaction with PCl_5 (screening analysis).

chain. Components having the phenyl attachment near the end of the alkyl chain eluted later than components with the phenyl attachment toward the middle of the alkyl chain. This elution order is analogous to that of their methyl sulfonate derivatives (*20*) and also to that of the desulfonated linear alkylbenzenes (*18, 26*). The sulfonyl chloride derivatives were well-amenable to HRGC, and no advantages was gained by further derivatization to their methyl esters.

HRGC/FID of Sludge Extracts. The screening analyses of sewage sludges, i.e., those that were dried, derivatized, extracted, and analyzed directly by HRGC without prior cleanup, showed that LAS were present in relatively large concentrations and that this method could be used routinely for rapid semiquantitative determinations. Figure 2 depicts the gas chromatogram of such a total extract of a sewage sludge sample after reaction with phosphorus pentachloride. This HRGC/FID trace shows that LAS were the major group of components present. Many other components were chlorinated during the reaction with PCl_5, with some artifacts being formed. For example, the distribution of steroidal compounds was altered. Prior to chlorination, sterols, stanols, and stanones were usually the major components observed by HRGC analysis, with coprostanol generally being predominant. Other compounds observed included 4-nonylphenols, fatty acids, *n*-alkanes, and linear alkylbenzenes. The screening method combined with HRGC/FID was advantageously rapid, and the Marlon A derived LAS chloride mixture could be used for coinjection experiments and hence for tentative identifications. Most of the 33 LAS components in the C_{10}–C_{15} range, which are listed in Table II, could be separated by HRGC/FID. Analysis by computerized HRGC/MS was required for both confirmed qualitative and reliable quantitative determinations due to the compositional complexity of the extracts obtained by the screening procedure.

Figure 1B shows the chromatogram obtained by HRGC/FID and using the confirmatory method of analysis for the same sewage sludge that was analyzed by the screening method for Figure 2. It is evident that the extracts of sewage sludges to which the internal standard had been added and which had been purified by TLC prior to HRGC (i.e., confirmatory analysis), showed no, or very little, interference from other components when analyzed by HRGC/FID. Thus, this method allowed the specific determination of LAS in sewage sludges. Quantitation of total LAS and of most individual components could be

Table II. Relative Distribution of Homologous and Isomeric Linear Alkylbenzenesulfonates in Digested Sewage Sludge from Helsinki-Herttoniemi, Finland

component[a]	homologue[b]	isomer[c]	relative amount, %
1	*n*-decyl	4, 5	0.9
2		3, 6	0.7
3		2, 7	0.9
4		1, 8	1.5
5	*n*-undecyl	5, 5	4.4
6		4, 6	4.4
7		3, 7	4.6
8		2, 8	5.1
9		1, 9	8.0
10	*n*-dodecyl	5, 6	5.8
11		4, 7	5.8
12		3, 8	6.1
13		2, 9	6.1
14		1, 10	8.1
15	*n*-tridecyl	6, 6	3.3
16		5, 7	3.3
17		4, 8	3.4
18		3, 9	3.5
19		2, 10	3.5
20		1, 11	4.0
21	*n*-tetradecyl	6, 7	1.8
22		5, 8	1.7
23		4, 9	2.2
24		3, 10	2.2
25		2, 11	2.2
26		1, 12	2.2
27	*n*-pentadecyl	7, 8	1.2
28		6, 9	
29		5, 10	0.5
30		4, 11	0.5
31		3, 12	0.7
32		2, 13	0.7
33		1, 14	0.7

[a] Number refers to HRGC/MS peaks in Figures 5 and 6. [b] Linear alkyl chain length. [c] Number of carbon atoms in the two aliphatic chains on either side of the carbon attached to the benzene ring.

accomplished by HRGC/FID, but again some coelution occurred rendering analysis by HRGC/MS necessary for maximum qualitative information. The LAS derived components have alkyl chains that range from C_{10} to C_{15}. The full range of secondary substituted C_{10}–C_{15} components was observed in this sewage sludge sample. Again Marlon A derivatives were used for coinjection experiments with HRGC/FID on both PS 255 and SE-54 columns for confirmation.

HRGC/MS: *Mass Spectra.* Figure 3A shows the mass spectrum, obtained by electron impact (EI) ionization, of the component with a dodecyl alkyl chain to which the phenyl group is attached to position 5 (component 11 in Table II). This spectrum is taken from the HRGC/MS analysis of a screening extract of sample I (see Table I). Figure 3B shows the mass spectrum of the corresponding component in the Marlon A derived LAS chloride mixture, with which it coeluted. The two spectra are very similar; differences are probably mainly due to interferences from coeluants in the sludge sample. The molecular ion ($M^{+}\cdot$) at m/z 344, and its isotope at m/z 346, indicated that the molecule contained one chlorine atom. The loss of chlorine generates the ion at m/z 309, $(M - 35)^+$. The loss of the smaller alkyl chain moiety by fragmentation is thought to give rise to the diagnostic ions at m/z 288 (loss of C_4H_8; $(M - 56)^{+}\cdot$) and at m/z 287 (loss of C_4H_9; $(M - 57)^+$). Similarly, the diagnostic ions at m/z 246 and m/z 245 are assigned due to the loss of the longer alkyl chain moiety,

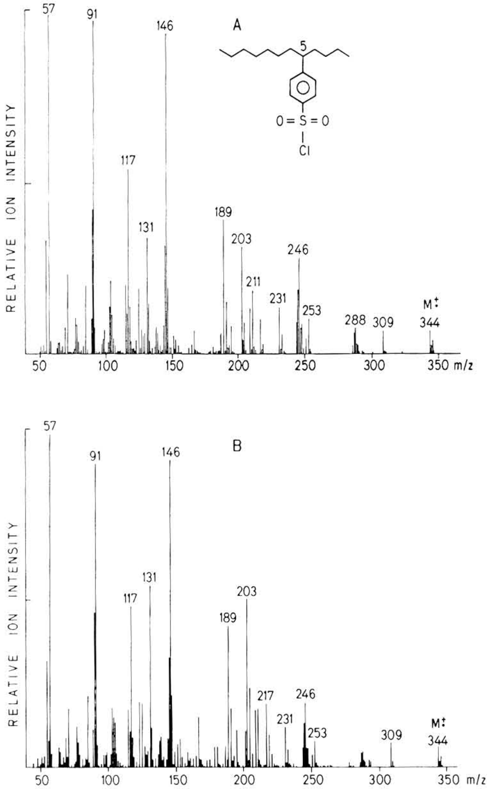

Figure 3. EI mass spectra of *p*-(dodec-5-yl)benzenesulfonyl chloride (component 11 in Table II) in (A) Marlon A and (B) Helsinki–Herttoniemi sewage sludge.

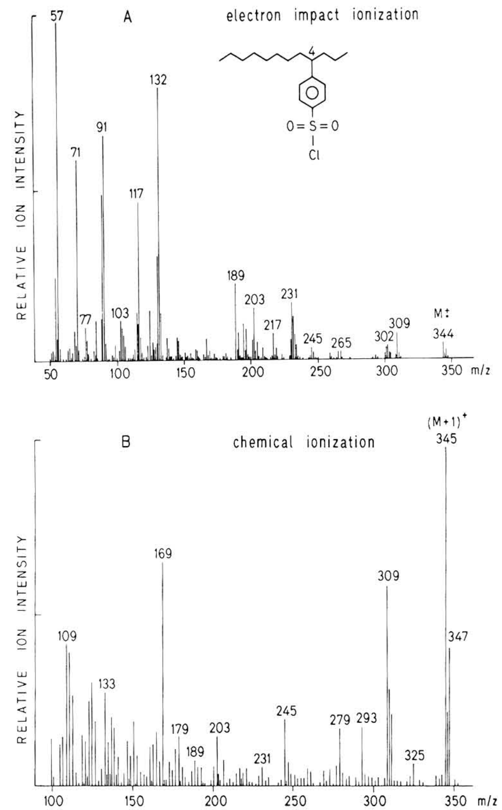

Figure 4. Mass spectra of *p*-(dodec-4-yl)benzenesulfonyl chloride (component 12 in Table II) in Helsinki–Herttoniemi sewage sludge: (A) electron impact ionization and (B) chemical ionization.

C_7H_{14}, $(M - 98)^{+\cdot}$ and C_7H_{15}, $(M - 99)^+$, respectively. These alkyl side chain cleavages together with the loss of Cl or HCl give rise to ions at m/z 253, $(M - C_4H_8 - Cl)^+$, m/z 251, $(M - C_4H_9 - HCl)^+$, m/z 211, $(M - C_7H_{14} - Cl)^+$, and at m/z 209, $(M - C_7H_{15} - HCl)^+$.

An important diagnostic ion for component 11 is the major ion observed at m/z 146. This ion results from the cleavage of both the sulfonyl chloride functionality and of the longest alkyl chain moiety. Components with the phenyl group attached to the alkyl chain at the 2, 3, 4, 5, 6, and 7 positions give major, diagnostic ions at m/z 104, 118, 132, 146, 160, and 174, respectiely. A further example of the major intensity of such a diagnostic ion is shown in Figure 4A. This is the EI mass spectrum of component 12 (Table II), which is an isomer of component 11, differing in that the phenyl is attached to position 4 of the dodecyl chain and hence the resulting fragment ion is at m/z 132. The mass spectrum obtained for this component under CI operation is shown in Figure 4B, where the protonated molecular ion at m/z 345 $(M + 1)^+$ and that of its isotope at m/z 347 predominate. The major ion at m/z 309 is due to the loss of hydrogen chloride.

Mass Chromatograms. Figures 5 and 6 show mass chromatograms (EI and CI mode, respectively) of LAS-chloride compounds isolated from sewage sludge from Helsinki–Herttoniemi, analyzed by the screening method (i.e., total extract, cf. with Figure 2). The numbering of the peaks in Figures 5 and 6 corresponds to the numbered components in Table II. The complementary use of EI and CI modes of operation was useful for obtaining maximum qualitative and quantitative information, particularly for resolving problems of coelution. The diagnostic ions, m/z 104, 118, 132, 146, and 160, observed in spectra obtained by EI give information about distributions of isomers and homologues (Figure 5). The use of these ions can help to quantitate peaks that coelute. For example, in the total ion chromatogram displayed in Figure 5, coelution occurred with the C_{11} alkyl chain isomers numbered 5 and 6. These components correspond to compounds having the phenyl attachment at positions 6 (i.e., 5, 5) and 5 (i.e., 4, 6), respectively (see Table II). These coelutants were resolved with the mass chromatograms of m/z 160 and m/z 146, respectively. Again in Figure 5 it can be seen that the C_{12} isomer (1, 10; peak 14 in Figure 5 and Table II) interfered with the C_{13} components 6, 6 (peak 15) and 5, 7 (peak 16). These components could be resolved by a combination of 104, 174, and 160, respectively (m/z 174, not shown in Figure 5). This particular problem can also be observed in the total ion current of Figure 6 where CI conditions were used. Here reconstructed mass chromatograms using the protonated molecular ions gave information on homologous distributions, and the C_{12} isomer (peak 14, $(M + 1)^+ = 345$), which coeluted with the C_{13} isomers (peaks 15 and 16, $(M + 1)^+ = 359$) could be fully resolved. The same is true for peak 20, a C_{13} component ($(M + 1)^+ = 359$), which elutes in the region of several C_{14} components ($(M + 1)^+ = 373$), the CI mode of operation fully resolving the different homologues.

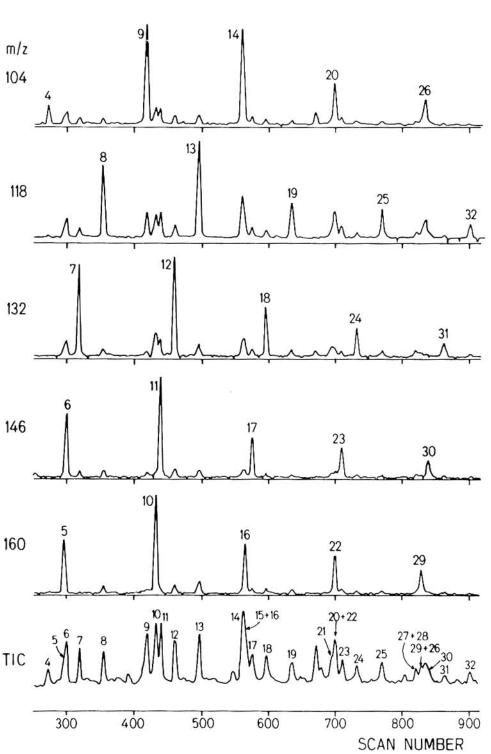

Figure 5. Partial mass chromatograms and total ion current chromatogram of linear alkylbenzenesulfonyl chlorides obtained from Helsinki-Herttoniemi sewage sludge (screening analysis) by electron impact ionization. Peak assignments are listed in Table II.

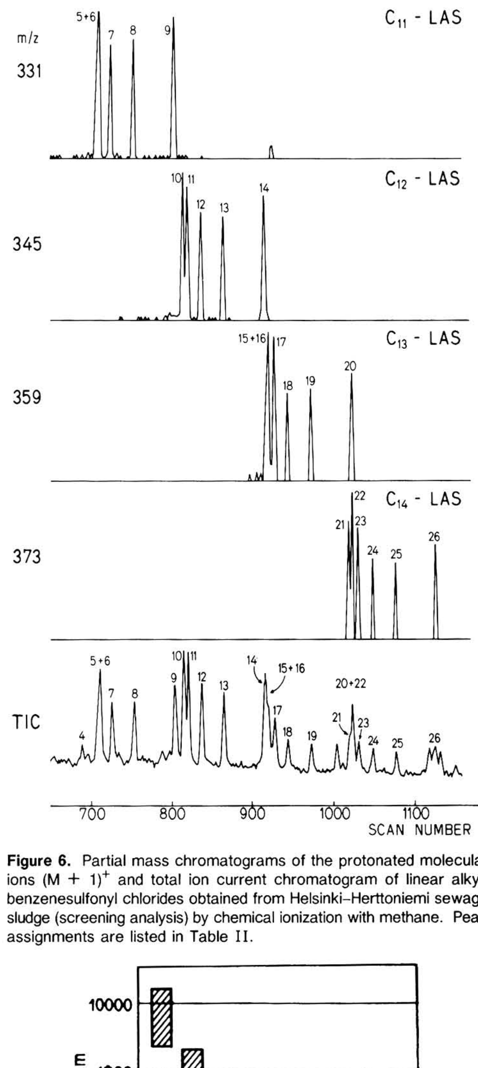

Figure 6. Partial mass chromatograms of the protonated molecular ions $(M + 1)^+$ and total ion current chromatogram of linear alkylbenzenesulfonyl chlorides obtained from Helsinki-Herttoniemi sewage sludge (screening analysis) by chemical ionization with methane. Peak assignments are listed in Table II.

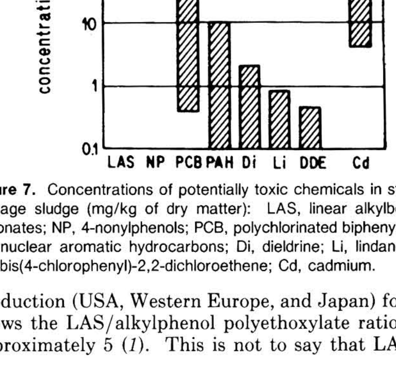

Figure 7. Concentrations of potentially toxic chemicals in stabilized sewage sludge (mg/kg of dry matter): LAS, linear alkylbenzenesulfonates; NP, 4-nonylphenols; PCB, polychlorinated biphenyls; PAH, polynuclear aromatic hydrocarbons; Di, dieldrine; Li, lindane; DDE, 1,1-bis(4-chlorophenyl)-2,2-dichloroethene; Cd, cadmium.

LAS Concentrations in Sewage Sludge. The total concentrations of LAS and the relative distribution of the homologues with C_{10}–C_{15} alkyl chains determined in 12 sewage sludges are given in Table I. The concentrations range from 2.9 to 11.9 g of LAS kg^{-1}. These extraordinarily high levels of up to 1.2% of the total dry matter, determined by this specific and unambiguous analysis, confirm the tentative results obtained by Holtzclaw and Sposito (*6*). These authors measured LAS in the fulvic acid fraction of sewage sludge by colorimetric determination and found that LAS could make up about 5% of this fraction.

These LAS levels are regarded with concern as they are well above the concentrations of the toxic pollutant 4-nonylphenyl (NP) in these same samples (*3* and unpublished results) and of other toxic chemicals reported in digested sludges (*27*). Figure 7 shows on a logarithmic scale the concentration ranges of organic pollutants and cadmium occurring in stabilized sewage sludges. Moreover, it is probable that the LAS values reported here for these samples have been underestimated as it is likely that a portion of LAS is bound to the solid matrix in a form that may not readily form extractable ion pairs with methylene blue, compared to the relative ease of ion pair formation and extraction of the internal standard that was added to the sludges just prior to analysis.

The high LAS concentrations reflect the massive input of these chemicals from household and industrial uses. The average concentration of LAS is about 7 times higher than the average concentration of 4-nonylphenol for these samples (*3* and unpublished results), whilst the world production (USA, Western Europe, and Japan) for 1982 shows the LAS/alkylphenol polyethoxylate ratio to be approximately 5 (*1*). This is not to say that LAS and

4-nonylphenol can be directly related as sewage sludge constituents. 4-Nonylphenol is a persistent metabolite formed from 4-nonylphenol polyethoxylates during wastewater and sludge treatment, particularly under anaerobic conditions (*3*), whereas the LAS reported here are unaltered anionic surfactants that have resisted biodegradation. No attempt was made to identify persistent degradation products of LAS in sewage sludges. The high concentrations of 4-nonylphenol in sludges is causing concern (*3*) as it is recognized as being highly toxic (*28, 29*). The toxicity values (LC_{50}) of NP are approximately an order of magnitude lower than those of individual LAS compounds (cf. ref 30). However, the concentrations of LAS in these sludges are approximately an order of magnitude above that of NP.

Biodegradation of LAS is generally accepted as being efficient in aerobic, aqueous environments (*30–32*), although there is some concern that certain metabolites are more stable (*33, 34*) and that the assessment of biodegradation (*10*) by spectroscopic measurement of methylene-blue-active substances is applicable only to assessing primary biodegradation (*34, 35*). The resolution of the discrepancy of how LAS accumulate in sludges when they are water soluble and rapidly degraded in wastewaters lies in their adsorptive behavior. As surfactants they exhibit both lipophilic and hydrophilic properties resulting from their hydrocarbon and sulfonate functionalities, respectively. The high concentrations of LAS in sludges reported in this work are assumed to be due to LAS compounds that adsorb to organic and inorganic particulates in sewage and are then deposited in the oxygen-low environment, which occurs at the primary (mechanical) stage of municipal wastewater treatment. It has been shown that the adsorption of LAS onto minerals inhibits their degradation in soils (*36*), and the same could hold when these chemicals are adsorbed to sewage sludge as LAS was shown to biodegrade very slowly in incubated soils with high water contents (*37*).

The distribution of the various isomers for a given alkyl chain length are approximately equal (Table II), but a slight predominance is observed for components with branching at the 2 positions (e.g., peak 9 in Figure 5) for C_{10}–C_{12} components. The majority of LAS in the Swiss samples consisted of compounds having alkyl chains of C_{11}–C_{13} (Table I). Those in samples from the USA and Finland also had high concentrations of C_{14} components with the latter having additional significant levels of C_{15} compounds. The difference in these distributions is presumably due to the makeup of the major LAS mixtures on the market, which have alkyl chain lengths primarily of either C_{10}–C_{13} or C_{11}–C_{14}. Generally, the Swiss samples tend to have a distribution similar to that of Marlon, but the latter has a greater predominance of C_{11} alkyl chains while the sludge samples show a greater proportion of C_{12}–C_{15} components with C_{12} predominant. There is evidence that LAS with longer chain lengths are biodegraded more rapidly than LAS with short chain lengths (*4, 33, 38*). LAS with C_{14} and C_{15} alkyl chains in these sludges may be an indication that biodegradation is retarded in the digesters. On the other hand it has been reported (*39*) that LAS components with longer alkyl chain lengths are preferentially adsorbed onto clays (and presumably also organic matter), which may also partly account for the higher proportion of C_{12}–C_{15} components observed. The increasing alkyl chain length increases the hydrophobic nature of these compounds making them more prone to adsorption. However, it is also possible that the greater abundance of LAS components with longer alkyl chains is representative of the overall composition of LAS used in Switzerland.

Further research is needed to understand the transport mechanisms and pathways of LAS during sewage and sludge treatment. Their sorption behavior with organic and inorganic particles should be further studied (*40*). Preliminary results suggest that LAS are not degraded in either mesophilic or thermophilic anaerobic sludge digestion (*41*). This is of particular relevance as in Switzerland approximately 70% of the digested sewage sludges are applied to agricultural land. Investigations on concentrations and effects of LAS in soils that have previously received inputs of sewage sludge should be undertaken to assess their possible impact on soil chemistry and soil biota. Studies into how long LAS persist in the soil and to what extent they can be taken up by plants should be undertaken.

Acknowledgments

We wish to thank P. H. Brunner, H. Motschi, and E. Stephanou for helpful discussions, the operators of the treatment plants who helped us during sample collection, the colleagues who sent us sludge samples, K. Grob, G. Grob, and C. Schaffner for supplying glass capillary columns, Unilever, Port Sunlight, G.B., for supplying LAS standard compounds, B. Schneider for typing the manuscript, and H. Bolliger for drawing the diagrams.

Registry No. DDE, 72-55-9; NP, 104-40-5; Cd, 7440-43-9; 4-decylbenzenesulfonate, 140-60-3; 4-undecylbenzenesulfonate, 39156-49-5; 4-dodecylbenzenesulfonate, 121-65-3; 4-tridecylbenzenesulfonate, 59599-57-4; 4-tetradecylbenzenesulfonate, 47377-16-2; 4-pentadecylbenzenesulfonate, 76964-45-9; dieldrin, 60-57-1; lindane, 58-89-9.

Literature Cited

(1) Werdelmann, B. W. In "Proceedings of the World Surfactants Congress II"; Kürle Verlag: Gelnhausen, FRG, 1984; pp 3–21, Vol. 1.

(2) Stephanou, E.; Giger, W. *Environ. Sci. Technol.* **1982**, *16*, 800–805.

(3) Giger, W.; Brunner, P. H.; Schaffner, C. *Science* **1984**, *225*, 623–625.

(4) Swisher, R. D. "Surfactant Biodegradation"; Marcel Dekker: New York, 1970.

(5) Linfield, W. M. "Anionic Surfactants"; Marcel Dekker: New York, 1976; Part I.

(6) Holtzclaw, K. M.; Sposito, G. *Soil Sci. Soc. Am. J.* **1978**, *42*, 607–611.

(7) Sposito, G.; Holtzclaw, K. M.; LeVesque, C. S.; Johnston, C. T. *Soil Sci. Soc. Am. J.* **1982**, *46*, 265–270.

(8) Schaumberg, G. D.; Holtzclaw, K. M.; LeVesque, C. S.; Sposito, G. *Soil Sci. Soc. Am. J.* **1982**, *46*, 310–314.

(9) Llenado, R. A.; Neubecker, T. A. *Anal. Chem.* **1983**, *55*, 93R–102R.

(10) Longwell, J.; Maniece, W. D. *Analyst (London)* **1955**, *80*, 167–171.

(11) Abbott, D. C. *Analyst (London)* 1962, *87*, 286–293.

(12) Greenberg, A. E.; Connors, J. J.; Jenkins, D. In "Standard Methods for the Examination of Water and Wastewater", 15th ed.; American Public Health Association: Washington, D. C., , 1980; Section 512A.

(13) Longman, G. F. "The Analysis of Detergents and Detergent Products"; Wiley: Great Britain, 1975.

(14) Webster, H. L.; Halliday, J. *Analyst (London)* **1959**, *84*, 552–559.

(15) Kunkel, E. *Tenside Deterg.* **1980**, *17*, 247–249.

(16) Nakae, A.; Tsuji, K.; Yamanaka, M. *Anal. Chem.* **1981**, *53*, 1818–1821.

(17) Sullivan, W. T.; Swisher, R. D. *Environ. Sci. Technol.* **1969**, *3*, 481–483.

(18) Leidner, H.; Gloor, R.; Wuhrmann, K. *Tenside Deterg.* **1976**, *13*, 122–130.

(19) Waters, J.; Garrigan, J. T. *Water Res.* **1983**, *17*, 1549–1562.
(20) Hon-nami, H.; Hanya, T. *J. Chromatogr.* **1978**, *161*, 205–212.
(21) Parsons, J. S. *J. Gas Chromatogr.* **1967**, *5*, 254–256.
(22) Watanabe, S.; Nukiyama, M.; Takagi, F.; Iida, K.; Kaise, T.; Wada, Y. *J. Food Hyg. Soc. Jpn.* **1975**, *16*, 212–217.
(23) Kirkland, J. J. *Anal. Chem.* **1960**, *32*, 1389–1393.
(24) Imaida, M.; Sumimoto, T.; Yada, M.; Yoshida, M.; Koyama, K.; Kunita, N. *J. Food Hyg. Soc. Jpn.* **1975**, *16*, 218–224.
(25) Grob, K.; Grob, G.; Blum, W.; Walther, W. *J. Chromatogr.* **1982**, *244*, 197–208.
(26) Eganhouse, R. P.; Blumfield, D. L.; Kaplan, I. R. *Environ. Sci. Technol.* **1983**, *17*, 523–530.
(27) Lester, J. N. In "Environmental Effects of Organic and Inorganic Contaminants in Sewage Sludge"; Davis, R. D., Hucker, G., L'Hermite, P., Eds.; Reidel: Dordrecht, Holland, 1983; pp 3–18.
(28) McLeese, D. W.; Zitko, W.; Sergeant, D. B.; Burridge, L.; Metcalfe, C. D. *Chemosphere* **1981**, *10*, 723–730.
(29) Bringman, G.; Kühn, R. *Z. Wasser Abwasser Forsch.* **1982**, *15*, 1–6.
(30) Divo, C.; Cardini, G. Tenside Deterg. **1980**, *17*, 30–36.
(31) Gledhill, W. E. *Appl. Microbiol.* **1975**, *30*, 922–929.
(32) Swisher, R. D. *Tenside Deterg.* **1981**, *18*, 57–63.
(33) Leidner, H.; Gloor, R.; Wüest, D.; Wuhrmann, K. *Xenobiotica* **1980**, *10*, 47–56.
(34) Pitter, P.; Fuka, T. *Tenside Deterg.* **1979**, *16*, 298–302.
(35) Wuhrmann, K.; Mechsner, K. *EAWAG News* **1974**, *3*, 1–2.
(36) Inoue, K.; Kaneko, K.; Yoshida, M. *Soil Sci. Plant Nutr. (Tokyo)* **1978**, *24*, 91–102.
(37) Schaumberg, G. D.; LeVesque-Madore, C. S.; Sposito, G.; Lund, L. J. *J. Environ. Qual.* **1980**, *9*, 297–303.
(38) Huddleston, R. L.; Allred, R. C. *Dev. Ind. Microbiol.* **1963**, *4*, 24–38.
(39) Wayman, G. H. In "Proceedings of the International Clay Conference"; Rosenquist, I. T., Ed.; Stockholm, 1963; pp 329–342, Vol. 1.
(40) Motschi, H.; McEvoy, J. *Naturwissenschaften* **1985**, *72*, 654–655.
(41) McEvoy, J.; Giger, W. *Naturwissenschaften* **1985**, *72*, 429–431.

Received for review April 8, 1985. Accepted Septemter 3, 1985. This project was mainly funded by the Swiss National Science Foundation (Nationales Forschungsprogramm 7D: "Organic Contaminants in Sewage Sludges").

α-Dicarbonyl Yields from the NO_x–Air Photooxidations of a Series of Aromatic Hydrocarbons in Air

Ernesto C. Tuazon,* Hélène Mac Leod, Roger Atkinson, and William P. L. Carter

Statewide Air Pollution Research Center, University of California, Riverside, California 92521

■ The yields of the ring cleavage products glyoxal, methylglyoxal, and biacetyl from the reactions of OH radicals with benzene, toluene, *o*-, *m*-, and *p*-xylene, and 1,2,3-, 1,2,4-, and 1,3,5-trimethylbenzene in the presence of parts per million concentrations of NO have been determined in 1 atm of air at 298 ± 2 K using in situ long-path-length Fourier transform infrared absorption spectroscopy and differential optical absorption spectroscopy with supplementary gas chromatographic analyses. The yields of glyoxal and methylglyoxal, after correction for their photolysis and reaction with OH radicals, were, respectively, as follows: from toluene, 0.105 ± 0.019 and 0.146 ± 0.006; from *o*-xylene, 0.087 ± 0.012 and 0.246 ± 0.020; from *m*-xylene, 0.086 ± 0.011 and 0.319 ± 0.009; from *p*-xylene, 0.225 ± 0.039 and 0.105 ± 0.034; from 1,2,3-trimethylbenzene, 0.058 ± 0.008 and 0.152 ± 0.025; and from 1,2,4-trimethylbenzene, 0.048 ± 0.005 and 0.357 ± 0.017. In addition, a glyoxal yield from benzene of 0.207 ± 0.019, a methylglyoxal yield from 1,3,5-trimethylbenzene of 0.602 ± 0.033, and biacetyl yields from 1,2,3- and 1,2,4-trimethylbenzene of 0.316 ± 0.036 and 0.048 ± 0.009, respectively, were determined. These data are important inputs to chemical models of the NO_x–air photooxidations of these aromatic hydrocarbons.

Introduction

Aromatic hydrocarbons are important constituents of commercial fuels (*1–3*) and of emissions from mobile sources (*1*, *3*). However, despite numerous experimental and computer modeling studies, the reaction pathways occurring during their atmospheric photooxidations are still not well-understood (*4–9*).

Kinetic and environmental chamber studies have shown that under atmospheric conditions the sole loss process of the aromatic hydrocarbons is due to reaction with the hydroxyl radical (*7*, *9–12*). These OH radical reactions have been shown to proceed via two pathways, namely H atom abstraction from the substituent alkyl groups and OH radical addition to the aromatic ring (*7*, *9–12*), as illustrated in eq 1 and 2 for toluene.

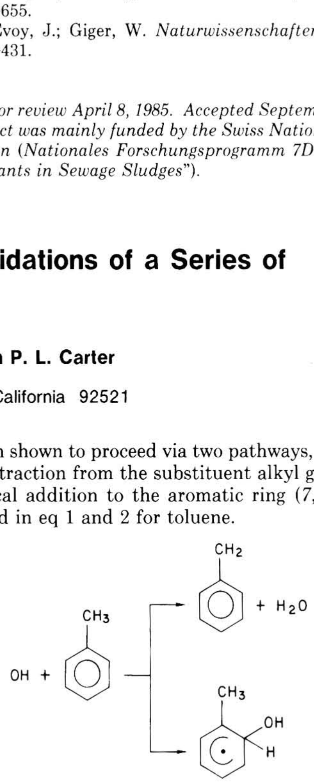

(1)

(2)

A

The H-atom abstraction route is relatively minor, accounting for ~8% of the overall reaction for toluene (*12*, *13*) and ~2–9% for the xylenes and trimethylbenzenes (*12*). While the subsequent chemistry of the benzyl and substituted benzyl radicals appears to be adequately understood (*7*, *9*, *10*), many uncertainties remain concerning the subsequent chemistry of the OH-aromatic adducts (A) under atmospheric conditions (*7–9*, *12*).

Reaction of the OH-aromatic adducts (i.e., hydroxycyclohexadienyl or methyl-substituted hydroxycyclohexadienyl radicals) with O_2 is expected to lead to the formation of hydroxyaromatics (*7*, *10*, *12*). Indeed the cresol isomers are formed from toluene in ~16% yield (*13*), with *o*-cresol being the dominant isomer (*14*). However, the observation of the α-dicarbonyls glyoxal, methylglyoxal, and biacetyl in significant yields from the methyl-substituted aromatic hydrocarbons (*8*, *13*, *15–19*) and of a variety of other acyclic oxygenated products from toluene (*5*, *6*, *20*), *o*-xylene (*5*), and 1,2,4-trimethylbenzene (*21*)

0013-936X/86/0920-0383$01.50/0

shows that ring cleavage is also an important overall reaction pathway.

In this work, in an extension of our recent investigation of the glyoxal and methylglyoxal yields from toluene and *m*- and *p*-xylene (*8*), we have used long-path-length Fourier transform infrared (FT-IR) absorption spectroscopy, long-path-length differential optical absorption spectroscopy (DOAS), and gas chromatography (GC) to determine the yields of the α-dicarbonyls glyoxal, methylglyoxal, and biacetyl from the NO_x–air photooxidations of benzene, toluene, the xylene isomers, and the trimethylbenzene isomers at ~740 torr total pressure of air and 298 ± 2 K.

Experimental Section

The experimental techniques used were essentially identical to those described previously (*8*). NO_x–air photooxidations of the aromatic hydrocarbons were carried out in the SAPRC 5800-L evacuable, Teflon-coated environmental chamber, with radiation being provided by a 25-kW xenon arc (*22*). This environmental chamber is equipped with two sets of multiple-reflection White-type optical systems. One set, on a diametrical axis with a base path of 1.30 m, was interfaced to a Nicolet FT-IR spectrometer. The second set, on a longitudinal axis with a base path of 3.77 m, was interfaced to a differential optical absorption spectrometer.

As in our previous study (*8*), DOAS measurements of glyoxal were carried out using path lengths from 45.2 to 150.8 m, utilizing the wavelength region 430–460 nm. The optimum detection sensitivity for glyoxal was $\sim 3 \times 10^{11}$ molecule cm^{-3} for the maximum path length used (150.8 m). Due to the much weaker spectral features of methylglyoxal (for which the detection sensitivity was $\sim 5 \times 10^{12}$ molecule cm^{-3} at 150 m) its unambiguous detection and measurement by DOAS during these experiments could not be carried out, particularly in the presence of interfering NO_2 absorption bands.

Glyoxal, methylglyoxal, and the aromatic hydrocarbons were monitored by FT-IR absorption spectroscopy simultaneously with the DOAS measurements of glyoxal. For the FT-IR measurements, a path length of 62.9 m was routinely used with a spectral resolution (unapodized) of 1 cm^{-1}. Spectra were recorded by utilizing both a liquid-N_2-cooled HgCdTe detector (600–2000 cm^{-1}) and a liquid-N_2-cooled InSb detector (2000–4000 cm^{-1}). Quantitative analysis was carried out by linear subtraction of a spectrum's absorption bands with the use of calibrated reference spectra of the authentic sample. For the aromatic hydrocarbons the subtraction procedure employed their characteristic absorption bands in both the regions 650–850 cm^{-1} and 2850–3100 cm^{-1}. Glyoxal and methylglyoxal were monitored at their absorptions centered, respectively, at ~2835 and 2829 cm^{-1}. The first step in the analysis of these superimposed absorption bands was the subtraction of the more highly structured band of glyoxal, as verified by the DOAS data, followed by the determination of the residual absorption of methylglyoxal. FT-IR detection sensitivities for glyoxal and methylglyoxal were similar, being $\sim 4 \times 10^{12}$ molecule cm^{-3} at the path length and resolution employed.

Biacetyl was analyzed by gas chromatography with electron capture detection, using a 18 in × 0.25 in. Teflon column of 5% Carbowax 400 on Chromosorb G (80/100 mesh) at 300 K. The detector response was calibrated periodically during this study, and gas samples were diluted as necessary to utilize the linear portion of the calibration curve.

Hydroxyl radicals were generated by the photolysis of methyl nitrite in air at wavelengths $\gtrsim$300 nm (*7*)

$$CH_3ONO + h\nu \rightarrow CH_3O + NO$$

$$CH_3O + O_2 \rightarrow HCHO + HO_2$$

$$HO_2 + NO \rightarrow OH + NO_2$$

NO was included in the reaction mixtures in order to minimize the formation of O_3 and NO_3 radicals. The initial concentrations of the CH_3ONO–NO–aromatic hydrocarbon–air mixtures were CH_3ONO, $\sim 2.4 \times 10^{14}$ molecule cm^{-3}; NO, $\sim 1.2 \times 10^{14}$ molecule cm^{-3}; aromatic hydrocarbon, $\sim(2.5\text{–}5) \times 10^{14}$ molecule cm^{-3}; with approximately 1 atm of synthetic air (80% N_2 + 20% O_2) as the diluent gas.

Each experiment consisted of cumulative, short-period (3–10-min) irradiations, with total irradiation times up to 60 min. DOAS and FT-IR spectra were recorded, and GC samples were taken, between these irradiation periods. This procedure minimized the effect of stray radiation on the DOAS instrument and ensured that all the analyses corresponded to the same extent of reaction. The light intensity in these experiments, as determined from an irradiation of a biacetyl–air mixture, corresponded to a biacetyl photolysis rate of 1.25×10^{-4} s^{-1}.

Results

CH_3ONO–NO–air irradiations of benzene, toluene, *o*-, *m*-, and *p*-xylene, and 1,2,3-, 1,2,4-, and 1,3,5-trimethylbenzene were carried out at 298 K and ~740 torr total pressure of air, with two or three separate experiments being carried out for all but *m*-xylene. The concentrations of the aromatic hydrocarbons, glyoxal, methylglyoxal, and biacetyl as analyzed by FT-IR, DOAS, and GC techniques are given in Tables II–IX. (Tables II–IX are available as supplementary material for this manuscript; see paragraph at end of text regarding supplementary material).

The observed α-dicarbonyl yields had to be corrected for reaction with OH radicals and photolysis (*8*) in order to derive the formation yields of these compounds. The reaction sequence is

$$OH + \text{aromatic} \rightarrow \xrightarrow{NO,\ O_2} Y\ \alpha\text{-dicarbonyl} \quad (3)$$

$$OH + \alpha\text{-dicarbonyl} \rightarrow \text{products} \quad (4)$$

$$\alpha\text{-dicarbonyl} + h\nu \rightarrow \text{products} \quad (5)$$

where reaction 3 is complex (*8*) and Y is the formation yield of the individual α-dicarbonyls from the aromatic hydrocarbon studied. By making the reasonable assumption that the OH radical concentrations were essentially constant over the small irradiation periods, then (*8*)

$$[\text{aromatic}]_{t_2} = [\text{aromatic}]_{t_1} e^{-k_3[OH](t_2-t_1)} \quad (I)$$

and

$$[\alpha\text{-dicarbonyl}]_{t_2} = [\alpha\text{-dicarbonyl}]_{t_1} e^{-(k_4[OH]+k_5)(t_2-t_1)} + \frac{Y_{t_1-t_2}[\text{aromatic}]_{t_1} k_3[OH]}{[(k_4 - k_3)[OH] + k_5]}[e^{-k_3[OH](t_2-t_1)} - e^{-(k_4[OH]+k_5)(t_2-t_1)}] \quad (II)$$

where $[\text{aromatic}]_{t_1}$, $[\alpha\text{-dicarbonyl}]_{t_1}$ and $[\text{aromatic}]_{t_2}$, $[\alpha\text{-dicarbonyl}]_{t_2}$ are the aromatic hydrocarbon and α-dicarbonyl concentrations observed at times t_1 and t_2, respectively, and $Y_{t_1-t_2}$ is the formation yield of the individual α-dicarbonyls over the time period t_1–t_2. Computer calculations showed that eq II yielded negligible (<1%) errors under the experimental conditions utilized in this study. In addition, we have determined (Table III of ref 8) that data obtained from a single long irradiation are indistinguishable from those obtained from several shorter irradiations of the same total duration, thus showing that

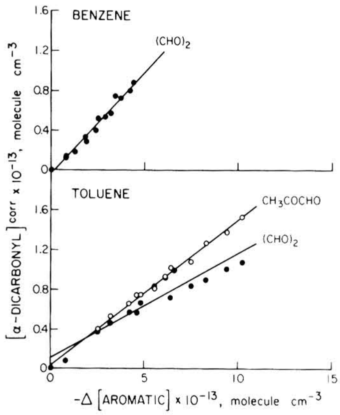

Figure 1. Plots of the glyoxal and methylglyoxal yields (corrected for photolysis and reaction with OH radicals; see text) against the amounts of benzene and toluene consumed.

thermal reactions during the dark analyses periods are of no consequence.

OH radical concentrations were calculated from the aromatic hydrocarbon decays (eq I). Rate constants k_3 and k_4 were taken from the literature (*11*, *23*), with values of k_3 and k_4 (in units of 10^{-12} cm^3 molecule^{-1} s^{-1}) of the following: benzene, 1.20; toluene, 6.4; *o*-xylene, 14.6; *m*-xylene, 24.0; *p*-xylene, 14.4; 1,2,3-trimethylbenzene, 33.3; 1,2,4-trimethylbenzene, 40.0; 1,3,5-trimethylbenzene, 62.4; glyoxal, 11.5; methylglyoxal, 17.3; and biacetyl, 0.24. Values of k_4 were obtained by ratioing the previously determined photolysis rates for glyoxal, methylglyoxal, and biacetyl (*23*) with the presently determined photolysis rate of biacetyl, yielding values of k_5 for these experimental conditions of 2.75×10^{-5} s^{-1} and 6.75×10^{-5} s^{-1} for glyoxal and methylglyoxal, respectively. Use of these rate constants together with eq I and II allow $Y_{t_1-t_2}$ to be calculated, and the α-dicarbonyl concentrations, corrected for reaction with OH radicals and photolysis, are then given by

$$[\alpha\text{-dicarbonyl}]_{t_2}{}^{\text{corr}} = [\alpha\text{-dicarbonyl}]_{t_1}{}^{\text{corr}} + Y_{t_1-t_2}([\text{aromatic}]_{t_2} - [\text{aromatic}]_{t_1}) \tag{III}$$

where $[\alpha\text{-dicarbonyl}]_{t_1}{}^{\text{corr}}$ and $[\alpha\text{-dicarbonyl}]_{t_2}{}^{\text{corr}}$ are the corrected α-dicarbonyl concentrations at times t_1 and t_2, respectively. The correction factors, $[\alpha\text{-dicarbonyl}]_t{}^{\text{corr}}/[\alpha\text{-dicarbonyl}]_t$, were in all cases ≤ 1.67 for glyoxal (for benzene) and ≤ 1.55 for methylglyoxal and were typically ~ 1.2.

The experimental data are given in Tables II–IX together with the corrected values derived from eq I–III. The corrected glyoxal and biacetyl concentrations, $[\alpha\text{-dicarbonyl}]_t{}^{\text{corr}}$, are plotted against the amounts of aromatic hydrocarbon consumed, $-\Delta[\text{aromatic}] = [\text{aromatic}]_t - [\text{aromatic}]_{t_0}$, according to eq III in Figures 1–3. The measurement errors were primarily given by the detection limits of the spectroscopic techniques, such that for glyoxal and methylglyoxal larger relative errors are, or course, associated with the lower yields during the early stage of a reaction. For the aromatic hydrocarbons, at the relatively high concentrations employed, the FT-IR determinations were well within $\pm 1\%$. In any case, the random scatter of the data plotted in Figures 1–3 shows the extent of these measurement errors in both $\Delta[\text{aromatic}]$ and $[\alpha\text{-dicarbonyl}]_t{}^{\text{corr}}$. The yields, Y, of glyoxal, methylglyoxal and biacetyl derived from the slopes of such plots by least-squares analyses are listed in Table I.

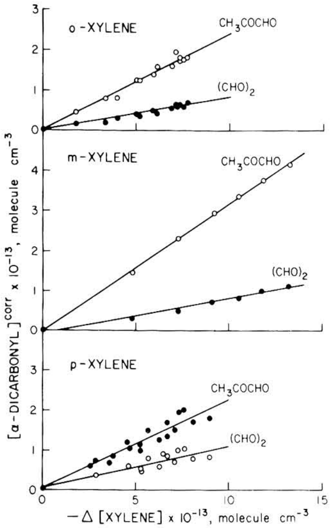

Figure 2. Plots of the glyoxal and methylglyoxal yields (corrected for photolysis and reaction with OH radicals; see text) against the amounts of *o*-, *m*-, and *p*-xylene consumed.

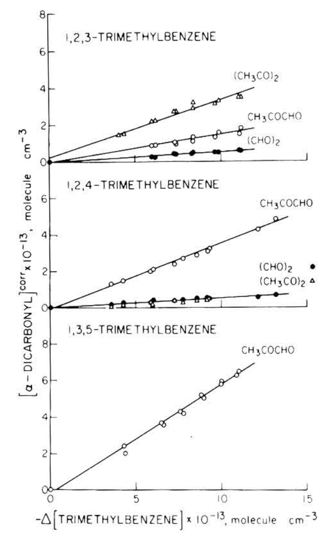

Figure 3. Plots of the glyoxal, methylglyoxal, and biacetyl yields (corrected for photolysis and reaction with OH radicals; see text) against the amounts of 1,2,3-, 1,2,4-, and 1,3,5-trimethylbenzene consumed.

Discussion

The glyoxal and methylglyoxal yields obtained in this work are compared in Table I with our previous glyoxal and methylglyoxal yields (*8*) for toluene and *m*- and *p*-xylene and with other available literature data for toluene, the xylenes, and the trimethylbenzenes. As we have noted previously (*8*), the present α-dicarbonyl yields should be independent (to within $\lesssim 10$–15%) of the initial aromatic and NO_x concentrations. This is confirmed by the study of Bandow et al. (*17*), in which the initial NO_x concentrations were varied from 2×10^{13} to 5×10^{13} molecule cm^{-3}, and no dependence of the product yields on the NO_x

Table I. Formation Yields of the α-Dicarbonyls Glyoxal, Methylglyoxal, and Biacetyl from Benzene and the Methyl-Substituted Benzenes, at Room Temperature and Atmospheric Pressure, together with Literature Data

aromatic	α-dicarbonyl yield[a] glyoxal	methylglyoxal	biacetyl	ref
benzene	0.207 ± 0.019			this work
toluene	0.15 ± 0.04	0.14 ± 0.04		17
	0.111 ± 0.013	0.146 ± 0.014		8
	0.105 ± 0.019	0.146 ± 0.006		this work
o-xylene			0.18 ± 0.04	15
			0.260 ± 0.102	16
			0.137 ± 0.016	13
	0.08 ± 0.04	0.23 ± 0.3	0.10 ± 0.02	18
	0.087 ± 0.012	0.246 ± 0.020		this work
m-xylene	0.13 ± 0.03	0.42 ± 0.05		18
	0.104 ± 0.020	0.265 ± 0.035		8
	0.086 ± 0.011	0.319 ± 0.009		this work
p-xylene	0.24 ± 0.02	0.12 ± 0.02		18
	0.120 ± 0.020	0.111 ± 0.015		8
	0.225 ± 0.039	0.105 ± 0.034		this work
1,2,3-trimethylbenzene	0.072 ± 0.001	0.18 ± 0.01	0.45 ± 0.02	19
	0.058 ± 0.008	0.152 ± 0.025	0.316 ± 0.036	this work
1,2,4-trimethylbenzene	0.078 ± 0.005	0.37 ± 0.01	0.11 ± 0.01	19
	0.048 ± 0.005	0.357 ± 0.017	0.048 ± 0.009	this work
1,3,5-trimethylbenzene		0.64 ± 0.03		19
		0.602 ± 0.033		this work

[a] Indicated error limits are 2 standard deviations.

concentration was reported.

It can be seen that the present glyoxal and methylglyoxal yields for toluene, the xylenes, and the trimethylbenzenes are generally in good agreement with those reported by Bandow and co-workers (*17–19*), with the only discrepancies outside of the combined stated error limits occurring for the glyoxal yields from 1,2,3- and 1,2,4-trimethylbenzene. Our glyoxal yield from benzene is the first reported for this aromatic hydrocarbon under conditions reasonably representative of the ambient atmosphere. Furthermore, with the exception of the glyoxal yield from *p*-xylene, our present glyoxal and methylglyoxal yields are in good agreement with those previously determined in this laboratory (*8*). The reasons for the discrepancies between our glyoxal yields from *p*-xylene are not clear, but a significant degree of scatter in the glyoxal yields from run to run for this aromatic hydrocarbon was observed. Our biacetyl yields from 1,2,3- and 1,2,4-trimethylbenzene are ~30–50% lower than those reported by Bandow and Washida (*19*).

Unsaturated 1,4-dicarbonyls have been postulated as counterpart products of the above α-dicarbonyls in the ring cleavage schemes of aromatic hydrocarbons (*7, 9, 10*). Thus for example, 3-hexene-2,5-dione and 2-methyl-2-butenedial have been postulated to be the respective coproducts of glyoxal and methylglyoxal from *p*-xylene (*10*). We attempted the detection of 3-hexene-2,5-dione among the irradiation products of *p*-xylene and 1,2,4-trimethylbenzene in the present experiments, since we have previously recorded the FT-IR spectra of both the *trans* and *cis* forms of this 1,4-unsaturated dicarbonyl compound (*24*). Infrared absorptions in the 1100–1400-cm^{-1} region of the residual spectra suggested the possible formation of 3-hexene-2,5-dione from both of these aromatic hydrocarbons, with the absorption features being consistent with the presence of more of the *cis* form than of the *trans* form. Estimates of yields could not be reliably made due to presence of interfering absorptions, among which were those most likely caused by peroxyacyl nitrates (other than peroxyacetyl nitrate). in the case of *p*-xylene the spectral data were not inconsistent with the upper limit yield of *cis*-3-hexene-2,5-dione being similar to that for glyoxal (i.e., $\lesssim$25%).

Consistent with our previous conclusions (*8*), it is obvious that the α-dicarbonyl yields do not fully account for the reaction pathways occurring. Thus these α-dicarbonyl yields account for ~20% of the overall reactions for benzene, ~25–30% for toluene, ~30–50% for the xylenes, and ~60% for the trimethylbenzenes if it is assumed that the corresponding unsaturated 1,4-dicarbonyls are formed together with the α-dicarbonyls. However, if the unsaturated 1,4-dicarbonyls are not formed in yields corresponding to the α-dicarbonyl coproducts, then these carbon balances are drastically lower.

The direct reactions of OH radicals with the aromatic hydrocarbons, via H-atom abstraction or, for benzene, H-atom elimination (*12, 25*) account for $\lesssim$10% of the overall OH radical reactions (*12*). Since the reaction pathway giving rise to hydroxyaromatic formation is quantitatively known only for toluene, the extent of presently unrecognized reaction pathways can be estimated only for this aromatic hydrocarbon. As discussed previously (*8*), for toluene only ~50% of the overall reaction pathways can be quantitatively accounted for, although Shepson et al. (*5*) and Dumdei and O'Brien (*6*) have identified a variety of polyfunctional products from the NO_x–air photooxidations of toluene (*5, 6*) and *o*-xylene (*5*).

Clearly, while the present data set is an important input to chemical computer models concerning the atmospheric chemistry of the aromatic hydrocarbons, work is urgently needed to quantify other products, such as those reported by Shepson et al. (*5*) and Dumdei and O'Brien (*6*), and to further elucidate the reaction pathways occurring during these NO_x–air photooxidations subsequent to the initial OH radical reaction with the parent aromatic hydrocarbons.

Supplementary Material Available

Tables II–IX, listing experimental data for the CH_3ONO–NO–aromatic hydrocarbon–air irradiations (8 pages), will appear following these pages in the microfilm edition of this volume of the journal. Photocopies of the supplementary material from this paper or microfiche (105 × 148 mm, 24× reduction, negatives) may be obtained from Microforms Office, American Chemical Society, 1155 16th St., N.W., Washington, DC 20036. Orders must state whether for photocopy or microfiche and give complete title of article, names of authors, journal issue data, and page numbers Prepayment, check or money order for $13.50 for photocopy ($15.50 foreign) or $6.00 for microfiche ($7.00 foreign), is required and prices are subject to change.

Acknowledgments

We thank William D. Long and Sara M. Aschmann for assistance in conducting these experiments.

Registry No. NO_x, 11104-93-1; OH, 3352-57-6; glyoxal, 107-22-2; methylglyoxal, 78-98-8; biacetyl, 431-03-8; benzene, 71-43-2; toluene, 108-88-3; *o*-xylene, 95-47-6; *m*-xylene, 108-38-3; *p*-xylene, 106-42-3; 1,2,3-trimethylbenzene, 526-73-8; 1,2,4-trimethylbenzene, 95-63-6; 1,3,5-trimethylbenzene, 108-67-8.

Literature Cited

(1) Black, F. M.; High, L. E.; Lang, J. M. *J. Air Pollut. Control Assoc.* **1980**, *30*,1216-1221.
(2) Carter, W. P. L.; Ripley, P. S.; Smith, C. G.; Pitts, J. N., Jr. "Atmospheric Chemistry of Hydrocarbon Fuels"; Experiments, Results and Discussion, USAF Final Report ESL-TR-81-53, Nov 1981; Vol. 1.
(3) Nelson, P. F.; Quigley, S. M.; Smith, M. Y. *Atmos. Environ.* **1983**, *17*, 439-449.
(4) Leone, J. A.; Seinfeld, J. H. *Int. J. Chem. Kinet.* **1984**, *16*, 159-193.
(5) Shepson, P. B.; Edney, E. O.; Corse, E. W. *J. Phys. Chem.* **1984**, *88*, 4122-4126.
(6) Dumdei, B. E.; O'Brien, R. J. *Nature (London)* **1984**, *311*, 248-250.
(7) Atkinson, R.; Lloyd, A. C. *J. Phys. Chem. Ref. Data* **1984**, *13*, 315-444.
(8) Tuazon, E. C.; Atkinson, R.; Mac Leod, H.; Biermann, H. W.; Winer, A. M.; Carter, W. P. L., Pitts, J. N., Jr. *Environ. Sci. Technol.* **1984**, *18*, 981-984.
(9) Leone, J. A.; Flagan, R. C.; Grosjean, D.; Seinfeld, J. H. *Int. J. Chem. Kinet.* **1985**, *17*, 177-216.
(10) Atkinson, R.; Carter, W. P. L.; Darnall, K. R.; Winer, A. M.; Pitts, J. N., Jr. *Int. J. Chem. Kinet.* **1980**, *12*, 779-836.
(11) Atkinson, R.; Darnall, K. R.; Lloyd, A. C.; Winer, A. M.; Pitts, J. N., Jr. *Adv. Photochem.* **1979**, *11*, 375-488.
(12) Atkinson, R. *Chem. Rev.*, in press.
(13) Atkinson, R.; Carter, W. P. L.; Winer, A. M. *J. Phys. Chem.* **1983**, *87*, 1605-1610.
(14) Hoshino, M.; Akimoto, H.; Okuda, M. *Bull. Chem. Soc. Jpn.* **1978**, *51*, 718-724.
(15) Darnall, K. R.; Atkinson, R.; Pitts, J. N., Jr. *J. Phys. Chem.* **1979**, *83*, 1943-1946.
(16) Takagi, H.; Washida, N.; Akimoto, H.; Nagasawa, K.; Usui, Y.; Okuda, M. *J. Phys. Chem.* **1980**, *84*, 478-483.
(17) Bandow, H.; Washida, N.; Akimoto, H. *Bull. Chem. Soc. Jpn.* **1985**, *58*, 2531-2540.
(18) Bandow, H.; Washida, N. *Bull. Chem. Soc. Jpn.* **1985**, *58*, 2541-2548.
(19) Bandow, H.; Washida, N. *Bull. Chem. Soc. Jpn.* **1985**, *58*, 2549-2555.
(20) Besemer, A. C. *Atmos. Environ.* **1982**, *16*, 1599-1602.
(21) Takagi, H.; Washida, N.; Akimoto, H.; Okuda, M. *Spectrosc. Lett.* **1982**, *15*, 145-152.
(22) Winer, A. M.; Graham, R. A.; Doyle, G. J.; Bekowies, P. J.; McAfee, J. M.; Pitts, J. N., Jr. *Adv. Environ. Sci. Technol.* **1980**, *10*, 461-511.
(23) Plum, C. N.; Sanhueza, E.; Atkinson, R.; Carter, W. P. L. Pitts, J. N., Jr. *Environ. Sci. Technol.* **1983**, *17*, 479-484.
(24) Tuazon, E. C.; Atkinson, R.; Carter, W. P. L. *Environ. Sci. Technol.* **1985**, *19*, 265-269.
(25) Lin, C.-Y.; Lin, M. C., presented at the Fall Technical Meeting, Eastern Section, Combustion Institute, 1984.

Received for review April 25, 1985. Accepted August 19, 1985. The authors gratefully acknowledge the financial support of the U.S. Environmental Protection Agency under Cooperative Agreement CR-810964-01 (Project Monitor, Marcia C. Dodge). Although the research described in this article has been funded by the Unites States Environmental Protection Agency, it has not been subjected to the Agency's required peer and policy review and therefore does not necessarily reflect the views of the Agency and no official endorsement should be inferred.

Formation of Methyl Nitrite in the Surface Reaction of Nitrogen Dioxide and Methanol. 1. Dark Reaction

Hiroo Takagi, Shiro Hatakeyama, and Hajime Akimoto*

Division of Atmospheric Environment, The National Institute for Environmental Studies, P.O. Tsukuba-gakuen, Ibaraki 305, Japan

Seiichiro Koda

Department of Reaction Chemistry, Faculty of Engineering, University of Tokyo, Hongo, Bunkyo-ku, Tokyo 113, Japan

■ The reaction of nitrogen dioxide and methanol, which has been known in the gas phase to proceed thermally as $CH_3OH + 2NO_2 \rightarrow CH_3ONO + HNO_3$, was found to proceed heterogeneously on various surfaces as well, in an 11-L Pyrex cell and a 6065-L evacuable smog chamber. An FTIR study has revealed that the reaction products are the same as in the homogeneous reaction, i.e., methyl nitrite and nitric acid. Neither methyl nitrate nor nitrous acid was observed. Among the surfaces studied, uncoated stainless steel, Pyrex, and the smog chamber wall surfaces were found to be the most active to induce the surface reaction. The apparent activation energy of the surface reaction in the smog chamber was determined to be -11.9 ± 3.3 kJ mol^{-1}.

Introduction

Thermal reaction of methanol and NO_2

$$CH_3OH + 2NO_2 \rightarrow CH_3ONO + HNO_3 \quad (1)$$

is of much interest to the atmospheric chemist in that (i) it could be a possible major source of methyl nitrite in the polluted atmosphere particularly when methanol is used as automobile fuel and (ii) it is an analogue to the reaction of water and NO_2,

$$H_2O + 2NO_2 \rightarrow HONO + HNO_3 \quad (2)$$

which would be an important source reaction of nitrous acid observed in the atmosphere (*1*). Since both methyl nitrite and nitrous acid accelerate efficiently photochemical smog formation by providing OH radicals under the irradiation of sunlight, it is of much significance to characterize reactions 1 and 2 under the simulated atmospheric conditions.

The classical gas-phase reaction of methanol and NO_2, eq 1, has recently been reinvestigated by Niki et al. (*2*) and

Koda et al. (3), and the stoichiometry and basic kinetics have been established. Niki et al. (2) confirmed the stoichiometric reaction 1 by direct observation of all the reactants and products, using the FTIR method, and showed the kinetics to follow the rate law, $d[CH_3ONO]/dt = k[NO_2]^2[CH_3OH]$ at the reactant pressures of 0.1–1.0 torr being consistent with earlier studies (4, 5). Koda et al. (3) found that the kinetic order with respect to methanol decreased with the increase of the methanol pressure in the range of ca. 1–10 torr, and proposed that *asym*-N_2O_4 rather than *sym*-N_2O_4 might be involved as intermediates of reaction 1. The termolecular rate constants of reaction 1 were reported to be $(5.7 \pm 0.6) \times 10^{-37}$ cm^6 $molecule^{-2}$ s^{-1} at 25 °C (2) and $(9.0 \pm 0.2) \times 10^{-37}$ cm^6 $molecule^{-2}$ s^{-1} at 21 °C (3).

On the other hand, the kinetics of the reaction of NO_2 and water in the gas phase have been studied by England and Corcoran (6), who reviewed the earlier studies and showed that the initial rate of disappearance of NO_2 was first order with respect to the water vapor concentration and greater than first order with respect to NO_2. More recently, the importance of the heterogeneous surface reaction of NO_2 and water vapor was pointed out by Sakamaki, Hatakeyama, and Akimoto (7) in relevance to the unknown radical supply (8, 9) in the smog chamber experiments. The kinetics of the surface reaction have been studied extensively by Sakamaki et al. (7) and by Pitts et al. (10) in air at the NO_2 concentration of 1–23 ppm and 0.1–20 ppm, respectively, and shown that the HONO formation follows the rate law, $d[HONO]/dt = k[NO_2][H_2O]$ rather than $d[HONO]/dt = k[NO_2]^2[H_2O]$, which is expected from the stoichiometry. However, gaseous HNO_3 could not be detected in any of the smog chambers employed at the National Institute for Environmental Studies (NIES) and at the Statewide Air Pollution Research Center (SAPRC). Thus, although the kinetic law has been established, the stoichiometry and the mechanism of the surface reaction of water vapor with NO_2 remain unresolved.

From the analogy of the reactions, the reaction of methanol and NO_2 may also proceed heterogeneously on the reactor surface to emanate products into the gas phase. The study of the heterogeneous reaction of methanol and NO_2 might give better insight into the nature of the reaction of water vapor and NO_2 also. In the present study, the dark reaction of methanol and NO_2 was studied at the pressure of 50–200 mtorr of reactants in 1 atm air in 11-L cells with different surface materials, and the heterogeneous component of the reaction was elucidated. The reaction was also studied in a 6056-L evacuable and bakable smog chamber, where the surface reaction was found to be predominant at the NO_2 pressure of 20–60 mtorr. This paper (Paper I) describes the kinetic study of the dark reactions of methanol and NO_2 on surfaces, and the following paper (Paper II) reports the observed enhancement of the rate of the methanol–NO_2 reaction in the smog chamber under the photoirradiation.

Experimental Section

Experiments were conducted by using a quartz or Pyrex cell (120-mm i.d., 1000-mm length, and 11-L volume) and an evacuable smog chamber (1400-mm diameter, 3500-mm length, and 6065-L volume). Details of the smog chamber system have been described elsewhere (11). Both the cells and the chamber were equipped with gold-coated, multireflection mirrors inside for FTIR measurement.

The surface area of the quartz and the Pyrex cell is 3770 cm^2, and the total surface-to-volume ratio is ca. 35 m^{-1}. A series of runs were carried out in the quartz cell inserting either a PFA (tetrafluoroethylene–perfluoroalkyl vinyl ether copolymer) coated or uncoated roll of stainless steel (SUS 304) plate (0.1 mm thickness, 700 mm × 380 mm rolled into a cylindrical form to contact closely to the quartz wall, 2660 cm^2 one side surface area) in order to enhance the heterogeneous surface reaction. The inner wall of the smog chamber is PFA coated 17 μm thick, and each end flange of the chamber holds 19 windows (250-mm diameter each) made of quartz and Pyrex. The surface area of the PFA-coated wall is ca. 39.4 m^2, and the quartz and Pyrex window surfaces are 0.9 and 1.0 m^2, respectively. Other surface materials in the smog chamber are gold (multireflection mirrors), aluminum (mirror covers), stainless steel (a part of mirror holders), and invar (mirror supporting rods). The total area of these metals is ca. 0.2 m^2. Thus, the total surface-to-volume ratio of the smog chamber is 6.9 m^{-1} including the contents. The PFA coating on the smog chamber wall and the SUS plate specimen, which was inserted into the quartz cell, contains primer coating underneath. The primer coating is polytetrafluoroethylene (PTFE) containing TiO_2 and carbon as pigments and Cr_2O_7 and H_3PO_4 to obtain better adhesiveness to the stainless-steel surface.

Temperature dependence of the reaction was studied in the smog chamber in the range 0–40 °C by varying the temperature of the wall, which is jacketed with thermostated heat transfer oil. Both end flanges of the chamber are not thermostated, and the temperature of the gas deviates from that of the wall to the extent of 4 °C at the most as the difference between the wall and the room temperature increases. The average gas temperature was measured by a thermometer fed through into the chamber. All the runs in the quartz and Pyrex cell were carried out at 22 ± 1 °C.

The concentrations of the products were measured by means of the long-path FTIR. The path lengths were 40.0 m and 221.5 m for the cells and the smog chamber, respectively. The same spectrometer was used for both systems by switching the optical path. The spectrum was typically obtained with 128 scans (scanning time ~4 min) at a resolution of 1.0 cm^{-1}. The absorptivities used were CH_3ONO, 0.161 (991 cm^{-1} Q-branch peak), and HNO_3, 1.38 (1326 cm^{-1} Q-branch peak) $torr^{-1}$ m^{-1}. The initial concentrations of methanol and NO_2 were determined by pressure reading in a known volume before flushing into the reactor. For a few runs the decrease of CH_3OH and NO_2 was monitored at the peaks 2846 and 2918 cm^{-1}, respectively.

In the quartz and Pyrex cell runs, NO_2 was first introduced into the cell with purified air up to ca. 400 torr, and then methanol was flushed with air to fill the cell at 760 torr. In the smog chamber runs, the chamber was first filled with the purified air at ca. 760 torr, and then NO_2 and methanol were introduced successively by using air as the carrier gas. The reaction mixture was stirred by a pair of fans during the run.

Results

Reaction in the Blank Quartz Cell. The dark reaction of methanol and NO_2 was first studied in a quartz cell at the pressure of methanol of ca. 38 mtorr, NO_2 of 35–150 mtorr, and 1 atm of air in order to assure the gas-phase reaction 1, which has been established in the 0.1–10-torr region (2, 3). Figure 1 shows typical data of CH_3ONO and HNO_3 formation in low conversion (open symbols). As shown in Figure 1, HNO_3 is observed in the gas phase right after the mixing of CH_3OH and NO_2 though the yield is only a fraction of CH_3ONO after the reaction proceeds. When the initial rates of CH_3ONO formation (*R*) are

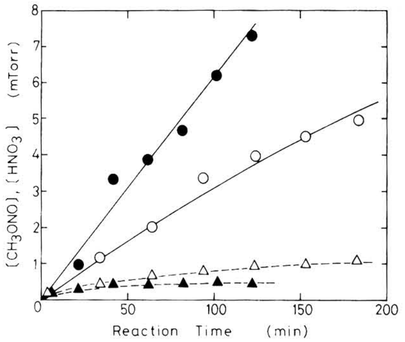

Figure 1. Time profiles of the formation of CH_3ONO (O, ●) and HNO_3 (△, ▲) for the reaction of CH_3OH and NO_2 in the blank quartz cell (open symbols) and in the quartz cell with a PFA-coated plate (solid symbols): $[CH_3OH]_0$ = 35.9, 38.1 mtorr and $[NO_2]_0$ = 113.8, 121.5 mtorr, respectively.

Table I. Kinetic Data for CH_3OH-NO_2 Mixtures in 760 torr of Air in the Quartz Cell (22 ± 1 °C)

$[CH_3OH]$, mtorr	$[NO_2]$, mtorr	$d[CH_3ONO]/dt$, mtorr min^{-1}	$k^{III} \times 10^{-36}$ cm^6 $molecule^{-2}$ s^{-1}
37.1	35.8	0.0051	1.94
38.1	76.2	0.0133	1.06
38.4	113.8	0.0297	1.09
35.9	133.0	0.0441	1.26
38.1	152.4	0.0566	1.18
			av[a] 1.15 ± 0.09

[a] Average of four runs with $[NO_2] \geq 76.2$ mtorr. Error limit cited is 1σ.

plotted against $[NO_2]_0^2$, a linear relationship was obtained confirming the major contribution of the termolecular reaction (eq 1). The termolecular rate constant (k^{III}) as defined by $d[CH_3ONO]/dt = k^{III}[NO_2]^2[CH_3OH]$ can be derived from an integrated equation

$$\frac{1}{(2a-b)}\left[\frac{1}{(b-2x)} - \frac{1}{b} - \frac{1}{(2a-b)}\ln\frac{b(a-x)}{a(b-2x)}\right] = k^{III}t \tag{3}$$

where a and b are the initial concentrations of CH_3OH and NO_2, x is the concentration of CH_3ONO at time t, and the stoichiometry of $-\Delta CH_3OH = -2\Delta NO_2$ is assumed. The rate constants obtained from eq 3 are given in Table I, and the average value was determined to be $(1.15 \pm 0.09) \times 10^{-36}$ cm^6 $molecule^{-2}$ s^{-1}. This value is appreciably higher than the homogeneous reaction rate constant reported before by Farlie et al. (*4*), $(0.45 \pm 0.08) \times 10^{-36}$ (25 °C), and by Niki et al. (*2*), $(0.57 \pm 0.06) \times 10^{-36}$ (25 °C), but only slightly higher than the value, $(0.90 \pm 0.02) \times 10^{-36}$ cm^6 $molecule^{-2}$ s^{-1} (21 °C), by Koda et al. (*3*), all of which were obtained at much higher reactant pressures (0.1–10 torr). In view of the results of the following experiments, the rate constant obtained in the quartz cell under the low reactant pressures in the present study may be subjected to a contribution of the heterogeneous surface reaction.

Reaction in the Quartz Cell with Extra Surfaces. When a cylinder of PFA-coated stainless steel was inserted into the quartz cell, the initial formation of CH_3ONO was also nearly linear with reaction time, but the rate was significantly enhanced as compared to the reaction in the blank cell (solid symbols in Figure 1). On the contrary, the formation of gaseous HNO_3 was suppressed in the presence of the PFA surface. No new product other than CH_3ONO and HNO_3 was observed in the presence of the foreign surface.

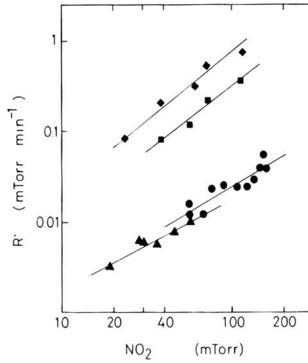

Figure 2. Log–log plot of the initial formation rate (R') of CH_3ONO due to the surface reaction vs. $[NO_2]_0$ for the reaction of NO_2 and methanol in the quartz cell with the PFA-coated plate (●) and uncoated SUS (♦), in the Pyrex cell (■), and in the evacuable smog chamber (▲): $[CH_3OH]_0 \sim 38$ mtorr.

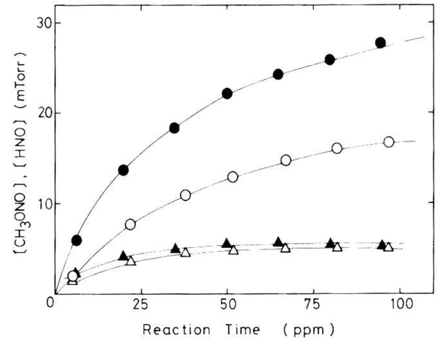

Figure 3. Time profiles of the formation of CH_3ONO (●, O) and HNO_3 (▲, △) in the quartz cell with a SUS plate (solid symbol) and in the Pyrex cell (open symbols): $[CH_3OH]_0 \sim 38$ mtorr and $[NO_2]_0 \sim 114$ mtorr.

The heterogeneous component of the CH_3ONO formation rate (R') due to the PFA surface was evaluated by subtracting the CH_3ONO formation rate due to the homogeneous reaction using the termolecular rate constant obtained in the blank cell. Figure 2 shows the log–log plot (●) of the heterogeneous reaction rate thus obtained vs. the initial concentration of NO_2. The slope of the plot is 1.11 ± 0.17, and thus, the heterogeneous component was found to be linearly dependent on NO_2 in contrast to the second-order dependence for the homogeneous reaction. The apparent bimolecular rate constant of the heterogeneous reaction due to the PFA surface was defined by $d[CH_3ONO]/dt = k^{II}[NO_2][CH_3OH]$ and was calculated from the plot of $\ln\{b(a-x)/a(b-2x)\}/(2a-b) = k^{II}t$. Here, a and b are the initial concentrations of CH_3OH and NO_2, and the stoichiometry of $-\Delta CH_3OH = -2\Delta NO_2$ was assumed as before. The obtained kinetic data are summarized in Table II.

When the uncoated SUS cylinder of the same dimension was substituted for the PFA-coated one, the formation rate of CH_3ONO was enhanced drastically (see solid symbols in Figure 3). The observed initial rate of CH_3ONO formation was more than an order of magnitude larger than the homogeneous reaction rate estimated by using the rate constant given above, even at the highest NO_2 pressures

Table II. Kinetic Data for CH_3OH–NO_2 Mixtures in 760 torr of Air in the Quartz Cell with PFA-Coated and Uncoated SUS Cylinder and in the Blank Pyrex Cell

$[CH_3OH]$, mtorr	$[NO_2]$, mtorr	R'^{a}, mtorr min^{-1}	$k^{II} \times 10^{-20}$ cm^3 $molecule^{-1}$ s^{-1}
	Quartz Cell (with PFA-Coated SUS)		
38.2	56.5	0.016	0.33
38.0	56.8	0.012	0.41
38.4	68.7	0.012	0.24
38.0	75.5	0.023	0.44
38.3	91.4	0.025	0.38
38.1	106.2	0.024	0.32
38.2	121.5	0.024	0.28
38.0	134.1	0.029	0.31
38.0	144.7	0.039	0.38
38.1	153.0	0.054	0.52
38.2	153.2	0.038	0.36
			av 0.36 ± 0.08
	Quartz Cell (with Uncoated SUS)		
37.4	23.3	0.08	5.0
37.9	38.1	0.21	7.7
38.0	61.5	0.32	7.9
38.1	70.4	0.54	9.5
38.0	114.1	0.77	11.9
			av 8.4 ± 2.5
	Pyrex Cell (Blank)		
38.5	37.9	0.08	3.0
37.3	56.8	0.12	3.1
37.8	72.6	0.23	4.7
38.1	113.3	0.37	4.9
			av 3.9 ± 1.0

[a] The initial formation rate of CH_3ONO due to the heterogeneous surface reaction.

employed. Nitric acid was observed as before, although the gaseous concentration shows a strong saturation. The initial rate of CH_3ONO formation was obtained by a curve fitting of a third-order polynomial to the time profile typified by Figure 3 and taking an initial slope at $t = 0$. The log–log plot of the initial heterogeneous reaction rate vs. NO_2 pressure reveals that the apparent reaction order is 1.43 ± 0.15 as shown in Figure 2 (♦). Nevertheless, the second-order rate analysis was made in the present work to make a comparison with the rates for the other surfaces easier. The second-order rate constant, k^{II}, given in Table II was obtained by taking an initial slope of the plot of ln $\{b(a-x)/a(b-2x)\}/(2a-b)$ vs. t and is slightly dependent on the reagents' partial pressure as expected. The average heterogeneous rate constant is 25 times as large as that for the PFA surface.

Reaction in the Pyrex Cell. The reaction in a blank Pyrex cell was found to proceed much faster than that in the blank quartz cell but slower than that in the quartz cell containing the SUS cylinder as shown in Figure 3 (open symbols). Figure 2 depicts that the initial rate of CH_3ONO formation was proportional to the 1.48 ± 0.18 degree to the initial concentration of NO_2, being close to the case of the reaction with the SUS surface in the quartz cell. The apparent second-order rate constant of the initial surface reaction was obtained by the curve-fitting method as before and is given in Table II. Thus, the observed rate constant is about 10 times larger than that in the quartz cell containing the PFA surface. The relative yield of HNO_3 is higher than in the case of other surfaces.

Reaction in the Smog Chamber. The dark reaction of methanol and NO_2 in the smog chamber also gave CH_3ONO and HNO_3 as reaction products, which increase nearly linearly with reaction time as depicted in Figure 4. Note that the initial concentration of CH_3OH employed in these runs is about 10 times smaller than those employed in the quartz and the Pyrex runs. The formation rate of CH_3ONO by the homogeneous reaction as calculated by using the termolecular rate constant is only less than 10% of that observed experimentally in Figure 4, indicating that the heterogeneous reaction is predominant also in the smog chamber under the present experimental conditions. The observed rate of CH_3ONO formation was found to be nearly proportional to the first order of NO_2 as in the case of the quartz cell with PFA surfaces (see (▲) in Figure 2). An apparent bimolecular rate constant of the surface reaction was calculated after subtracting the contribution of the homogeneous reaction and the results are given in Table III. The dependence of the CH_3ONO formation rate on the CH_3OH concentration was also studied in the smog chamber. The results are given in Table III and shown in Figure 5.

The effect of agitating the reaction mixture was checked by terminating the stirring fan at the middle of the run. The difference in the CH_3ONO formation rate before and after the stopping of the fan was within experimental error. This result indicates that the reaction rate is not determined by the transportation of species in the bulk gas phase.

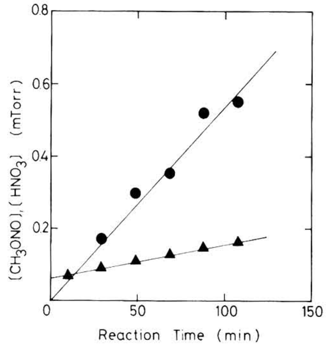

Figure 4. Time profiles of the formation of CH_3ONO (●) and HNO_3 (▲) in the evacuable smog chamber: $[CH_3OH]_0$ = 3.7 mtorr and $[NO_2]_0$ = 36.5 mtorr.

Table III. Kinetic Data for CH_3OH–NO_2 Mixtures in 760 torr of Air in the Evacuable Smog Chamber

$[CH_3OH]$, mtorr	$[NO_2]$, mtorr	temp, K	R'^{a}, mtorr min^{-1}	$k^{II} \times 10^{-20}$ cm^3 $molecule^{-1}$ s^{-1}
3.8	19.1	303	0.0031	2.4
3.8	28.1	303	0.0043	2.2
3.9	30.4	303	0.0058	2.8
3.7	36.5	303	0.0045	1.7
3.5	45.4	303	0.0070	2.7
3.9	56.7	303	0.0093	2.5
				av 2.4 ± 0.4
6.8	38.3	303	0.0045	
9.2	38.3	303	0.0071	
12.2	38.1	303	0.0079	
15.5	38.4	303	0.0055	
			R^{b}	
3.9	38.4	277	0.0068	
3.6	38.1	285	0.0072	
3.6	38.0	294	0.0057	
3.7	36.5	303	0.0054	
3.9	38.1	311	0.0038	

[a] The formation rate of CH_3ONO due to the heterogeneous surface reaction. [b] The formation rate of CH_3ONO including the homogeneous reaction.

Table IV. Material Balance of the Gaseous Species in the Surface Reaction of NO_2 and CH_3OH

surface	$[CH_3OH]$, mtorr	$[NO_2]$, mtorr	$-\Delta CH_3OH$	$-\Delta NO_2$	ΔCH_3ONO	ΔHNO_3
quartz/SUS	37.4	23.3	1.69 ± 0.18[a]	1.00	0.93 ± 0.08	0.20 ± 0.02
	37.9	38.1	1.14 ± 0.09	1.00	1.01 ± 0.15	n.d.[b]
Pyrex	38.5	37.9	1.31 ± 0.30	1.00	0.76 ± 0.10	0.12 ± 0.05
	37.3	56.8	1.13 ± 0.12	1.00	0.94 ± 0.17	0.13 ± 0.04
smog chamber/PFA	15.5	38.4	0.51 ± 0.08	1.00	0.41 ± 0.03	0.13 ± 0.01

[a] Error range is 1σ. [b] Not determined due to the strong saturation of the gaseous HNO_3.

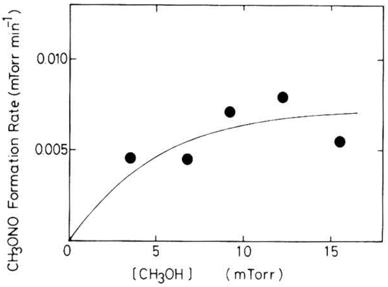

Figure 5. Formation rate of CH_3ONO vs. $[CH_3OH]_0$ for the reaction of NO_2 and methanol in the smog chamber: $[NO_2]_0$ = 38 mtorr.

Temperature dependence of the overall reaction studied in the smog chamber is shown in Table III. Although the data are rather scattered, the formation rates of CH_3ONO and HNO_3 are slightly negatively dependent on temperature. An Arrhenius plot gives the apparent activation energy of -11.9 ± 3.3 kJ mol^{-1}.

Material Balance. The material balance of the gaseous species in the surface reaction of NO_2 and CH_3OH was studied for a few runs employing comparable initial concentrations of NO_2 and CH_3OH. For each run, $-\Delta CH_3OH$, ΔCH_3ONO, and ΔHNO_3 were plotted against $-\Delta NO_2$ at different reaction time, and the slopes were determined from least-squares plots. The results are summarized in Table IV. Only for the smog chamber run is the material balance of $-\Delta CH_3OH$, $-\Delta NO_2$, and ΔCH_3ONO close to the stoichiometric relation of $CH_3OH + 2NO_2 = CH_3ONO + HNO_3$. In other cases, the apparent ratio of $-\Delta CH_3OH$, $-\Delta NO_2$, and ΔCH_3ONO in the gas phase is closer to 1:1:1, and the consumption ratio of $\Delta CH_3OH/\Delta NO_2$ exceeds unity particularly when the ratio of $[NO_2]/[CH_3OH]$ gets lower. The increment of $\Delta CH_3ONO + \Delta HNO_3$ in the gas phase exceeds $-\Delta NO_2$ in some cases in the smaller cells.

Discussion

Surface Reaction of NO_2 with Methanol. The characteristics of the surface reaction can be summarized as follows: (i) The reaction products are the same as those in the gas phase, i.e., CH_3ONO and HNO_3, and neither CH_3ONO_2 nor HONO was detected. (ii) The surface reaction rate follows the first-order kinetics with respect to NO_2 in the smog chamber and in the quartz cell with a PFA surface, in contrast to the gas-phase reaction, which follows the second-order dependence (*2, 3*). In the quartz cell containing SUS surface and in the Pyrex cell, the reaction rate was proportional approximately to the 1.5 power of NO_2 pressure. (iii) The formation rate of CH_3ONO increases with the concentration of CH_3OH at the lower concentration range but tends to saturate as the concentration increases. (iv) The rate of the surface reaction is very much dependent on the materials. The observed heterogeneous reaction rate constants per geometric S/V ratio are 1.5×10^{-22}, 3.5×10^{-21}, and 1.1×10^{-21} cm^3 molecule^{-1} s^{-1} m, for the PFA, SUS, and Pyrex surfaces, respectively ($[CH_3OH] \simeq 38$ mtorr, $[NO_2]$ = 30–150 mtorr). Among the surfaces employed the SUS surface is the most active, followed by the Pyrex and PFA-coated plate, and the quartz surface is the most inactive. However, since the dependence of the reaction rate on the CH_3OH concentration was not studied for each surface, the relative rate obtained above may not be representative of the catalytic activity under different conditions. The smog chamber surface was also found to be very reactive giving the normalized reaction rate of 3.5×10^{-21} cm^3 molecule^{-1} s^{-1} m for the runs with 3.8 mtorr of CH_3OH.

The above findings indicate that the reaction of NO_2 and methanol,

$$CH_3OH + 2NO_2 \rightarrow CH_3ONO + HNO_3 \qquad \Delta H^\circ = -65 \text{ kJ mol}^{-1} \quad (1)$$

which has been well-known in the gas phase (*2, 3*), is enhanced catalytically on various surfaces. The material balance of the gaseous species has shown that the ratio of $-\Delta CH_3OH$, $-\Delta NO_2$, and ΔCH_3ONO is approximately 1:2:1 as expected from the stoichiometry of eq 1 in the case of the smog chamber. The yield of gaseous HNO_3 is ca. one-third of that of CH_3ONO. These results suggest that the overall surface reaction of NO_2 and CH_3OH proceeds following the stoichiometric reaction 1 as in the gas phase, but most of HNO_3 formed remains on the surface. In the quartz cell with the SUS surface and in the Pyrex cell, however, the ratio of $-\Delta CH_3OH/(-\Delta NO_2)$ exceeds unity as opposed to the stoichiometry of eq 1. The ratio tends to increase as the concentration ratio of CH_3OH to NO_2 increases. In these smaller cells, unreactive adsorption of CH_3OH and NO_2 may be considerable, which would give the deviation of the ratio from the stoichiometry. As the ratio of CH_3OH to NO_2 decreases, most of adsorbed CH_3OH would react with nitrogenous species on the surface to emit a nearly stoichiometric amount of CH_3ONO to that of CH_3OH consumed. The fact that the ratio of $\Delta CH_3ONO/(-\Delta NO_2)$ is close to unity rather than to 0.5 as expected from eq 1 may be ascribed to the contribution of the reaction of NO_2 preadsorbed on the surface right after the reactant is introduced into the cell.

Relation of NO_2 and Water Reaction. It would be worthwhile to compare the present results for reaction 1 with those of the reaction of water and NO_2,

$$H_2O + 2NO_2 \rightarrow HONO + HNO_3 \qquad \Delta H^\circ = -37 \text{ kJ mol}^{-1} \quad (2)$$

which has been reported earlier (*6, 7, 10*). Both reactions proceed on the gas–solid interface as well as homogeneously in the gas and liquid phase (*12, 13*). The kinetic dependence with respect to the NO_2 pressure is the same, i.e., the second order in the homogeneous gas-phase reaction and the first order in the heterogeneous surface reaction. The heterogeneous second-order rate constants of the methanol–NO_2 and the water–NO_2 reactions in the evacuable smog chamber at NIES are $(2.4 \pm 0.4) \times 10^{-20}$ and $(7.0 \pm 0.9) \times 10^{-24}$ cm^3 molecule^{-1} s^{-1} (*7*), respectively. Thus, the surface reaction of the methanol and NO_2 is ca.

3000 times faster than that of water and NO_2.

The surface reaction of H_2O and NO_2 has been written as a nonstoichiometric reaction,

$$NO_2 + H_2O \xrightarrow{\text{wall}} HONO \quad (4)$$

in our previous study (7) due to the failure of detecting HNO_3 in the gas phase. In view of the similarity of the reaction to that of methanol and NO_2, the surface reaction of water and NO_2 may also proceed as written by eq 2, but the reason for the stay of HNO_3 on the surface in this case remains unresolved.

Mechanism of the Surface Reactions. From the kinetic dependence on NO_2 and CH_3OH as observed in this study, the surface kinetics can be conceived, e.g.,

$$CH_3OH(g) \rightarrow (CH_3OH)_{ad} \quad (5)$$

$$NO_2(g) \rightarrow (NO_2)_{ad} \quad (6)$$

$$(NO_2)_{ad} + NO_2(g) \rightarrow [(NO_2)_2]_{ad} \quad (7)$$

$$[(NO_2)_2]_{ad} + (CH_3OH)_{ad} \rightarrow [CH_3OH{\cdot}(NO_2)_2]_{ad} \quad (8)$$

$$[CH_3OH{\cdot}(NO_2)_2]_{ad} \rightarrow (CH_3ONO{\cdot}HNO_3)_{ad} \quad (9)$$

$$(CH_3ONO{\cdot}HNO_3)_{ad} \rightarrow CH_3ONO(g) + HNO_3(g) \quad (10)$$

Although the present study does not give any details on these steps, the dependences on NO_2 (smaller than second order) and CH_3OH (smaller than first order) seem to be consistent with the above mechanism. The observed negative temperature dependence of the overall reaction suggests that the steps of eq 5–8 rather than the rearrangement step, eq 9, are rate determining.

Being relevant to the reactive nitrogenous intermediate, Koda et al. (3) have noted that the alternative pathways of the methanol–NO_2 reaction,

$$CH_3OH + 2NO_2 \rightarrow CH_3ONO_2 + cis\text{-}HONO \qquad \Delta H^\circ_{300} = -61 \text{ kJ mol}^{-1} \quad (11)$$

$$CH_3OH + 2NO_2 \rightarrow CH_3ONO_2 + trans\text{-}HONO \qquad \Delta H^\circ_{300} = -64 \text{ kJ mol}^{-1} \quad (12)$$

have comparable exothermicity to that of reaction 1, but the reaction pathway to form CH_3ONO and HNO_3 has been observed exclusively in the gase phase. From this fact and the kinetic analysis they proposed a six-membered ring transition state involving *asym*-N_2O_4, which is known only in low-temperature matrices (*14–16*) and also postulated in the liquid phase (*17, 18*). On the other hand, Cooney and Tsai (*19*) have observed by Raman spectroscopy that a self-ionization of NO_2/N_2O_4 occurs to a far greater extent than in the liquid phase to generate nitrosonium (NO^+) and nitrate (NO_3^-) ions on the alkali cation-exchanged zeolites. Such a self-ionization has also been reported in a low-temperature solid of NO_2/N_2O_4 (*15*), while *asym*-N_2O_4 is known to be predominant in diluted matrices (*14, 16*). Although it is premature to assess the reaction intermediate involved in the surface reaction, the fact that the exclusive reaction channel (eq 1) is also the case for the surface reaction as in the gas phase is suggestive that for similar type of transition state or reaction intermediate might be involved in the surface reaction. It would be interesting to note here that in our previous study (7) of the surface reaction of NO_2 and water, the use of $H_2{}^{18}O$ gave $H^{18}ONO$ exclusively, which could be interpreted by the same mechanism as proposed (3) for the case of methanol.

The difference in the surface activity as observed in the present study may be related to the chemical form of the adsorbed nitrogenous species as well as the acidity of the hydroxyl group of the adsorbed CH_3OH. The NO_2-catalyzed surface reaction of the double bond migration of 2-butenes on porous Vicor and several types of zeolites has been studied by Wada, Otsuka, and Morikawa (*20*) and is ascribed to the formation of acidic hydroxyl group in the presence of surface NO_2.

Atmospheric Implications. Methanol is a potential candidate of the alternative liquid fuel to petroleum, in particular as an automobile fuel in the near future. In fact fleet tests for pure methanol engines have been already performed in a number of countries. Methyl nitrite has been reported as one of the new emissions from practical engines (*21, 22*) as well as from more fundamental constant-volume combustion vessels (*23*). It is now established that the nitrite is not produced during the bulk combustion but is produced through a certain postcombustion reaction during the exhaust as well as analytical processes. The most probable reaction is that between NO_2 and the unburnt methanol emitted from the combustion process, but the rate of the homogeneous reaction 1 seems to be too slow for explaining the relatively large production of methyl nitrite under several performance conditions. For example, methyl nitrite production of more than 100 ppm was reported (*22*) at 20 s after sampling the exhaust gas from the engine exhaust line of an ordinary 4-cycle S.I. engine. Thus, the heterogeneous reaction seems to play a decisive role in these practical systems, though any quantitative estimation is not yet possible due to the unresolved temperature dependence over the necessary wide range and also due to the difficulty in characterizing the surface condition in these practical systems.

Several workers (*24, 25*) have recently discussed the effect of methanol replacement of a part of gasoline on the photochemical smog formation. The methanol substitution was stated to help decrease the calculated ozone level in some cases. But they did not take into account the dark reaction (eq 1) (both of homogeneous and heterogeneous nature) to yield methyl nitrite, which is an important source of radicals when photolyzed. The heterogeneous rate constant for the methanol reaction is about 3000 times as large as that of the water reaction with NO_2, at least as far as the heterogeneous reactions are concerned; thus, although it is not possible to assess quantitatively the heterogeneous rate of CH_3ONO formation in the atmosphere, the nitrite-forming reaction should be as important as the HONO-forming reaction from water and NO_2 if the concentration of methanol exceeds the order of 1 ppm. The monitoring of methanol and nitrite concentrations in the atmosphere as well as the detailed estimation of the fate of the emitted methanol is considered to be important if methanol is to be used practically.

Acknowledgments

We thank A. Morikawa of Tokyo Institute of Technology and H. Bandow for helpful discussions.

Registry No. CH_3OH, 67-56-1; CH_3ONO, 624-91-9; HNO_3, 7697-37-2; stainless steel, 12597-68-1.

Literature Cited

(1) Harris, G. W.; Carter, W. P. L.; Winer, A. M.; Pitts, J. N., Jr.; Platt, U.; Perner, D. *Environ. Sci. Technol.* **1982**, *16*, 414–419.

(2) Niki, H.; Maker, P. D.; Savage, C. M.; Breitenbach, L. P. *Int. J. Chem. Kinet.* **1982**, *14*, 1199–1209.

(3) Koda, S.; Yoshikawa, K.; Okada, J.; Akita, K. *Environ. Sci. Technol.* **1985**, *19*, 262–264.

(4) Fairlie, A. M., Jr.; Corberry, J. J.; Treacy, J. C. *J. Am. Chem. Soc.* **1953**, *75*, 3786–3789.

(5) Silverwood, R.; Thomas, J. H. *Trans. Faraday Soc.* **1967**, *63*, 2476–2479.

(6) England, C.; Corcoran, W. H. *Ind. Eng. Chem. Fundam.* **1974**, *13*, 373–384.
(7) Sakamaki, F.; Hatakeyama, S.; Akimoto, H. *Int. J. Chem. Kinet.* **1983**, *15*, 1013–1029.
(8) Carter, W. P. L.; Atkinson, R.; Winer, A. M.; Pitts, J. N., Jr.; *Int. J. Chem. Kinet.* **1981**, *13*, 735–740.
(9) Carter, W. P. L.; Atkinson, R.; Winer, A. M.; Pitts, J. N., Jr.; *Int. J. Chem. Kinet.* **1982**, *14*, 1071–1103.
(10) Pitts, J. N., Jr.; Sanhueza, E.; Atkinson, R.; Carter, W. P. L.; Winer, A. M.; Harris, G. W.; Plum, C. N. *Int. J. Chem. Kinet.* **1984**, *16*, 919–939.
(11) Akimoto, H.; Hoshino, M.; Inoue, G.; Sakamaki, F.; Washida, N.; Okuda, M. *Environ. Sci. Technol.* **1979**, *13*, 471–475.
(12) Schwartz, S. E.; White, W. H. *Adv. Environ. Sci. Technol.* **1983**, *12*, 1–46.
(13) Schwartz, S. E. In "SO_2, NO and NO_2 Oxidation Mechanisms: Atmospheric Considerations", Calvert, J. G., Ed.; Butterworth: Boston, MA, 1984; pp 173–208.
(14) Fateley, W. G.; Bent, H. A.; Crawford, B., Jr. *J. Chem. Phys.* **1959**, *31*, 204–217.
(15) Bolduan, F.; Jodl, H. J.; Loewenschuss, A. *J. Chem. Phys.* **1984**, *80*, 1739–1743.
(16) Bandow, H.; Akimoto, H.; Akiyama, S.; Tezuka, T. *Chem. Phys. Lett.* **1984**, *111*, 496–500.
(17) Anbar, M.; Taube, H. *J. Am. Chem. Soc.* **1955**, *77*, 2993–2994.
(18) White, E. H.; Feldman, W. R. *J. Am. Chem. Soc.* **1957**, *79*, 5832–5833.
(19) Cooney, R. P.; Tsai, P. *J. Raman Spectrosc.* **1980**, *9*, 33–38.
(20) Wada, Y.; Otsuka, K.; Morikawa, A. *J. Catal.* **1981**, *71*, 136–143.
(21) Jonsson, A.; Persson, K. -A.; Bertilsson, B. M. "Organic Nitrites in the Exhaust Emissions from Alcohol Fueled Vehicles", Proceedings of the Fifth International Alcohol Fuel Technology Symposium, Auckland, New Zealand, 1982; pp 3-179–3-186.
(22) Ito, K.; Yano, T.; Takahashi, F. "Methyl Nitrite Formation in Exhaust Gases Emitted from a Methanol Fueled S.I. Engine", Proceedings of the Fifth International Alcohol Fuel Technology Symposium, Auckland, New Zealand, 1982; pp 3-171–3-178.
(23) Okada, J.; Koda, S.; Akita, K. *Fuel* **1985**, *64*, 553–557.
(24) Whitten, G. Z.; Pullman, J. B. "Methanol Fuel Substitution Can Reduce Urban Ozone Pollution", Proceedings of the Sixth International Alcohol Fuel Technology Symposium, Ottawa, Canada, 1984; pp 2-61–2-65.
(25) Wilson, K. W.; McCormack, M. C. "Methanol As an Ozone Control Strategy in the Los Angeles Area", Proceedings of the Sixth International Alcohol Fuel Technology Symposium, Ottawa, Canada, 1984; pp 2-68–2-74.

Received for review April 29, 1985. Accepted November 5, 1985.

Formation of Methyl Nitrite in the Surface Reaction of Nitrogen Dioxide and Methanol. 2. Photoenhancement

Hajime Akimoto* and Hiroo Takagi

Division of Atmospheric Environment, The National Institute for Environmental Studies, P.O. Tsukuba-gakuen, Ibaraki 305, Japan

■ The surface reaction of NO_2 and methanol described in the preceding paper was studied in the evacuable smog chamber under the irradiation of UV–visible light ($\gtrsim$290 nm). Kinetic analysis of the gaseous reactant and products with the aid of computer modeling revealed that the surface reaction to yield CH_3ONO and HNO_3 is enhanced by the irradiation. The apparent second-order rate constant of the surface reaction increases linearly with light intensity, and the photoenhancement factor ranged from 1.8 to 5.9 for the k_1 value (primary NO_2 photolysis rate) of 0.16–0.38 min^{-1} and for the NO_2 and methanol initial concentrations of 5 and 30 ppm, respectively.

Introduction

In the preceding paper (*1*) (referred to as paper 1), a thermal surface reaction of NO_2 and methanol

$$CH_3OH + 2\,NO_2 \xrightarrow{\text{wall}} CH_3ONO + HNO_3 \qquad (1)$$

has been characterized in dark in the smog chamber. In the present study, the kinetics of the surface reaction of NO_2 and methanol have been studied under UV–visible irradiation. The observed evidence that the apparent rate of reaction 1 is enhanced under the irradiation will be reported in the present paper. This result may be of interest being relevant to the analogous reaction of NO_2 and water,

$$H_2O + 2NO_2 \xrightarrow{\text{wall}} HONO + HNO_3 \qquad (2)$$

which has been discussed (*2, 3*) in relation to the unknown radical source issue for the smog chamber studies raised by Carter et al. (*4, 5*).

Experimental Section

Several runs of CH_3OH (5–20 ppm)–NO_2 (37–60 ppm)–dry air (1 atm) were carried out at 30 °C using the evacuable and bakable smog chamber at the National Institute for Environmental Studies (NIES). Full accounts of the chamber system have been reported previously (*6*), and a brief description has been given in paper 1. In each run, the chamber was first filled with purified dry air, and then methanol was injected using air as the carrier gas. After a reference spectrum had been recorded, NO_2 was next introduced with the carrier gas, and the IR measurement was made approximately every 10–20 min. The formation of CH_3ONO in the dark was monitored for the first ca. 2 h after the injection of NO_2, and then the irradiation by a solar simulator (*6*) was commenced and continued for another ca. 2 h. The reaction mixture in the chamber was mixed with the two fans during runs. The light intensity was measured by primary NO_2 photolysis rate (*6*) and was varied in the range of 0.16–0.38 min^{-1}.

Concentrations of the reactants and the products were measured by means of a long-path (221.5-m) FTIR set in the chamber. Spectral resolution of 1 cm^{-1} was employed, and 128 scans were accumulated to obtain a spectrum. Absorption peaks and absorption coefficients (base 10, torr^{-1} m^{-1}) used for the quantitative measurement are as follows: CH_3OH (2847 cm^{-1}; 0.0711, Q-branch), CH_3ONO (1445 cm^{-1}; 0.0408, peak only), HCHO (1745 cm^{-1}, 0.690, Q-branch), and CH_3ONO_2 (1292 cm^{-1}; 0.476, Q-branch peak to P-branch valley).

Computer Simulation and Reaction Model. Computer simulation for the reaction system studied was carried out by using the reaction model given in Table I.

Table I. Photochemical Reaction Model for CH_3OH-NO_x-Air System

no.	reaction	rate constant,[a] molecule^{-1} cm^3 s^{-1}	ref
	Photochemical Reactions		
1	$NO_2 + h\nu \rightarrow NO + O(^3P)$	1.0	9, 11
2	$O_3 + h\nu \rightarrow O_2 + O(^1D)$	7.6×10^{-3}	10, 11
3	$O_3 + h\nu \rightarrow O_2 + O(^3P)$	5.1×10^{-2}	10, 11
4	$HONO + h\nu \rightarrow OH + NO$	1.8×10^{-1}	12
5	$H_2O_2 + h\nu \rightarrow 2OH$	7.1×10^{-4}	13
6	$NO_3 + h\nu \rightarrow NO + O_2$	3.0	14
7	$NO_3 + h\nu \rightarrow NO_2 + O(^3P)$	$2.4 \times 10^{+1}$	14
8	$HCHO + h\nu \xrightarrow{O_2} 2HO_2 + CO$	2.5×10^{-3}	15, 16
9	$HCHO + h\nu \rightarrow H_2 + CO$	4.2×10^{-3}	15, 16
10	$CH_3ONO + h\nu \rightarrow CH_3O + NO$	1.6×10^{-1}	15
	Inorganic Reactions		
11	$O(^3P) + O_2 \xrightarrow{M} O_3$	1.4×10^{-14}	17
12	$O(^3P) + NO_2 \rightarrow NO + O_2$	9.3×10^{-12}	17
13	$O(^3P) + NO_2 \xrightarrow{M} NO_3$	1.5×10^{-12}	17
14	$O(^3P) + NO \xrightarrow{M} NO_2$	2.1×10^{-12}	17
15	$O(^3P) + O_3 \rightarrow 2O_2$	8.9×10^{-15}	17
16	$O(^1D) \xrightarrow{M} O(^3P)$	$7.0 \times 10^{+8}$	17
17	$O(^1D) + H_2O \rightarrow 2OH$	2.2×10^{-10}	17
18	$O(^1D) + O_3 \rightarrow O_2 + O_2$	1.2×10^{-10}	17
19	$O(^1D) + O_3 \rightarrow O_2 + 2O(^3P)$	1.2×10^{-10}	17
20	$O_3 + NO \rightarrow NO_2 + O_2$	1.9×10^{-14}	17
21	$O_3 + NO_2 \rightarrow NO_3 + O_2$	3.7×10^{-17}	17
22	$O_3 + OH \rightarrow HO_2 + O_2$	7.2×10^{-14}	17
23	$O_3 + HO_2 \rightarrow OH + 2O_2$	2.1×10^{-15}	17
24	$2NO + O_2 \rightarrow 2NO_2$	1.9×10^{-38}	19
25	$NO + NO_3 \rightarrow 2NO_2$	2.0×10^{-11}	17
26	$NO + OH \xrightarrow{M} HONO$	4.8×10^{-12}	17
27	$NO + HO_2 \rightarrow OH + NO_2$	8.2×10^{-12}	17
28	$NO_2 + NO_3 \xrightarrow{M} N_2O_5$	1.2×10^{-12}	20
29	$NO_2 + OH \xrightarrow{M} HNO_3$	1.1×10^{-11}	17
30	$NO_2 + HO_2 \rightarrow HO_2NO_2$	1.4×10^{-12}	17
31	$HO_2NO_2 \rightarrow HO_2 + NO_2$	9.3×10^{-2}	18
32	$HONO + OH \rightarrow NO_2 + H_2O$	6.6×10^{-12}	21
33	$N_2O_5 \rightarrow NO_2 + NO_3$	9.5×10^{-2}	17
34	$2HO_2 \rightarrow H_2O_2 + O_2$	2.5×10^{-12}	17
35	$2HO_2 + H_2O \rightarrow H_2O_2 + O_2 + H_2O$	6.0×10^{-30}	23
36	$H_2O_2 + OH \rightarrow H_2O + HO_2$	1.7×10^{-12}	17
37	$CO + OH \xrightarrow{O_2} HO_2 + CO_2$	2.4×10^{-13}	17
	Surface Reactions		
38	$NO_2 + H_2O \rightarrow HONO$	7.0×10^{-24}	4
39	$N_2O_5 + H_2O \rightarrow 2HNO_3$	2.0×10^{-21}	23
40	$CH_3OH + NO_2 \rightarrow CH_3ONO$	2.2×10^{-20}	1
	Organic Reactions		
41	$CH_3OH + 2NO_2 \rightarrow CH_3ONO + HNO_3$	1.2×10^{-36}	1
42	$CH_3OH + O(^3P) \xrightarrow{O_2} HCHO + HO_2 + OH$	1.5×10^{-14}	24
43	$HCHO + O(^3P) \xrightarrow{O_2} HO_2 + CO + OH$	1.7×10^{-13}	17
44	$CH_3OH + OH \xrightarrow{O_2} HCHO + HO_2 + H_2O$	1.1×10^{-12}	25
45	$CH_3ONO + OH \xrightarrow{O_2} OOCH_2ONO + H_2O$	1.8×10^{-13}	26
46	$HCHO + OH \xrightarrow{O_2} HO_2 + CO + H_2O$	1.0×10^{-11}	17
47	$OOCH_2ONO + NO \rightarrow HCHO + 2NO_2$	7.6×10^{-12}	17
48	$CH_3O + O_2 \rightarrow HCHO + HO_2$	1.4×10^{-15}	17
49	$CH_3O + NO \xrightarrow{M} CH_3ONO$	1.7×10^{-11}	27, 28
50	$CH_3O + NO \xrightarrow{O_2} HCHO + HO_2 + NO$	3.0×10^{-12}	27, 28
51	$CH_3O + NO_2 \xrightarrow{M} CH_3ONO_2$	1.6×10^{-11}	28
52	$CH_3O + NO_2 \rightarrow HCHO + HONO$	1.0×10^{-12}	28

[a] Relative rate for photochemical reactions.

Calculations were performed on a Hitac 180 computer using a CHEMK program for the integration of coupled kinetic equations originally written by Whitten and Hogo (7). The subroutines employ the Gear algorithm (8) for the variable step-size integration. Accounts on the reaction model are given below.

(*i*) *Relative Photolysis Rates*. All the photolysis rates were calculated by using the typical spectral distribution of our solar simulator given before (6). The summation $\sum J_\lambda \sigma_\lambda \phi_\lambda$ was taken at 5-nm intervals at <450 nm and at 10-nm intervals at ≥450 nm, where J_λ, σ_λ, and ϕ_λ are the relative photon flux of the solar simulator, absorption cross section, and photodecomposition quantum yield, respectively. For NO_2 and O_3, absorption coefficients given by Bass et al. (9) and Griggs (*10*) were used, respectively, and ϕ_λ values were obtained from the figures given by Demerjian et al. (*11*). The photolysis rate of HONO and H_2O_2 were calculated by using σ_λ values given by Stockwell and Calvert (*12*) and Lin et al. (*13*), respectively, assuming the quantum yield of unity. The σ_λ and ϕ_λ given by Magnotta and Johnston (*14*) were used to calculate the photolysis rate of NO_3. The absorption coefficients of HCHO and CH_3ONO were taken from the figures given by Calvert and Pitts (*15*). The quantum yields of photolysis of HCHO were taken from the figure of Moortgat et al. (*16*), and that of CH_3ONO was assumed to be unity. All the photolysis

Table II. Initial Conditions and the Best-Fit Values of the Rate Constants of the Surface Reaction of NO_2 and CH_3OH in Dark (k_{40}) and Under Irradiation (k'_{40})

run	CH_3OH, ppm	NO_2, ppm	k_1, min^{-1}	k_{40}, cm^3 $molecule^{-1}$ $s^{-1} \times 10^{-20}$	k'_{40}, cm^3 $molecule^{-1}$ $s^{-1} \times 10^{-20}$	k'_{40}/k_{40}
1	5.1	36.9	0.24	2.0	5.7	2.9
2	4.6	59.7	0.24	2.2	5.8	2.6
3	20.4	50.6	0.24	0.53	3.0	5.7
4	5.0	30.0	0.16	2.1	3.8	1.8
5	5.2	30.1	0.32	1.5	7.7	5.1
6	5.0	30.0	0.38	1.4	8.3	5.9

rates are given in Table I as relative values with respect to that of NO_2.

(*ii*) *Inorganic Reactions.* Most of the rate constants are adopted from the recent evaluation by NASA Panel (*17*) by calculating the values at 303 K using the given temperature dependences. Some of the rate constants are also taken from the evaluation by Baulch et al. (*18*) and from the complication of Hampson (*19*). For the reaction

$$NO_2 + NO_3 \xrightarrow{M} N_2O_5$$

a more recent value of the rate constant by Kircher et al. (*20*) was adopted, although the simulated results are not critical to this value in the present study. The rate constant of the reaction of OH and HONO reported by Cox et al. (*21*) was used in the model. The effect of H_2O vapor on the self-reaction of HO_2 was modeled according to the evaluation by Atkinson and Lloyd (*22*).

(*iii*) *Surface Reactions.* The surface reaction rate of CH_3OH and NO_2 was determined for each run to obtain the best fit of CH_3ONO formation as will be discussed later. For the purpose of keeping generality, the model includes the surface reactions of NO_2 with H_2O and N_2O_5 with H_2O, whose reaction rates were determined in our previous study (*4*), and were selected based on the fitting of the computer simulation (*23*) to the NIES smog chamber experiments of the propylene–NO_x–air system, respectively, although the results of the present study are not affected by these reactions due to the very low level of H_2O. It should be noted that the nonreactive surface decay of CH_3OH and NO_2 was not included in the model, since the inclusion of these rates determined individually always gives much higher predicted decay than the experimental value when CH_3OH and NO_2 coexist.

(*iv*) *Organic Reactions.* The rate constants are taken from the review by the NASA panel (*17*) when available. The rate constants for the reaction of CH_3OH with $O(^3P)$ and OH are taken from the values reported by Owens and Roscoe (*24*) and by Overand and Paraskevopoulous (*25*), respectively. The value reported by Tuazon et al. (*26*) for the reaction of CH_3ONO + OH was adopted. For the reaction of peroxy radicals produced in the reaction of CH_3ONO with OH, only the reaction with NO was included in the model, since the high concentration of NO always coexists when irradiated under the present experimental conditions. The same rate constant as that of the reaction of CH_3O_2 + NO (*18*) was assumed for this reaction. The rate constant by Sanders et al. (*27*) for the overall reaction of CH_3O and NO and the branching ratio, 1:0.17, for the association and disproportionation reported by Wiebe et al. (*28*) were adopted.

Since the above rate constant for the CH_3O + NO reaction may be in the fall-off region, trial calculations using the value of $k(CH_3O + NO)$ increased by 50% were also made. Although the increased value gave better fit of the calculated concentration of CH_3ONO to the experimental one, the results using the original literature value will be reported in this paper, since the conclusion was found not to be affected by this variation of the rate constant. There is no direct measurement for the reaction of $CH_3O + NO_2$, and the rate constant ratio to that of CH_3O + NO was reported to be 1/1.2 and 1/2.03 by Wiebe et al. (*28*) and Batt et al. (*29*). The branching ratio of disproportionation has been reported as 8%, ≤5%, and 30% by Wiebe et al. (*28*), Batt et al. (*29*), and Barker et al. (*30*). In the present study, the rate constant ratio of $k(CH_3O + NO)/k(CH_3O + NO_2) = 1.2$, and the disporportionation/association ratio of 6%, which is close to the values reported by Wiebe et al. (*28*), were selected so as to reproduce the yield of CH_3ONO_2 properly. As for the homogeneous reaction of CH_3OH and NO_2, the rate constant determined in paper 1 was used.

Results and Discussion

Three runs with different initial concentrations of NO_2 and CH_3OH under the same light intensity were conducted first, and then another three runs with the same initial conditions with different light intensity were carried out in the present study. In each run, irradiation was started after following the dark reaction for ca. 2 h. The kinetic data are summarized in Table II. During the dark period, the products observed were solely CH_3ONO and HNO_3 as revealed in paper 1. After irradiation was complete the products observed were HCHO, CH_3ONO_2, CO, and NO in addition to CH_3ONO and HNO_3. In the present study computer fitting was attempted for CH_3OH, CH_3ONO, HCHO, and CH_3ONO_2 using the reaction model shown in Table I. The rate constant of the surface reaction of NO_2 and CH_3OH, k_{40}, was first adjusted to obtain a best fit to the formation curve of CH_3ONO in the dark period for each run, and then the simulation for the irradiated period was conducted by use of the selected value of k_{40}. Since the initial concentration of NO_2 employed in this study is much in excess of that of CH_3OH, the consumption of NO_2 is less than 10% of the initial value and the computed results are not significantly affected by the stoichiometric factor of the surface reaction of CH_3OH and NO_2. One-to-one stoichiometry of the reaction was assumed in the model calculation.

Figure 1 depicts the comparison of the observed and predicted time profiles of CH_3OH, CH_3ONO, HCHO and CH_3ONO_2 for run 6 (see Table II) during the irradiated period. The dashed lines are the prediction when the selected value of $k_{40} = 1.4 \times 10^{-20}$ cm^3 $molecule^{-1}$ s^{-1}, which gives the best-fit profile for CH_3ONO in the dark period, was used. As shown in Figure 1, the simulation clearly overpredicts the photolytic decay rate of CH_3ONO and underpredicts the decay rate of CH_3OH and the yields of HCHO and CH_3ONO_2. These deviations can be explained neither by simply decreasing the photolysis rate of CH_3-ONO (k_{10}) nor by increasing the rate constants of the reaction of CH_3OH with OH or $O(^3P)$ (k_{44} or k_{42}). The decrease of k_{10} to fit the decay rate of CH_3ONO gives even

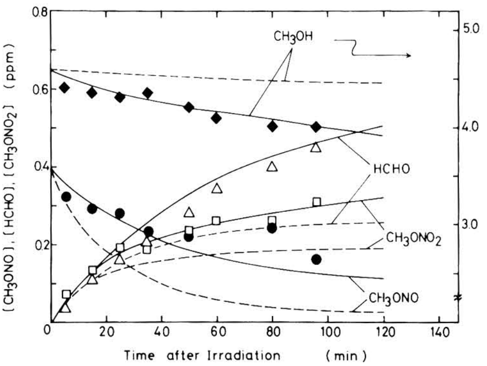

Figure 1. Experimental (points) and predicted (solid and dashed lines) time profiles of the reactant and products for the reaction of NO_2 and CH_3OH under the irradiation in the smog chamber. Initial concentrations of CH_3OH and NO_2 are 5.0 and 30.0 ppm, respectively: k_1 = 0.38 min^{-1}; k_{40} = 1.4 × 10^{-20} (---), 8.3 × 10^{-20} cm^3 molecule^{-1} s^{-1} (—).

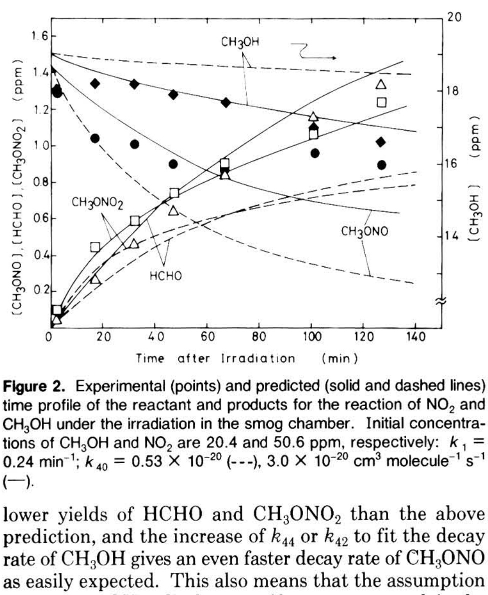

Figure 2. Experimental (points) and predicted (solid and dashed lines) time profile of the reactant and products for the reaction of NO_2 and CH_3OH under the irradiation in the smog chamber. Initial concentrations of CH_3OH and NO_2 are 20.4 and 50.6 ppm, respectively: k_1 = 0.24 min^{-1}; k_{40} = 0.53 × 10^{-20} (---), 3.0 × 10^{-20} cm^3 molecule^{-1} s^{-1} (—).

lower yields of HCHO and CH_3ONO_2 than the above prediction, and the increase of k_{44} or k_{42} to fit the decay rate of CH_3OH gives an even faster decay rate of CH_3ONO as easily expected. This also means that the assumption of unknown OH radical source, if any, cannot explain the experimental results. In order to explain the enhanced consumption of CH_3OH and the enhanced yields of CH_3ONO, HCHO, and CH_3ONO_2 under the irradiation, the possibility of the photoenhancement of the surface reaction of NO_2 and CH_3OH was considered. The best-fit curves for CH_3OH, CH_3ONO, HCHO, and CH_3ONO_2 were obtained by adjusting the value of k_{40} keeping all the other rate constants unvaried, and the results are shown in Figure 1 indicated by the solid lines. By selecting the photoenhanced rate constant (designated as k'_{40}) of 8.3 × 10^{-20} cm^3 molecule^{-1} s^{-1}, good fits to the time profile of CH_3OH, CH_3ONO, HCHO, and CH_3ONO_2 were obtained as depicted in Figure 1.

Figure 2 shows another example for run 3 (see Table II). The consumption rate of CH_3OH is apparently enhanced during the irradiation, which implies that a reaction of CH_3OH with a certain species gives an additional amount of products, CH_3ONO, HCHO, and CH_3ONO_2. Here again it should be stressed that the unknown OH radical source,

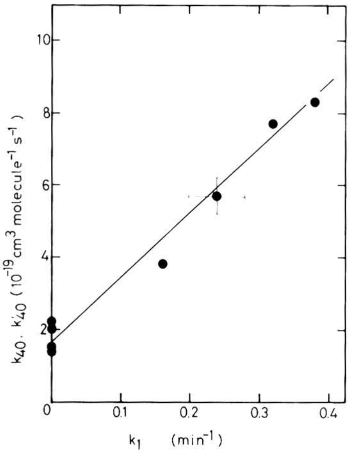

Figure 3. Best-fit values of the rate constant of the surface reaction of NO_2 and CH_3OH (k_{40} in dark and k'_{40} under irradiation) vs. primary photolysis rate of NO_2 (k_1). Bars are the estimated error limits for the photolysis rate measurement and rate constant determination by the computer modeling.

if any, cannot explain the additional yield of CH_3ONO. Assuming the value of k'_{40} = 3.0 × 10^{-20} cm^3 molecule^{-1} s^{-1}, which is ca. 6 times as large as the k_{40} value giving the best fit for the dark period, good agreement between the observed and predicted time profiles of all the products was obtained as demonstrated by solid lines in Figure 2.

Table II summarized the best fit values of k_{40} and k'_{40} for all the runs studied. As shown in Table II, all the experimental results of the present study can be explained by assuming 2–6 times as large rate constant, k'_{40}, of the heterogeneous NO_2–CH_3OH reaction under irradiation, as that of the dark reaction, k_{40}. Figure 3 plots the k_{40} and k'_{40} values for the series of runs with $[CH_3OH]_0 \simeq 3$ ppm and $[NO_2]_0 \simeq 30$ ppm as a function of light intensity as expressed by the primary photolysis rate of NO_2, k_1. As seen in Figure 3, the apparent reaction rate increases linearly with light intensity, which strongly suggests that the surface reaction of NO_2 and methanol is photoenhanced. Under the experimental condition of NO_2 in large excess of CH_3OH, the apparent rate constant of the surface reaction in the smog chamber can be expressed as a function of k_1, i.e.,

$$k'_{40} = (1.76 \pm 0.20) \times 10^{-19} k_1 + (1.67 \pm 0.40) \times 10^{-20} \text{ cm}^3 \text{ molecule}^{-1} \text{ s}^{-1} \quad (3)$$

thus giving the photoenhancement factor of 1.8–5.9 for the k_1 value range of 0.16–0.38 min^{-1}. The two NO_2-excess runs (runs 1 and 2) with different initial concentrations of NO_2 but with the same initial concentration of CH_3OH and the same k_1 value gave the same photoenhancement factor within experimental error, while the run with the higher methanol/NO_2 ratio (run 3) gave the higher photoenhancement by a factor of 2. The initial concentration of CH_3OH for this run is apparently in the saturation range of k_{40} as seen by Figure 5 of paper 1; the difference in the photoenhancement factor may be attributed to the different surface reaction mechanism.

Although a detailed mechanism cannot be assessed in the present study, it is concluded that the photoenhancement of the surface reaction of NO_2 and CH_3OH has been observed to emanate additional CH_3ONO into the gas phase in the smog chamber. This conclusion would suggest that the analogous type of surface reaction between

NO_2 and H_2O might also be enhanced under irradiation in the smog chamber. If this is actually the case, it will solve the puzzle of the unknown radical source issue that the observed rate of heterogeneous HONO formation from NO_2 and H_2O in the dark is only a fraction of the unknown OH radical flux observed in the smog chamber experiments (5). Study of the reaction system of NO_2 and H_2O is under way in our laboratory.

Registry No. NO_2, 10102-44-0; HCHO, 50-00-0; HNO_3, 7697-37-2; CO, 630-08-0; NO, 10102-43-9; CH_3ONO, 598-58-3; CH_3OH, 67-56-1.

Literature Cited

(1) Takagi, H.; Hatakeyama, S.; Akimoto, H.; Koda, S. *Environ. Sci. Technol.* **1986**, *20* (3), preceding paper in this issue.
(2) Sakamaki, F.; Hatakeyama, S.; Akimoto, H. *Int. J. Chem. Kinet.* **1983**, *15*, 1013-1029.
(3) Pitts, J. N., Jr.; Sanhueza, E.; Atkinson, R.; Carter, W. P. L.; Winer, A. M.; Harris, G. W.; Plum, C. N. *Int. J. Chem. Kinet.* **1984**, *16*, 919-939.
(4) Carter, W. P. L.; Atkinson, R.; Winer, A. M.; Pitts, J. N., Jr.; *Int. J. Chem. Kinet.* **1981**, *13*, 735-740.
(5) Carter, W. P. L.; Atkinson, R.; Winer, A. M.; Pitts, J. N., Jr.; *Int. J. Chem. Kinet.* **1982**, *14*, 1071-1103.
(6) Akimoto, H.; Hoshino, M.; Inoue, G.; Sakamaki, F.; Washida, N.; Okuda, M. *Environ. Sci. Technol.* **1979**, *13*, 471-475.
(7) Whitten, G. Z.; Hogo, H. "Modeling of Simulated Photochemical Smog with Kinetic Mechanism", CHEMK: A Computer Modeling Scheme for Chemical Kinetics, EPA-600/3-80-0286, Feb. 1980; Vol. 2.
(8) Gear, C. W. *Commun. ACM* **1971**, *14*, 176-190.
(9) Bass, A. M.; Ledford, A. E., Jr.; Laufer, A. H. *J. Res. Natl. Bur. Stand. Sect. A* **1976**, *80A*, 143-166.
(10) Griggs, M. *J. Chem. Phys.* **1968**, *49*, 857-859.
(11) Demerjian, K. L.; Schene, K. L.; Peterson, J. T. *Adv. Environ. Sci. Technol.* **1980**, *10*, 369-459.
(12) Stockwell, W. R.; Calvert, J. G. *J. Photochem.* **1978**, *8*, 193-203.
(13) Lin, C. L.; Rohatgi, N. K.; DeMore, W. B. *Geophys. Res. Lett.* **1978**, *5*, 113-115.
(14) Magnotta, F.; Johnston, H. S. *Geophys. Res. Lett.* **1980**, *7*, 769-772.
(15) Calvert, J. G.; Pitts, J. N., Jr. "Photochemistry"; Wiley: New York, 1966; p 368, 455.
(16) Moortgat, G. K.; Seiler, W.; Warneck, P. *J. Chem. Phys.* **1983**, *78*, 1185-1190.
(17) NASA Panel for Data Evaluation: DeMore, W. B.; Molina, M. J.; Watson, R. T.; Golden, D. M.; Hampson, R. F.; Kurylo, M. J.; Howard, C. J.; Ravishankara, A. R. "Chemical Kinetics and Photochemical Data for Use in Stratospheric Modeling Evaluation No. 6", JPL Publication 83-62, Pasadena, Sept 1983.
(18) Baulch, D. L.; Cox, R. A.; Crutzen, P. J.; Hampson, R. F., Jr.; Kerr, J. A.; Troe, J.; Watson, R. T. *J. Phys. Chem. Ref. Data* **1982**, *11*, 327-496.
(19) Hampson, R. F., Jr. Chemical Kinetic and Photochemical Data Sheets for Atmospheric Reactions, FAA-EE-80-17. U.S. Department of Transformation, Washington DC, Apr 1980.
(20) Kircher, C. C.; Margitan, J. J.; Sander, S. P. *J. Phys. Chem.* **1984**, *88*, 4370-4375.
(21) Cox, R. A.; Derwent, R. G.; Holt, P. M. *J. Chem. Soc. Faraday Trans. 1* **1976**, *72*, 2031-2043.
(22) Atkinson, R.; Lloyd, A. C. *J. Phys. Chem. Ref. Data* **1984**, *13*, 315-331.
(23) Akimoto, H.; Sakamaki, F., unpublished data.
(24) Owens, C. M.; Roscoe, J. M. *Can. J. Chem.* **1976**, *54*, 984-989.
(25) Overend, R.; Paraskevopoulous, G. *J. Phys. Chem.* **1978**, *82*, 1329-1333.
(26) Tuazon, E. C.; Carter, W. P. L.; Atkinson, R.; Pitts, J. N., Jr. **1983**, *15*, 619-629.
(27) Sanders, N.; Butler, J. E.; Pasternack, L. R.; McDonald, J. R. *Chem. Phys.* **1980**, *48*, 203-208.
(28) Wiebe, H. A.; Villa, A.; Hellman, J. H.; Heicklen, J. *J. Am. Chem. Soc.* **1973**, *95*, 7-13.
(29) Batt, L.; Pathray, G. N. *Int. J. Chem. Kinet.* **1979**, *11*, 1183-1196.
(30) Barker, J. R.; Benson, S. W.; Golden, D. M. *Int. J. Chem. Kinet.* **1977**, *9*, 31-53.

Received for review April 29, 1985. Accepted November 5, 1985.

Measurement of the Water–Octanol Partition Coefficient of 2,3,7,8-Tetrachlorodibenzo-*p*-dioxin[†]

Leland Marple,* Bernard Berridge, and Lewis Throop

Analytical and Environmental Research, Syntex Research, Palo Alto, California 94303

■ The problems inherent in the "shake flask" method for measurement of water–octanol partition coefficients were avoided by the use of a cell in which dioxin was allowed to diffuse from the octanol phase into the water phase. Starting from mutually presaturated water and octanol phases, dioxin equilibration appears to be complete within 1 week. Partition coefficients ranged from 3.48×10^6 to 8.87×10^6. Starting from unsaturated phases, we observed a rapid transport of dioxin from the octanol phase into the water phase, followed by a reversal that corresponds to the formation of hydrated dioxin. The average of all partition coefficient measurements for systems at equilibrium is $(4.24 \pm 2.73) \times 10^6$, giving a log K_{ow} of 6.64.

The octanol–water partition coefficient is recognized as one of the most important physical properties of dioxin. It has been used in the estimation of water solubility (*1*), the adsorption and mobility in soils (*2*), and the bioaccumulation in fish and other animals (*3–5*) and for risk assessment. Previous efforts to establish the partition coefficient of dioxin have consisted of estimates based on structural features (*6, 7*), estimates based on retention time of reversed-phase high-performance liquid chromatography (HPLC) columns (*8*), and one value of unspecified experimental origin (*9*). The reported values of log K_{ow} (Table I) vary from 6.14 to 8.92, or approximately a thousandfold. Clearly, it is important to have reliable

Table I. Summary of Reported Dioxin Octanol–Water Partition Coefficients

log K_0	method	ref
6.84	fragment additivity	Johnson (*6*)
8.93	HPLC-fragment additivity	Webster et al. (*8*)
6.15	(not reported)	Kenaga (*5*)
7.16	fragment additivity	Perkow et al. (*7*)

[†]Analytical and Environmental Research Contribution No. 22.

estimate of the octanol partition coefficient, as so many other physical properties may be calculated from it.

The measurement of the octanol–water partition coefficient presents a number of experimental problems. Dioxin has such a low water solubility (*1*) that the dioxin concentration in the octanol phase must be nearly 10% of its saturation concentration (*10*) in order to have a measurable amount in the equilibrated water phase, even when one samples a large volume of water compared to the volume of octanol present. The resulting disparity of dioxin levels in the two phases also makes it essential that the dioxin analysis be done when phase sepration is complete. Although an octanol–water suspension appears to break rapidly, a slight persistent opalescence shows the presence of very small particles or micelles. The dioxin trapped in suspension may be considerably more than the solubilized dioxin in the water phases. Our initial trials at equilibration by the "shake flask" technique resulted in suspensions that were exceptionally slow to break and an opalescent aqueous phase that persisted for months. Formation of a suspension must therefore be avoided in order to obtain meaningful data. Lastly, it is essential that the sampling of the water phase be done in a way that prevents contamination of the water sample with octanol.

We addressed these experimental problems by making equilibration cells in which diffusion across the octanol–water interface is the main method of dioxin transfer from the octanol into the water phase. A very small magnetic stir bar was used to establish a slight convective current in the aqueous phase and thereby hasten the distribution of dioxin in the aqueous phase. Sampling of the aqueous phase was done by removal of water from a low volume side-arm standpipe that was connected to the bottom of the equilibration cell. The size of the cell was large enough to withdraw a sample without having octanol get into the standpipe.

Experimental Section

The equilibrations were carried out in two cells that differed only slightly. Cell 1 was made from a 400-mL beaker by sawing off the rim, polishing the cut, and then connecting a 11 mm o.d. glass standpipe to the bottom edge. A glass plate was cut to fit on the top. Cell 2 was made from a 500-mL Erlenmeyer flask with a 24/40 standard taper neck by connecting a 11 mm o.d. glass standpipe to the bottom edge. A female 14/40 joint was attached to the top of the standpipe so that the entire system could be tightly stoppered. The cells were first cleaned in boiling, fuming nitric acid, and then rinsed several times with water purified by ion exchange and carbon filters.

Two procedures were used for equilibration, but both monitor the transfer of dioxin from the octanol to the water phase. The first procedure started by adding the dioxin–octanol solution to pure water and taking water samples over a period of 4 weeks. Makeup water was added after each sampling. The second experiment differed from the first in that the phases were mutually presaturated at the beginning of the experiment. All equilibrations were carried out at ambient temperature (22 ± 1 °C), and the solutions were protected at all times from the light by covering the entire apparatus with aluminum foil. A $^1/_2$ in. × $^1/_8$ in. magnetic stirbar was used to produce a very slight convective motion in the water phase. The water in the standpipe was periodically forced back into the main equilibration chamber by pressurizing the standpipe with a small rubber bulb.

Solutions of dioxin (>98% 2,3,7,8-tetrachlorodibenzo-*p*-dioxin; Cambridge Isotope Labs) in octanol were prepared from a standard solution of dioxin in hexane by adding 10 μL of octanol (Fisher-Certified) to 10 mL of hexane stock solution and evaporating to near dryness with a stream of nitrogen. The octanol that remained was diluted to 4 mL with octanol and then transferred to the equilibration cell.

Table II. Variation of Octanol–Water Partition Coefficients with Equilibration Time[a]

equilibration	procedure 1, cell 1		procedure 2, cell 2	
time, days	C_{dioxin}, ng/L	K_{ow}	C_{dioxin}, ng/L	K_{ow}
5	26	0.064×10^6		
6			2.5	3.48×10^6
12	16	0.504×10^6		
15			0.9	8.87×10^6
20	2.5	3.32×10^6		
31	4.1	1.65×10^6	2.2[4]	3.88×10^6

[a] Mutually presaturated phases at start of equilibration. Dioxin concentration in octanol is 8.07×10^6 ng/L.

Analysis of dioxin in the water phase started by removing 1–2 mL of water phase from the side arm and then transferring 100–200 mL of equilibrated water phase to a 500-mL separatory funnel. After 10 ng of 2,3,7,8-[^{14}C]-dioxin (Cambridge Isotope Labs) in toluene/acetone solvent was added as internal standard, dioxin was extracted with 2 × 50 mL of hexane (Mallinckrodt-Nanograde). The combined hexane extracts were dried over anhydrous sodium sulfate and reduced to about 10 mL in a rotary evaporator. The remaining hexane was evaporated under a stream of nitrogen, concentrating the dioxin into a small volume of residual octanol. The sample was transferred to a silanized 1-mL microreaction vessel with redistilled toluene (Mallinckrodt-Nanograde) and again concentrated to about 0.1 mL with a stream of nitrogen. Dioxin was quantitated by capillary column GC using low resolution mass spectrometry (LRMS) detection. Details of the GC/LRMS procedure are given in an earlier publication (*1*).

Analysis of the octanol phase started by diluting a 50-μL aliquot of octanol to 100 mL with hexane and then evaporating 2 mL of the dilution and 10 ng of [^{13}C]dioxin internal standard to near dryness with a stream of nitrogen. The residual octanol was taken up in toluene, the toluene concentrated to about 0.1 mL, and the dioxin quantitated by GC/LRMS.

Results and Discussion

Results for the amount of dioxin in aqueous solution and corresponding values for partition coefficients for samples taken of the course of the equilibrations are collected in Table II. Clearly, the two procedures initially give quite different results. The high concentration of dioxin observed when the equilibration started with mutually unsaturated phases is due to the transport of octanol-solvated dioxin into the water phase, along with the octanol that ultimately saturates the aqueous phase. Eventually, the octanol-solvated dioxin hydrolyzes, owing to the low octanol content of the water phase. This hydrolysis, coupled with a dilution that takes place when makeup water was added after each sampling, accounts for the decreasing dioxin concentration with time of equilibration. When hydrolysis is started with mutually saturated phases, equilibrium appears to be achieved within 6 days. This is attributed to the large interfacial area to water volume ratio as well as the fact that the concentration of dioxin in the octanol phase does not measurably change upon transfer of dioxin to the water phase. An average value of the partition coefficient, (4.24 ± 2.73) × 10^6 g/g, was calculated from the values after 20 days by procedure 1 and all values by procedure 2.

The partition coefficients measured in this study may be compared to values calculated from the solubilities in octanol and water and by use of the distributive law, $K_{ow} = S_{octanol}/S_{water}$. The current literature values for $S_{octanol}$, 48 ppm (*11*), and S_{water}, 200 parts per trillion (ppt) (*11*), yield a ratio of 0.24×10^6. This value is inconsistent with the reported K_{ow} values given in Table I. However, when our earlier experimental values of 12.5 and 19.3 ppt (*1*) are used, the corresponding ratios are 3.84×10^6 and 2.49×10^6, respectively. These ratios are well within the range defined by the mean and experimental error of the partition coefficient measurement and agree quite well with calculated K_{ow} values. This agreement is remarkably close when one considers that the amount of dioxin present in the equilibrated water-phase samples is very near our limit of detection, 0.1 ng.

A common source of error in estimating partition coefficients from the distributive law arises from the mutual solubility of the two "immiscible" phases. Organic solvents present in the water phase will enhance the amount of materials such as dioxin found in the water phase when the mole fraction of solvent is significant compared to the mole fraction water. Fortunately, this does not happen in the water–octanol partition system, for the mutual solubility of the two solvents is small. Butler et al. (*12*) have measured the solubility of octanol in water and report a mean value of 0.0000811 for the mole fraction of octanol. Clearly, the interaction of the water-solvated dioxin molecule with its nearest neighbors will not be affected by the insignificant change in bulk composition from water to water saturated with octanol. Thus, even though the amount of octanol dissolved in the water phase is very much larger than the amount of dioxin present (586 000 000 ppt vs. 1–3 ppt), one may still expect good agreement of the experimental values of partition coefficients with values predicted from the distributive law.

Registry No. 2,3,7,8-Tetrachlorodibenzo-*p*-dioxin, 1746-01-6; octanol, 111-87-5.

Literature Cited

(1) Marple, L.; Brunck, R.; Throop, L. *Environ. Sci. Technol.* **1986**, *20*, 180–182.

(2) Kearney, P.; Isensee, A.; Helling, C.; Woolson, E.; Plimmer, J. In "Chlorodioxins-Origin and Fate"; American Chemical Society: Washington, DC, 1973; Adv. Chem. Ser. No. 120.

(3) Branson, K.; Takahashi, I.; Parker, W. Environmental Sciences Research, The Dow Chemical Co.; Midland, MI, Nov 15, 1978, unpublished report.

(4) Isensee, A.; Jones, G. *Environ. Sci. Technol.* **1975**, *9*, 668.

(5) Kenaga, E. *Environ. Sci. Technol.* **1980**, *14*, 553.

(6) Johnson, H. "Aquatic Fate Process Data for Organic Priority Pollutants"; Mabey, W. R., Ed.; 1982, EPA Final Report, Contract 68-01-3867.

(7) Perkaw, J.; Eschenroeder, A.; Goyer, M.; Stevens, J.; Wechsler, A. "An Exposure and Risk Assessment for 2,3,7,8-Tetrachlorodibenzo-*p*-dioxin"; Office of Water Regulations and Standards, U.S. EPA: Washington, DC, 1980.

(8) Webster, G.; Sarna, L.; Muir, D. "K_{ow} of 1,3,6,8-T CDD and 0 CDD by Reverse Phase HPLC"; University of Manitoba: Winnepeg, Manitoba, Canada R3T 2N2; publication preprint.

(9) Schroy, J. "Dioxin Physical Property Data Sheet", Monsanto Chemical Co., St. Louis, MO, revised Nov 6, 1984.

(10) Esposito, M.; Teirnan, T.; Dryden, E. "Dioxins", US EPA, IERL, Office of Research and Development, U.S. EPA: Cincinnati, OH, 1980; EPA 600/2-80-197.

(11) Crummett, W.; Stehl, R. *Environ. Health Perspect.* **1973**, *5*, 15.

(12) Butler, J.; Thompson, E.; MacLennan, W. *J. Chem. Soc.* **1933**, 674–686.

Received for review June 27, 1985. Accepted December 20, 1985.

Environ. Sci. Technol. 1986, 20, 400–404

Mutagenic Effluents from a Coal-Fired Power Plant: Short-Term Variations and Relation to Power Load and Other Load-Dependent Emissions

Katarina Victorin,*,† Matti J. Jantunen,*,‡ Ahti Itkonen,§ Ulf G. Ahlborg,† Margareta Ståhlberg,† and Sirpa Honkasalo†

National Institute of Environmental Medicine, Stockholm, Sweden, Department of Environmental Hygiene and Toxicology, National Public Health Institute, Kuopio, Finland, and Department of Environmental Hygiene, University of Kuopio, Kuopio, Finland

■ Fly ash was sampled with a standard high-volume sampler at temperatures of 110–125 °C after the electrostatic precipitator of a 300-MW_t pulverized coal-fired power plant to investigate short-term variations in the mutagenicity of fly ash emissions. Fifty-eight 1–2-h samples were collected during 9 days. Organics were extracted with acetone and analyzed by the Ames test with *Salmonella typhimurium* strain TA100 and S9 activation. Other measured parameters were CO_2, SO_2, NO, CO, and particulate emissions, steam load, and sampling temperature. The mutagenicity of the fly ash (rev/mg; rev = revertants) did not correlate with any of the measured parameters. The mutagenic emission (rev/MJ) correlated with steam load ($r = 0.62$) and the fly ash emission ($r = 0.59$) but not with any other measured parameter. The mutagenicity of the fly ash, as well as the mutagenic emission, varied considerably from sample to sample. The mean mutagenic emission was 350 (44–3000) rev/MJ. Six peak emission samples raised the mean by 36%. While the steam load followed a regular diurnal variation, the average hourly emission of NO, CO, and fly ash, mutagenic emission, and the mutagenicity of the fly ash all presented different diurnal patterns. Both the mutagenicity of the fly ash and the mutagenic emission reacted to power load changes differently from the CO emission.

Introduction

Emissions of certain carcinogenic substances from coal combustion were first reported in 1964 (*1–3*). In these early works polynuclear hydrocarbons and other emissions were analyzed from 19 different combustion units fired with coal, oil, and gas. Known and suspected inorganic carcinogens (Cd, As, U, Th, Cr, Be, and Ni) are also emitted (*4, 5*). Many of these are volatile at furnace temperatures and condense after the furnace on fly ash particles so that the smallest particles collect the highest concentrations (*6*). Chrisp and co-workers were the first to show that coal combustion products are mutagenic when tested by the Ames *Salmonella* assay. They found direct-acting mutagens in extracts of fly ash collected at 95–100 °C downstream of an electrostatic precipitator of a large coal-fired power plant (*4, 7*). The compounds reponsible for the observed mutagenicities in coal combustion products have not been identified, although the presence of aromatic hydrocarbons and polar organic compounds, especially nitroorganics, has been demonstrated (*8–11*).

Fly ash samples collected from electrostatic precipitators at large power plants, consisting primarily of large particles, have not been found to be mutagenic in the *Salmonella* assay (*7, 12*). Sampling temperatures around 100 °C appear to be critical for condensation of mutagens, and fly ash loses its mutagenicity when heated to 350 °C (*7*). A large but varying part of the mutagenicity is in the particulate phase at 160 °C (*13, 14*). Fly ash emitted from experimental fluidized bed combustors has shown considerable mutagenicity in the *Salmonella* assay (*15–17*). The mutagenicities of the fly ash collected during start-up conditions and during high CO emissions have been several times higher than under steady-state operation in one of these fluidized bed combustors (*16, 17*).

Within the Swedish Coal-Health-Environment project (*18*) emission measurements have been performed in 14 coal- or oil-fired plants of different sizes and types. Both chemical characterization and biological tests have been performed. The mutagenicities of the effluents from large, well-operated plants were very low (*13, 14, 18–20*). The results are, however, based on (3–7-h) sampling periods during presumably optimal combustion conditions. No information concerning short-term variations in mutagenic effluents during a longer period of time can be derived from these measurements, nor from other results found in the literature. The following investigation on the short-term variations of emission of mutagenic particulates from a large, coal-fired plant was performed as a part of the Swedish Coal-Health-Environment project.

Materials and Methods

Collection and Preparation of Samples. The plant from which the samples were collected is a modern (1977) 300-MW_t pulverized coal-fired boiler in Helsinki, Finland. It produces district heat and electricity and is equipped with a high-efficiency electrostatic precipitator (ESP). The sampling of fly ash emissions for mutagenicity testing was a part of a 2-week sampling and emission analysis program. The other results of this experiment are published elsewhere (*21*).

The fly ash samples were collected isokinetically at 110–125 °C from a duct that connects the ESP to the stack. The sampling probe was a 4.5-cm-i.d. aluminum tube, and glass-fiber filters and a modified GMW 3 B-L-X high-volume sampler were used. A complete system for collecting both particles and vapors at high volume rates was not available. Fifty-eight samples of 0.8–2.6-h duration were taken, and the total sampling time was 99 h. Intervals between the samples were 10–40 min, and in four occasions over 3 h.

For fly ash mutagenicity testing, an extraction procedure was considered necessary because direct testing of the fly ash particles has been shown to be a much less sensitive method (*10*). Acetone was chosen as the solvent for the extraction mainly because it has been used for the same purpose in other measurements of organic and mutagenic effluents within the Swedish Coal-Health-Environment project (*13, 14, 20*). Acetone yields the highest total recovery of mutagenic activity when calculated per milligram

*Address reprint request to Katarina Victorin, National Institute of Environmental Medicine, Box 60208, S-104 01 Stockholm, Sweden, or to Matti Jantunen, Department of Environmental Hygiene and Toxicology, National Public Health Institute, Box 95, SF-70701 Kuopio, Finland.

†National Institute of Environmental Medicine.

‡Department of Environmental Hygiene and Toxicology, National Public Health Institute.

§Department of Environmental Hygiene.

0013-936X/86/0920-0400$01.50/0

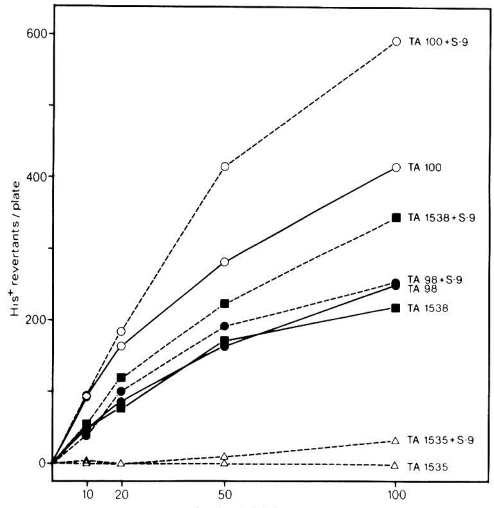

Figure 1. Mutagenicity of a combined fly ash sample tested with different bacterial strains: 20 μL of S9, means of triplicate plates. Spontaneous revertants per plate were as follows: TA98, 14; TA1535, 8; TA1538, 6; TA98 + S9, 15; TA1535 + S9, 6; TA1538 + S9, 10; TA100, 91; TA100 + S9, 95.

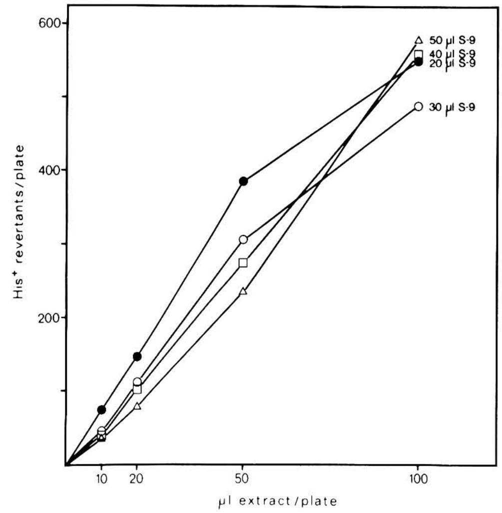

Figure 2. Test for optimum amount of S9. A combined sample was tested with different doses of sample and S9 with TA100: means of triplicate plates. Spontaneous revertants per plate were as follows: 20 μL of S9, 83; 30 μL of S9, 100; 40 μL of S9, 88; 50 μL of S9, 83.

of coal fly ash compared to cyclohexane, dichloromethane, or methanol (*10*). After sampling, the filters were stored in a dark refrigerator until extraction (less than 2 weeks). Each filter was weighed and Soxhlet-extracted in preextracted soxhlet-caps for 18 h with 300 mL of acetone (p.a.). The extract was evaporated to 10–20 mL on an evaporator at 30 °C and then under a nitrogen stream to near dryness, dissolved in 5.0 mL of Me_2SO, and stored at −20 °C in darkness until testing.

Mutagenicity Testing. The *Salmonella*/microsome plate incorporation assay was used for mutagenicity testing. The recommended standardized procedure was followed. The bacterial strains were kindly provided by B. Ames. Their genotypes were checked before and during the testing. A fresh overnight culture (15-h incubation) was used for each day's tests. The S9 was prepared from pooled liver from four Arochlor-treated male Sprauge-Dawley rats. Triplicate plates were used for each dose (*22*).

Extracts of four samples were combined and assayed to select the most sensitive bacterial strain, the appropriate doses, and the optimal amount of S9 for mutagenicity testing (see Figures 1 and 2). *Salmonella* TA100 was found to be the most sensitive strain by the slope of the dose–response curve (Figure 1). The amount of S9 chosen for all subsequent tests was 20 μL/plate. Selected doses were 0, 5 (in some samples), 10, 20, 50, and 100 μL/plate. Eight of the samples were tested with both TA98 and TA100 ± S9. For all but one sample TA100 was also the most sensitive strain for these separate samples (data not shown).

Dose–response curves were plotted for each sample, tested both with and without S9 activation. Toxicity was indicated for most samples from the shape of the dose–response curves by deviations from linearity at the highest dose tested (100 μL/plate) especially in tests without S9. The toxicity was confirmed by treating the diluted bacteria suspension with the same doses and plating on complete media. Because mutagenicity testing with S9 addition reduced sample toxicities and increased the numbers of revertants in most cases, only the results for TA100 + S9 were used in the statistical analyses of the material.

The specific mutagenicities of the samples (rev)/μL of extract) were calculated with a computerized regression analysis program as the slope of the regression line, toxic doses excluded. The test included significance testing of the slope of the regression line against the O-hypothesis. The numbers of revertants per plate were used as separate values in the regression analysis. All samples were mutagenic according to the significance tests ($p < 0.01$) with TA100 + S9.

All samples were retested with TA100 + S9 3–6 months after the first testing (100-μL dose excluded). The difference between the specific mutagenicity of the two tests varied between 0 and 29% of the mean value. The mean difference between repeated tests was 11.5% for all samples. The mutagenicity showed no tendency to decrease during storage. The mean of the two repeated tests was used as the final mutagenicity of the extract. The mean number of spontaneous revertants per plate from all experiments was 106 ± 30 with TA100 + S9. As positive control for TA 100 + S9, benzo[*a*]pyrene (Ega-Chemie) was used. The mean net revertants for 2 μg/plate in single doses was 940. Blank glass-fiber filters were prepared and tested in the same way as the particulate samples. Neither the filter nor the solvent showed mutagenicity.

Results

Because 116 mutagenicity tests were performed, all original data are not presented here. Instead, examples of dose–response curves from three fly ash sample extracts are presented in Figure 3, representing extracts with low, moderate, and high mutagenicity. Results from first and repeated tests are shown.

Sample mutagenicities were computed as the specific mutagenicity of the fly ash mass (rev/mg of fly ash) and as the emission of mutagenic substances per energy input (rev/MJ fuel energy), i.e., revertants per the volume of flue gas produced in combustion of 1 MJ worth of coal (see Table I) with excess air computed for each sample from the CO_2 concentration. The mutagenicities are presented in Figure 4a,b. Mutagenicity of the effluent varied con-

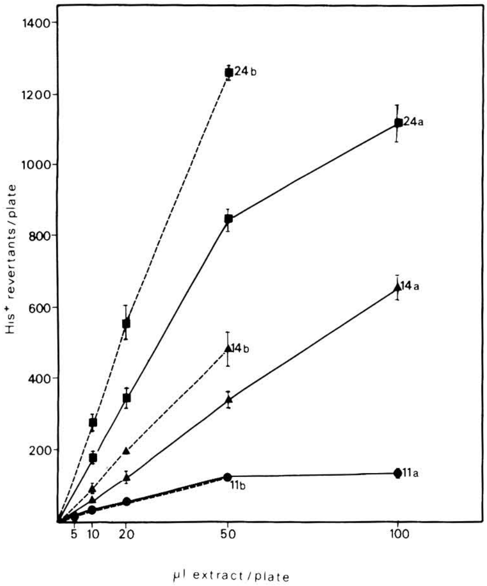

Figure 3. Dose–response curves for three different samples with TA100 + S9. Both first and repeated test results are shown. The standard deviations between triplicate plates are indicated.

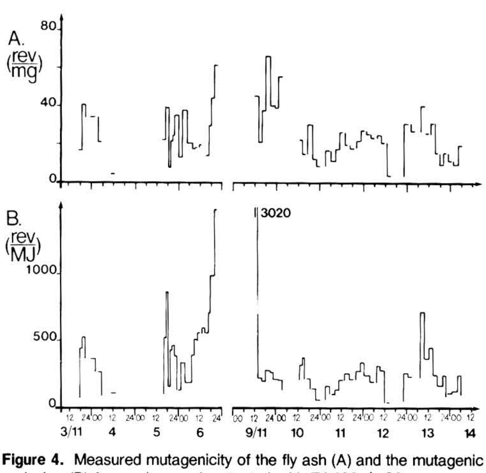

Figure 4. Measured mutagenicity of the fly ash (A) and the mutagenic emission (B) for each sample: tested with TA100 + S9.

Table I. Specifications of the Coals Used during the Sampling in the 300-MW$_t$ Boiler

	coal type		
	1[a]	2[a]	3[b]
moisture content, %	13.3	12.8	7.2
ash in dry matter, %	10.7	12.2	10.3
volatile matter, ash and water free, %	36.7	36.6	39.5
sulfur content in dry matter, %	1.78	1.67	2.01
effective heat value, MJ/kg	26.6	25.0	28.7

[a] English bituminous coal. [b] American bituminous coal.

siderably from sample to sample. The emission statistics for CO, NO, SO_2, particles, mutagenicity of the fly ash, and the mutagenic emission are presented in Table II. The mutagenicity of the fly ash (rev/mg) and the mutagenic

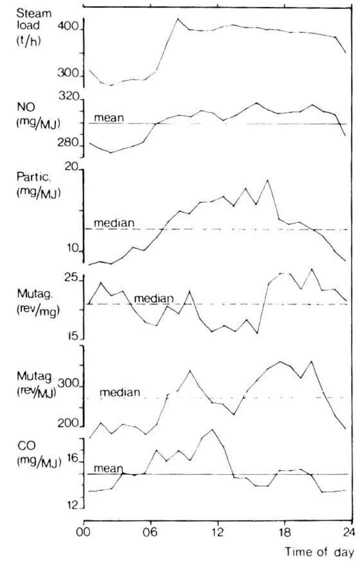

Figure 5. Diurnal patterns of the steam load and the load or combustion efficiency related emissions: hourly mean values during 8 days for the normally distributed NO and CO emissions, median values for the log-normally distributed fly ash and mutagenic emissions.

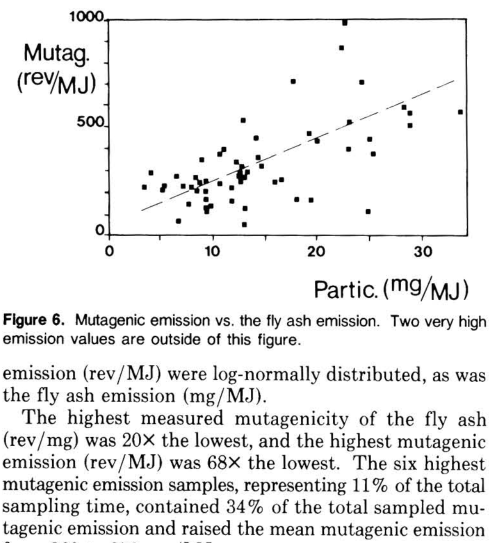

Figure 6. Mutagenic emission vs. the fly ash emission. Two very high emission values are outside of this figure.

emission (rev/MJ) were log-normally distributed, as was the fly ash emission (mg/MJ).

The highest measured mutagenicity of the fly ash (rev/mg) was 20× the lowest, and the highest mutagenic emission (rev/MJ) was 68× the lowest. The six highest mutagenic emission samples, representing 11% of the total sampling time, contained 34% of the total sampled mutagenic emission and raised the mean mutagenic emission from 260 to 350 rev/MJ.

Because the sampling temperature could not be kept constant, but varied from 110 to 125 °C, it was necessary to verify that this variation did not affect the sampling of organic mutagens. The correlation between the mutagenicity of the fly ash (rev/mg) and the sampling temperature is $r = -0.14$; i.e., they are independent. The mean particulate emission after the electrostatic precipitator was low, 17 mg/MJ. The emissions of CO and NO remained under normal operating values (see Table II).

The power plant is run to meet municipal heat and power demand. Steam load was increased at 06–09 h in the morning, and decreased after 22 h in the evening. The average steam load was 30% lower during nighttime than daytime. Because of the regular diurnal load variation,

Table II. Emission Statistics of the Studied 300-MW_t Pulverized Coal-Fired Boiler (99-h Sampling Time)

emission	median	Sg^a	mean	std dev, %	range	n^b	distribution
CO^c			15	25	6–28	396	normal
NO^c			300	11	220–390	396	normal
SO_2^c			1200	5.5	960–1300	396	normal
particles[c]	15	1.7	17		3–50	188	log-normal
particles[c,d]	13	1.6	14		2.6–47	58	log-normal
mutagenicity of the particles[e]	21	1.8	25		3–66	58	log-normal
mutagenic emission[f]	270	2.1	350		44–3000	58	log-normal

[a] Geometric dispersion, dimensionless. [b] Number of samples. [c] In mg/MJ (*21*). [d] Sampled with a high-volume sampler at the same place and during the same period as in the study of Jantunen et al. (*21*), where particles were sampled with a modified 5-stage cascade centripeter. [e] In rev/mg. [f] In rev/MJ.

diurnal patterns of all the measured load-related emissions were plotted. The results are presented in Figure 5 as hourly means for the normally distributed emissions of NO and CO and hourly medians for the log-normally distributed emissions of particulates, mutagens, and the mutagenicity of the particulates. The data are derived from 9 days of sampling.

Discussion

The mutagenic emission is the product of the specific mutagenicity of the fly ash and the fly ash emission. Inefficient combustion gives rise to increased emission of CO and has also been shown to produce increased amounts of organics and mutagenic substances (*13, 14, 17, 18*). During our sampling, the emissions of CO were low and varied 8–25 mg/MJ as 1-h averages. No correlation was found between the specific mutagenicity of the particles (rev/mg) and CO ($r = 0.17$) or the mutagenic emission (rev/MJ) and CO ($r = 0.12$).

Fly ash penetration through an ESP is proportional to $\exp(-1/Q)$, where Q is the flue gas flow rate (*23*). Therefore the fly ash emission depends on the flue gas stream, which again depends on the steam load. This makes all these three variables interdependent. The correlation between the mutagenic emission and the particulate emission was $r = 0.59$ (see Figure 6), and the steam load, $r = 0.62$. The mutagenicity of the fly ash did not correlate with the fly ash emission ($r = 0.24$).

Figure 6, which presents the mutagenic emission vs. the fly ash emission, indicates that the mutagenic emission in this power plant would be proportional to the fly ash emission—with considerable variation—i.e., 25 (±20) rev/1 mg of emitted fly ash.

Figure 5 shows that the manner is more complicated: The mutagenicity of the fly ash (rev/mg) follows a diurnal pattern, which is not related either to the steam load or the fly ash emission. It decreases during the night (01–06 h) when the steam load and the fly ash emission remain low. Is has a peak during the hours of power increase in the morning (07–10 h) and decreases then to the lowest daily levels between 10 and 15 h. It shows the highest levels late in the afternoon and evening. The median mutagenicity of the fly ash during "high emission" (16–22 h) was significantly higher than during "low emission" (10–15 h), when tested in the t test ($p < 0.05$).

Diurnal pattern of the CO emission is different from both the steam load and the mutagenic emission. It increases through the night and morning until noon, then decreases, and remains low until midnight. The mean CO emission during "high emission" (06–12 h) was significantly higher than during "low emission" (20–02 h), when tested in the t test ($p < 0.001$). Both CO and mutagenic emissions result from incomplete combustion. Production of PAH compounds, many of which are mutagens, has been suggested to relate to soot formation in the reducing atmospheres found in early combustion stages (*24*). While both CO and mutagenic emissions of this power plant were low, they did not correlate with each other, and their diurnal patterns, i.e., reactions to power load changes, were different.

This study does not include the effects of mutagens that remain in the gaseous phase at the sampling temperatures (110–125 °C) and were not adsorbed by the filter or the particulate matter on it. However, according to the results of Alfheim et al. (*13, 14*), we conclude that a large part of the mutagenic substances in our sampling was in particulate form and, thus, collected.

Conclusions

The mutagenicity of the fly ash as well as the mutagenic emission varies considerably from sample to sample even in the properly functioning, large and efficient coal-fired power plant studied. However, the peak emissions did not as much as double the long-term average.

In the conditions of this experiment, the mutagenic emission depends mainly on the fly ash emission; i.e., the fly ash collector also controls mutagenic emissions.

While the CO and the mutagenic emissions were low, both the mutagenicity of the fly ash and the mutagenic emission are statistically independent of the CO emission, and they react to power load changes differently from the CO emission.

Registry No. CO_2, 124-38-9; SO_2, 7446-09-5; NO, 10102-43-9; CO, 630-08-0.

Literature Cited

(1) Cuffe, S. T.; Gerstle, R. N *J. APCA* **1964**, *14*(9), 358–363.
(2) Hangerbrauck, R. P.; Lehmden, D. J.; Meeker, J. E. *J. APCA* **1964**, *14*(7), 267–278.
(3) Gerstle, R. N.; Cuffe, S. T. *J. APCA* **1965**, *15*(2), 59–64.
(4) Chrisp, C. E.; Fisher, G. L.; Lammert, J. E. *Science* **1978**, *199*, 73–75.
(5) Natusch, D. F. S *Environ. Health Perspect* **1978**, *22*, 79–90.
(6) Davison, R. L.; Natusch, D. F. S.; Wallace, R. R.; Evans, A. *Environ. Sci. Technol.* **1974**, *8*(13), 1107–1113.
(7) Fisher, G. L.; Chrisp, D. E.; Raabe, O. G. *Science* **1979**, *204*, 879–881.
(8) Griest, W. H.; Caton, J. E.; Rao, T. K.; Harmon, S. H.; Yeatts L. B., Jr.; Henderson, G. M. *Int. J. Environ. Anal. Chem.* **1982**, *12*, 241–252.
(9) Wei, C.; Raabe, O. G.; Rosenblatt, L. S. *Environ. Mutagen.* **1982**, *4*, 249–258.
(10) Mumford, J. L.; Lewtas, J. *J. Toxicol. Environ. Health* **1982**, *10*, 565–586.
(11) Hanson, R. L.; Henderson, T. R.; Hobbs, C. H.; Clark, C. R.; Carpenter, R. L.; Dutcher, J. S. *J. Toxicol. Environ. Health*, **1983**, *11*, 971–980.
(12) Kubitschek, H. E.; Venta, L. *Environ. Mutagen.* **1979**, *1*, 79–82.
(13) Alfheim, I.; Møller, M. The Coal-Health-Environment Project, Technical Report, No. 60, Swedish State Power Board, Stockholm, 1983.

(14) Alfheim, I.; Bergström, J.; Jenssen, D.; Møller, M. *Environ. Health Perspect.* **1983**, *47*, 177–187.
(15) Clark, C. R.; Hobbs, C. H. *Environ. Mutagen* **1980**, *2*, 101–105.
(16) Kubitschek, H. E.; Williams, D. M.; Kirdiner, F. R. *Mutat. Res.* **1980**, *74*, 329–333.
(17) Kubitschek, H. E.; Williams, D. M. *Mutat. Res.* **1980**, *77*, 287–291.
(18) K.H.M. The Coal-Health-Environment Project, Final Report, Swedish State Power Board, Stockholm (In Swedish), Sweden, 1983.
(19) Jenssen, D.; Magnusson, J. The Coal-Health-Environment Project, Technical Report No. 61, Swedish State Power Board, Stockholm (In Swedish with English summary), Sweden, 1983.
(20) Ahlberg, M.; Berghem, L.; Nordberg, G.; Persson, S. A.; Rudling, L.; Steen, B. *Environ. Health Perspect.* **1983**, *47*, 85–102.
(21) Jantunen, M. J.; Itkonen, A.; Lihtamo, H.; Savolainen, T. The Coal-Health-Environment Project, Technical Report No. 53, Swedish State Power Board, Stockholm, 1983.
(22) Ames, B. N.; McCann, J.; Yamasaki, E. *Mutat. Res.* **1975**, *31*, 347–364.
(23) White, H. J. "Industrial Electrostatic Precipitation"; Addison-Wesley: Reading, MA, 1963.
(24) Ström, B. The Coal-Health-Environment Project, Technical Report No. 22, Swedish State Power Board, Stockholm (in Swedish with English Summary), 1982.

Received for review May 14, 1985. Revised manuscript received October 28, 1985. Accepted November 18, 1985. This study was initiated and funded by the Swedish Coal-Health-Environment project and performed by the National Institute of Environmental Health in Sweden and the University of Kuopio in Finland.

Polybrominated Dibenzofurans and Dibenzo-*p*-dioxins: Thermal Reaction Products of Polybrominated Diphenyl Ether Flame Retardants

Hans-Rudolf Buser

Swiss Federal Research Station, CH-8820 Wädenswil, Switzerland

■ Thermolysis of three technical polybrominated diphenyl ether (PBDPE) flame retardants in quartz minivials at 510–630 °C produced a range of potentially hazardous and toxic polybrominated dibenzofurans (PBDFs) and dibenzo-*p*-dioxins (PBDDs) at total yields of up to 10%. HRGC–MS analysis revealed the formation of various mono- to octabrominated species. EI mass spectra of PBDPEs, PBDFs, and PBDDs were found to be similar to those of the chlorinated analogues. The technical PBDPEs, consisting of a rather small number of components, lead to reasonably simple mixtures of reaction products with, often, one or two main PBDF and PBDD isomers. Except 2,3,7,8-tetrabromodibenzofuran, which was not among the main thermolysis products, isomer assignments were not possible due to the lack of authentic reference compounds. PBDPEs are of environmental concern; the formation of PBDFs and PBDDs is of additional concern. These adverse effects should be carefully evaluated against the possible merits of these products as flame retardants.

Introduction

Polychlorinated dibenzo-*p*-dioxins (PCDDs) and dibenzofurans (PCDFs) are groups of hazardous compounds, among which are some extremely toxic isomers (*1*). During recent years, PCDDs and PCDFs have received much scientific and public attention. The most toxic isomers appear to be the 2,3,7,8-substituted compounds, e.g., 2,3,7,8-tetrachlorodibenzo-*p*-dioxin (2,3,7,8-tetra-CDD) and 2,3,7,8-tetrachlorodibenzofuran (2,3,7,8-tetra-CDF). Polybrominated dibenzo-*p*-dioxins and dibenzofurans, PBDDs and PBDFs, seem to have similar or even higher toxicity than the chlorinated analogues; high toxicity or biological activity was shown for the 2,3,7-tribromodibenzo-*p*-dioxin (2,3,7-tri-BDD), the 2,3,7,8-tetra-BDD, and the 2,3,7,8-tetrabromodibenzofuran (2,3,7,8-tetra-BDF) (*2–4*).

PCDDs and PCDFs are trace contaminants of certain industrial chemicals such as chlorophenols, polychlorinated biphenyls (PCBs), and other chloroaromatics. In addition, PCDDs and PCDFs can be formed from these industrial chemicals in substantial yields in thermal reactions. This conversion into PCDDs or PCDFs has been shown for the chlorophenols, PCBs, polychlorinated diphenyl ethers (PCDPEs), and benzenes (PCBzs) (*5–9*). The brominated aromatics can be expected to behave in a similar fashion, and in fact the formation of PBDFs from polybrominated biphenyls (PBBs) was reported (*10, 11*).

Flame retardants are chemicals added to plastic, textiles, carpets, and other materials to reduce flammability and protect these materials in case of fire accidents (*12*). They are added to these materials at levels up to 10–20%. A variety of different flame retardants exist and include polyhalogenated compounds, among which PBBs and polybrominated diphenyl ethers (PBDPEs) play an important role (*13, 14*). These materials are of ecological concern because significant amounts are released eventually into the environment. The formation of toxic compounds from incineration, accidental burning, or in fires of such materials would certainly be of additional concern and constitute a potential danger and health risk for the public.

In the present study, the formation of significant quantities of PBDFs and PBDDs from thermal reactions of technical PBDPE flame retardants is reported. Mass spectral and gas chromatographic data of these brominated aromatics are reported and compared to those of the chlorinated analogues.

Experimental Section

PBDPE Flame Retardants. The technical products investigated were mixtures of PBDPEs with different degrees of bromination from a commercial source. Manufacturer literature listed the following details: Pentabromo, 71% bromine; Octabromo, 79% bromine, predominantly hexa- to nonabrominated; Decabromo, 83% bromine, 97% deca-BDPE.

The products were dissolved in toluene (1 mg/mL). They were analyzed directly by gas chromatography–mass spectrometry (GC–MS) for composition and for the ab-

0013-936X/86/0920-0404$01.50/0

Table I. Composition of PBDPE Flame Retardants

product	PBDPE congeners present[a]							
	tri-	tetra-	penta-	hexa-	hepta-	octa-	nona-	deca-
Pentabromo	+ (1)	+++ (3)	+++ (3)	++ (5)	+ (1)			
Octabromo			+ (1)	++ (3)	+++ (3)	++ (4)	++ (1)	
Decabromo							+ (1)	+++ (1)

[a] Amounts indicated semiquantitatively by number of marks (+); number of isomers observed is in parentheses.

sence of PBDFs, PBDDs, and PBBs. None of the products contained detectable quantities (0.01–0.1%) of the latter compounds.

Reference Compound. A few micrograms of 2,3,7,8-tetra-BDF was available as a qualitative reference compound (courtesy A. S. Kende, University of Rochester, NY).

Micropyrolyses. The PBDPE flame retardants were thermally reacted in separate quartz minivials (volume ca. 0.3 mL) in the presence of air in an electrical oven at 510 and 630 °C. The conditions were as previously described with reaction periods of 60 s of which 3–5 s were within 20 °C of the stated final temperatures (*6, 7*). Quantities of 200 μg (200 μL of solution) were placed into vials. The vials were sealed by flame after evaporation (vacuum) of the toluene. After reaction and cooling to room temperature, the vials were opened, 50 μL of toluene added, and the mixture refluxed on a hot plate for a few seconds. A 2-μL aliquot was directly analyzed by GC–MS. No cleanup of sample extracts was necessary.

GC–MS Analysis. High-resolution (HR) GC–MS analysis was carried out with a Finnigan 4000 GC–MS instrument operating in the electron impact (EI) mode and a 25-m SE 54 glass capillary column (0.31 mm i.d., cross-linked, 0.15-μm film thickness). The HRGC column was temperature programmed as follows: 80 °C, 2 min isothermal (splitless for 60 s), 20 °C/min to 180 °C, 5 °C/min to 280 °C, then isothermal at 280 °C. The column was interfaced to the mass spectrometer via a fused silica line (0.15 mm i.d., temperature 220 °C). Other GC conditions were as follows: injector temperature, 250 °C; helium carrier gas velocity, 35–45 cm/s.

For the analysis of Decabromo (deca-BDPE) and its reaction products an 8-m SE 54 glass capillary column (0.1-μm film thickness) was used because of the otherwise extremely long retention times of these compounds. In this case, injector and interface temperatures were raised to 300 and 260 °C, respectively; the same column temperature program (splitless for 40 s) was used.

The medium-polar SE 54 columns were suitable for separating the various bromo congeners of each group of compounds within reasonable analysis times. These columns were not expected to give best isomer separation, and therefore, the actual number of isomers present in a sample may be larger than observed in the analyses.

Mass spectra (m/z 35–985, 3.2 s/scan) were recorded starting at a column temperature of 180 °C. Operating the EI ion source of our instrument at 50 eV gave higher sensitivity for the compounds analyzed. However, mass spectra recorded under this condition should not differ significantly from those recorded at 70 eV. Quantitations (semiquantitatively) were made from computer-reconstructed chromatograms and comparison of peak areas.

Results and Discussion

Analysis of the Technical PBDPE Flame Retardants. GC–MS analysis of technical PBDPEs using packed columns has been reported (*15*). In the present study, we used HRGC–MS with persilylated, cross-linked SE 54 glass capillary columns for analysis. A 25-m column proved suitable for the analysis of all except the highest brominated congeners. For Decabromo and its reaction products a shorter (8-m) column was used. The results of these analyses are summarized in Table I. EI mass spectra and gas chromatographic data of PBDPE congeners will be reported and discussed below.

Pentabromo was found to consist predominantly of tetra-, penta-, and hexabromo congeners with the very minor amounts of tri- and hepta-BDPEs. Major components were a tetra- and a penta-BDPE present at about 40 and 45%, respectively. Octabromo was found to consist of hexa-, hepta-, octa-, and nona-BDPEs with only a very small quantity of penta-BDPE present. The main component was a heptabromo isomer present at about 50%. Decabromo was found to contain deca-BDPE as the main component with some (2–5%) nona-BDPE present. The average bromination degrees calculable from these analyses were in agreement with information listed by the manufacturer.

The rather small number of isomers observed in these technical PBDPEs is in contrast to the complex isomer composition found in technical PCBs and PBBs. Direct analysis of PBDPE reaction products was thereby possible without the need for cleanup of samples; this was not possible in case of the technical PCBs (*6*).

The smaller number of isomers present in these PBDPEs is likely due to a strong directing effect of the ether group (ortho, para director) in a synthesis starting with bromination of diphenyl ether. In this way 2,4-(2,6-), 2,4,6-, 2,3,4,6-, and 2,3,4,5,6-substitutions should dominate; this however is in contrast to the finding of 2,4,5,2′,4′-penta-BDPE as a main component in a technical pentabrominated product (*14*). From the EI mass spectra (see below) substitution patterns (distribution of the Br substituents among the two carbon rings) of PBDPEs were discernible. With only one exception, all tetra- to octabrominated isomers were 2-2′, 2-3′, 3-3′, 4-3′, and 4-4′ substituted, indicating a preferred bromination of the lower substituted carbon ring during synthesis.

Analysis of Pyrolyzed PBDPE Flame Retardants. From bond strength consideration (97 and 82 kcal/mol for aromatically bound chlorine and bromine, respectively) the brominated congeners are expected to be thermally decomposed to a similar or even greater extent than the chlorinated analogues. Thermolysis at 510 and 630 °C was chosen because temperatures around 600 °C resulted in significant decomposition of PCBs and PCDPEs in similar experiments (6, 8); these temperatures are also easily reached in fires. We observed the formation of significant quantities of PBDFs and PBDDs from PBDPEs as summarized in Table II.

Analysis of Pentabromo thermolyzed at 510 °C indicated a decomposition of around 10%. PBDFs and PBDDs were present at a combined level of around 0.5–1%. Thermolysis of Pentabromo at 630 °C lead to almost complete destruction (97–98%) of the PBDPEs and formation of PBDFs and PBDDs at a combined level of around 10%. The formation of carbon and HBr was also observed. The

Table II. PBDFs and PBDDs from the Thermal Reaction of PBDPE Flame Retardants

product	reaction temp, °C	decompn %	total amt PBDFs/PBDDs, %	PBDFs (F) and PBDDs (D) formed							
				mono-	di-	tri-	tetra-	penta-	hexa-	hepta-	octa-
Pentabromo	510	10	0.5–1	(F) +	+	+	+	+			
				(D) +	++	+	+				
	630	97–98	10	(F) +	+	++	+++	+++	+		
				(D) +	+++	+++	++	+			
Octabromo	630	96	5	(F)			+	++	+++	+	
				(D)		+	++	+++	++	+	
Decabromo	630	90	1–2	(F)			+	+	+	++	
				(D)			+	++	++	+	+

[a] Amounts indicated semiquantitatively by number of marks (+).

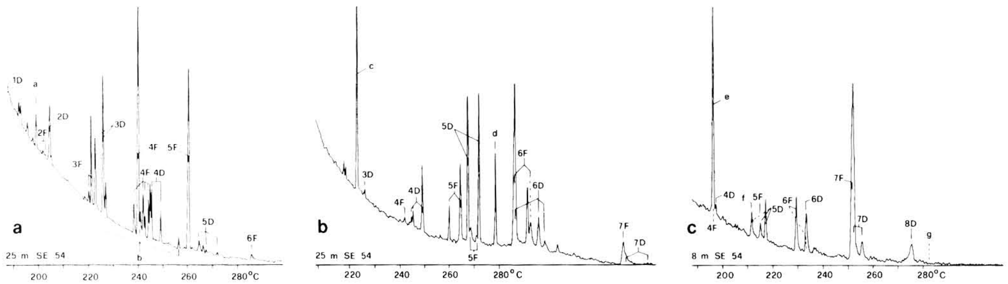

Figure 1. Total ion chromatograms (m/z 100–985) of thermal reaction products of PBDPE flame retardants: (a) from Pentabromo, (b) from Octabromo, and (c) from Decabromo; analysis on 25- and 8-m SE 54 HRGC columns as indicated; peak identifications: PBDFs as 4F (tetra-BDF), etc.; PBDDs as 4D (tetra-BDD), etc.; other peak assignments: a, pentabromobenzene; b, tetra-, penta-, and hexa-BDPEs (from undecomposed Pentabromo); c, hexabromobenzene; d, hepta-BDPE (from undecomposed Octabromo); e, hexabromobenzofuran; f, hexabromonaphthalene; g, elution of deca-BDPE (absent).

major products formed were polybrominated benzenes (PBBzs, predominantly tri- and tetrabrominated); smaller amounts of other brominated compounds (phenols, benzofurans, naphthalenes, etc.) were also present. Among the PBDFs and PBDDs were mono- to hexa-BDFs and mono- to penta-BDDs; the major components were a tetra- and a penta-BDF and two isomeric tri-BDDs (see chromatogram in Figure 1a).

Thermolysis of Octabromo at 630 °C gave a decomposition of around 96% and lead to the formation of PBBzs and about 5% of PBDFs and PBDDs. Major products were two penta-BDDs and a hexa-BDF; additionally, tri- to hepta-BDDs and tetra- to hepta-BDFs were present (see Figure 1b). Again the number of isomers was small. Pyrolysis of Decabromo gave a total of about 1–2% of PBDFs and PBDDs; the decomposition of the PBDPEs was greater than 90%. Major products were PBBzs (tri- to hexabrominated). Among the tricyclic products, a hepta-BDF was the main product; additionally tetra- to hepta-BDFs and tetra- to octa-BDDs were present (see Figure 1c).

In these experiments, the formation of only a few PBDF and PBDD components was observed. These PBDFs and PBDDs contained at least one and two, respectively, Br substituents less than the PBDPEs in the technical products and often the same major isomers were observed from all three flame retardants.

With the exception of 2,3,7,8-tetra-BDF, PBDF and PBDD isomers were not identified due to the lack of reference compounds. Analysis of the thermolysis samples showed that among the tetra-BDFs formed the 2,3,7,8-isomer was not a major component. From PBDPEs with 2,4,6-bromine substitution and the reaction routes identified from the pyrolysis of PCDPEs, a direct formation of 2,3,7,8-substituted PBDFs and PBDDs is not expected,

Scheme I

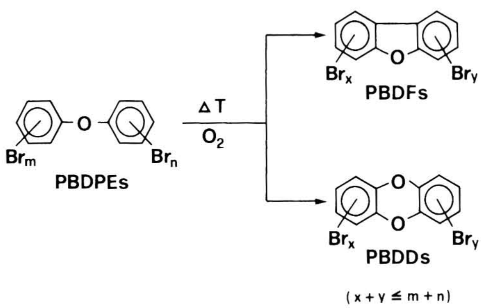

although their formation cannot be completely ruled out, due to the possibility of rearrangement reactions (8).

Debromination reactions leading to lower brominated PBDF and PBDD congeners were observed with all PBDPEs. The source of the hydrogen required was not elucidated. Possible sources are moisture or traces of solvent left in the vials. In general, the higher the bromination degree of the PBDPE, the higher brominated were the reaction products.

Most likely the PBDFs and PBDDs are formed in intramolecular cyclization reactions involving the attack of oxygen on the diphenyl ether system (see Scheme I). Other brominated thermolysis products may be cleavage and oxidation products (PBBzs and phenols, respectively); some (naphthalenes, benzofurans), however, may also have been formed in recombination reactions, after breakdown of PBDPEs to small reactive (possibly C_2–) species.

EI Mass Spectrometric Properties of Polybrominated Aromatics (PBDPEs, PBDFs, PBDDs).

Table III. Molecular Ions (M^+, ^{79}Br Isotopes) of PBDPEs, PBDFs, and PBDDs

compd	bromo congeners									
	mono-	di-	tri-	tetra-	penta-	hexa-	hepta-	octa-	nona-	deca-
PBDPEs	248	326	404	482	560	638	716	794	872	950
PBDFs	246	324	402	480	558	636	714	792		
PBDDs	262	340	418	496	574	652	730	808		

Scheme II

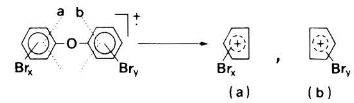

Molecular (M^+) and fragment ions in the EI mass spectra of these polybrominated compounds showed the expected clustering due to the bromine ^{79}Br and ^{81}Br isotopes. M^+ ions of all these compounds were prominent and often base peaks; the m/z values of these ions (^{79}Br values) are listed in Table III. Due to the cluster formation from the Br isotopes, the most prominent ions in these clusters may be at higher m/z values depending on the degree of bromination, e.g., at $M^+ + 2$ for di- and tri-, at $M^+ + 4$ for tetra- and penta-, at $M^+ + 6$ for hexa- and hepta-, at $M^+ + 8$ for octa- and nona-, and at $M^+ + 10$ for decabrominated species.

PBDPEs. EI mass spectra of a tetra- and a penta-BDPE (major products of Pentabromo) as typical representatives of this group of compounds are shown in Figure 2a,b. All PBDPEs had very strong M^+ ions and major, often base peak fragment ions $M^+ - Br_2$ ($M^+ - 158$). The latter ions have the same exact mass and number of bromine atoms as a PBDF. Further fragment ions of PBDPEs were $M^+ - Br$ (very weak), $M^+ - Br_3$ (weak), $M^+ - Br_2 - COBr$ (medium), $M^+ - Br_4$ (medium), etc.; this fragmentation behavior is similar to that of the PCDPEs (*16*). Doubly charged ions were present as M^{2+} (very weak) and $(M - Br_2)^{2+}$. A series of lower mass ions were also present, and among these were fragment ions from cleavage near or at the oxygen of the etheral bridge of the PBDPE structure. Ions due to this cleavage (a and b, Scheme II) are characteristic of the substitution type of a PBDPE (number of Br substituents in each carbon ring). These ions (m/z 143, 221, 299, 377, and 455 for mono- to pentabrominated carbon rings) were sometimes of low intensity but could always be readily identified (see Figure 2a, b).

PBDFs. EI mass spectra of a tetra- and a penta-BDF (major products from the pyrolysis of Pentabromo) are presented in Figure 2c, d. All PBDFs had M^+ ions as base peaks. Fragment ions were $M^+ - Br$ (weak), $M^+ - COBr$ (medium/weak), $M^+ - Br_2$ (weak/medium), $M^+ - COBr - Br$ (weak), $M^+ - Br_3$ (very weak), $M^+ - COBr - Br_2$ (medium) and ions (c) due to the complete removal of all Br substituents and CO ($C_{11}H_{8-x}$, where x is the number of bromines of the PBDF, e.g., m/z 136 for a tetra-BDF). Doubly charged ions were present as M^{2+} and $(M - Br_2)^{2+}$ (weak). Some differences were observed for PBDF isomers in the relative ratios of some fragment ions, e.g., in the ratio $(M^+ - Br_2)/(M^+ - COBr)$. The $M^+ - Br_2$ ions are much more intense than the $M^+ - Cl_2$ ions in case of the PCDFs (*16*); otherwise the EI mass spectral behavior of the PBDFs is similar to that of the PCDFs. The PBDFs can be easily distinguished from interfering PBDPEs ($M^+ - Br_2$ fragment ions with same m/z and number of bromines as M^+ of PBDFs) through a search for the presence of the M^+ ions of the latter compounds.

PBDDs. EI mass spectra of a tetra- and a penta-BDD (products from the pyrolysis of Octabromo) are given in Figure 2e, f. M^+ ions were observed as base peaks for all PBDDs. Fragment ions were $M^+ - Br$ (weak), $M^+ - COBr$ (weak/medium), $M^+ - Br_2$ (medium), $M^+ - COBr - Br$ (weak), $M^+ - 2COBr$ (medium), $M^+ - 2COBr - Br_2$ (medium), $M^+ - Br_4$, etc. Doubly charged ions were present as M^{2+} and $(M - Br_2)^{2+}$. Ions (d) due to the complete loss of all Br substituents and 2CO were present in the low mass range ($C_{10}H_{8-x}$, where x is the number of bromines of the PBDD, e.g., m/z 124 for a tetra-BDD). A systematic study on low mass fragment ions that might be indicative of the substitution type of a PBDD isomer was not possible for lack of a sufficient number of isomers. In the case of PCDDs such ions (m/z 70–150) were used to determine substitution types of congeners (*17*). The $M^+ - Br_2$ ion in the mass spectra of PBDDs was much more intense than the corresponding $M^+ - Cl_2$ ions in case of the PCDDs; doubly charged ions $(M - Cl_2)^{2+}$ were not observed for PCDDs (*16, 17*). Otherwise, similar fragmentation patterns were observed for the two groups of compounds.

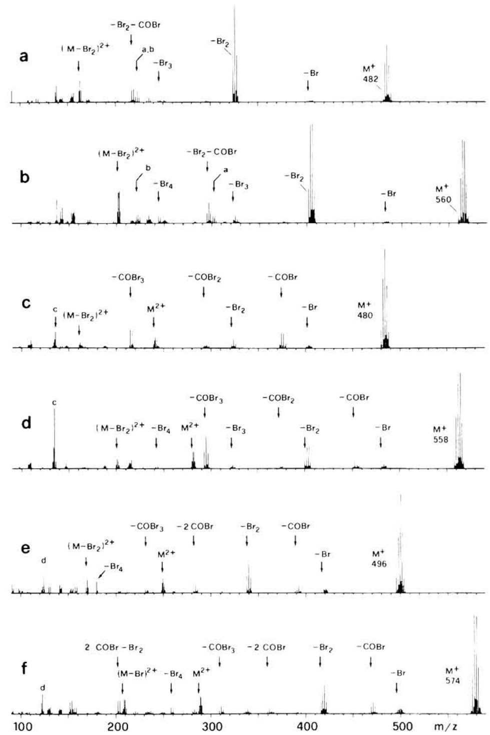

Figure 2. Mass spectra (EI, m/z 90–590) of polybrominated aromatic compounds: (a,b) tetra- and penta-BDPE (main components of Pentabromo); (c,d) tetra- and penta-BDF (major reaction products from Pentabromo); (e,f) tetra- and penta-BDD (reaction products from Octabromo); fragment ions abbreviated, e.g., $M^+ - Br$ as $-Br$; low-mass ions (a–d), see text.

Mass chromatograms of selected ions (M^+ or a cluster ion) were used to search and aid in identification of these

Table IV. Observed Elution Temperatures of PBDPEs, PBDFs, and PBDDs

congener	HRGC column (SE 54), m	elution temp, °C[a,b] PBDPEs	PBDFs	PBDDs
mono-	25	not observed	184–187	187–188
di-	25	not observed	200–203	205
tri-	25	210	219–224	222–227
tetra-	25	225–232	238–249	241–251
penta-	25	240–255	260–268	264–273
hexa-	25	257–272	280+	280+
hepta-	25	280+	280+	280+
octa-	25	280+	not observed	280+
nona-	8	265		
deca-	8	280		

[a] See Experimental Section for column temperature program; temperatures marked by + indicate elution in isothermal phase at 280 °C; for PBDDs and PBDFs see also Figure 1. [b] Comparison of elution temperatures of brominated and chlorinated congeners: 2,3,7,8-tetra-CDF/BDF, 215 and 248 °C (25-m SE 54), 180 and 223 °C (8-m SE 54), octa-CDD/BDD, 269 and 280+ °C (25-m SE 54), 217 and 280 °C (8-m SE 54).

brominated compounds. The ions monitored were the following: PBDPEs, $M^+ + 4$ (tri- to hepta-) and $M^+ + 6$ ions (octa- and higher); PBDFs, M^+ (mono- to tetra-), $M^+ + 2$ (penta-), or $M^+ + 4$ ions (hexa- and higher); PBDDs, $M^+ + 2$ (mono- to tetra-), $M^+ + 4$, and $M^+ + 6$ ions (penta- and higher brominated species). These ions were not always the base peaks of the clusters, but their use resulted in less interference from higher brominated congeners that also respond at these m/z values due to the presence of $M^+ - Br_2$ ions. These congeners however can be easily identified from complete mass spectra and increased retention times. Final identification was always from complete mass spectra.

Gas Chromatographic Data of PBDPEs, PBDFs, and PBDDs. These brominated compounds have greatly increased retention times and higher elution temperatures (+30–40 °C) compared to their chlorinated analogues. In Table IV, we list the elution temperatures of the PBDPEs, PBDFs, and PBDDs observed in the samples investigated. For comparison, the retention times of 2,3,7,8-tetra-BDF and octa-BDD are listed and compared to those of the chlorinated analogues. Due to the extremely long retention times and high elution temperatures of the higher brominated congeners (octa-BDF/BDD and nona- and deca-BDPE) the shorter (8-m) column was used. This column had reasonable elution temperatures and still sufficient resolution, however the column had a low capacity (around 100 ng) for these very-high-boiling compounds.

Conclusions

This investigation revealed the formation of hazardous compounds such as PBDFs and PBDDs, in substantial yields, from thermal reactions of PBDPE flame retardants. PBDFs and PBDDs were formed in similar quantities and ranged from the mono- to hepta- or octabrominated species. Excepting 2,3,7,8-tetra-BDF, which was not among the main PBDFs formed, isomer identifications were not made. The higher brominated PBDPEs generally lead to higher brominated PBDFs and PBDDs. Debromination reactions to lower brominated species were observed for all technical PBDPEs including deca-BDPE. Reaction routes were not determined due to the lack of individual PBDPE, PBDF, and PBDD isomers.

Materials containing these flame retardant chemicals are eventually discarded. A part of the PBDPEs is then directly released into the environment. In addition, significant quantities of these materials are incinerated. The thermal experiments with PBDPEs reported here were carried out under laboratory conditions. Similar model experiments were carried out with PCBs and other chlorinated aromatics (*6–9*). The formation of PCDFs and PCDDs from PCBs and PCBzs in these experiments was later confirmed in additional studies (*18*) and on a larger scale in accidents such as PCB transformer and capacitor fires (*19, 20*). PBDFs and PBDDs may thus form to some degree in fires, from incineration or accidential burning of materials containing PBDPEs. Formation of these hazardous compounds would pose an additional potential health risk to the public and a threat to the environment. These adverse effects should be carefully compared against the possible merits of these products and should encourage reevaluation of PBDPEs as flame retardant additives. Additional investigations under more realistic conditions (burning of materials containing PBDPEs) seem appropriate for final evaluation.

Acknowledgments

I thank H. Lohmann, Bundestag, Bonn, for discussion, M. D. Müller, Wädenswil, for preparation of the HRGC columns, and A. S. Kende for the 2,3,7,8-tetra-BDF reference compound.

Literature Cited

(1) Nicholson, W. J.; Moore, J. A. *Ann. N. Y. Acad. Sci.* **1979**, *320*, 1–730.
(2) Moore, J. A.; McConnell, E. E.; Dalgard, D. W.; Harris, M. W. *Ann. N. Y. Acad. Sci.* **1979**, *320*, 151.
(3) Poland, A.; Greenlee, W. F.; Kende, A. S. *Ann. N. Y. Acad. Sci.* **1979**, *320*, 214.
(4) Poland, A.; Glover, E.; Kende, A. S. *J. Biol. Chem.* **1976**, *251*, 4936.
(5) Rappe, C.; Marklund, S.; Buser, H. R.; Bosshardt, H. P. *Chemosphere* **1978**, *7*, 269.
(6) Buser, H. R.; Bosshardt, H. P.; Rappe, C. *Chemosphere* **1978**, *7*, 109.
(7) Buser, H. R.; Rappe, C. *Chemosphere* **1979**, *8*, 157.
(8) Lindahl, R.; Rappe, C.; Buser, H. R. *Chemosphere* **1980**, *9*, 351.
(9) Buser, H. R. *Chemosphere* **1979**, *8*, 415.
(10) Buser, H. R. Ph.D. Thesis, University of Umeå, Umeå, Sweden, 1978.
(11) O'Keefe, P. *EHP, Environ. Health Perspect.* **1978**, *23*, 347.
(12) Blum, A.; Ames, B. N. *Science* **1977**, *195*, 17.
(13) Norström, A.; Andersson, K.; Rappe, C. *Chemosphere* **1976**, *5*, 255.
(14) Sundström, G.; Hutzinger, O. *Chemosphere* **1976**, *5*, 187.
(15) De Kok, J. J.; De Kok, A.; Brinkman, U. A. Th. *J. Chromatogr.* **1979**, *171*, 269.
(16) Buser, H. R. *J. Chromatogr.* **1975**, *107*, 295.
(17) Buser, H. R. *Chemosphere* **1978**, *7*, 199.
(18) Erickson, M. D.; Cole, C. J.; Flora, J. D., Jr.; Gorman, P. G.; Haile, C. L.; Hinshaw, G. D.; Hopkins, F. C.; Swanson, S. E. EPA Report 560/5-84-009, U.S. Environmental Protection Agency: Washington, DC.
(19) Schecter, A. *Chemosphere* **1983**, *12*, 669.
(20) Rappe, C.; Marklund, S.; Bergqvist, P. A.; Hansson, M. *Chemica Scripta* **1982**, *20*, 56.

Received for review July 12, 1985. Accepted October 8, 1985.

Environ. Sci. Technol. 1986, 20, 409–413

NOTES

Morphological and Chemical Characterization of Iron-Rich Fly Ash Fractions

Glenn A. Norton,* Richard Markuszewski, and Howard R. Shanks

Ames Laboratory, Iowa State University, Ames, Iowa 50011

■ Fly ash samples collected from the electrostatic precipitator of a coal-fired power plant were separated into relatively magnetic and nonmagnetic fractions. The magnetic portions of these samples were examined by scanning electron microscopy, optical microscopy, and X-ray diffraction. The fly ash particles in the magnetic concentrates were predominantly spherical and were generally solid in cross section, although vesicular particles were common in the larger sizes (e.g., >50 μm). The larger particles also exhibited the most diversity with respect to internal morphology. A variety of dendritic growths were among the features observed. X-ray diffraction analyses revealed that the magnetic fly ash fraction was composed primarily of magnetite and lesser amounts of hematite. Results of this study suggest a potential for increasing ash density and purity by selecting a particle size range that will optimize these parameters. This in turn could make it more suitable for use as a heavy medium in physical coal beneficiation.

Introduction

As increasingly greater quantities of coal are consumed for the production of electrical energy, concern over the resulting fly ash continues to mount. Annual fly ash production from coal-fired power plants is presently on the order of 50 million tons (*1*). About 90% of this material is buried or is disposed of in settling ponds (*2*). In either case, the material poses potential environmental problems from leaching (*3–7*).

Fly ash from coal combustion contains typically about 20 wt % magnetic iron oxides (*2*). The characterization of these magnetic phases is important from both an environmental and a technological point of view. Environmentally, the magnetic phases are of concern since they are probably less inert in natural waters than the silicate phases (*6*) and could thus act as agents for the slow release of toxic elements into the environment (*8*). This may be particularly significant for first-row transition metals, which have been reported to be concentrated in the magnetic phases (*6, 8, 9*). From a technological standpoint, magnetic fly ash fractions can be used to substitute for commercial magnetite in heavy-media coal preparation facilities (*2, 3, 10*). Thus, a more thorough characterization of this material could provide an insight for improving their quality and enhancing their suitability for technological applications.

Morphology can affect physical and chemical properties of the ash, which in turn relate to environmental and technological aspects of fly ash disposal and utilization. Results of morphological examinations on coal fly ash have been published frequently and have included observations of pleurospheres, cenospheres, surface crystals, solid spheres, and general particle morphology (*11–15*). However, relatively little attention has been given specifically to the magnetic fractions.

Crystalline phases in the ash also affect the chemical and physical properties (*8*). Mullite and quartz phases (*6, 7, 9, 16*) in nonmagnetic ash fractions and internal crystalline structures in magnetic concentrates (*2, 3, 17*) have been observed previously. But again, studies on internal crystallinity and general morphology of the magnetic concentrates are sparse.

In this study, the interiors of magnetic fly ash particles were examined more extensively to acquire morphological information pertinent to improving ash quality for technological applications and to gain insight into potential environmental hazards associated with ash disposal. In this regard, information on various parameters such as homogeneity, crystallinity, and porosity in the magnetic phases was sought. Information on the chemical makeup of these magnetic phases was also obtained to supplement these observations.

Experimental Section

Fly ash samples were collected from the cold-side electrostatic precipitator (ESP) of a 35-MW tangentially fired steam-generating facility at the City of Ames Municipal Power Plant. The pulverized coal unit has been modified to burn refuse-derived fuel (RDF) as a fuel supplement, burning a nominal maximum of 20% RDF on the basis of the heating value of the individual fuel components. Samples were collected while the unit was operating at 80% of the design capacity and while burning 20% RDF with a 55/45 mixture of Iowa/Colorado coal.

By use of a small hand magnet, the ash samples were separated into nonmagnetic and relatively magnetic fractions, the latter portion comprising about 15% of each sample. Some of the magnetic fraction was ground to −200 mesh and was analyzed by X-ray diffraction (XRD) with an automated Picker theta–theta X-ray diffractometer utilizing Mo Kα radiation. Data were collected while scanning from 2.5 to 30° (2θ) in increments of 0.05° (2θ) with a counting time of 1 s per step. Because of the short counting times and relatively narrow 2θ scanning range, data collection was much quicker with Mo rather than with the more common Cu radiation. The XRD patterns obtained were computer-generated plots of 2θ values vs. relative peak intensity. In addition, a software package provided a listing of peak positions and distances between atomic planes in the crystal lattices ("*d*" values) by using the Bragg equation (*18*) to relate the experimental peak positions to *d* values. Compounds were identified by comparing these values to those in standard JCPDS files (*19*) and by comparing the diffraction pattern to those obtained previously at this laboratory (*20*) on the individual mineralogical components.

Portions of the magnetic fraction were also mounted in copper-bearing diallyl phthalate, a conductive potting compound, and subsequently ground and polished to reveal cross-sectional features. In some instances, individual

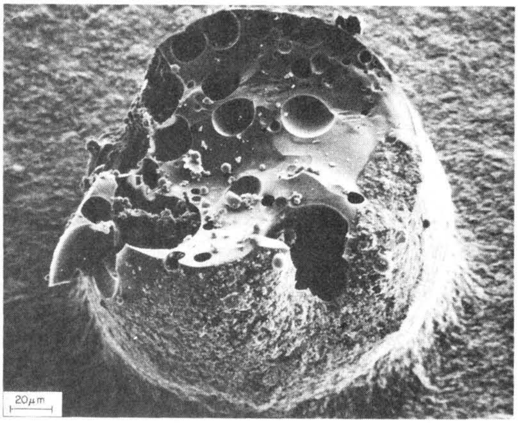

Figure 1. Iron-rich particle that was removed from the magnetic fraction and then fractured, showing a vesicular interior and concoidal fracture in a glassy matrix.

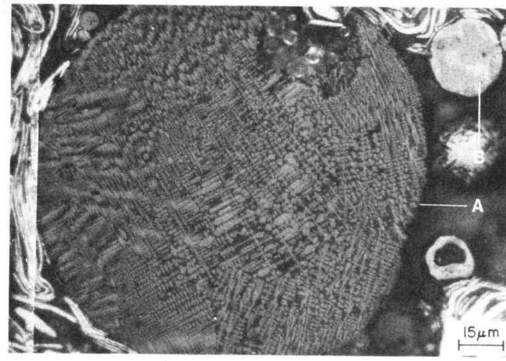

Figure 2. Cross-sectional view showing fine dendritic growth in a large particle (A) from the magnetic fraction. A smaller, more typical particle (B) exhibiting relatively simple internal morphology can also be seen.

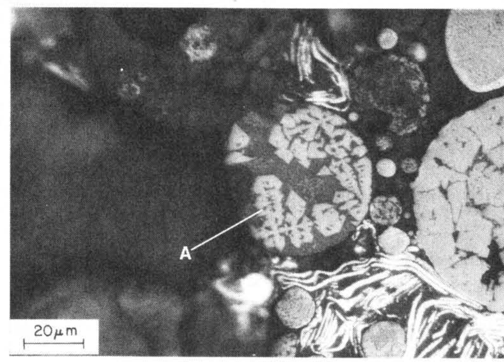

Figure 3. Coarse dendritic growth (A) typical of many of the larger particles observed in the magnetic fraction.

particles were removed from the magnetic fraction and mounted on a carbon stub with carbon paint. Morphological studies on these samples were conducted with optical microscopes using polarized light and with an International Scientific Instruments Alpha-9 scanning electron microscope (SEM). Because the examined particles were rich in iron, they were sufficiently conductive for the SEM studies and did not require any additional preparation. The SEM was sometimes operated to produce images from backscattered primary electrons to show differences in mass between various chemical phases. Chemical information on one of the samples was obtained by energy-dispersive X-ray analysis (EDX) with a Cambridge S-4 SEM in conjunction with an ORTEC 6250 multichannel analyzer.

Results and Discussion

Results of our work have shown that magnetic and nonmagnetic portions of fly ash from the combustion of coal/RDF mixtures consist predominantly of spherical particles. This agrees with the observations reported for whole (not magnetically separated) samples (*11*, *15*) and magnetic concentrates (*2*, *3*, *8*, *17*) of fly ashes obtained from the combustion of coal alone. Although other researchers have reported that combustion of coal/RDF mixtures produced fly ash particles that were mostly nonspherical (*21*), numerous parameters such as firing method, boiler design, the physical nature of the RDF, and the coal-to-RDF ratios were substantially different between studies. In our study, firing coal/RDF mixtures did not appear to substantially alter combustion conditions or firing parameters, only moderate percentages of RDF were fired, and concentrations of matrix elements were not significantly affected (*20*). Thus, the morphological and chemical composition of this fly ash is believed to be equivalent to coal fly ash for the purposes of this study.

The largest particles such as those shown in Figures 1–4 tended to exhibit the most diversity with respect to internal morphology and contained all of the pleurospheres observed in this study. Vesicular particles such as the one shown in Figure 1 were quite common in the larger sizes. The smaller particles (e.g., <50 μm) tended to be more solid and exhibited less dendritic growth than the larger ones.

The iron found in the magnetic fractions can be present as magnetic spinels or it can be dissolved in aluminosilicate material (*16*). Figure 1 shows a particle in which the iron is presumably in solid solution in a glassy aluminosilicate matrix. This particle was removed from the magnetic ash and was subsequently fractured, revealing a vesicular interior and the concoidal fracture indicative of a glassy matrix. Although no chemical determination for iron was made on this particle, it was presumed to be iron rich because it was black and highly magnetic. In many of the magnetic particles observed, much of the iron was in the form of dendritic iron oxide growths. Figures 2 and 3 show examples of fine and coarse dendritic growth, respectively. Similar growths in magnetic fly ash fractions have been reported in other studies (*3*). In Figure 2, a smaller particle with relatively simple internal features can also be seen.

Figure 4, representing a particle observed with an optical microscope using polarized light, shows coarse and fine dendritic growth in a predominantly glassy particle. One of the coarse dendrites and the adjacent matrix material are shown at higher magnification in Figure 5, and results of chemical analyses by SEM–EDX on these two regions are shown in Figure 6. The dendrite was composed mostly of iron, with small amounts of calcium and manganese also being detected. The matrix material was composed of calcium, iron, silicon, aluminum, potassium, and sodium.

Figures 7 and 8 show a particle from the magnetic fraction that was observed with an optical microscope using polarized light and in an SEM using backscattered primary electrons, respectively. Backscattered electrons were used to emphasize differences in mass between different phases

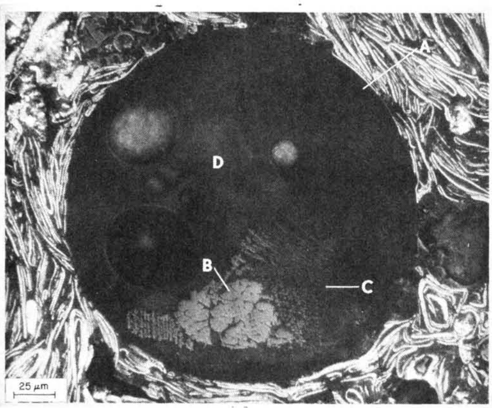

Figure 4. Iron-rich particle (A) seen in cross section with polarized light. Note the coarse (B) and fine (C) dendritic growth and the inhomogeneity of the glassy matrix (D).

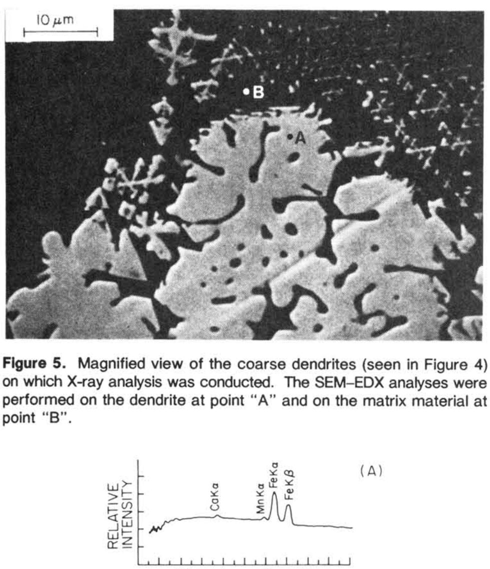

Figure 5. Magnified view of the coarse dendrites (seen in Figure 4) on which X-ray analysis was conducted. The SEM-EDX analyses were performed on the dendrite at point "A" and on the matrix material at point "B".

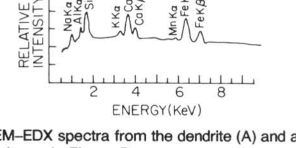

Figure 6. SEM-EDX spectra from the dendrite (A) and adjacent matrix material (B) shown in Figure 5.

in the particle. Figure 8 does not show as much detail in the glassy matrix, but it dramatically shows differences in mass between the iron-rich crystalline material and the glassy matrix which is relatively rich in lighter elements such as aluminum and silicon. From these photographs, it appears that an iron oxide particle crystallized and was

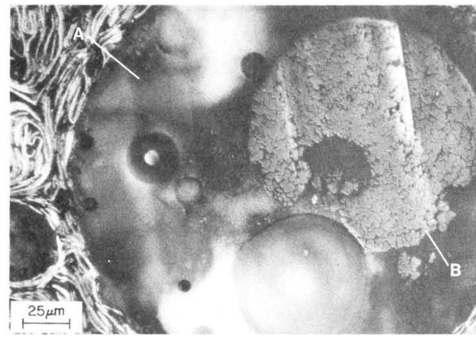

Figure 7. Glassy particle (A) containing a crystalline iron-rich particle (B). This photograph was taken with polarized light in an optical microscope.

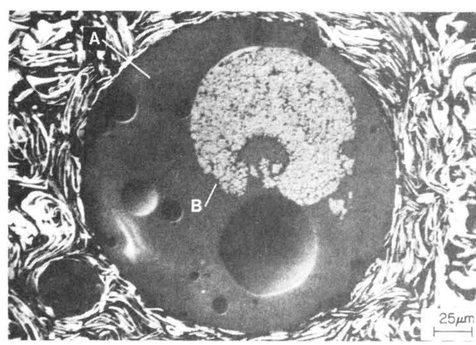

Figure 8. Particle in Figure 7 as seen with an SEM in the backscattering mode to show differences in mass. The glassy particle (A) appears much darker than the iron-rich crystalline particle (B), indicating that it is composed of relatively light elements.

later engulfed by molten silicates. The inhomogeneity of the glassy matrix is readily discernible in Figures 4 and 7. On the basis of chemical and morphological observations, the larger particles observed in this study appeared to contain a significant amount of nonferrous material in the magnetic fraction, although the chemical composition of various size fractions from the magnetic concentrates require a more quantitative evaluation.

Acicular surface microcrystals appearing as growths from the particle surfaces were also observed and were most prevalent in the magnetic portion of most of the samples examined. In previous studies, electron microprobe analyses have shown similar acicular surface crystals to consist of calcium and sulfur, suggesting that those crystals may be gypsum or anhydrite (*11*, *15*).

The XRD pattern and the experimental *d* values obtained for the magnetic concentrates in this study are shown in Figure 9. These results indicate that the crystalline portion of the magnetic ash fraction was composed primarily of magnetite, with lesser amounts of hematite and possibly a small amount of quartz. The presence of quartz is inconclusive since the identification is based on only a single peak for this compound ($d = 3.34$). Hematite tends to concentrate in the magnetic fraction because of its close association with magnetite (*22*).

By contrast, in a study by other researchers (*8*), the magnetic concentrate of ESP fly ash was found to contain

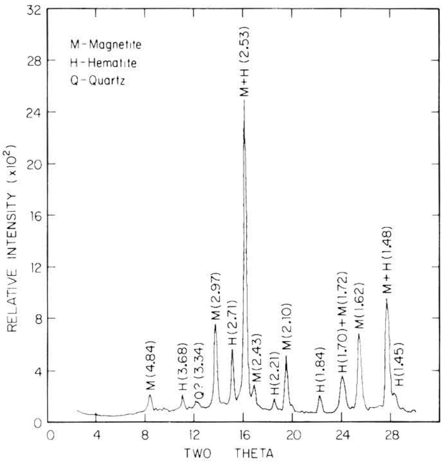

Figure 9. X-ray diffraction pattern showing peaks and experimental *d* values for the magnetic fraction of a fly ash sample.

mostly magnetite and lesser amounts of maghemite (γ-Fe_2O_3), a polymorph of hematite; little or no hematite was detected. In another study, it was reported that the magnetic component of fly ash was "ferrite" rather than magnetite because significant amounts of aluminum and iron were extracted from the ash with hydrochloric acid and because lattice constants from their XRD data were too small for magnetite (*7*).

Other researchers have sought to improve the magnetic fly ash to make it more suitable for use as a heavy medium in coal preparation. In one study, levels of aluminum and silicon were reduced substantially by various acid and alkali extractions (*2*). In other work, grinding was used to break the larger fly ash particles, resulting in increased density of the magnetic fraction, and washing was used to remove some of the smallest particles from the ash (*3*).

Results of our own observations suggest that the quality of magnetic fly ash fractions destined for use as heavy media might be improved by determining and utilizing a particle size range which will optimize parameters such as density and chemical composition. Removing the larger (e.g., >50 μm) sizes might increase the density of the ash by eliminating the pleurospheres and the majority of the vesicular particles. In addition, ash density and purity could possibly be increased if the aluminosilicate material is most concentrated in these larger sizes.

From an environmental perspective, the association of iron with either crystalline or glass phases in magnetic fly ash fractions has important implications. Trace elements that tend to concentrate in the magnetic fraction could occur as isomorphic substitutions in spinel crystal lattices or could be associated with iron which is dissolved in a glassy matrix. Because the rates of particle decomposition in natural waters and in lung fluids are different between the glassy and crystalline phases (*6, 9*), the rate of release of trace elements in magnetic fly ash fractions in various leaching environments will be partially a function of the distribution of trace elements and their association in the magnetic concentrates.

Conclusions

The internal morphology of magnetic fly ash fractions is both complex and diverse. Thus, a deeper understanding of the chemistry and morphology of magnetic fly ash fractions could shed light on ways to improve the ash quality for technological applications. Although this study reveals the complex and diverse nature of some iron-rich fly ash particles, a more in-depth study is required before definitive conclusions can be drawn on ways to make such improvements. However, indications are that removing the larger (>50 μm) particle sizes would remove the majority of the pleurospheres and vesicular particles from the magnetic fly ash fraction, which may increase the density of this fraction and possibly improve its performance as heavy media in coal beneficiation. Combined chemical and physical treatments may be particularly effective at improving the quality of the magnetic concentrates. If particle chemistry is significantly different between various size fractions, it may be possible to select specific size ranges that will optimize the chemical composition of the magnetic fly ash fraction. The leaching potential of trace elements concentrated in the magnetic fly ash fraction cannot be adequately assessed without additional information on their distribution between glassy and crystalline phases.

Acknowledgments

We thank Harlan Baker for mounting and polishing the samples and Ed Gibson for performing the chemical analyses by SEM-EDX.

Registry No. Magnetite, 1309-38-2; hematite, 1317-60-8; quartz, 14808-60-7.

Literature Cited

(1) Fisher, G. L.; Chrisp, C. E.; Raabe, O. G. *Science (Washington, D.C.)* **1979**, *204*, 879.
(2) Murtha, M. J.; Burnet, G. *Proc. Iowa Acad. Sci.* **1978**, *85*, 10.
(3) Roy, N. K.; Murtha, M. J.; Burnet, G. In "Industrial Applications of Magnetic Separation"; Liu, Y. A., Ed.; Institute of Electrical and Electronic Engineers: New York, 1979; pp 32–38.
(4) Edwards, L. O.; Muela, C. A.; Sawyer, R. E.; Thompson, C. M.; Williams, D. H.; Delleney, R. D. "Trace Metals and Stationary Conventional Combustion Processess". 1980, EPA-600/7-80-155a; Vol. 1, Section 5, pp 22–52.
(5) Libicki, J. "Effect of the Disposal of Coal Waste and Ashes in Open Pits". 1978, EPA-600/7-78-067.
(6) Hulett, L. D.; Weinberger, A. J.; Ferguson, N. M.; Northcutt, K. J.; Lyon, W. S. "Trace Element and Phase Relations in Fly Ash". prepared for Electric Power Research Institute, 1981, Final Project Report, EPRI EA-1822, pp 55–59.
(7) Hulett, L. D., Jr.; Weinberger, A. J.; Northcutt, K. J.; Ferguson, M. *Science (Washington, D.C.)* **1980**, *210*, 1356.
(8) Hansen, L. D.; Silberman, D.; Fisher, G. L. *Environ. Sci. Technol.* **1981**, *15*, 1057.
(9) Hulett, L. D.; Lauf, R. "Mineralogical Properties of Coal Ash". Proceedings of the Resources from Coal, Coal Wastes, and Ash Workshop, Reston, VA, June 1982.
(10) Birlingmair, D.; Murtha, M.; Killmeyer, R. "Characterization and Performance Evaluation of Fly Ash Derived Heavy-Media Material", Ames Laboratory, March 1983, IS-4839 (available from NTIS).
(11) Fisher, G. L.; Prentice, B. A.; Silberman, D.; Ondov, J. M.; Biermann, A. H.; Ragaini, R. C.; McFarland, A. R. *Environ. Sci. Technol.* **1978**, *12*, 447.
(12) Carpenter, R. L.; Clark, R. D.; Su, Y.-F. *J. Air. Pollut. Control Assoc.* **1980**, *30*, 679.
(13) Campbell, J. A.; Laul, J. C.; Nielson, K. K.; Smith, R. D. *Anal. Chem.* **1978**, *50*, 1032.
(14) Smith, R. D.; Campbell, J. A.; Nielson, K. K. *Atmos. Environ.* **1979**, *13*, 607.
(15) Fisher, G. L.; Chang, D. P. Y.; Brummer, M. *Science (Washington, D.C.)* **1976**, *192*, 553.
(16) Hulett, L. D.; Weinberger, A. J. *Environ. Sci. Technol.* **1980**, *14*, 965.

(17) Dobbins, M. S.; Burnet, G. *Resour. Conserv.* **1982**, *9*, 231.
(18) Cullity, B. D. "Elements of X-Ray Diffraction"; Addison-Wesley: Reading, MA, 1956; pp 78–85.
(19) "1982 Powder Diffraction File, Inorganic Phases". JCPDS International Centre for Diffraction Data, Swarthmore, PA, 1982.
(20) Norton, G. A., unpublished data.
(21) Taylor, D. R.; Tompkins, M. A.; Kirton, S. E.; Mauney, T.; Natusch, D. F. S.; Hopke, P. K. *Environ. Sci. Technol.* **1982**, *16*, 148.
(22) Bruns, J. J. M.S. Thesis, Iowa State University, Ames, IA, 1980.

Received for review February 14, 1985. Revised manuscript received December 6, 1985. Accepted December 17, 1985. Ames Laboratory is operated for the U.S. Department of Energy by Iowa State University under Contract W-7405-Eng-82. This work was supported by the U.S. Department of Energy through the Office of Health and Environmental Research, Basic Energy Sciences, and through Fossil Energy, Division of Coal Utilization.

Reduction of NO_2 to NO by Rush and Other Plants

Hajime Nishimura,* Teruyoshi Hayamizu,[†] and Yukio Yanagisawa[‡]

Department of Chemical Engineering, University of Tokyo, 7-3 Hongo, Bunkyo-ku, Tokyo 113, Japan

■ Previously we reported (*3*) that rush carpets used in Japanese houses had the capacity to adsorb ambient NO_2 and the capacity endured for several years. The fate of adsorbed NO_2 was investigated in the present report. The outlet gas of a contacting tube packed with test material was monitored with a chemiluminescence analyzer for NO_2 and NO. Rush, lawn grass, and ginkgo leaves were found to adsorb NO_2 and to liberate NO. At steady state, the conversion of adsorbed NO_2 to NO reached 70%. The high conversion meant the reduction of adsorbed NO_2 by some organic matter. The reducing component was isolated by fractionation and identified as a kind of polysaccharide contained in the free sugar fraction of rush. The reduction rate was highly dependent on humidity, and a relation with clustered water in sugar was suggested.

Introduction

Depletion of NO_2 in ambient air occurs through various processes such as nitrate aerosol formation, photochemical reaction, etc., though many points remain unknown.

We had already noticed that the concentration of NO_2 was usually lower indoors than outdoors (*1*, *2*) when there was no internal emission source of NO_2. We examined the rates of sorption of NO_2 into several interior materials and found that tatami-omote, rush carpet commonly used in Japanese houses, contributed considerably to elimination of NO_2 from indoor air. It could adsorb or absorb NO_2 continuously at an appreciable rate without noticeable accumulation of nitrate or nitrite even after use of several years. Our previous study (*3*) showed that although biological denitrification can occur in tatami when it was soaked in water and kept in anaerobic condition, it is very unlikely that it occurs under actual conditions. Some other reaction removing the absorbed nitrogen must be working.

In this study, NO was found to be generated when rush was contacted with air containing the ambient level NO_2. The generation was found to be caused by reduction of NO_2 by some reducing material in rush. Rush was fractionated, and the responsible constituent was characterized.

Materials and Methods

Materials. Rice straw and rush stem are the member material of "tatami", a typical flooring of Japanese houses, which consists of a thick rice straw mat and a covering rush carpet. The rush used for tatami is *Juncus effusus L. var. decipiens Buch.* having a long stem used for carpet. Ususally a stained stem is used for the purpose, but we used an unstained one harvested and weather-dried 1 month before being tested. The used rush sample fractioned by the method of Figure 1 had a composition of 0.4% lipid, 13.9% free sugar, 2.6% pectic substances, 18.4% lignin, 33.3% hemicellulose, and 31.4% cellulose. Rice straw used in the experiment was taken from a tatami mat that had been used for 2 years.

The leaves of lawn grass, *Poa pratensis L.*, and leaves of a tree, *Ginkgo biloba L.*, were harvested on the campus of Tokyo University a day before the experiment and sacrificed for the test.

Methods. The feed gas to the experimental system was prepared by diluting NO_2 gas exuded from the permeation tube with NO_2-free air. The humidity of the gas was controlled with a humidity controller (Honeywell R670 1015) by bypassing a part of the gas through a humidifier. A Pyrex glass tube (17.5 mm i.d. and 300 mm long) packed with test material was used as the contacting tube and placed in a thermostatic oven. The concentrations of NO_2 and NO were measured by a chemiluminescent analyzer (Kimoto Model 258) at the outlet of the packed tube. The blank concentrations were measured at the beginning and the end of each experiment by removing the test material. The flow rate to the packed tube was monitored by an orifice flowmeter which was calibrated at a definite interval by diverting the exhaust flow from the tube to a wet test meter.

The water content of the material was determined by drying at 100 °C for 5–20 h.

Nitrite and nitrate accumulated in the material were determined by extracting 2 g of the material with 100 g of distilled water for 15 min on a shaker and for 5 min in an ultrasonic bath. Nitrite in the extract was determined from the absorbance at 545 nm after addition of sulfanilamide and N-(1-naphthyl)ethylenediamine dihydrochloride solution. Nitrate was determined after reduction to nitrite with a Cu–Cd column (*4*). Each sample was divided into two, and the known amounts of nitrite and nitrate were added to one of them as internal standards.

The fractionation of the structural polysaccharide in rush was performed as shown in Figure 1. The rush was cut to 5 cm, washed with distilled water, and dried. Lipid, free sugar, the pectic substance (*5*), lignin, and hemicellulose (*6*) were removed by successive extraction with petroleum ether, hot ethanol, hot water, $NaClO_2$, and KOH solution. The product of each step was weighted after drying at 100 °C, and a portion was used as the test material.

[†] Present address: Japan Environmental Agency, Kasumigaseki, Chiyodaku, Tokyo 100, Japan.

[‡] Present address: Harvard School of Public Health, Boston, MA 02115.

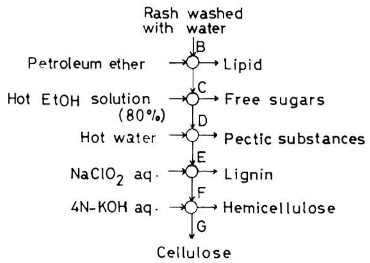

Figure 1. Schematic diagram of the procedure for successive removal of fractions of structural polysaccharides in rush.

Table I. Conversion of the Sorbed NO_2 to NO at Steady State[a]

material	preparation	conversion ratio, %
rush	raw	0.1
(*Juncus effusus L.*)	dried at 100 °C	70
	vacuum dried	48
lawn grass	raw	2
(*Poa pratensis L.*)	dried at 100 °C	69
	sun-dried	41
tree leaves	raw	30
(*Ginkgo biloba*)	dried at 100 °C	60

[a] The measurements were made when the outlet concentrations reached the steady state in the experimental system under the following conditions: feed NO_2 concentration 430 ppb; relative humidity 75%; temperature 20 °C.

The free sugar fraction was analyzed by high-performance liquid chromatography (HPLC) (Shimadzu LC-3A) with a column packed with Shodex Ionpak KS-802 and Shimadzu Gel SCR-101N in a series under the following conditions: water 0.5 mL/min as solvent; temperature 70 °C. UV (188 nm) was used for detection.

Results

Figure 2 shows the outlet concentrations of packed tube when it was fed with humidified air containing 300–450 ppb of NO_2. Zeolite, aged rice straw, and dried rush were used as test materials. Zeolite showed the typical response of a tube packed with adsorbent material. The NO_2 concentration, initially zero, rose rather abruptly and reached an almost steady state after 10 h. In case of aged rice straw, the outlet concentration was in the steady state from the beginning, though it increased slightly with time. In both cases, the outlet NO concentration was actually zero. A remarkable feature for rush was that the outlet NO concentration rose from zero and reached an appreciably high level after 10 h. The corresponding NO_2 concentration was close to its steady-state level from the beginning, though it approached it from above.

Similar experiments were made for various materials under various treatments. The ratio of NO generation rate to NO_2 sorption rate was calculated for each case when the outlet gas concentrations became steady. A part of the results is shown in Table I. Rush and turf did not raise NO when they were raw but converted 70% of adsorbed NO_2 to NO after they were dried at 100 °C. Dried ginkgo leaves showed a similar performance though the leaves could raise NO even in the raw state. The ratio can be taken as the steady conversion ratio of NO_2 to NO if we can assume a complete steady state for the accumulation of all related molecular species in the material.

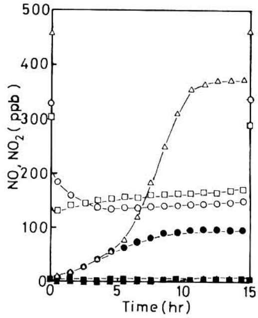

Figure 2. Sorption of NO_2 and its conversion to NO for some typical materials. The ordinate shows the outlet NO_2 or NO concentration of the tube packed with synthetic zeolite A-4 [NO_2 (△); NO (▲)], aged rice straw [NO_2 (□); NO (■)], or dried rush [NO_2 (O); NO (●)] and fed with air of 75% RH containing the shown level of NO_2. The tube was kept at 20 °C. Each of three pairs of points on both ordinates stands for the blank NO_2 concentrations measured at the beginning or the end of each experiment by removing the test material.

The conversion observed for dried rush or turf is higher than can be expected from the reaction associated with absorption of NO_2 into water, which is described as

$$2NO_2 + H_2O = HNO_3 + HNO_2 \quad (1)$$

$$2HNO_2 = NO_2 + H_2O + NO \quad (2)$$

or in summary

$$3NO_2 + H_2O = 2HNO_3 + NO \quad (3)$$

According to reaction 3, the conversion can never exceed 33.3%. Higher conversion must result from the reduction of NO_2 by some reducing material. The view was confirmed by the analysis of adsorbed compounds. Table II shows the amounts of nitrite and nitrate extracted from rush as well as the total amount of NO generated. The sum of these three nitrogen compounds was found to explain the deficit of NO_2. The relative amounts of the three compounds were plotted on a triangle diagram in Figure 3, in which line A corresponds to the progress of the reaction represented by eq 2 after completion of the reaction represented by eq 1, whereas line B corresponds to the progress of the reaction represented by eq 2 after a reaction which reduces NO_2 totally to HNO_2 as

$$NO_2 + H = HNO_2 \quad (4)$$

The presence of some reducing material was supposed. In order to identify the reducing material contained in rush, the change of NO generation rate was examined by

Table II. Amounts of Nitrogen Compounds Produced by Sorption of NO_2 to Dried Rush[a]

sample	temp, °C	RH, %	blank NO_2 concn, ppb	time, h	decreased NO_2, μmol	generated NO, μmol	accumulated NO_3^-, μmol	accumulated NO_2^-, μmol
1	26	75	392	37	14.90 (100%)	8.50 (57%)	2.38 (16%)	3.58 (24%)
2	21	75	332	15	7.06 (100%)	2.40 (34%)	2.96 (42%)	2.05 (29%)

[a] After the experiment, rush was rinsed with distilled water for 15 min on a shaker and for 5 min in an ultrasonic bath, and the extract was analyzed for nitrite and nitrate according to the method described in the text.

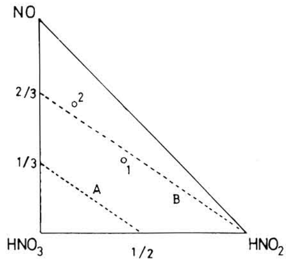

Figure 3. Relative compositions of NO, HNO_2, and HNO_3 produced by sorption of NO_2 into dried rush. Data were taken from Table II. Line A represents the composition when the reaction $2NO_2 + H_2O = HNO_3 + HNO_2$ was followed by the reaction $2HNO_2 = NO_2 + H_2O + NO$ whereas line B when the latter reaction was preceded by the reaction $NO_2 + H = HNO_2$.

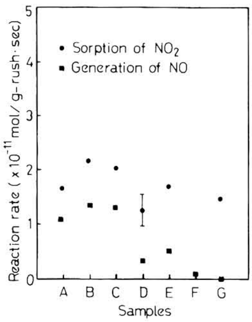

Figure 4. NO_2 sorption and NO generation rates of dried rush (A) compared with the rates of the same material after successive removal of water-soluble matter (B), lipid (C), free sugar (D), pectic substance (E), lignin (F), and hemicellulose (G). Rates were expressed with the unit mass of the starting material as the basis. Experimental conditions: NO_2 concentration 420 ppb; RH 90%; temperature 20 °C.

Table III. NO_2 Sorption and NO Generation Rates of Free Sugar Fraction at Steady State

	rates, 10^{-11} mol/(g of rush·s)	
solution	NO_2 sorption	NO generation
(A) free sugar fraction[a]	4.71	1.89
(B) solution A filtered with membrane filter[b]	4.22	2.06
(C) solution B treated with ion-exchange resin[c]	1.52	1.04

[a] Fraction defined by Figure 1. [b] Milipore Filter 0.45 μm. [c] A 25-mL sample was contacted with 2 g of Dowex 50W and 3 g of Dowex 1 for 2 h.

successively removing the constituents in rush. The result is shown in Figure 4. The NO generation rate dropped drastically when free sugar fraction was removed while the NO_2 sorption rate showed no such appreciable change throughout the successive removal.

Thus, the free sugar fraction was suspected to be responsible for the NO generation. In order to obtain positive evidence for it, a filter paper (Toyo Roshi No. 50 750 cm^2) soaked with the fraction was contacted with the test gas (Table III). The NO generation rate, when expressed on the basis of original dry rush, was as high as that for the original rush (Figure 4). Thus, free sugar fraction was ascertained to be responsible for the NO generation.

The free sugar fraction in rush contains chlorophyll and protein besides the ethanol-soluble sugar. In order to remove chlorophyll, the extract was filtered with a Mil-

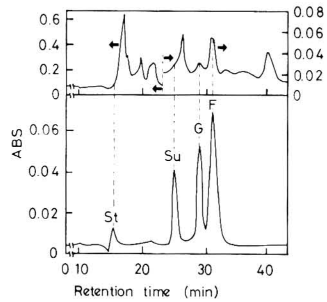

Figure 5. HPLC chromatogram of the free sugar fraction of rush purified by ion-exchange resin with reference to that of a standard solution. G, glucosef F, fructose; Su, sucrose, St, starch. See text for conditions of analysis.

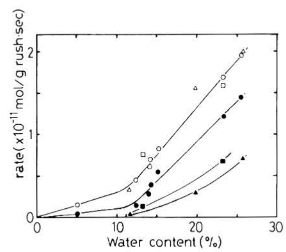

Figure 6. NO_2 sorption (△, □, ○) and NO generation (▲, ■, ●) rates of rush as a function of its water content and temperature. The rates were measured in the experimental system by feeding air containing 430 ppb of NO_2. The experiments were done by varying the humidity of air, and the water content was estimated from Figure 7 assuming equilibrium. Temperature was varied at three levels: 5.0 °C (△, ▲); 10.5 °C (□, ■); 20.0 °C (○, ●).

lipore filter (0.45 μm), and then a part of it was treated by ion-exchange resin to remove protein. The resultant two solutions were also tested for the activity of NO generation (Table III). The isolated sugar fraction, before the ion-exchange treatment, showed the almost same activity as the original rush when expressed on the basis of rush weight. After the treatment, the activity decreased to half of the original level. It might mean that the removed fraction, protein, was half responsible for NO generation or that the ion-exchange treatment half damaged the structure related to NO generation.

The ion-exchanged solution was analyzed with HPLC and found to contain, besides fructose and glucose, three to five components between starch and sucrose (Figure 5).

The NO generation activity was checked for glucose fructose, starch, and sugar by the same method as used for the free sugar fraction. Neither of them showed the activity.

The effects of the feed gas concentration, the feed gas humidity, and the temperature were also investigated. Both the NO_2 sorption and NO generation rates varied linearly with NO_2 concentration in the range 50–2000 ppb. The NO_2 sorption rate did not vary appreciably in the temperature range 5–20 °C, while the NO generation rate varied with an activation energy, 9.6 kcal/mol. It means that at a lower temperature the conversion ratio to NO becomes smaller than the value shown in Table I.

Both rates showed remarkable responses to the water content of rush under experimental conditions (Figure 6). They rose sharply in the range above 10% which corresponds to the range of the steep increase of water content with humidity (Figure 7).

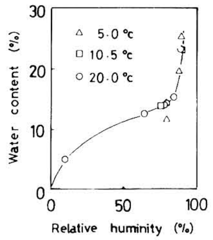

Figure 7. Equilibrium water content of rush as a function of the relative humidity of air, with temperature as a parameter.

Discussion

The conversion as high as 70% as shown in Table I cannot be explained by the scheme of reactions represented by eq 1, and the product composition of sorbed NO_2 as shown in Figure 3 cannot be elucidated by a combined reaction represented by eq 1 and 2. It implies that a hydrogen atom is removed from the adsorbent material for every NO_2 molecule absorbed.

The possibility of abstraction of hydrogen by nitrogen dioxide from organic compound was reported by Pryor and Lightsey (7). In his experiment with cyclohexene, he could demonstrate that, at a concentration below 100 ppm, NO_2 reacts with cyclohexene almost exclusively, abstracting allylic hydrogen to form nitrous acid and an allylic radical.

$$NO_2 + -HC=CH-CH_2- \rightarrow HONO + -\overline{CH-\dot{C}H-CH}- \quad (5)$$

The radical can combine with NO_2 to yield unsaturated nitro or nitrite compound.

We did not check for allylic hydrogen in our rush. Although the observed activation energy, 10 kcal/mol, seems to be a little small for the reaction of eq 5, a similar mechanism is supposed to be working on our reducing material.

It will be important to note that the reaction is strongly dependent on humidity. The higher reaction rate corresponds to the region where the humidity–water content curve shows a very steep rise. An interesting interpretation of the curve was given by Zimm and Lundberg (8). Applying statistical mechanical theory of solution, they could demonstrate that the steep rise of the curve reflects clustering of water. Clustering means that the probability of finding another molecule around a water molecule is higher than would be expected from the average concentration. A clustered structure of water seems to be necessary for the reaction.

NO generation rate, initially zero, rose very slowly and attained the steady-state value after 10 h in Figure 2. The delay would probably be related to the establishment of the steady-state water content in the material.

The humidity and water content relation of rush stem would probably be determined by that of cellulose. As cellulose or the water in cellulose was shown to have no direct effect on NO generation, the clustering of water responsible for reaction is supposed to be occurring on the free sugar fraction.

Conclusion

Rush, lawn grass, and ginkgo leaves were found to convert up to 70% of adsorbed NO_2 to NO. The conversion was concluded as the result of reduction of the adsorbed NO_2 by some organic reducing matter. The matter was identified as a kind of low molecular weight polysaccharide contained in free sugar fraction of plants. The reduction reaction is suggested to be closely related to the clustering of adsorbed water.

Registry No. NO_2, 10102-44-0; NO, 10102-43-9.

Literature Cited

(1) Yanagisawa, Y.; Nishimura, H. 21st Annual Meeting of the Japanese Society of Air Pollution, Miyazaki, 1980.
(2) Nitta, H.; Yokoyama, Y.; Aoki, S.; Maeda, K. *Nippon Koshu Eisei Zasshi* **1982**, *29*, 343.
(3) Hayamizu, T.; Yanagisawa, Y.; Nishimura, H. *Taiki Osen Gakkaishi* **1983**, *18*, 18.
(4) In "Method of Ocean Environment Study"; Japan Society of Oceanography, Ed.; Koseisha-Koseikaku: Tokyo, 1979; pp 273–275.
(5) In "The Analytical Method for Crops"; Special Editorial Committee, Ed.; Yokendo: Tokyo, 1975.
(6) Jermyn, M. A.; Iserwood, F. L. *Biochem. J.* **1956**, *64*, 123.
(7) Pryor, W. A.; Lightsey, J. W. *Science (Washington, D.C.)* **1981**, *214*, 436.
(8) Zimm, B. H.; Lundberg, J. L. *J. Phys. Chem.* **1956**, *60*, 425.

Received for review July 17, 1985. Accepted December 11, 1985.

ADDITIONS AND CORRECTIONS

1985, Volume 19, Pages 796–804

Gregory R. Markowski* and Roy Filby: Trace Element Concentration as a Function of Particle Size in Fly Ash from a Pulverized Coal Utility Boiler.

The barium size distribution in Figure 2 on page 801 should be labeled micrograms instead of nanograms.

corrected
M.S
29 July 86